The photochemical reflectance index (PRI) as an indicator of changes in photosynthetic dynamics and gross primary productivity in response to climate change

Chao Zhang

The photochemical reflectance index (PRI) as an indicator of changes in photosynthetic dynamics and gross primary productivity in response to climate change

Doctoral Thesis

Chao Zhang

July 2017

Global Ecology Unit (CREAF-CSIC)

Center for Ecological Research and Forestry Applications

Universitat Autònoma de Barcelona, July 2017

Universitat Autònoma
de Barcelona

The photochemical reflectance index (PRI) as an indicator of changes in photosynthetic dynamics and gross primary productivity in response to climate change

PhD Thesis

Chao Zhang

With the approval of the supervisors

Dr. Josep Peñuelas
Professor d'Investigació CSIC
Unitat d'Ecologia Global
CREAF-CSIC-UAB
CREAF,
Universitat Autònoma de Barcelona

Dr. Iolanda Filella
Investigadora Científica CSIC
Unitat d'Ecologia Global
CREAF-CSIC-UAB
CREAF
Universitat Autònoma de Barcelona

July 24, 2017

Table of Contents

Abstract

Quantifying photosynthetic dynamics from different spatiotemporal scales is highly important for carbon uptake research, particularly under ongoing climate changes. The photochemical reflectance index (PRI) has shown to be useful to remotely asses the physiological functioning of vegetation and it constitutes a promising method to estimate gross primary productivity (GPP) at global scale. In the last years, several works have presented possible improvements on PRI understanding and formulation to improve its applicability at larger temporal and spatial scales. The main objective of this dissertation was to clarify the mechanisms that elicit the variability in PRI and to evaluate the applicability of PRI in detecting photosynthetic dynamics and carbon uptake under various stress conditions at different spatiotemporal scales.

Three special objectives were addressed in six chapters in this thesis. The first objective was to summarize the main factors that affect PRI variation according the most recent publications, also the relationships between PRI and RUE/GPP and other ecophysiological variables across diurnal and seasonal scales at foliar, canopy and ecosystemic levels, as well as the improvements in PRI implementation. The second objective was to evaluate the capacity of PRI in monitoring the dynamics of photosynthetic activity of evergreen species seasonally or under water or temperature stresses. The last objective was to assess whether the PRI retrieved from MODerate resolution Imaging Spectroradiometer (MODIS) can be utilized to detect the effects of extreme drought on GPP and isoprenoid emissions at ecosystem scale.

The main conclusion of this thesis in the first chapter was that PRI is a good proxy of RUE and GPP at different spatial and temporal scales and was mainly constrained by facultative changes of xanthophyll-cycle pigments at short-term scales and by constitutive changes of chlorophyll and carotenoid pool sizes at long-term scales. Correcting PRI to decrease the effects of physical or physiological factors or combining PRI with solar-induced fluorescence (SIF) and conventional greenness biomass indices could greatly improve remote estimation of RUE and GPP. The second chapter showed

that leaf-level fluorescence spectra from all wavelengths (670 to 800 nm) have similar potential to track the dynamics of photosynthetic seasonality during spring recovery period in Scots pine needles and that PRI and WI also acted as good indicators to track the recovery of photosynthesis. The third chapter demonstrated that both PRI and reflectance-ratio based fluorescence (R690/R630) were not only sensitive to progressively enhanced drought stress but also sensitive enough to the recovery of photosynthesis for Mediterranean evergreen leaves. The fourth chapter illustrated that PRI and ΔPRI (morning PRI subtracted from midday PRI) were able to monitor the seasonality and the midday depression of photosynthesis of Mediterranean evergreen shrub in response to experimental warming and drought. In the fifth chapter the conclusion was that the MODIS PRI normalized by absorbed light (APAR) (sPRIn) detected the effects of drought events on GPP for Mediterranean forest but not for grassland ecosystem. In the final chapter we concluded that PRI is a promising index to estimate isoprene emissions, especially when it is complemented by information on potential emission.

Keywords: canopy level, carbon uptake, climate change, drought, ecosystem level, eddy covariance, fluorescence, gross primary productivity (GPP), leaf level, photochemical reflectance index (PRI), photosynthesis, radiation-use efficiency (RUE), recovery, remote sensing, seasonality.

Acknowledgements

Four years in CREAF have been giving me a great experience, and a new sight of work and life. My special word of appreciation would like to give to my supervisors Prof. Josep Peñuelas and Dr. Iolanda Filella who always give their guidance and explanation with patience, give me encouragement and trust, teach me how to be confidence, and encourage me to move on and fulfil my PhD work step by step. I have always been learning from Josep who always keeps full of energy and enthusiasm to enjoy work and life with his lovely smile and keeps thinking scientific questions from multiple angles, and from Iolanda who always has new ideas to find a way to improve our work and can balance well her work and family (especially with her kid).

My most sincere thanks also would like to give to Dr. Albert Porcar-Castell and Dr. Jon Atherton for their guidance in my two month stay in Hyytiälä, their patience as co-authors during my writing, and theirs instructions of the way of thinking about science. Many thanks to all the co-authors and people in SMEAR-II station who enable me to finish my work and enjoy life there with special thanks to Prof. Jaana Bäck, Dr. Juho Aalto, Dr. Pasi Kolari, Pauliina Schiestl-Aalto, Beñat Olascoaga, Dr. Risto Taipale, and Ella karvonen.

I would very like to thank to Dr. Josep-Maria Espelta Morral, Dr. Sandra Saura Mas, and Dr. Francesc Peters for their patience and instructions during every year's evaluation of my PhD program.

Many thanks to all the friends and colleagues at CREAF which is a big family with nice people always and great working environment. I am always indebted to their great help in my work and life, and enjoy daily work, lunch, and all the pleasuring time with them. Among many others, many thanks to Gerard, Xavier, Helena, Loles, Catherine, Marcos, Dominic, Chaoting, Irene, Victor, Vicenç, Albert Rivas, Albert Gargallo, Javier, Manuel, Sara, Anna, Carlos, Janette, Boira …. I am also very grateful to Anna, Magda, Marta, Carlos Carreño, Daniel, and Youssef who always prepare to help me solve the practical matters.

The European Research Council Synergy grant, the Spanish Government, the Catalan Government, the COST Action ES1309/OPTIMISE, the Academy of Finland, the University of Helsinki were acknowledged for their supporting of this thesis. A very special acknowledgement to Chinese Scholarship Council for giving me opportunity to conduct my PhD and funding this thesis.

Most important, I want to give my appreciation to my dear friends who always look forward me to back to China. Thanks for their friendship all these years.

To all my family, my parents and parents in law, sister in law and brother in law. Thanks for your supporting and understanding, keeping me moving and growing.

And to all the coauthors who make this thesis possible.

感谢所有人的陪伴，支持与鼓励！Muchas gracias!

General Introduction

Photosynthesis is a key physiological process that regulates terrestrial ecosystem functioning and productivity (Lambers *et al*., 2008), particularly in response to global environmental change (Kirschbaum, 2004; Niinemets *et al*., 2017). Climatic drought and warming can negatively affect plant ecophysiological traits, growth and survival, and positively trigger plant mortality, greatly disturbing carbon balance (Peñuelas & Filella, 2001; Peñuelas *et al*., 2009), particularly in the Mediterranean ecosystems with a climatic interaction between heat and aridity (Valladares *et al*., 2013). Along with ongoing climate change, the advanced timing of spring recovery and growing season has also been detected in different regions of the world, especially at more northern latitudes (Wang *et al*., 2015). Quantifying photosynthetic dynamics is of high importance under climate change, and to find a rapid, efficient, and non-destructive method to estimate photosynthesis dynamics from leaf, canopy, to ecosystem and regional levels at various temporal scales remains a challenging issue for carbon uptake research.

During photosynthetic process, the excessive reducing power that cannot be used by photochemistry decreases radiation-use efficiency (RUE) and can be safely dissipated through xanthophyll de-exposition status (DEPS) (Demmig-Adams & Adams, 2006). The DEPS of xanthophyll pigments is associated to reflectance at 531nm due to increased zeaxanthin during xanthophyll cycle (Gamon *et al*., 1990). The photochemical reflectance index was thus firstly defined through normalized zeaxanthin sensitive band by an insensitive wavelength ((R531-R570)/(R531+R570), where R is the reflectance and numbers are wavelength in nanometers) as an indirect optical signal of RUE and reducing power availability (Gamon *et al*., 1992; Peñuelas *et al*., 1995). Several studies had proved that PRI was a good proxy of RUE and could be used to estimate gross primary productivity (GPP) at different vegetation functional types from multiple spatiotemporal scales (Garbulsky *et al*., 2011; Peñuelas *et al*., 2011). Many studies also demonstrated that PRI was also a good indicator of RUE even under

environmental stresses conditions such as water shortage, nutrient deficit, and low and high temperature (Filella *et al*., 2004; Suárez *et al*., 2008; Mänd *et al*., 2010; Porcar-Castell *et al*., 2012; Zinnert *et al*., 2012; Gamon & Bond, 2013; Rossini *et al*., 2013). However, the variations of PRI are affected and controlled by many biochemical and physical properties, such as foliar pigment pool size, canopy structure, solar geometry, spectrometer/satellite view angles, illumination, soil background and also vegetation functional types (Filella *et al*., 2004, 2009; Hilker *et al*., 2009; Garbulsky *et al*., 2011; Hernández-Clemente *et al*., 2011; Gamon & Berry, 2012; Gamon & Bond, 2013). The extent to what these factors control PRI changes and how these effects can be minimized or avoided, and how to improve the estimation of RUE using PRI are still need to be clarified.

For example, during the winter-spring transition period, the photosynthetic downregulation induced by cold temperature is generally accompanied by multiple and concomitant physiological process, and biochemical and structural adjustments (Öquist & Huner, 2003). In overwintering evergreen trees, changes in photosynthetic and photoprotective pigments content and the afore mentioned adjustments drive to wondering whether PRI can still be a good indicator to track photosynthetic dynamics during spring recovery period. The fluorescence emitted by chlorophyll a (ChlF) compete with photochemistry and heat dissipation and can be obtained through active (pulse amplitude modulated (PAM) fluorometer) and passive (e.g. spectral fluorescence, reflectance ratio (e.g. R690/R630), and solar-induced chlorophyll fluorescence (SIF)) methods (Porcar-Castell *et al*., 2014). Fluorescence measurements have also been widely applied to detect changes in photosynthetic activity and GPP, even at canopy and global scales by way of SIF (Meroni *et al*., 2009). At seasonal scale, the relationship between leaf spectral fluorescence and photosynthesis has not been studied so far and it is worth to evaluate this promising optical signal, particularly for overwintering evergreen trees.

Although studies had shown that PRI is sensitive to water stress (Dobrowski *et al*., 2005; Suárez *et al*., 2009, 2010; Hernández-Clemente *et al*., 2011; Zarco-Tejada *et al*.,

2012), no studies have demonstrated that PRI was able to efficiently track photosynthetic recovery after progressive drought stress. It should also be further evaluated the applicability of ChlF obtained from reflectance-ratio in detecting photosynthetic response to water stress. Photosynthetic midday depression can affect the global carbon balance (Arora *et al*., 2009). We hypothesized that PRI could be sensitive to midday depression of photosynthesis, and, thus could be useful for detecting changes in RUE or GPP under extreme drought condition.

Addressing the above mentioned questions is important to improve the remote sensing of photosynthesis and carbon uptake of global terrestrial ecosystems in response to climate change. At this regard, the main objectives of this dissertation are (1) to better understand the mechanisms of PRI changes and (2) to evaluate and improve the capacity of PRI in assessing photosynthesis and carbon uptake under various stress conditions from leaf, canopy to ecosystem levels and at diurnal to seasonal scales. With this aim this thesis was divided into 3 blocks (one chapter in block 1, three chapters in block 2, and two chapters in block 3). Block 1 synthesizes the most recent publications of using PRI to remote estimate RUE and GPP. Block 2 was focused on exploiting the applicability of leaf and canopy PRI in assessing photosynthetic dynamics for evergreen species in response to water or temperature stresses. Block 3 was conducted to use satellite-based PRI to assess the effect of extreme drought on GPP and estimate isoprene emissions at ecosystem level.

The first chapter updates the review regarding the application of PRI in remotely sensing RUE. We summarized the main factors that affect PRI variation and its assessment of RUE across diurnal and seasonal scales at foliar, canopy and ecosystemic levels, and the applications of PRI to assess ecophysiological variables, as well as the improvements in PRI implementation.

The second chapter explores the optical cues likely to reveal the spring recovery of photosynthesis in Scots pine needles. We assessed the relationships of spectral fluorescence, PRI, NDVI and WI with photosynthesis, with long-term and *in situ* monitoring measurements and high frequency laboratory measurements.

In the third chapter, we addressed the assessment of photosynthetic activity in response to progressive drought and recovery using PRI and passive ChlF (R690/R630) in a Mediterranean evergreen species.

In the fourth chapter, we evaluated the diurnal and seasonal responses of photosynthesis to long-term experimental warming and drought using PRI in an evergreen Mediterranean shrub, *Erica multiflora*.

In the fifth chapter, we used different satellite indicators to detect the effects of extreme drought on GPP in a beech forest with a comparison with three additional ecosystems: a Mediterranean holm oak forest, a temperate beech forest and a semi-grassland.

The last chapter addressed the capability of satellite-based (MODIS) PRI to detect the isoprenoid emission during growing season and in response to mild and extreme drought conditions in a temperate deciduous forest.

This dissertation ends with conclusions.

References

Arora VK, Boer GJ, Christian JR, Curry CL, Denman KL, Zahariev K, Flato GM, Scinocca JF, Merryfield WJ, Lee WG. **2009**. The effect of terrestrial photosynthesis down regulation on the twentieth-century carbon budget simulated with the CCCma Earth System Model. *Journal of Climate* **22**: 6066–6088.

Demmig-Adams B, Adams WW. **2006**. Photoprotection in an ecological context: the remarkable complexity of thermal energy dissipation. *New Phytologist* **172**: 11–21.

Dobrowski SZ, Pushnik JC, Zarco-Tejada PJ, Ustin SL. **2005**. Simple reflectance indices track heat and water stress-induced changes in steady-state chlorophyll fluorescence at the canopy scale. *Remote Sensing of Environment* **97**: 403–414.

Filella I, Peñuelas J, Llorens L, Estiarte M. **2004**. Reflectance assessment of seasonal and annual changes in biomass and CO_2 uptake of a Mediterranean shrubland submitted to experimental warming and drought. *Remote Sensing of Environment* **90**: 308–318.

Filella I, Porcar-Castell A, Munné-Bosch S, Bäck J, Garbulsky MF, Peñuelas J. **2009**. PRI assessment of long-term changes in carotenoids/chlorophyll ratio and short-term changes in de-epoxidation state of the xanthophyll cycle. *International Journal of Remote Sensing* **30**: 4443–4455.

Gamon JA, Berry JA. **2012**. Facultative and constitutive pigment effects on the photochemical reflectance index (PRI) in sun and shade conifer needles. *Israel Journal of Plant Sciences* **60**: 85–95.

Gamon JA, Bond B. **2013**. Effects of irradiance and photosynthetic downregulation on the photochemical reflectance index in Douglas-fir and ponderosa pine. *Remote Sensing of Environment* **135**: 141–149.

Gamon J a, Field CB, Bilger W, Björkman O, Fredeen a L, Peñuelas J. **1990**. Remote sensing of the xanthophyll cycle and chlorophyll fluorescence in sunflower leaves and canopies. *Oecologia* **85**: 1–7.

Gamon JA, Peñuelas J, Field C. **1992**. A narrow-waveband spectral index that tracks diurnal changes in photosunthetic efficiency. *Remote Sensing of Environment* **41**: 35–44.

Garbulsky MF, Peñuelas J, Gamon J, Inoue Y, Filella I. **2011**. The photochemical reflectance index (PRI) and the remote sensing of leaf, canopy and ecosystem radiation use efficiencies. A review and meta-analysis. *Remote Sensing of Environment* **115**: 281–297.

Hernández-Clemente R, Navarro-Cerrillo RM, Suárez L, Morales F, Zarco-Tejada PJ. **2011**. Assessing structural effects on PRI for stress detection in conifer forests. *Remote Sensing of Environment* **115**: 2360–2375.

Hilker T, Lyapustin A, Hall FG, Wang Y, Coops NC, Drolet G, Black TA. **2009**. An assessment of photosynthetic light use efficiency from space: Modeling the atmospheric and directional impacts on PRI reflectance. *Remote Sensing of Environment* **113**: 2463–2475.

Kirschbaum MUF. **2004**. Direct and indirect climate change effects on photosynthesis and transpiration. *Plant Biology* **6**: 242–253.

Lambers H, Chapin FS, Pons TL. **2008**. Photosynthesis, respiration, and long-distance transport. In: Plant physiological ecology. 11–162.

Mänd P, Hallik L, Peñuelas J, Nilson T, Duce P, Emmett BA, Beier C, Estiarte M, Garadnai J, Kalapos T, *et al.* 2010. Responses of the reflectance indices PRI and NDVI to experimental warming and drought in European shrublands along a north-south climatic gradient. *Remote Sensing of Environment* **114**: 626–636.

Meroni M, Rossini M, Guanter L, Alonso L, Rascher U, Colombo R, Moreno J. **2009**. Remote sensing of solar-induced chlorophyll fluorescence: review of methods and applications. *Remote Sensing of Environment* **113**: 2037–2051.

Niinemets Ü, Berry JA, von Caemmerer S, Ort

DR, Parry MAJ, Poorter H. **2017**. Photosynthesis: ancient, essential, complex, diverse … and in need of improvement in a changing world. *New Phytologist* **213**: 43–47.

Öquist G, Huner NPA. **2003**. Photosynthesis of overwintering evergreen plants. *Annual Review of Plant Biology* **54**: 329–355.

Peñuelas J, Filella I. **2001**. Responses to a warming world. *Science* **294**: 64–66.

Peñuelas J, Filella I, Gamon JA. **1995**. Assessment of photosynthetic radiation use efficiency with spectral reflectance. *New Phytologist* **131**: 291–296.

Peñuelas J, Garbulsky MF, Filella I, Papp T. **2011**. Photochemical Reflectance Index (PRI) and Remote Sensing of Plant CO2 Uptake. *New Phytologist* **191**: 596–599.

Peñuelas J, Rutishauser T, Filella I. **2009**. Phenology feedbacks on climate change. *Science* **324**: 887–888.

Porcar-Castell A, Garcia-Plazaola JI, Nichol CJ, Kolari P, Olascoaga B, Kuusinen N, Fernández-Marín B, Pulkkinen M, Juurola E, Nikinmaa E. **2012**. Physiology of the seasonal relationship between the photochemical reflectance index and photosynthetic light use efficiency. *Oecologia* **170**: 313–323.

Porcar-Castell A, Tyystjärvi E, Atherton J, Van Der Tol C, Flexas J, Pfündel EE, Moreno J, Frankenberg C, Berry JA. **2014**. Linking chlorophyll a fluorescence to photosynthesis for remote sensing applications: mechanisms and challenges. *Journal of Experimental Botany* **65**: 4065–4095.

Rossini M, Fava F, Cogliati S, Meroni M, Marchesi A, Panigada C, Giardino C, Busetto L, Migliavacca M, Amaducci S, *et al.* 2013. Assessing canopy PRI from airborne imagery to map water stress in maize. *ISPRS Journal of Photogrammetry and Remote Sensing* **86**: 168–177.

Suárez L, Zarco-Tejada PJ, Berni JAJ, González-Dugo V, Fereres E. **2009**. Modelling PRI for water stress detection using radiative transfer models. *Remote Sensing of Environment* **113**: 730–744.

Suárez L, Zarco-Tejada PJ, González-Dugo V, Berni JAJ, Sagardoy R, Morales F, Fereres E. **2010**. Detecting water stress effects on fruit quality in orchards with time-series PRI airborne imagery. *Remote Sensing of Environment* **114**: 286–298.

Suárez L, Zarco-Tejada PJ, Sepulcre-Cantó G, Pérez-Priego O, Miller JR, Jiménez-Muñoz JC, Sobrino J. **2008**. Assessing canopy PRI for water stress detection with diurnal airborne imagery. *Remote Sensing of Environment* **112**: 560–575.

Valladares F, Benavides R, Rabasa S, D'\iaz M, Pausas JG, Paula S, Simonson WD. **2013**. Global change and Mediterranean forests: current impacts and potential responses. *Forests and Global Change*: 47–75.

Wang X, Piao S, Xu X, Ciais P, Macbean N, Myneni RB, Li L. **2015**. Has the advancing onset of spring vegetation green-up slowed down or changed abruptly over the last three decades? *Global Ecology and Biogeography* **24**: 621–631.

Zarco-Tejada PJ, González-Dugo V, Berni JAJ. **2012**. Fluorescence, temperature and narrow-band indices acquired from a UAV platform for water stress detection using a micro-hyperspectral imager and a thermal camera. *Remote Sensing of Environment* **117**: 322–337.

Zinnert JC, Nelson JD, Hoffman AM. **2012**. Effects of salinity on physiological responses and the photochemical reflectance index in two co-occurring coastal shrubs. *Plant and Soil* **354**: 45–55.

Block I. The progress in using PRI to remotely estimate RUE and GPP

Chapter I. Affecting factors and recent improvements of the photochemical reflectance index (PRI) for remotely sensing foliar, canopy and ecosystemic radiation-use efficiencies

Chao Zhang, Iolanda Filella, Martín F. Garbulsky and Josep Peñuelas

This chapter was published in ***Remote Sensing*** in 2016, 8(9), 1-33.

Abstract

Accurately assessing terrestrial gross primary productivity (GPP) is crucial for characterizing the climate-carbon cycle. Remotely sensing the photochemical reflectance index (PRI) across vegetation functional types and spatiotemporal scales has received increasing attention for monitoring photosynthetic performance and simulating GPP over the last two decades. The factors confounding PRI variation, especially on long timescales, however, require the improvement of PRI understanding to generalize its use for estimating carbon uptake. In this review, we summarize the most recent publications that have reported the factors affecting PRI variation across diurnal and seasonal scales at foliar, canopy and ecosystemic levels; synthesize the reported correlations between PRI and ecophysiological variables, particularly with radiation-use efficiency (RUE) and net carbon uptake; and analyze the improvements in PRI implementation. Long-term variation of PRI could be attributed to changes in the size of constitutive pigment pools instead of xanthophyll de-epoxidation, which controls the facultative short-term changes in PRI. Structural changes at canopy and ecosystemic levels can also affect PRI variation. Our review of the scientific literature on PRI suggests that PRI is a good proxy of photosynthetic efficiency at different spatial and temporal scales. Correcting PRI by decreasing the influence of physical or physiological factors on PRI greatly strengthens the relationships between PRI and RUE and GPP. Combining PRI with solar-induced fluorescence (SIF) and optical indices for green biomass offers additional prospects.

Keywords: gross primary productivity (GPP); radiation-use efficiency (RUE); photochemical reflectance index (PRI); affecting factors; spatiotemporal scales

1. Introduction

Terrestrial gross carbon uptake, expressed as gross primary productivity (GPP), and its response to climatic changes play a key role in projections of future carbon cycles and climate [1,2]. Increasing attention has been concentrated on accurately and continuously quantifying and modeling GPP over large regions and long timescales [3–5]. Observations of vegetation primary productivity in situ, and empirical [6] or process-based [1,7] models have been successfully used to estimate the global distribution of GPP. These measurements, however, rarely provide high-quality data and contain errors originating from the uncertainties of field work, which impede a comprehensive understanding of the global terrestrial carbon cycle [2,7].

Remotely sensing carbon uptake provides a unique opportunity for extending the spatial coverage of carbon fluxes [2,8–11]. The quantification of GPP variation by remote-sensing techniques is generally based on a model of radiation-use efficiency (RUE) [12,13]. This model mainly considers the absorbed photosynthetically active radiation (APAR) and the actual photochemical efficiency [12,13]. APAR has been extensively analyzed and is usually derived from vegetation indices of greenness such as the normalized difference vegetation index (NDVI) and the enhanced vegetation index (EVI) [10,14–17]. The remote sensing of RUE, however, has been less extensively analyzed, perhaps because it is influenced by many factors [10,18–20].

RUE is commonly remotely estimated using the photochemical reflectance index (PRI), which is a proxy of ecophysiological parameters linked to the competition between energy dissipation and photochemical conversion [11,18–23]. Reflectance at 531 nm rapidly decreases in response to the dissipation of excess energy by xanthophyll de-epoxidation due to an increase in zeaxanthin concentration and to chloroplast shrinkage following an increase in thylakoid ΔpH, which is insensitive to short-term changes at 570 nm [18,19]. PRI is thus defined as (R531 − R570)/(R531 + R570), where R is the reflectance and the numbers are central wavelengths of narrow bands in nanometers. The remote sensing of photosynthetic performance and plant stress has advanced considerably over the last two decades [9,11,20,24], with tower- [25], aircraft- [26,27] and satellite- [9,28–31] based PRI at both short (hours to days) and long (days to seasons) terms since Gamon, Peñuelas and Field [18] and Peñuelas et al. [19] proposed this reflectance index. The short-term change in PRI associated with the xanthophyll cycle, as proposed by Gamon et al. [18] and Peñuelas et al.

[19], is able to track photosynthetic performance and RUE, the actual or maximum photochemical efficiency of photosystem II (PSII) and non-photochemical quenching (NPQ) over a wide range of species, plant functional types and nutrient levels at foliar, canopy and ecosystemic levels under various stress conditions (e.g., water shortage, nutrient levels, disease and contamination) [19,20,23,28,32–46]. PRI has also been useful for studying aquatic vegetation [47], mosses [48–50] and lichens [51]. Photosynthetic activation can be efficiently tracked by PRI, particularly during special seasonal periods of alteration such as spring recovery in coniferous [52–55], and across years in boreal deciduous forests [56], Mediterranean holm-oak forests [29] and shrubland [22]. PRI obtained from MODIS (Moderate Resolution Imaging Spectroradiometer) [25,29,56–58], AVIRIS (Airborne Visible/Infrared Imaging Spectrometer) [59] and CHRIS/PROBA (Compact High Resolution Imaging Spectrometer launched aboard the Proba satellite) [60] can also track changes in photosynthetic performance and primary productivity at larger spatial scales. The rapid changes in carbon uptake for evergreen vegetation in densely vegetated areas have been captured by PRI, but not by widely used greenness indices such as NDVI which can be saturated due to stabilized canopy greenness [20,28,39,61–63]. PRI, a narrow-band spectral index as a proxy of ecophysiological parameters based on the changes in energetic status thus provides a quick, simple, nondestructive, labor-saving and cost-efficient means of optical sampling for exploring interactions of plant-ecosystem carbon fluxes and for promisingly monitoring and mapping RUE/GPP at larger spatiotemporal scales [11,20,64–66].

Several studies, however, have shown that PRI can be affected by solar angle, illumination, canopy structure, atmosphere, pigments and soil background [10,11,20,23,54,67–75]. Additionally, the interpretation of PRI becomes more difficult for mixed species or landscapes with varying canopy fractions [76,77], although several studies have reported correlations between PRI and photosynthetic performance [34,35,78,79]. The variation in PRI also depended on the site difference caused by vegetation types and canopy structure [62,77], which generally affected the PRI-RUE relationships. Much of the long-term variation in PRI and its tracking of carbon assimilation has recently been attributed to changes in the sizes of constitutive (slow) pigment pools that also impacted long-term tracking of carbon assimilation by PRI [23,54,55,67,76]. However, such studies have not been expanded to a wide range of species and sites, so the physiological mechanism of long-term PRI variation still remains to be clearly understood. Furthermore, the not yet resolved physiological mechanism of PRI and its high sensitivity to various extraneous effects might

impede the evaluation of photosynthetic performance, when scaling up from foliar to canopy, and ultimately, landscape and global scales [24]. Even so, recent findings of links between RUE/GPP and PRI and the integration of PRI with other parameters such as foliar pigments [80], solar-induced fluorescence (SIF) [81] or vapor-pressure deficit (VPD) [77] may provide new opportunities for the continuous assessment of carbon uptake.

In a review of the literature, Garbulsky et al. [20] found that PRI was significantly correlated with RUE and other relevant ecophysiological variables across vegetation types and spatiotemporal scales. The consistent relationships with RUE-PRI at different spatiotemporal scales were summarized by synthetic analyses of publications from 1992 to 2009. The kinds of factors that control PRI variation in different plant functional types, organizational levels and temporal scales, how and the extent to which these factors control changes in PRI and how these effects can be decreased or avoided, however, remain to be clarified. An integrated and robust model for remotely sensing carbon uptake using PRI at different scales will also need to be developed for using PRI as an estimator of carbon uptake.

In this review, we analyze the main factors that drive changes in PRI and its assessment of RUE at foliar, canopy and ecosystemic levels based on the scientific literature reviewed by Garbulsky et al. [20] and on an additional review of the literature published between 2010 and 2015, and we summarize the applications of PRI for interpreting ecophysiological variables. We also describe the principal suggestions for improving the estimation of RUE and carbon uptake using PRI. The primary purpose of this study is thus to determine if PRI, a simple, optical remote-sensing index, is a good proxy of RUE at both short and long timescales from foliar to global levels.

2. Affecting Factors

We found more than 110 publications in the Science Citation Index published from 2010 to 2015 that studied remotely sensed PRI; among those, 73 studies analyzed the disparately functional mechanisms of PRI at varying spatiotemporal scales and the factors that drive PRI variation and hinder its use at longer timescales and larger regions. Here, we reviewed these affecting factors of PRI over temporal (daily and seasonal) and spatial scales (from leaves to ecosystems).

2.1. Daily Changes

2.1.1. Foliar Level

Leaves in different canopy positions with changing illumination and varying temperature have different PRI values. For example, shaded leaves had higher PRI values than sunlit leaves with higher irradiance that generated a larger xanthophyllic pigment pool and a higher potential diurnal pigment conversion [67,82,83]. In particular, illumination also led to a lower PRI toward midday [83] and a recovery in late afternoon on sunny days [76,84–87] but to a higher PRI toward midday on cloudy days [76]. PRI changed little over time with weak light [88] and did not vary with maximum photochemical efficiency (Fv/Fm) [87,89], relative water content (RWC), CO_2 assimilation or stomatal conductance under low photosynthetic photon flux density (PPFD) (<700 μmol m^{-2} s^{-1}) [90]. In contrast, PRI values decreased under light saturation, due to the generation of a photoprotective reaction, which decreased the epoxidation state (EPS) [85]. PRI was also sensitive to increased NPQ during the initial growing stages in crops and to xanthophyllic pigments during the later growing stages [91]. PRI, however, was a poor diurnal indicator of the de-epoxidation state (DEPS) in different crown levels for spruce needles, probably due to the variation in the chlorophyll/carotenoid ratio [92].

Drought [30,93], temperature stress [87,93], low nitrogen concentration [91,94], iron deficiency [95], high altitude [96], high ultraviolet A/B [97,98] and disease [99–102] can potentially induce biochemical and physiological changes (e.g., chlorophyllic and carotenoid contents, xanthophyll cycle and NPQ) and inhibit the photochemistry of PSII, thus leading to a decrease in PRI, which was more apparent in young than in mature leaves as cadmium stress increased [103]. Variations in the angle and direction of illumination [104] and instrumental FWHM (full width at half-maximum) [69] can also change the optical properties, which then influence PRI values. Gamon and Berry [67] reported that the sizes of both the facultative xanthophyllic and constitutive pigment pools affected PRI and that the latter but not the former caused PRI to vary with canopy position; they also suggested that lutein de-epoxidation might influence PRI variability in nature. Other studies have also reported that foliar chlorophyllic and carotenoid pigment pools, which characterize the plant physiological status, contribute greatly to the variability of PRI [91,92,105], so incorporating

the effects of other photosynthetic pigments is necessary to use PRI as a more accurate proxy for biophysical parameters or plant status [88,91].

2.1.2. Canopy Level

Fifteen of the publications studied the diurnal response of canopy PRI to the ecophysiological status of the vegetation and to photosynthetic performance. The status of epoxidation of the xanthophyllic cycle accounted for most of the diurnal PRI variability [76,106], especially in the early morning and afternoon [107], and short-term adaptations to varying levels of solar irradiance increased PRI variability [106]. Damm et al. [108] demonstrated the sensitivity of canopy reflectance and vegetation indices derived from spatial and spectral high-resolution data to varying irradiances, and reported that unknown direct/diffuse irradiance caused by complex interactions of surface irradiance and reflectance anisotropy accounted for up to 32% of the uncertainty of PRI for crops. Another study found that spectra were best obtained ca. 10 a.m. but that deviation from the zenith affected PRI, although the effect of the departure of 10° from the nadir view precision on PRI accuracy was acceptable [109]. Further, a high relative azimuth angle showed higher PRI values at any view zenith angles by capturing more shaded foliage and thus decreasing the effect of soil background [82,83]. In addition, PRI tracked RUE poorly when chlorophyllic concentrations during senescence were low [109] and when wheat canopies at the elongation stage were sparse [110]. In contrast, PRI values were lower for dark soil, even with dense vegetation, but estimated RUE and PSII efficiency better [62,82,110]. PRI has also been used as an indicator of salinity stress in coastal species but varied with tissue chlorides and not with pigments [111]. Some studies have also reported that soil reflectance [62], species [110], canopy structure [75,82], tree age and illumination patterns [84] complicated the interpretation of PRI. Gamon and Bond [84], however, supported the hypothesis that photosynthesis is coordinately regulated, allowing PRI to be used as an indicator of diurnal photosynthetic activity.

2.2. Seasonal Changes

2.2.1. Foliar Level

PRI is intended as a measure of the responses of a constitutive component dependent on the pigment content of leaves and on a facultative component varying on a short timescale because of the xanthophyllic cycle [67]. Hmimina et al. [86] reported foliar pigment content had a stronger impact on PRI than on the relationship with RUE at seasonal timescales and proposed a procedure for correcting PRI that clarified this pigment effect at the foliar level.

PRI values during growth were lower for sunlit than shaded leaves [83,112] and were higher for dark-green than either light- or yellow-green leaves [83,87]. PSII efficiency could not be efficiently tracked by PRI in varying light intensities, seasons and leaf colors due to the influence of chlorophyll, low temperature at night or low illumination on reflectance, which inhibit the epoxidation of the xanthophyllic cycle and retain more xanthophyllic pigments [87,113]. Likewise, the tracking of seasonal levels of Chlorophyll a/b (Chl a/b) using PRI was affected by high non-photochemical dissipation from the senescence of the vegetation and drought stress in desert species during growth [114]. PRI decreased throughout the soybean growing season due to elevated ozone concentrations, which increased the protective dissipation of excess energy and decreased the foliar contents of nitrogen and chlorophyll [115,116]. PRI, however, correlated well with NPQ in evergreens during most of the year except during spring recovery after winter down-regulation [72] and throughout the stages of crop leaves unless PRI was corrected for pigment effects [88]. Similarly, EPS could not account for the variation in PRI during spring recovery [54,55] due to the changes in the constitutive pigment pool, but not the facultative xanthophyllic cycle, which led to the primary variation of PRI during spring recovery and over the year in evergreen conifers. Hernández-Clemente et al. [117] found that changes in chlorophyllic and carotenoid concentrations caused the variation of PRI values due to the seasonal fluctuation of foliar optical signals. Similar findings were also reported for *Salix viminalis* trees [112], eggplant [88] and oak and beech trees [86], where the sizes of the pigment pools contributed to most of the PRI variability and thus limited its use for RUE estimation on long timescales. Changes in pigment concentrations due to water stress, however, could also potentially affect the seasonal variability of PRI [118–120], but these changes varied between species such as *Umbilicaria arctica* and *U. hyperborean* [118]. PRI clearly differentiated between normal and stressed holm oaks but was not very informative under a severe drought [121], and could generally detect the physiological status of water-stressed plants but was not useful for the drought-tolerant species *Elaeagnus umbellate* [122].

2.2.2. Canopy Level

Recent studies have indicated that the changes in the patterns of seasonal and inter-annual PRI were correlated with chlorophyllic and carotenoid pool sizes and structural properties [76,107,123,124]. Structural changes of the canopy caused by sustained water stress [120,123,125,126] or a varying leaf area index (LAI) [127] over the season led to PRI

variability and loss of the seasonal relationship between PRI and RUE. PRI calculated from pure crown reflectance for fruit trees under different irrigation regimes varied with xanthophyllic pigment contents and not with vegetation structure or chlorophyllic content [128]. The sensitivity of PRI to physiological indicators of stress when calculated for entire canopies, however, was considerably lower for dark soil [128]. PRI has shown sensitivity to both the zenith angle and relative azimuth angle [83]. Differences in the correlations between PRI and RUE for different types of vegetation can be due to differences in the canopy structure and shadow fraction, however, when the canopy is detected from only one angle (as with MODIS) [4], highlighting the importance of the effect of the canopy structure on PRI. PRI was also sensitive to changes in the structure and physiology during the soybean growing season caused by elevated CO_2 and O_3 concentrations [127]. Canopy PRI values were higher during the growth phase than other phases [83,129] and did not efficiently track RUE variability during the ripening stage [129]. Canopy PRI values were higher on cloudy days with low irradiance than on sunny days [130], and were correlated most strongly with RUE under clear or slightly overcast skies [123]. For some vegetation such as *Elaeagnus umbellate*, a drought-tolerant invasive species, PRI decreased slightly during water stress because of the plant's special physiological and morphological characteristics [122].

2.2.3. Ecosystemic Level

MODIS and CHRIS/PROBA are common operational instruments for studying PRI at ecosystemic and regional scales [9,60,131,132]. Alterations in the angle at which satellites detect seasonal fluctuations of illumination, the shadow fraction detected by the sensor and atmospheric effects were identified as critical influences on PRI signals on a spatial scale [31,71,79,133], with the exception of some relatively uniform and dense canopy structures and a low variability of shadow fractions [71]. PRI obtained from the backscatter direction [25,60,132] nonetheless minimized the effect of shadows, and near-nadir satellite observations [79] that reduced the effects of soil background and atmospheric scattering were also optimal and improved the accuracy of RUE detection. PRI performance was improved in forward-scattering directions after replacing the PRI formulation wavelength, which indicates a possible shift in the signal of xanthophyllic de-epoxidation with the direction of detection. In contrast, Sims et al. [134] found no difference between backward and forward effects on MODIS PRI in a dense evergreen and two deciduous forest ecosystems. MODIS PRI has detected the impacts of water stress on RUE [25], but not for severe droughts

[31,135]. Intra-annual changes in MODIS PRI were dependent on the composition of foliar pigments at evergreen sites and on the dynamics of canopy structure at deciduous sites [79], but a universally applicable model for correlating ecosystemic RUE with MODIS PRI for all types of ecosystems could not be found. Vegetation indices designed to be more sensitive to chlorophyllic content explained most of the variability in GPP in a subalpine grassland ecosystem characterized by a strong seasonally dynamic GPP, and the accuracy only slightly improved by adding PRI to the model formulation [136]. The combined use of PRI and VPD was also one of the better models for estimating RUE in tropical evergreen rainforests [77].

2.3. Other Factors

Several studies have concentrated on the influence of the configuration and calibration of field spectroradiometers on PRI variation. Most spectroradiometers are designed for periodic use, but continuous measurements and the validation of remote-sensing data are needed to improve PRI accuracy and application in assessing carbon uptake [137,138]. Regular calibration and the correction of data based on the effect of nonlinearity were therefore recommended to ensure data quality [85,137,139]. Radiometric and spectral stability have high impacts on the uncertainty of PRI. The accurate measurement of near-surface spectral data can provide an important groundwork for the calibration and validation of satellite measurements [85].

3. Application

PRI has been used as an indicator of photosynthetic function at long timescales and in large areas and of carbon uptake at large scales [8,9,11,20]. We summarized various aspects of the applications of PRI based on the review by Garbulsky et al. [20]. Sixty percent of the articles published between 2010 and 2015 linked PRI to plant physiological variables (Table 1 [4, 25, 28, 30, 31, 54, 55, 60, 62, 69, 71, 72, 75–77, 79, 81, 84–95, 98, 101, 103, 105, 107, 109–115, 117, 119–124, 126, 128–130, 132, 136, 140–153]). We included only the studies that calculated PRI as (R531 − R570)/(R531 + R570) or (R570 − R531)/(R570 + R531) [18,19] to allow analysis and comparisons. The coefficients of determination (R^2) and uncharted correlations were extracted from the figures, and were analyzed and drawn using boxplots for each type of vegetation (e.g., broadleaved, coniferous and herbaceous/crop plants),

timescale (daily or seasonal, i.e., changes within or across seasons) and organizational level (foliar, canopy for a single plant or a monospecific stand, or ecosystemic for a stand of mixed species). We also included the results by Garbulsky et al. [20] in our boxplots. The correlations obtained from 153 publications were thus analyzed. All variables except the six most common ecophysiological variables linked to PRI in Table 2 in Garbulsky et al. [20] were also analyzed and plotted. The overall relationships between RUE and PRI reported during the last two decades were analyzed at daily and seasonal scales and at foliar to ecosystemic levels.

3.1. Foliar Level

3.1.1. Diurnal Changes

A total of 33 articles published from 1992 to 2015 analyzed the relationships between foliar-level PRI and actual photochemical efficiency (ΔFv/Fm'), NPQ, the chlorophyll/carotenoid ratio, EPS, DEPS, RUE or net CO_2 uptake (Figure 1). The correlations between PRI and ΔFv/Fm' (n = 57, n is the number of the correlations reported in the literature) and RUE (n = 28) were among the most relevant. Most of the relationships were focused on broadleaved and herbaceous/crop plants. The correlations for broadleaved and coniferous plants were stronger than those for herbaceous/crop plants, except for the correlations between PRI and EPS (or DEPS). R^2 for all variables other than the chlorophyll/carotenoid ratio also showed high differentiation for herbaceous/crop plants (Figure 1). PRI for broadleaved species represented medians of 80%, 76% and 78% of the variability of ΔFv/Fm', RUE and net CO_2 uptake, respectively (Figure 1a,d,f).

The R^2 of PRI with other physiological variables is presented in Figure 2. All studies focused on broadleaved and herbaceous/crop plants, for which PRI explained averages of 68% or 67%, respectively, of the variation of emissions of volatile organic compounds (monoterpenes and isoprenes). PRI was significantly correlated with foliar nitrogen content and seed yield (R^2 = 0.29, p < 0.0001 and R^2 = 0.30, p < 0.0001, respectively) [115] for soybean leaves exposed to elevated ozone. PRI was also significantly correlated in six broadleaved species with water potential under water stress (0.60 < R^2 < 0.95) [30] and with RWC (R^2 = 0.32) under water and temperature stress [93].

Table 1. List of published studies (2010–2015) linking photochemical reflectance index (PRI) with ecophysiological variables. Specrad, spectroradiometer. Abbreviations for the ecophysiological variables: RWC, relative water content; gS, stomatal conductance; RUE, radiation-use efficiency; net CO_2 uptake, net photosynthetic rate, gross primary productivity or light-saturated photosynthesis; EPS or DEPS, epoxidation or de-epoxidation state of the xanthophylls; Fv/Fm, maximum photochemical efficiency of PSII; ΔF/Fm', effective quantum yield, actual photochemical efficiency or photochemical efficiency of photosystem II (ΦPSII); Fs, steady-state fluorescence; NPQ, non-photochemical quenching; Chl/Car or Car/Chl, chlorophyll/carotenoid or carotenoid/chlorophyll ratio; VAZ, xanthophyll-cycle pigment pools; V, violaxanthin; A, antheraxanthin; Z, zeaxanthin; L, lutein; qN, non-photochemical quenching; PPFD, photosynthetic photon flux density; fAPAR, fraction of absorbed photosynthetically active radiation; fIPARg, fraction of photosynthetically active radiation intercepted by vegetation; α_s, canopy shadow fraction; Tl-Tair, leaf minus air temperature; Tc-Ta, crown minus air temperature.

Article Order by Published Date	Year	Reference	Scale	Variance Factor	Species/Vegetation Type	Vegetation Type	Sensor	Figure #	Ecophysiological Variable
3	2010	(Ibaraki et al. [140])	Leaves	Diurnal	Strawberry, lettuce and potato	Herbaceous and crop	PRI imaging system	1a	ΔF/Fm'
2	2010	(Ibaraki and Gupta [89])	Leaves	Diurnal	Potato	Herbaceous and crop	PRI imaging system	2	Fv/Fm
35	2013	(Kováč et al. [92])	Leaves	Diurnal	Norway spruce (*Picea abies*)	Conifers	Spectrad	1e	Chl/Car
38	2013	(Peñuelas et al. [141])	Leaves	Diurnal	*Populus nigra* and *Quercus ilex*	Broadleaf	Spectrad	2	Monoterpene emission rates Isoprene emission rates
48	2014	(Magney et al. [91])	Leaves	Diurnal	Sunflower, wheat, *Quercus macrocarpa*, *Betula papyrifera*, and *Populus tremuloides*	Herbaceous and crop and Broadleaf	Spectrad	1c 1b	NPQ DEPS
58	2016	(Harris et al. [112])	Leaves	Diurnal	*Salix viminalis*	Broadleaf	Specrad	1d and 9	RUE
								1f	Net CO_2 uptake
								1e	Car/Chl
								2	Isoprene emission rates VAZ Neoxanthin Lutein Chl

									Car VAZ/Chl
63	2015	(Stratoulias et al. [142])	Leaves	Diurnal	Shore reed	Herbaceous and crop	Specrad	2	Chl Fs Fm' ETR
43	2014	(Ainsworth et al. [115])	Leaves	Diurnal (Ozone)	Soybean	Herbaceous and crop	Specrad	2	Leaf N (%) Chl Seed Yield
55	2014	(Xue et al. [103])	Leaves	Diurnal (Cd polution)	Soybean	Herbaceous and crop	Specrad	1d and 9	RUE
								1f	Net CO_2 uptake
								1a	ΔF/Fm'
64	2015	(Su et al. [95])	Leaves	Diurnal (Fe deficiency)	Peanut	Herbaceous and crop	Specrad	1d and 9	RUE
								1f	Net CO_2 uptake
40	2013	(Sun et al. [143])	Leaves	Diurnal (Genetic transformation)	Barley	Herbaceous and crop	Spectrad	1d and 9	RUE
								1f	Net CO_2 uptake
21	2012	(Osório et al. [93])	Leaves	Diurnal (Moisture and temperature stress)	*Ceratonia siliqua*	Broadleaf	Spectrad	1a	ΔF/Fm'
								1c	NPQ
								2	RWC Water potential
25	2012	(Shrestha et al. [94])	leaves	Diurnal (N supply)	Rice	Herbaceous and crop	PlantPen PRI 200	1c	NPQ
37	2013	(Pallozzi et al. [98])	Leaves	Diurnal (UVA stress)	*Populus Canadensis*	Broadleaf	Spectrad	1d and 9	RUE
								1f	Net CO_2 uptake
								1a	ΔF/Fm'
30	2013	(Calderón et al. [101])	Leaves	Diurnal (Vericillium wilt)	Olive orchard	Broadleaf	PlantPen	2	Tc-Ta gS
7	2010	(Sarlikioti et al. [90])	Leaves	Diurnal (Water stress)	Tomato	Herbaceous and crop	PlantPen PRI 200	1f	Net CO_2 uptake
								2	RWC gS
8	2010	(Shahenshah et al. [144])	Leaves	Diurnal (Water stress)	Cotton and Peanut	Herbaceous and crop	PMA-11	1a	ΔF/Fm'
								1c	NPQ
13	2011	(Garrity et al. [105])	Leaves	Diurnal (Water stress)	Bur oak and 10 sugar maple	Broadleaf	Specrad	1e	Car/Chl
								2	Chl Car
18	2011	(Ripullone et al. [30])	Leaves	Diurnal (Water stress)	*Arbutus unedo*, *Quercus ilex*, *Quercus pubescens*, *Quercus cerris*, *Quercus robur*, *Cannabis sativa*, *Fagus sylvatica* and *Populus euroamericana*	Broadleaf	Specrad	1d and 6	RUE
								1f	Net CO_2 uptake
								1a	ΔF/Fm'
								1b	DEPS
								2	Water potential
27	2012	(Weng et al. [113])	Leaves	Diurnal/ Seasonal	*Pinus taiwanensis*, *Stranvaesia niitakayamensis*, two *Miscanthus* spp. and mango	Broadleaf, conifers and Herbaceous and crop	Spectrad	1a and 3a	ΔF/Fm'
								4	Fv/Fm

23	2012	(Rahimzadeh-Bajgira et al. [88])	Leaves	Diurnal/ Seasonal	*Solanum melongena*	Herbaceous and crop	Spectrad	1c	NPQ
								4a	ΔF/Fm'
								2 and 4	ETR
67	2015	(Wong and Gamon, [55])	Leaves	Diurnal/ Seasonal/ Internnual	*Pinus contorta* and *Pinus ponderosa*	Conifers	Specrad	3e	Car/Chl
								3b	EPS
11	2010	(Weng et al. [87])	Leaves	Diurnal/ Seasonal	Mango	Broadleaf	Specrad	1a and 3a	ΔF/Fm'
								3b	EPS
								4	Fv/Fm Minimum temperature
46	2014	(Harris et al. [85])	Leaves/ Canopy	Diurnal	*Pinus contorta*	Conifers	Specrad	1b and 5b	EPS
32	2013	(Gamon and Bond [84])	Leaves/ Canopy	Diurnal	Douglas-fir and ponderosa pine	Conifers	Spectrad	6	PPFD
16	2011	(Hernández-Clemente et al. [69])	Leaves/ Canopy	Diurnal (Water stress)	*Pinus sylvestris* and *Pinus nigra*	Conifers	Specrad AHS airborne	1b and 5b	EPS
								6	gS Water potential
22	2012	(Porcar-Castell et al. [72])	Leaves	Seasonal	*Pinus sylvestris*	Conifers	Spectrad	3d and 9	RUE
								3c	NPQ
								3a	ΔF/Fm'
								3e	Car/Chl
								3b	DEPS
								4	Fv/Fm Car Chl VAZ VAZ/Chl
47	2014	(Hmimina et al. [86])	Leaves	Seasonal	*Quercus robur* and *Fagus sylvatica*	Broadleaf	Specrad	3d, 9 and 10a	RUE
								3a	ΔF/Fm'
60	2015	(Nyongesah et al. [114])	Leaves	Seasonal	*Haloxylon ammodendron*	Shrubland	Specrad	4	Chl a/b
62	2015	(Šebela et al. [145])	Leaves	Seasonal (High night temperature)	Rice	Herbaceous and crop	Specrad	3a	ΔF/Fm'
								4	Fs
53	2014	(Sun et al. [119])	Leaves	Seasonal (Interannual)	Olive	Broadleaf	Specrad	3d and 9	RUE
								3f	Net CO_2 uptake
								3e	Car/Chl
								4	Car RWC
54	2014	(Tsonev et al. [121])	Leaves	Seasonal	*Quercus ilex*	Broadleaf	Specrad	3d and 9	RUE

				(Water stress)				3f	Net CO_2 uptake
								4	RWC
10	2010	(Suárez et al. [128])	Leaves/ Canopy	Seasonal	Peach, nectarine and orange	Broadleaf	Specrad Airborne	3b and 7b	EPS
19	2012	(Hernández-Clemente et al. [117])	Leaves/ Canopy	Seasonal	*Pinus sylvestris*	Conifers	Camera	3e	Car/Chl
								4	Car Chl
66	2015	(Wong and Gamon [54])	Leaves/ Canopy	Seasonal	*Pinus contorta*, *Pinus ponderosa* and *Picea glauca*	Conifers	Specrad	3f	Net CO_2 uptake
								3b	EPS
								3a	ΔF/Fm’
								3e	Car/Chl
								4	ETR Z/Chl L/Chl β-carotene/Chl VAZ/Chl
36	2013	(Liu et al. [110])	Canopy	Diurnal	Maize and winter wheat	Herbaceous and crop	Spectrad	5d and 9	RUE
								5f	Net CO_2 uptake
								5c	NPQ
29	2012	(Zinnert et al. [111])	Canopy	Diurnal (Salinity stress)	*Baccharis Halimifolia* and *Myrica cerifera*	Broadleaf	Spectrad	5d and 9	RUE
								5f	Net CO_2 uptake
								5a	ΔF/Fm’
								5c	NPQ
								6	gS Water potential Total chlorides
44	2014	(Delalieux et al. [146])	Canopy	Diurnal (Water stress)	Citrus orchard	Herbaceous and crop	APEX	6	Water potential
57	2015	(Gamon et al. [76])	Canopy	Diurnal/ Seasonal	*Pinus contorta*	Conifers	SRS sensor	5b	EPS
								7c	Chl/Car
4	2010	(Mänd et al. [62])	Canopy	Diurnal	*Calluna vulgaris*, *Vaccinium myrtillus*, *Empetrum nigrum*, *Populus alba*, *Erica multiflora*, *Globularia alypum*, *Cistus monspeliensis* and *Pistacia lentiscus*	Mixture	Specrad	5a	ΔF/Fm’
								6	Fv/Fm qN
12	2010	(Wu et al. [109])	Canopy	Diurnal	Wheat	Herbaceous and crop	Specrad	5d, 9 and 10a	RUE
								5f	Net CO_2 uptake
61	2015	(Rossini et al. [147])	Canopy	Diurnal	Maize	Herbaceous and crop	Airborne	5a	ΔF/Fm’
								6	gS
28	2012	(Zarco-Tejada et al. [120])	Canopy	Diurnal (Water stress)	Orange and mandarin	Broadleaf	PlantPen SKR 1800 camera	6	gS Water potential
41	2013	(Zarco-Tejada et al. [75])	Canopy	Diurnal	Vineyard	Herbaceous and crop	Airborne	6	gS

				(Water stress)					Water potential
50	2014	(Panigada et al. [148])	Canopy	Diurnal (Water stress)	Maize and sorghum	Herbaceous and crop	AISA Eagle	5a	ΔF/Fm'
26	2012	(Stagakis et al. [126])	Canopy	Diurnal/ Seasonal (Water stress)	Orange	Broadleaf	Camera	6	Water potential
5	2010	(Naumann et al. [122])	Canopy	Seasonal	*Elaeagnus umbellata*	Broadleaf	Specrad	7a	ΔF/Fm'
42	2013	(Zarco-Tejada et al. [149])	Canopy	Seasonal	Olive orchard	Broadleaf	Airborne	7e	Net CO_2 uptake
59	2015	(Hmimina et al. [107])	Canopy	Seasonal	*Quercus robur*, *Fagus sylvatica* and *Pinus sylvestris*	Mixture	Specrad	7d, 9 and 10a	RUE
65	2015	(van Leeuwen et al. [130])	Canopy	Seasonal	Douglas-fir	Conifers	PRiAnalyze	7d and 9	RUE
6	2010	(Rossini et al. [129])	Canopy	Seasonal	Rice	Herbaceous and crop	Specrad	7d and 9	RUE
								7e and 10c	Net CO_2 uptake
39	2013	(Rossini et al. [150])	Canopy	Seasonal (Water stress)	Maize	Herbaceous and crop	Airborne	7a	ΔF/Fm' RWC Tl-Tair
1	2010	(Hilker et al. [4])	Canopy	Seasonal (Interannual)	Douglas-fir and Aspen	Broadleaf and Conifers	Specrad	7d and 9	RUE
									α_s
15	2011	(Hall et al. [151])	Canopy	Seasonal (Interannual)	Douglas-fir and Aspen	Broadleaf and Conifers	CHRIS/ PROBA		RUE
31	2013	(Cheng et al. [81])	Canopy	Seasonal (Interannual)	Corn	Herbaceous and crop	Spectrad	7d, 9 and 10b	RUE
								7e and 10c	Net CO_2 uptake
68	2015	(Wu et al. [124])	Canopy	Seasonal (Interannual)	Wheat	Herbaceous and crop	Specrad	7d, 9 and 10a	RUE
52	2014	(Stagakis et al. [60])	Leaves/ Ecosystem	Seasonal	*Phlomis fruticosa* forest	Broadleaf	Specrad CHRIS/ PROBA	3d, 8a and 9	RUE
34	2013	(Kefauver et al. [152])	Ecosystem	Ozone	*Pinus ponderosa*, *Pinus jeffreyi* and *Pinus uncinata*	Conifers	AVIRIS and CASI		O_3
56	2015	(Balzarolo et al. [153])	Ecosystem	Seasonal	grassland	Herbaceous and crop	Specrad	8a and 9	RUE
								8b	Net CO_2 uptake
24	2012	(Rossini et al. [136])	Ecosystem	Seasonal	Subalpine grassland	Herbaceous and crop	HIS	8a and 9	RUE
								8b and 10c	Net CO_2 uptake
									Chl fIPARg
9	2010	(Stagakis et al. [132])	Ecosystem	Seasonal (Interannual)	*Phlomis fruticosa* forest	Broadleaf	CHRIS/ PROBA		Chl Chl a Car Water potential
45	2014	(Guarini et al. [25])	Ecosystem	Seasonal	*Quercus cerris* forest	Broadleaf	MODIS	8a and 9	RUE

14	2011	(Goerner et al. [79])	Ecosystem	Seasonal (Interannual)	Savanna (*Combretum apiculatum*, *Sclerocarya birrea* and *Acacia nigrescens*), *Pinus ponderosa* forest, deciduous broad-leaved forest and *Quercus ilex* forest	Broadleaf and Conifers	MODIS	8a and 9	RUE
									fAPAR
20	2012	(Moreno et al. [31])	Ecosystem	Seasonal (Interannual)	Mediterranean *Pinus pinaster* forests	Conifers	MODIS	8a and 9	RUE
17	2011	(Hilker et al. [71])	Ecosystem	Seasonal (Interannual)	*Pseudotsuga Menziesii*, *Thuja plicata*, *Tsuga heterophylla*, *Quercus rubra*, *Acer rubrum*, *Betula lenta*, *Pinus strobes*, *Tsuga Canadensis*, *Pinus banksiana*, *Picea rubens*, *Picea mariana*, *Pinus banksiana*, *Eucalyptus delegatensis* and *Eucalyptus dalrympleana*	Mixture	CHRIS/ PROBA		α_s
49	2014	(Nakaji et al. [77])	Ecosystem	Seasonal (Interannual)	Dipterocarp forest (many species)	Mixture	Specrad	8a, 9 and 10b	RUE
51	2014	(Soudani et al. [123])	Ecosystem	Seasonal (Interannual)	Deciduous forest (*Quercus robur* and *Quercus petraea*) and Mediterranean evergreen forest (*Quercus ilex*)	Broadleaf	SKR 1800	8a, 9 and 10a	RUE
								8b	Net CO_2 uptake
									aPAR VPD
33	2013	(Garbulsky et al. [28])	Ecosystem	Seasonal/ Interannual	*Quercus ilex*	Broadleaf	MODIS	8a and 9	RUE
								8b	Net CO_2 uptake
									Diametric-increment

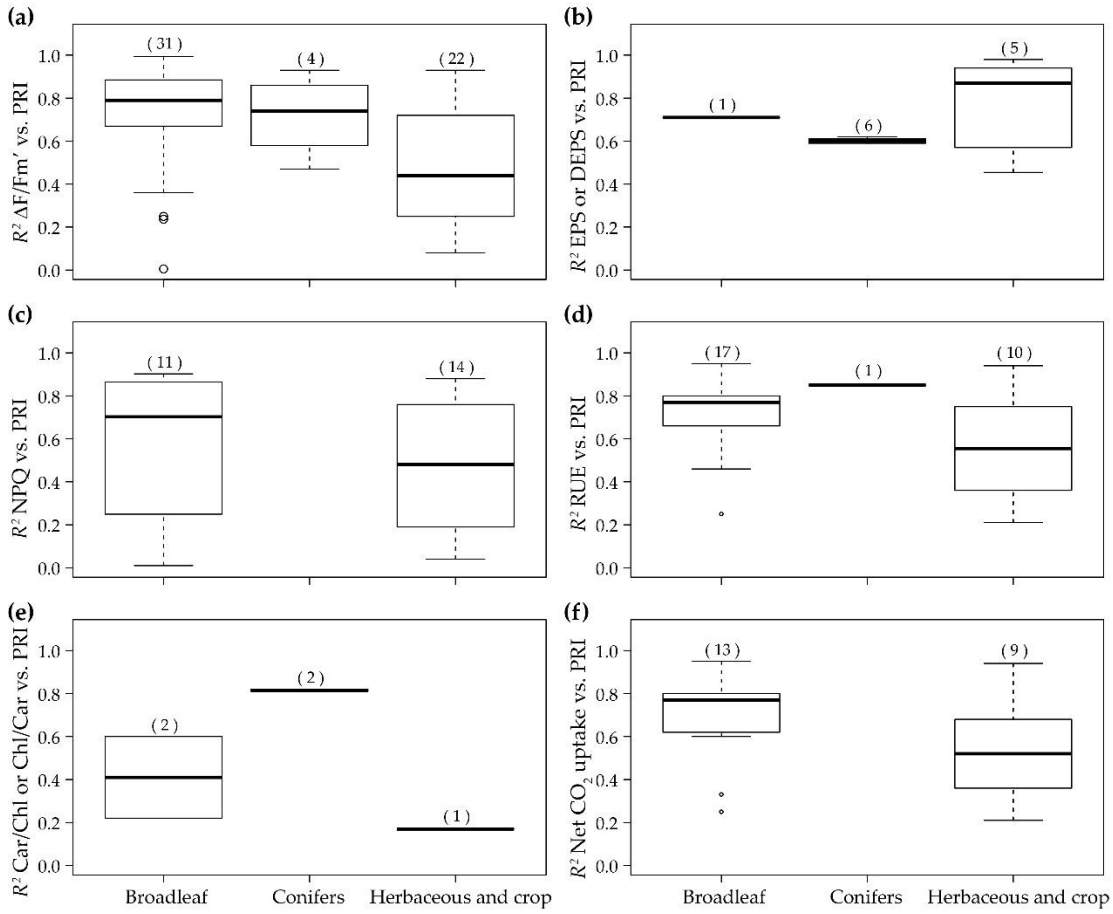

Figure 1. Boxplots of the coefficients of determination of the relationships between PRI and physiological variables at the foliar level and diurnal timescale: (**a**) Actual photochemical efficiency (ΔF/Fm'); (**b**) Epoxidation or de-epoxidation state of xanthophylls (EPS or DEPS); (**c**) Non-photochemical quenching (NPQ); (**d**) Radiation-use efficiency (RUE); (**e**) Carotenoid/chlorophyll (Car/Chl) or chlorophyll/carotenoid (Chl/Car) ratio; and (**f**) Net CO_2 uptake. Central lines represent medians, boxes represent 50% of the data, whiskers represent minima and maxima and circles represent outliers. The numbers of correlations reported in the literature are shown in brackets.

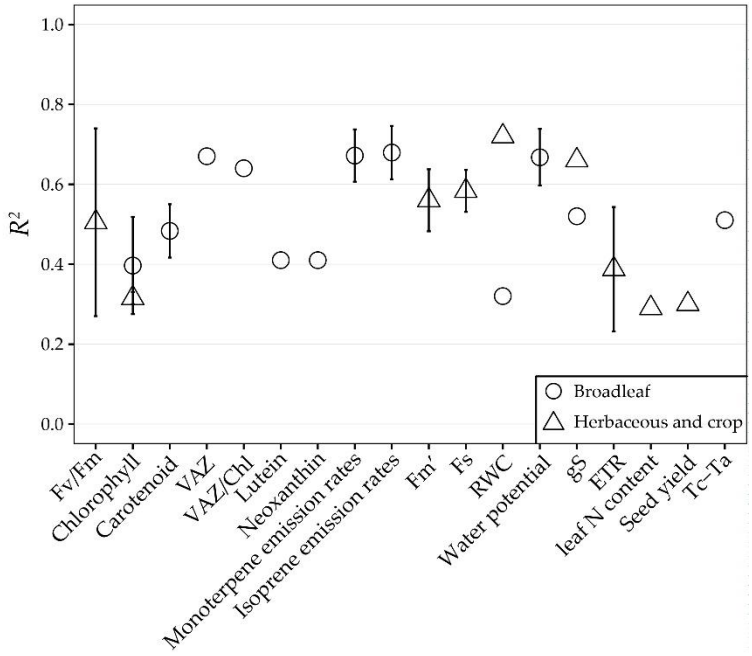

Figure 2. The mean values of coefficients of determination of the relationships between PRI and several physiological variables at the foliar level and short daily timescale. All the correlations were significant ($p < 0.05$). Error bars indicate standard error.

3.1.2. Seasonal Changes

Thirty articles published since 1992 linked PRI with ecophysiological changes at the seasonal scale (Figure 3). PRI was most often correlated with actual photochemical efficiency ΔFv/Fm' (n = 57) and explained 17%–90% of its variability (Figure 3a). Median R^2 was higher for conifers than for other species groups. PRI accounted for 0%–86% of the variability of NPQ for broadleaved and coniferous trees (Figure 3c) and was more strongly correlated with the chlorophyll/carotenoid ratio (R^2 between 0.55 and 0.89) than with EPS (or DEPS) (Figure 3b,e). The correlations between PRI and RUE and net CO_2 uptake for broadleaved species were highly variable (R^2 ranged from 0.0 to 0.84 and 0.0 to 0.92, respectively; Figure 3d,f), but median R^2 was 0.12 and 0.19 higher, respectively, than those reported by Garbulsky et al. [20].

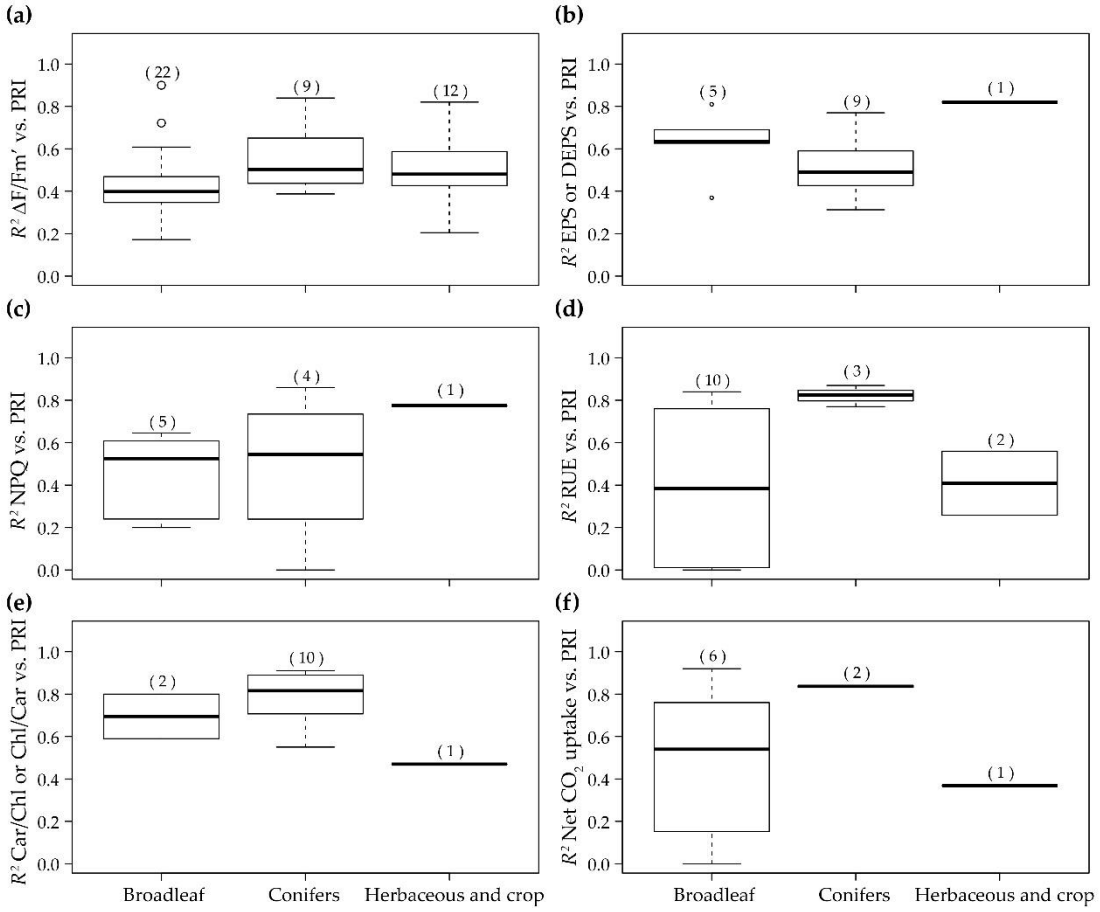

Figure 3. Boxplots of the coefficients of determination of the relationships between PRI and physiological variables at the foliar level and seasonal timescale: (**a**) Actual photochemical efficiency (ΔF/Fm'); (**b**) Epoxidation or de-epoxidation state of xanthophylls (EPS or DEPS); (**c**) Non-photochemical quenching (NPQ); (**d**) Radiation-use efficiency (RUE); (**e**) Carotenoid/chlorophyll (Car/Chl) or chlorophyll/carotenoid (Chl/Car) ratio; and (**f**) Net CO_2 uptake. Central lines represent medians, boxes represent 50% of the data, whiskers represent minima and maxima and circles represent outliers. The numbers of correlations reported in the literature are shown in brackets.

PRI was significantly correlated with other pigments or pigment ratios (e.g., chlorophyll, xanthophyll-cycle pigment pools: chlorophyll (VAZ/Chl) and lutein/chlorophyll; mean R^2 between 0.40 and 0.86; Figure 4). PRI was significantly correlated with Fv/Fm, RWC and the electron transport rate (ETR), and predawn PRI decreased with the minimum temperature and explained 55% of the variability for mango leaves [87].

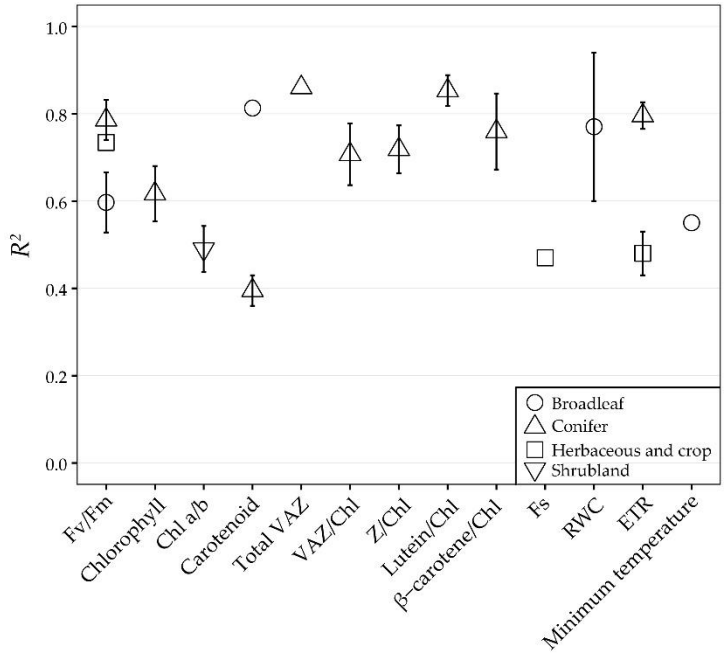

Figure 4. The mean values of coefficients of determination of the relationships between several physiological variables and PRI at the foliar level and seasonal timescale. All the correlations were significant ($p < 0.05$). Error bars indicate standard error.

3.2. Canopy Level

3.2.1. Diurnal Changes

Only 12 articles in the last two decades reported canopy PRI for tracking ecophysiological changes at short daily timescales. Ten studies published after 2010 illustrated the increasing applicability of PRI at the canopy scale. The correlations between PRI and ecophysiological variables were lower at the canopy than the foliar level. PRI explained 44%–74% of the variability of the actual quantum yield for broadleaved and herbaceous/crop plants but accounted for only 1%–40% of the variability of ΔFv/Fm' for mixed forests (Figure 5a). PRI also explained 23% and 38% of the variability of RUE for two broadleaved species under salinity stress (Figure 5d) [111]. Median R^2 between PRI and RUE and net CO_2 was as high as 0.66 and 0.63, respectively, for herbaceous/crop species (Figure 5d,f). One article reported an R^2 between PRI and the chlorophyll/carotenoid ratio of 0.65 in *Pinus sylvestris* (Figure 5e) [117]. Two articles reported that PRI correlated well with NPQ, with a median R^2 of

0.73 (Figure 5c). Three other articles reported slightly variable relationships between PRI and EPS for conifers (Figure 5b).

Changes in PRI were significantly correlated with pigment contents, similar to the correlation at the foliar level (Figure 6). PRI was strongly correlated with Fv/Fm and non-photochemical quenching (qN) for shrubland at three sites in northern Europe but not for shrubland at southern sites due to the dominance of soil reflectance [62]. PRI explained a mean of 21%–46% and 21%–56% of the variability of water potential and stomatal conductance, respectively. The change in PPFD explained 86% of the change in diurnal PRI patterns for conifers [84], which demonstrated a strong effect of illumination on diurnal PRI patterns.

3.2.2. Seasonal Changes

Only a few studies reported correlations between PRI and ΔFv/Fm' (n = 2), EPS (n = 1) and the chlorophyll/carotenoid ratio (n = 1) at long-term (seasonal to inter-annual) timescales, with R^2 between 0.44 and 0.78 (Figure 7a–c). Twenty-four articles, however, linked seasonal or inter-annual changes in PRI with RUE at individual-plant to stand levels. Median R^2 (0.79 and 0.65, respectively; Figure 7d) was 7.0% and 4.0% higher for broadleaved and coniferous trees, respectively, than those (R^2 =0 .72 and 0.61, respectively) in Figure 5 in Garbulsky et al. [20]. PRI accounted for 66% of the variability of RUE over an entire growing season for a mixed forest [107]. Four articles published after 2010 illustrated that PRI was strongly correlated with changes in net CO_2 uptake for broadleaved (R^2 = 0.59 and 0.75) and herbaceous/crop (R^2 = 0.54 and 0.81) plants (Figure 7e).

Some studies also analyzed the correlations of PRI with water content (RWC, R^2 = 0.64) [150] and stomatal conductance (gS, R^2 = 0.46) [125]. One study reported that PRI varied with the difference between foliar and air temperature for maize (R^2 = 0.82) [150]. Another study illustrated that PRI obtained from a multi-angular spectroradiometer varied with the change in the fraction of the canopy shadow (α_s) [4] under constant RUE (0.45 g CMJ^{-1}) for Douglas fir (R^2 = 0.45) and Aspen (R^2 = 0.83).

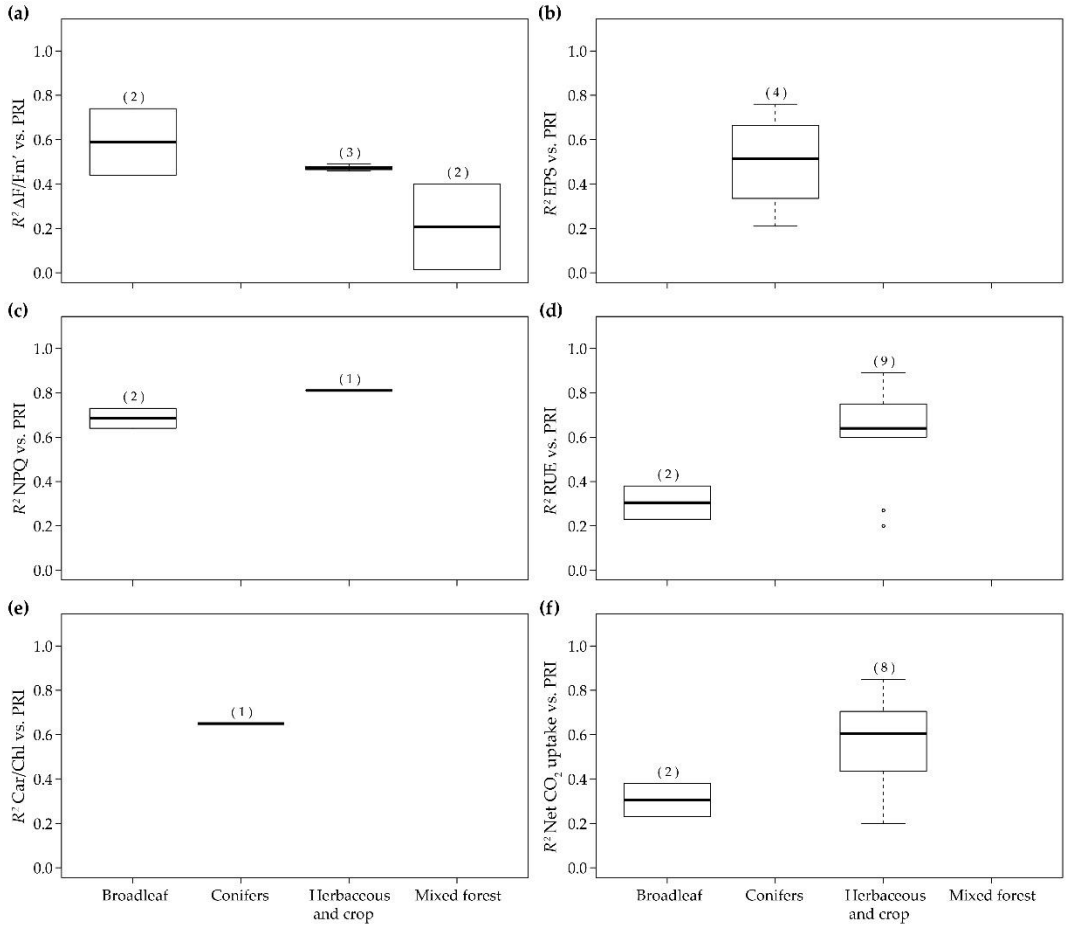

Figure 5. Boxplots of the coefficients of determination of the relationships between PRI and the physiological variables at the canopy level and diurnal timescale: (**a**) Actual photochemical efficiency (ΔF/Fm'); (**b**) Epoxidation state of xanthophylls (EPS); (**c**) Non-photochemical quenching (NPQ); (**d**) Radiation-use efficiency (RUE); (**e**) Carotenoid/chlorophyll (Car/Chl); and (**f**) Net CO_2 uptake. Central lines represent medians, boxes represent 50% of the data, whiskers represent minima and maxima and circles represent outliers. The numbers of correlations reported in the literature are shown in brackets.

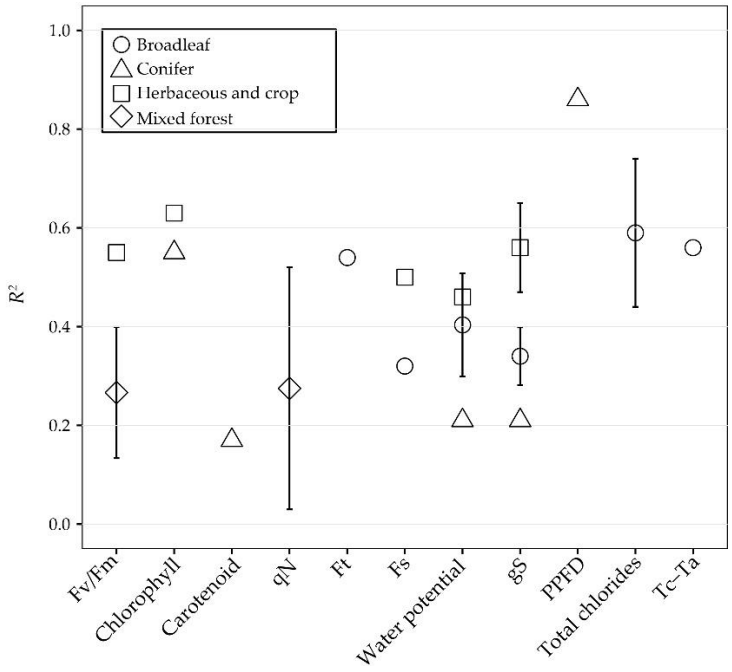

Figure 6. The mean values of coefficients of determination of the relationships between PRI and several physiological variables at the canopy level and short daily timescale. All the correlations were significant ($p < 0.05$) except for one relationship between PRI and carotenoid in *Pinus sylvestris* [117] and one between PRI and steady-state chlorophyll fluorescence (Ft) [73]. Error bars indicate standard error.

3.3. Ecosystemic Level

PRI obtained from MODIS using different reference bands was generally used for estimating ecosystemic RUE and GPP [20]. Tower or tripod-mounted spectroradiometers were also used to study ecosystemic carbon uptake at long timescales [77,123]. Forty relationships in 14 articles linked PRI with RUE based on eddy covariance in various kinds of ecosystems (e.g., Mediterranean forests, temperate deciduous forests, mountain grassland, evergreen tropical rainforest and boreal and coniferous forests; Table 1). Median R^2 for the correlations between RUE and PRI ranged from 0.12 to 0.59 (Figure 8a), with few non-significant relationships during severe drought years [25]. The correlation between PRI and RUE ($R^2 = 0.12$, $p < 0.001$) for a tropical evergreen forest [77] was lower than that for broadleaf (0.59 of median R^2) and coniferous forests (0.39 of median R^2), indicating a site-specific difference for the PRI-RUE relationships. PRI was significantly correlated with net CO_2 uptake for

Mediterranean forests (R^2 was 0.28 [123] and 0.38 [28]; Figure 8b) and grassland ecosystems (R^2 ranged between 0.13 and 0.81 [136,153]; Figure 8b).

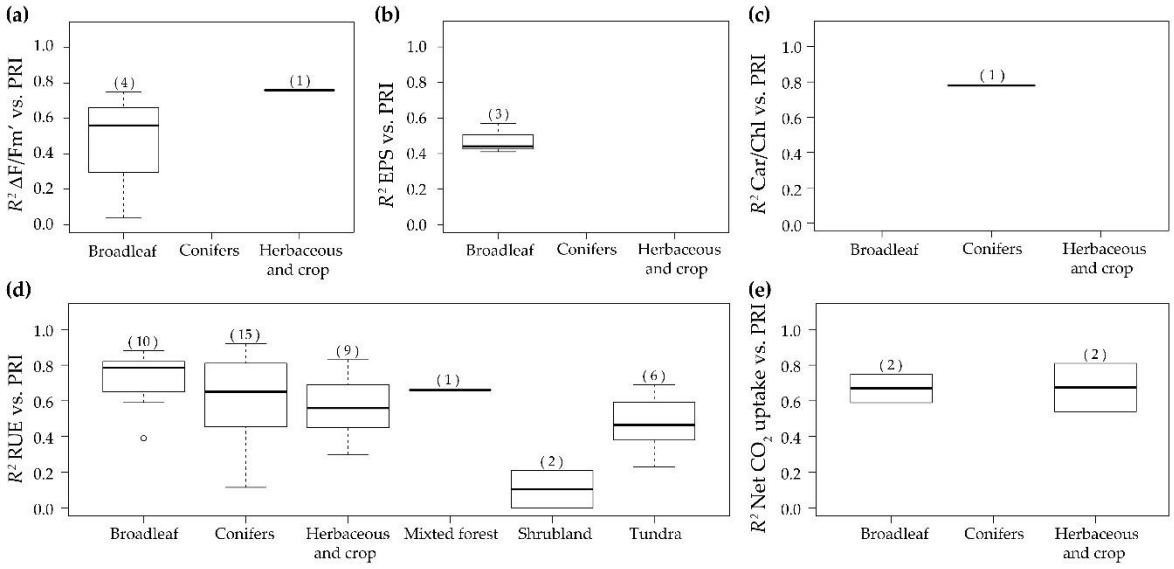

Figure 7. Boxplots of the coefficients of determination of the relationships between PRI and physiological variables at the canopy level and seasonal timescale: (**a**) Actual photochemical efficiency (ΔF/Fm'); (**b**) Epoxidation state of xanthophylls (EPS); (**c**) Carotenoid/chlorophyll ratio (Car/Chl); (**d**) Radiation-use efficiency (RUE); and (**e**) Net CO_2 uptake. Central lines represent medians, boxes represent 50% of the data, whiskers represent minima and maxima and circles represent outliers. The numbers of correlations reported in the literature are shown in brackets.

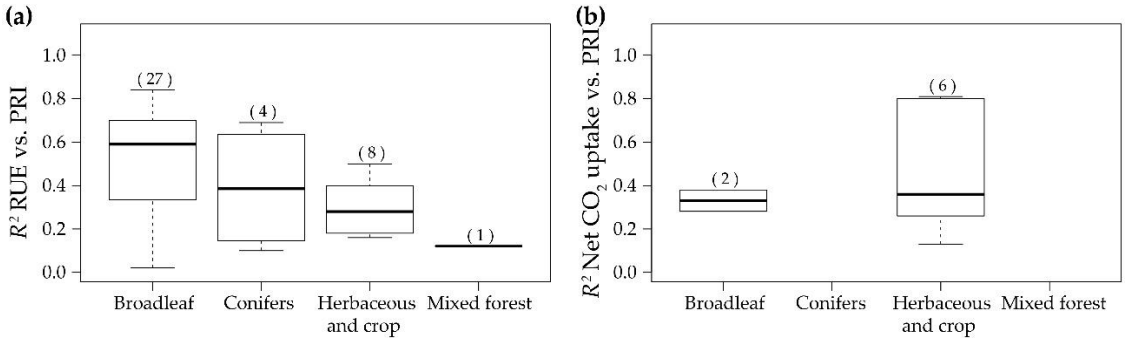

Figure 8. Boxplots of the coefficients of determination of the relationships between PRI and (**a**) Radiation-use efficiency (RUE) and (**b**) Net CO_2 uptake at the ecosystemic level and seasonal timescale. Central lines represent medians, boxes represent 50% of the data and whiskers represent minima and maxima. The numbers of correlations reported in the literature are shown in brackets.

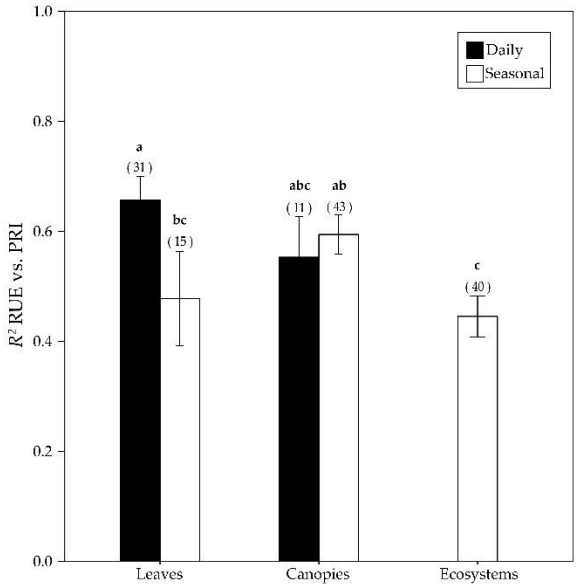

Figure 9. Comparison of the strength of the relationships between PRI and RUE across temporal and spatial scales. Each bar represents the average coefficient of determination for each source of temporal variation (daily or seasonal) and spatial scales (leaf, canopy and ecosystem). Different letters indicate significant differences ($p < 0.05$). Error bars represent the standard errors, and the numbers of reported correlations are shown in brackets.

3.4. RUE-PRI Relationships Across Scales

We calculated the mean R^2 between RUE and PRI at short daily and long seasonal scales from foliar to ecosystemic levels (Figure 9). All correlations were strong across spatiotemporal scales, with the mean R^2 ranging between 0.45 and 0.66. Mean R^2 values at daily timescales were similar to those in Figure 10 in Garbusky et al. [20] at foliar and canopy levels. The mean R^2 values at seasonal scales, however, were 20% and 7% higher for foliar and canopy levels, respectively, than those in Figure 10 in Garbusky et al. [20]. Also, the mean R^2 was higher for seasonal than diurnal relationships at the canopy scale. Forty relationships linked changes in RUE with PRI at the ecosystemic level, which was the second largest number of relationships, with a standard error of 0.04. Thirty-four of these relationships were reported after 2010. Daily PRI was thus better correlated with RUE at the foliar than the canopy level, whereas seasonal PRI tracked the changes in RUE better at the canopy than the foliar and ecosystemic levels.

4. Improvements in PRI Implementation

As stated above, a series of factors hinder the interpretation of PRI and its capacity to detect RUE from foliar to ecosystemic levels and at different temporal scales. The minimization and avoidance of these influences on PRI variation has thus become an urgent problem given its significance in the study of global carbon fixation. Improving the accuracy of PRI interpretation and particularly its application to long-term and global carbon uptake will require: (1) employing different kinds of instruments and models, from ground-based to space-borne satellite sensors; (2) choosing reference bands for PRI calculation (Table 2) and (3) combining other parameters and generating PRI models.

4.1. Instruments

Various instruments have been used for obtaining PRI in addition to the traditional ground-based spectroradiometer. A PRI imaging system was developed using a low-cost CCD camera and band-pass filters (530 and 570 nm) to non-destructively evaluate micropropagated plantlets, and has been successfully tested in cultured plantlets and from outside the culture vessels [89,140]. An automated multi-angular spectroradiometer (AMSPEC I and II system) [4] was designed and CHRIS/PROBA was used [71,90,151,154] for instantaneously measuring the spectra of a canopy at multiple detection angles along the tracking path, and for illustrating the effect of canopy structure and detection geometry at various spatial scales. CHRIS/PROBA, however, can only provide a very limited spatial coverage, which inhibits the monitoring of multiple-angular PRI at regional and global scales [154]. A temperature-controlled spectrometric system was also designed to collect high resolution spectral data to detect the diurnal and seasonal variation of RUE and fluorescence [137]. Other instruments, such as a simple filtered photodiode (QuadPod) [155], a low-cost spectroscopic instrumentation (PRiAnalyze) [130] and an automated PRI sensor with upward- and downward-facing sensors [76], were developed to explore the environmental and physiological constraints on photosynthesis and to improve remote-sensing studies of carbon uptake.

Table 2. PRI formulations for assessing RUE or net CO_2 uptake.

	Formulation	References
Original	PRI = (R531 − R570)/(R531 + R570)	Gamon et al. [18] Peñuelas et al. [19]
Different bands	PRI586 = (R531 − R586)/(R531 + R586)	Panigada et al. [148]
	PRI515 = (R531 − R515)/(R531 + R515) PRI512 = (R531 − R512)/(R531 + R512)	Calderón et al. [101] Hernández-Clemente et al. [69,117] Rossini et al. [136,150] Stagakis et al. [126] Zarco-Tejada et al. [120]
	PRI = (R525 − R570)/(R525 + R570) PRI = (R539 − R570)/(R539 + R570) PRI = (R545 − R570)/(R545 + R570) PRI = (R532 − R701)/(R532 + R701)	Stagakis et al. [60,132] Porcar-Castell et al. [72]
	PRI551 = (R531 − R551)/(R531 + R551) PRI555 = (R531 − R555)/(R531 + R555) PRI645 = (R531 − R645)/(R531 + R645) PRI667 = (R531 − R667)/(R531 + R667)	Rossini et al. [136] (simulated MODIS bands)
	PRI = (Band11 − Band1)/(Band11 + Band1) PRI = (Band11 − Band12)/(Band11 + Band12) PRI = (Band11 − Band13)/(Band11 + Band13)	Garbulsky et al. [28] (MODIS) Guarini et al. [25] (MODIS) Moreno et al. [31] (MODIS) Sims et al. [134] (MODIS) Vicca et al. [135] (MODIS)
Different formulations	PRI600 = (R531 − R602)/(R531 + R602) PRI670 = (R531 − R668)/(R531 + R668)	Rossini et al. [150]
	ΔPRI = cPRI − PRI (cPRI is dark-state PRI)	Gamon and Berry [67]
	PRIc = PRI − PRI0	Soudani et al. [123] Hmimina et al. [86,107]
	PRIs = (PRI + 1)/2	Ainsworth et al. [115] Guarini et al. [25] Rossini et al. [129] Wu et al. [109]
	$\Delta PRI = PRI_{midday} - PRI_{pre\text{-}dawn}$	Ripullone et al. [30]
	$\Delta PRI = PRI - PRI_{Ref}$ (PRI_{Ref} is the minimum PRI near midday)	Liu et al. [110]
Combination with other indices	PRInorm = PRI/(RDVI × R700/R670)	Zarco-Tejada et al. [75]
	Chlorophyll index (NDVI, NDSI, MTCI, NDI and CI)	Garrity et al. [105] Rossini et al. [129,136] Hernández-Clemente et al. [117]
	$\Delta PRI \Delta\alpha_s^{-1}$	Hall et al. [151] Hilker et al. [4,71]
	CPRI = PRI − (0.645 × ln(mNDVI705) + 0.0688)	Rahimzadeh-Bajgiran et al. [88]
	PRI_{R1} = (R550 − R531)/(R550 − R570) PRI_{R2} = (R531 − R570)/(2R550 − R531 − R570)	Wu et al. [109]
	sPRI = 0.15 × (1 − exp (−0.5 × LAI)) − 0.2 rPRI = PRI − sPRI	Wu et al. [124]
	SIF	Cheng et al. [81] Rossini et al. [129]
	VPD	Nakaji et al. [77]
	fAPAR estimated as MTCI	Rossini et al. [136] (MODIS)
	PRIn = PRI − PRI0 sPRIn = (1 + PRIn)/2	Vicca et al. [135] (MODIS)

4.2. Modeling

Models of radiative transfer have been applied to explore the changes in PRI influenced by a variety of detection geometries, illumination conditions and canopy structures in conjunction with in situ measurements [4, 31, 69, 75, 82, 83, 109, 117, 128, 133, 151, 154]. The accuracy of the simulated PRI from ACRM (A Markov chain Analytical two-layer Canopy Reflectance Model) was affected by canopy structural change and thus led to inaccurate estimates of RUE and GPP [83]. Empirical regression models were effectively used to assess PRI and ecophysiological variation [87,109,113,124]. Devising a valid model is therefore important for accurately estimating PRI and providing a continuous assessment of GPP.

4.3. Different Formulations of PRI

The application of the xanthophyllic cycle and different reference bands has been discussed extensively for better understanding PRI (Table 2). Porcar-Castell et al. [72] used PRI calculated as (R545 − R570)/(R545 + R570), which has been associated with the rapidly conformational changes contributing to protonation in key proteins in the thylakoid membrane during reversible NPQ and has improved the correlations between NPQ and PRI, especially during early spring decoupling in conifers. A combination of a vegetation index of the xanthophyllic de-epoxidation band (531 nm) with a band associated with chlorophyllic content (701 nm from CHRIS) performed better than PRI for estimating seasonal RUE from the backscatter direction [60]. PRI515 (or PRI512) has recently been proposed to minimize the effects of canopy structure under different stresses [69,101,117,120,126] but was not significantly correlated with GPP for an olive orchard [149] and performed slightly weaker than PRI for crops under water stress [148,150]. Panigada et al. [148] reported that PRI570 and PRI586 correlated with $\Delta F/Fm'$ (R^2 = 0.49 and 0.51, respectively) for cereal crops under water stress better than other PRIs based on different reference wavelengths. Additionally, PRIs based on green reference bands at 555 and 551 nm correlated mostly with RUE, and PRIs based on reference bands at 645 and 667 nm correlated better with the leaf chlorophyllic concentration than with RUE [136].

The first derivative of PRI with respect to shadow fractions viewed by the sensor ($\Delta PRI\Delta\alpha_s^{-1}$ or PRI') was developed to alleviate the impacts of vegetation structure and radiometric properties on the basis of a multi-angular observation algorithm, which has been used to infer RUE across different biomes [4,71,151,154]. The proposed PRI' technique, however, was probably not applicable to infer RUE for canopies with reduced variability in shadow fractions as noted by Hilker et al. [71]. Gamon and Berry [67] showed that a combination of dark-state sampling (cPRI) and dark-to-light conversion (ΔPRI) could experimentally isolate the two (constitutive and facultative) effects on PRI in situ without extensive destructive sampling, which could help to interpret the variation in the PRI signal from remote platforms. Differences in canopy PRI (ΔPRI) from the minimum reference PRI near midday [110] were similarly applied and improved the correlations between RUE and PRI (R^2 = 0.24 for PRI and 0.5 for ΔPRI). Differences in foliar PRI (ΔPRI, dawn PRI minus midday PRI) [30] improved the correlation with the maximum photosynthetic rate (R^2 = 0.21 for PRI and 0.44 for ΔPRI). Some studies also reported the use of scaled PRI (sPRI = (PRI + 1)/2) to avoid negative values and for comparable analysis [25,115,129,135].

A corrected PRI (PRIc = PRI − PRI0), after subtracting an estimated PRI0 defined as PRI of perfectly dark-adapted leaves, correlated well with RUE at diurnal [86], seasonal [86,123] and inter-annual scales [123]. This approach considered the impacts of changes in canopy structure and pigments, which greatly improved the correlations between PRI and RUE (Figure 10a) with a increment of R^2 by 71% and 92% at the foliar level in oak and beech, respectively [86], and by 22% for a deciduous broadleaved forest [123]. The correlation between PRI and RUE, however, was not improved by correcting with PRI0 for an evergreen forest, because PRI0 varied little across the season [123]. Hmimina et al. [107] developed an accurate deconvolution model for further improving PRI0 and PRIc to identify the influences of pigment and physiological changes on PRI variation and improved the correlation with RUE from an exponential correlation of 0.66 to a highly significant linear correlation of 0.93. Vicca et al. [135] similarly applied PRIc (method from Soudani et al. [123]) using MODIS data, successfully removed the impact of pigment and illumination and detected the severe drought and GPP variation for a deciduous broadleaved forest that was not detected by EVI. Wu et al. [109] also revised PRI by introducing the optical signal of chlorophyllic content at 550 nm to decrease the effect of the sizes of pigment

pools; two revised indices, PRI_{R1} = (R550 − R531)/(R550 − R570) and PRI_{R2} = (R531 − R570)/(2R550 − R531 − R570), correlated better with RUE, particularly during senescence when chlorophyllic content and LAI were low (R^2 = 0.57 and 0.59 for PRI_{R1} and PRI_{R2}, respectively; R^2 = 0.20 for PRI). The residual PRI (rPRI = PRI − sPRI), which removed the structural-related signal in PRI (sPRI) as a function of LAI, increased by 42% the correlation in the estimation of RUE over PRI [124]. In other studies, the calibrated PRI (CPRI = PRI – (0.645 × ln(mNDVI705) + 0.0688)) adjusted the effects of the pigments and improved the correlation between PRI and NPQ [88]. PRI calculated as PRInorm = PRI/(RDVI × R700/R670) (RDVI, Renormalized Difference Vegetation Index [156]) which normalizes for decreases in chlorophyllic content and canopy leaf area induced by stress was better correlated with stomatal conductance, water potential and pigment content and detected water stress better than the standard PRI [75].

4.4. Combining with Other Parameters to Evaluate Carbon Fixation

Combining PRI with other vegetation indices (VIs) was a promising approach in the review by Garbulsky et al. [20] to improve the detection of carbon uptake. The conventional and widely used RUE model expresses GPP as the product of APAR and RUE. PRI is a proxy of RUE, so some VIs (e.g., normalized difference spectral indices (NDSI), NDVI, the MERIS terrestrial chlorophyll index (MTCI) and EVI) correlate well with the fraction of APAR (fAPAR) [10,14–17,20,24,129,136]. GPP can thus be efficiently assessed with the combination of MODIS VIs and PRI, and the correlations were 22%–77% higher than with PRI (Figure 10c) [136]. Estimation of seasonal GPP based on MTCI-related fAPAR and PRI-related RUE (PRI551, MODIS band 4 as the reference band) modeled a subalpine grassland best (R^2 = 0.90) [136].

SIF, another photoprotective mechanism successfully sensed from space, is also an indicator of vegetation function and is used for carbon modeling [157,158]. The combination of SIF with PRI is strongly correlated with RUE and GPP for crops (Figure 10b,c). Combining PRI and SIF in a linear regression model improved GPP estimation for a cornfield (R^2 = 0.8 for SIF at red band and 0.78 for SIF at far-red band, Figure 10c) [81]. Gross ecosystemic productivity (GEP) for a rice crop was best estimated based on APAR as a function of steady-state SIF computed at 760 nm (SIF(far-red))

and on RUE as a function of sPRI (Figure 10c) [129], which was the first study that modeled seasonal courses of GEP based on measurements of remotely sensing fluorescence. Nakaji et al. [77] demonstrated that the accuracy of estimating RUE (Figure 10b) and the estimation error were improved for an evergreen tropical rainforest by applying a regression model using PRI and VPD, probably due to the influence of the water conditions on unseasonal variation in RUE.

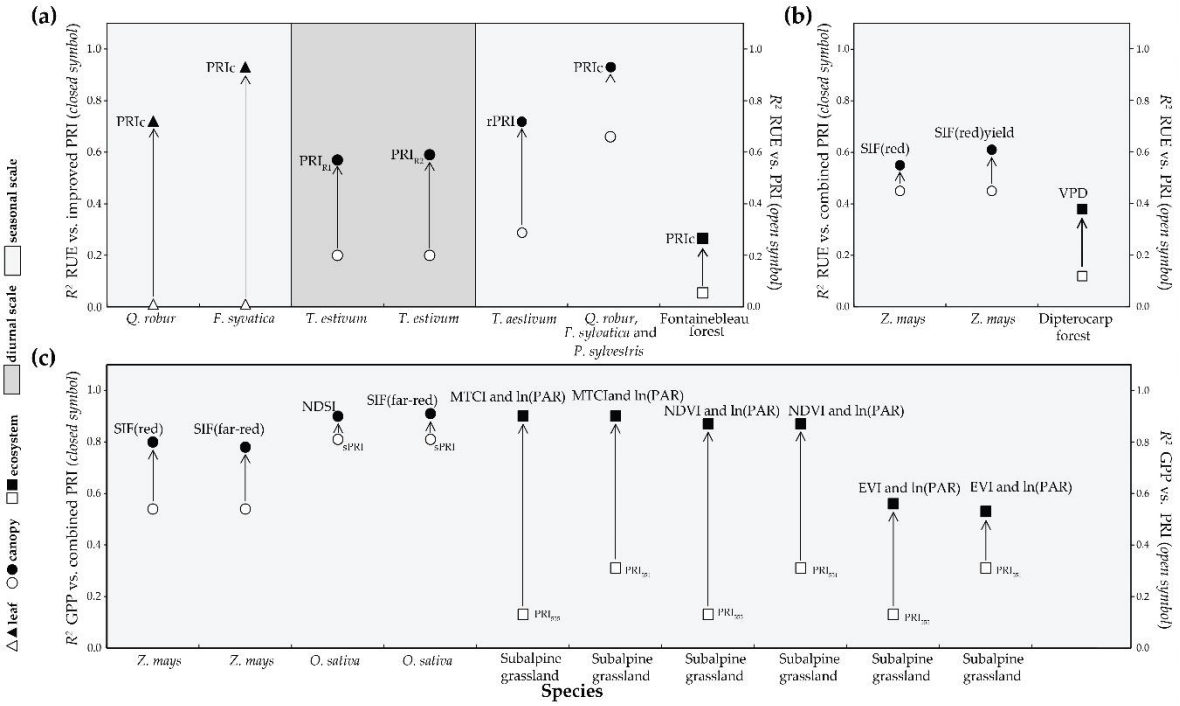

Figure 10. Comparison of the relationships between RUE/GPP vs. PRI and RUE/GPP vs. improved/combined PRI. (**a**) PRIc was used for *Q*. *robur* and *F*. *sylvatica* [86], a mixed canopy of *Q*. *robur*, *F*. *sylvatica* and *P*. *sylvestris* [107] and a deciduous broadleaved forest [123]; PRI_{R1} and PRI_{R2} were used for *T*. *aestivum* [109] and rPRI for *T*. *aestivum* (mixed non-linear model, rPRI = PRI − (0.15 × (1 − exp(−0.5 × LAI)) − 0.2)) [124]; (**b**) Tracking RUE combining PRI with SIF (red) or SIF (far-red) yield in *Z*. *mays* (RUE = a + b × PRI + c × SIF + d × PRI × SIF) [81] and with VPD in a dipterocarp forest (RUE = 0.153 × PRI − 0.00067 × VPD + 0.029) [77]; (**c**) Tracking GPP combining PRI with SIF (red) or SIF (far-red) in *Z*. *mays* (GPP = a + b × PRI + c × SIF + d × PRI × SIF) [81], with NDSI (GPP = (a0 × sPRI + a1) × (a2 × NDSI + a3) × PARi, sPRI = (1 + PRI)/2) and SIF (far-red, GPP = (a0 × sPRI + a1) × (a2 × SIF + a3), sPRI = (1 + PRI)/2) in *O*. *sativa* [129] and with VI (MTCI, NDVI and EVI) and ln(PAR) (GPP = (a0 × PRI + b0) × (a × VI + b) × ln(PAR)) [136] in a subalpine grassland.

5. Discussion

The factors affecting PRI variation at different spatiotemporal scales were reviewed in this study based on the most recent publications in which PRI has received increasing attention and on the previous publications reviewed by Garbulsky et al. [20]. Our more than 20 years' analysis shows that diurnal changes in PRI were strongly correlated with EPS at both the foliar and canopy levels (Figures 1 and 5) across more vegetation species than those reported in the first study reviewed by Garbulsky et al. [20]. Interestingly, the relationships of seasonal PRI with Chl/Car ratios were stronger than with EPS at both foliar and canopy levels for different species (Figures 1 and 3). Such results indicate the significant impacts of xanthophyll-cycle pigments on short-term changes of PRI, and chlorophyll and carotenoid pool sizes on long-term changes of PRI, in accordance with the reported studies by Wong and Gamon [54,55]. Our analysis thus further supports that taking into account the changes in chlorophyll and carotenoid pool sizes is critical for PRI interpretation on long timescales. Our summarized correlations between PRI and ecophysiological variables linked to RUE (Figures 1–8) show that PRI is a good proxy of photosynthetic efficiency at foliar, canopy and ecosystemic levels. The mean R^2 values between PRI and RUE at diurnal and seasonal scales from foliar to ecosystemic levels in this study (Figure 9) were even higher than in the first study reviewed by Garbulsky et al. [20]. Further, the significant relationships of PRI with water status (relative water content (RWC) and water potential) suggest that PRI also could be appropriate for water stress assessment.

Nevertheless, the factors complicating PRI interpretation still hinder the use of generalized PRI-RUE relationships. Our summarized review of improvements in PRI implementation found, however, that key factors driving PRI variation, such as the sizes of pigment pools and canopy structure could be minimized or avoided in part to make PRI an efficient indicator of RUE. Such improvement could be possible through subtracting the dark-adapted PRI and introducing the optical signal of pigment pools or the structural-related signal. Moreover, our analysis also showed that combining RUE-related PRI with APAR-related greenness biomass indices (e.g., NDVI, MTCI and EVI; Table 2) efficiently explores GPP (Figure 10), as expected in the previous review by Garbulsky et al. [20]. On the other hand, most reported publications focused on

broadleaf and herbaceous and crops during last two decades (Table 1), so expanding the study to a wide range of plant functional types is necessary.

The strong correlations of PRI with actual photochemical efficiency, especially with RUE and net CO_2 uptake across different plant functional types and spatiotemporal scales, indicate the possibility of assessing photosynthetic activity at larger scales. Besides, MODIS PRI has been increasingly and successfully used to assess ecosystemic RUE, allowing us to expect a PRI product in platforms such as the commonly used NDVI.

6. Conclusions and Perspectives

The mechanisms involved in PRI variation can be complex due to varying spatial and temporal scales. Many physical, biochemical and physiological factors can affect diurnal and seasonal PRI patterns at foliar, canopy and ecosystemic levels. Most of the variation of PRI when scaling up from diurnal to seasonal measurements is likely due to the changes in the size of the constitutive pigment pools other than facultative xanthophyllic de-epoxidation [54,55,67]. Other physical or external factors, such as illumination, temperature or water stress, soil background, disease and low nitrogen levels, have the potential to produce biochemical and physiological changes that can also generate PRI variation. The structural properties of canopies and the solar/spectrometric (or satellite) directions of detection at the canopy and ecosystemic levels are also important factors that contribute to changes in PRI. Our analysis, however, also indicated that PRI was often significantly correlated with ecophysiological variables and RUE. R^2 values between PRI and RUE ranged between 0.41 and 0.66 (Figure 9), even higher than in the first studies reviewed by Garbulsky et al. [20]. In particular, PRI was a good indicator of diurnal changes in RUE and a good proxy of seasonal changes in photosynthetic efficiency at different spatial scales.

Our understanding of the ecophysiological mechanisms of PRI variation and the implementation of PRI, particularly for assessing carbon uptake, have progressed. Further, other photoprotective mechanisms, for example chloroplast avoidance movement, have been proposed to have an effect on light-induced optical changes related to zeaxanthin formation [159] that probably also play a role in the PRI variation. Such influences on PRI variation should be further analyzed. The correlations between

PRI and RUE have been greatly improved by decreasing the impact of the canopy structure and the sizes of the pigment pools. These impacts can be decreased by subtracting the dark-adapted PRI to minimize the influence of the canopy structure and the pigment pools and by introducing the optical signal of the pigment pools or the structural-related signal. GPP, though, can be better assessed by combining the RUE-related PRI with APAR-related greenness indices, thus using the approach of the RUE model. Combining SIF with PRI is another promising opportunity for interpreting RUE and monitoring GPP from local to regional scales.

Studies of the optical remote sensing of RUE, especially using PRI to estimate or model RUE, have focused mainly on temperate forests and grassland, with limited studies of tropical forests. More attention should thus be paid to the assessment of RUE and GPP using PRI for different species, especially for tropical forests. We should also further explore the PRI mechanisms across vegetation types and at various spatial and temporal scales. Unmanned aerial vehicles (UAVs) with various multispectral cameras can increasingly provide an exciting opportunity to obtain canopy PRI and also SIF with high spatiotemporal resolution [74,75,149,160], which could be very beneficial for our understanding of the variation in canopy PRI. Our results indicate that corrected PRI (PRIc) proposed by Soudani et al. [123] is an outstanding improved PRI, which could be a promising proxy of RUE and is warranted to be tested over a wide range of species and spatiotemporal scales. Furthermore, PRIc was successfully obtained from MODIS and tracked the severe drought episode and GPP variation. Thus, we advocate efforts to produce a PRI product in platforms (e.g., MODIS PRI) as existing MODIS NDVI/EVI products. Additionally, PRI coupled with SIF or indices of greenness biomass is a promising approach to build an integrated and robust model of remotely sensed carbon uptake. We can attempt to combine PRI corrected or calibrated by the most influential factors (e.g., pigment pool sizes and structural changes) with SIF or other greenness indices to establish a generalized global model of carbon uptake. The satellite data from MODIS and GOME (Global Ozone Monitoring Experiment) provide potential regional and global calculations of PRI. The Sentinel program [161] of the ESA (European Space Agency), the new hyperspectral instruments built by the DLR (German Aerospace Center), such as EnMAP (Environmental Mapping and Analysis Program [162]) or DESIS (Earth Sensing Imaging Spectrometer [163]) on board the ISS (International Space Station), as well as the forthcoming missions built by NASA

(National Aeronautics and Space Administration), such as the HyspIRI (Hyperspectral Infrared Imager [164]) or the EIS (Europa Imaging System [165]) allow space-based calculation of the PRI and estimation of the RUE at a higher spatial resolution. Incorporating satellite data with over 685 eddy covariance flux sites (FLUXNET [166]) even further enhances the global continuous and accurate monitoring of carbon uptake by terrestrial ecosystems.

References

1. Beer, C.; Reichstein, M.; Tomelleri, E.; Ciais, P.; Jung, M.; Carvalhais, N.; Rödenbeck, C.; Arain, M.A.; Baldocchi, D.; Bonan, G.B.; et al. Terrestrial gross carbon dioxide uptake: Global distribution and covariation with climate. *Science* **2010**, *329*, 834–838.
2. Schimel, D.; Pavlick, R.; Fisher, J.B.; Asner, G.P.; Saatchi, S.; Townsend, P.; Miller, C.; Frankenberg, C.; Hibbard, K.; Cox, P. Observing terrestrial ecosystems and the carbon cycle from space. *Glob. Chang. Biol.* **2015**, *21*, 1762–1776.
3. Guanter, L.; Zhang, Y.; Jung, M.; Joiner, J.; Voigt, M.; Berry, J.A.; Frankenberg, C.; Huete, A.R.; Zarco-Tejada, P.; Lee, J.-E.; et al. Global and time-resolved monitoring of crop photosynthesis with chlorophyll fluorescence. *Proc. Natl. Acad. Sci. USA* **2014**, *111*, E1327–1333.
4. Hilker, T.; Hall, F.G.; Coops, N.C.; Lyapustin, A.; Wang, Y.; Nesic, Z.; Grant, N.; Black, T.A.; Wulder, M.A.; Kljun, N.; et al. Remote sensing of photosynthetic light-use efficiency across two forested biomes: Spatial scaling. *Remote Sens. Environ.* **2010**, *114*, 2863–2874.
5. Joiner, J.; Yoshida, Y.; Vasilkov, A.P.; Schaefer, K.; Jung, M.; Guanter, L.; Zhang, Y.; Garrity, S.; Middleton, E.M.; Huemmrich, K.F.; et al. The seasonal cycle of satellite chlorophyll fluorescence observations and its relationship to vegetation phenology and ecosystem atmosphere carbon exchange. *Remote Sens. Environ.* **2014**, *152*, 375–391.
6. Mäkelä, A.; Pulkkinen, M.; Kolari, P.; Lagergren, F.; Berbigier, P.; Lindroth, A.; Loustau, D.; Nikinmaa, E.; Vesala, T.; Hari, P. Developing an empirical model of stand GPP with the LUE approach: Analysis of eddy covariance data at five contrasting conifer sites in Europe. *Glob. Chang. Biol.* **2008**, *14*, 92–108.
7. Piao, S.; Sitch, S.; Ciais, P.; Friedlingstein, P.; Peylin, P.; Wang, X.; Ahlström, A.; Anav, A.; Canadell, J.G.; Cong, N.; et al. Evaluation of terrestrial carbon cycle models for their response to climate variability and to CO_2 trends. *Glob. Chang. Biol.* **2013**, *19*, 2117–2132.
8. Gamon, J.A. Reviews and syntheses: Optical sampling of the flux tower footprint. *Biogeosciences* **2015**, *12*, 4509–4523.
9. Garbulsky, M.F.; Filella, I.; Verger, A.; Peñuelas, J. Photosynthetic light use efficiency from satellite sensors: From global to Mediterranean vegetation. *Environ. Exp. Bot.* **2014**, *103*, 3–11.
10. Hilker, T.; Coops, N.C.; Wulder, M.A.; Black, T.A.; Guy, R.D. The use of remote sensing in light use efficiency based models of gross primary production: A review of current status and future requirements. *Sci. Total Environ.* **2008**, *404*, 411–423.
11. Peñuelas, J.; Garbulsky, M.F.; Filella, I. Photochemical reflectance index (PRI) and remote sensing of plant CO_2 uptake. *New Phytol.* **2011**, *191*, 596–599.
12. Monteith, J.L. Solar radition and productivity in tropical ecosystems. *J. Appl. Ecol.* **1972**, *9*, 747–766.
13. Monteith, J.L. Climate and the efficiency of crop production in Britain. *Philos. Trans. R. Soc. London B Biol. Sci.* **1977**, *281*, 277–294.
14. Balzarolo, M.; Vicca, S.; Nguy-Robertson, A.L.; Bonal, D.; Elbers, J.A.; Fu, Y.H.; Grünwald, T.; Horemans, J.A.; Papale, D.; Peñuelas, J.; et al. Matching the phenology of net ecosystem exchange and vegetation indices estimated with MODIS and FLUXNET *in-situ* observations. *Remote Sens. Environ.* **2016**, *174*, 290–300.
15. Baret, F.; Guyot, G. Potentials and limits of vegetation indices for LAI and APAR assessment. *Remote Sens. Environ.* **1991**, *35*, 161–173.
16. Rouse Jr, J.W.; Haas, R.H.; Schell, J.A.; Deering, D.W. *Monitoring Vegetation Systems in the Great Plains with ERTS*; Freden, S.C., Mercanti, E.P., Becker, M.A., Eds.; NASA: Washington, D.C., USA, 1974; Volume 1, pp. 309–317.
17. Running, S.W.; Nemani, R.R.; Heinsch, F.A.; Zhao, M.; Reeves, M.; Hashimoto, H. A continuous satellite-derived measure of global terrestrial primary production. *Bioscience* **2004**, *54*, 547–560.

18. Gamon, J.A.; Peñuelas, J.; Field, C.B. A narrow-waveband spectral index that tracks diurnal changes in photosynthetic efficiency. *Remote Sens*. *Environ*. **1992**, *44*, 35–44.
19. Peñuelas, J.; Filella, I.; Gamon, J.A. Assessment of photosynthetic radiation-use efficiency with spectral reflectance. *New Phytol*. **1995**, *131*, 291–296.
20. Garbulsky, M.F.; Peñuelas, J.; Gamon, J. A.; Inoue, Y.; Filella, I. The photochemical reflectance index (PRI) and the remote sensing of leaf, canopy and ecosystem radiation use efficiencies: A review and meta-analysis. *Remote Sens*. *Environ*. **2011**, *115*, 281–297.
21. Gamon, J.A.; Field, C.B.; Bilger, W.; Björkman, O.; Fredeen, A.L.; Peñuelas, J. Remote sensing of the xanthophyll cycle and chlorophyll fluorescence in sunflower leaves and canopies. *Oecologia* **1990**, *85*, 1–7.
22. Filella, I.; Peñuelas, J.; Llorens, L.; Estiarte, M. Reflectance assessment of seasonal and annual changes in biomass and CO_2 uptake of a Mediterranean shrubland submitted to experimental warming and drought. *Remote Sens*. *Environ*. **2004**, *90*, 308–318.
23. Filella, I.; Porcar-Castell, A.; Munné-Bosch, S.; Bäck, J.; Garbulsky, M.F.; Peñuelas, J. PRI assessment of long-term changes in carotenoids/chlorophyll ratio and short-term changes in de-epoxidation state of the xanthophyll cycle. *Int*. *J*. *Remote Sens*. **2009**, *30*, 4443–4455.
24. Coops, N.C.; Hilker, T.; Hall, F.G.; Nichol, C.J.; Drolet, G.G. Estimation of light-use efficiency of terrestrial ecosystems from space: A status report. *Bioscience* **2010**, *60*, 788–797.
25. Guarini, R.; Nichol, C.; Clement, R.; Loizzo, R.; Grace, J.; Borghetti, M. The utility of MODIS-sPRI for investigating the photosynthetic light-use efficiency in a Mediterranean deciduous forest. *Int*. *J*. *Remote Sens*. **2014**, *35*, 6157–6172.
26. Nichol, C.J.; Huemmrich, K.F.; Black, T.A.; Jarvis, P.G.; Walthall, C.L.; Grace, J.; Hall, F.G. Remote sensing of photosynthetic-light-use efficiency of boreal forest. *Agric*. *For. Meteorol*. **2000**, *101*, 131–142.
27. Peñuelas, J.; Inoue, Y. Reflectance assessment of canopy CO_2 uptake. *Int*. *J*. *Remote Sens*. **2000**, *21*, 3353–3356.
28. Garbulsky, M.F.; Peñuelas, J.; Ogaya, R.; Filella, I. Leaf and stand-level carbon uptake of a Mediterranean forest estimated using the satellite-derived reflectance indices EVI and PRI. *Int*. *J*. *Remote Sens*. **2013**, *34*, 1282–1296.
29. Garbulsky, M.F.; Peñuelas, J.; Papale, D.; Filella, I. Remote estimation of carbon dioxide uptake by a Mediterranean forest. *Glob*. *Chang*. *Biol*. **2008**, *14*, 2860–2867.
30. Ripullone, F.; Rivelli, A.R.; Baraldi, R.; Guarini, R.; Guerrieri, R.; Magnani, F.; Peñuelas, J.; Raddi, S.; Borghetti, M. Effectiveness of the photochemical reflectance index to track photosynthetic activity over a range of forest tree species and plant water statuses. *Funct*. *Plant Biol*. **2011**, *38*, 177–186.
31. Moreno, A.; Maselli, F.; Gilabert, M.A.; Chiesi, M.; Martínez, B.; Seufert, G. Assessment of MODIS imagery to track light-use efficiency in a water-limited Mediterranean pine forest. *Remote Sens*. *Environ*. **2012**, *123*, 359–367.
32. Evain, S.; Flexas, J.; Moya, I. A new instrument for passive remote sensing: 2. Measurement of leaf and canopy reflectance changes at 531 nm and their relationship with photosynthesis and chlorophyll fluorescence. *Remote Sens*. *Environ*. **2004**, *91*, 175–185.
33. Filella, I.; Amaro, T.; Araus, J.L.; Peñuelas, J. Relationship between photosynthetic radiation-use efficiency of barley canopies and the photochemical reflectance index (PRI). *Physiol*. *Plant*. **1996**, *96*, 211–216.
34. Gamon, J.A.; Serrano, L.; Surfus, J.S. The photochemical reflectance index: An optical indicator of photosynthetic radiation use efficiency across species, functional types, and nutrient levels. *Oecologia* **1997**, *112*, 492–501.
35. Guo, J.; Trotter, C.M. Estimating photosynthetic light-use efficiency using the photochemical reflectance index: Variations among species. *Funct*. *Plant Biol*. **2004**, *31*, 255–265.
36. Meroni, M.; Rossini, M.; Picchi, V.; Panigada, C.; Cogliati, S.; Nali, C.; Colombo, R. Assessing steady-state fluorescence and PRI from hyperspectral

proximal sensing as early indicators of plant stress: The case of ozone exposure. *Sensors* **2008**, *8*, 1740–1754.

37. Meroni, M.; Picchi, V.; Rossini, M.; Cogliati, S.; Panigada, C.; Nali, C.; Lorenzini, G.; Colombo, R. Leaf level early assessment of ozone injuries by passive fluorescence and photochemical reflectance index. *Int. J. Remote Sens.* **2008**, *29*, 5409–5422.
38. Middleton, E.M.; Cheng, Y.B.; Hilker, T.; Black, T.A.; Krishnan, P.; Coops, N.C.; Huemmrich, K.F. Linking foliage spectral responses to canopy-level ecosystem photosynthetic light-use efficiency at a Douglas-fir forest in Canada. *Can. J. Remote Sens.* **2009**, *35*, 166–188.
39. Nakaji, T.; Ide, R.; Takagi, K.; Kosugi, Y.; Ohkubo, S.; Nasahara, K.N.; Saigusa, N.; Oguma, H. Utility of spectral vegetation indices for estimation of light conversion efficiency in coniferous forests in Japan. *Agric. For. Meteorol.* **2008**, *148*, 776–787.
40. Peguero-Pina, J.J.; Morales, F.; Flexas, J.; Gil-Pelegrín, E.; Moya, I. Photochemistry, remotely sensed physiological reflectance index and de-epoxidation state of the xanthophyll cycle in *Quercus coccifera* under intense drought. *Oecologia* **2008**, *156*, 1–11.
41. Peñuelas, J.; Llusià, J.; Pinol, J.; Filella, I. Photochemical reflectance index and leaf photosynthetic radiation-use-efficiency assessment in Mediterranean trees. *Int. J. Remote Sens.* **1997**, *18*, 2863–2868.
42. Sims, D.A.; Gamon, J.A. Relationship between leaf pigment content and spectral reflectance across a wide range species, leaf structures and development stages. *Remote Sens. Environ.* **2002**, *81*, 337–354.
43. Sims, D.A.; Luo, H.; Hastings, S.; Oechel, W.C.; Rahman, A.F.; Gamon, J.A. Parallel adjustments in vegetation greenness and ecosystem CO_2 exchange in response to drought in a southern California chaparral ecosystem. *Remote Sens. Environ.* **2006**, *103*, 289–303.
44. Strachan, I.B.; Pattey, E.; Boisvert, J.B. Impact of nitrogen and environmental conditions on corn as detected by hyperspectral reflectance. *Remote Sens. Environ.* **2002**, *80*, 213–224.
45. Weng, J.H.; Jhaung, L.H.; Jiang, J.Y.; Lai, G.M.; Liao, T.S. Down-regulation of photosystem 2 efficiency and spectral reflectance in mango leaves under very low irradiance and varied chilling treatments. *Photosynthetica* **2006**, *44*, 248–254.
46. Weng, J.H.; Chen, Y.N.; Liao, T.S. Relationships between chlorophyll fluorescence parameters and photochemical reflectance index of tree species adapted to different temperature regimes. *Funct. Plant Biol.* **2006**, *33*, 241–246.
47. Peñuelas, J.; Filella, I.; Gamon, J.A.; Field, C.B. Assessing photosynthetic radiation-use efficiency of emergent aquatic vegetation from spectral reflectance. *Aquat. Bot.* **1997**, *58*, 307–315.
48. Lovelock, C.E.; Robinson, S.A. Surface reflectance properties of antarctic moss and their relationship to plant species, pigment composition and photosynthetic function. *Plant Cell Environ.* **2002**, *25*, 1239–1250.
49. Yamano, H.; Chen, J.; Zhang, Y.; Tamura, M. Relating photosynthesis of biological soil crusts with reflectance: Preliminary assessment based on a hydration experiment. *Int. J. Remote Sens.* **2006**, *27*, 5393–5399.
50. Van Gaalen, K.E.; Flanagan, L.B.; Peddle, D.R. Photosynthesis, chlorophyll fluorescence and spectral reflectance in *Sphagnum* moss at varying water contents. *Oecologia* **2007**, *153*, 19–28.
51. Jupa, R.; Hájek, J.; Hazdrová, J.; Barták, M. Interspecific differences in photosynthetic efficiency and spectral reflectance in two *Umbilicaria* species from Svalbard during controlled desiccation. *Czech Polar Rep.* **2012**, *40*, 31–41.
52. Louis, J.; Ounis, A.; Ducruet, J.M.; Evain, S.; Laurila, T.; Thum, T.; Aurela, M.; Wingsle, G.; Alonso, L.; Pedros, R.; et al. Remote sensing of sunlight-induced chlorophyll fluorescence and reflectance of Scots pine in the boreal forest during spring recovery. *Remote Sens. Environ.* **2005**, *96*, 37–48.
53. Nichol, C.J.; Lloyd, J.; Shibistova, O.; Arneth, A.; Röser, C.; Knohl, A.; Matsubara, S.; Grace, J. Remote sensing of photosynthetic-light-use efficiency of a Siberian boreal forest. *Tellus B* **2002**, *54*, 677–687.
54. Wong, C.Y.S.; Gamon, J.A. The photochemical reflectance index provides

an optical indicator of spring photosynthetic activation in evergreen conifers. *New Phytol*. **2015**, *206*, 196–208.

55. Wong, C.Y.S.; Gamon, J.A. Three causes of variation in the photochemical reflectance index (PRI) in evergreen conifers. *New Phytol*. **2015**, *206*, 187–195.
56. Drolet, G.G.; Huemmrich, K.F.; Hall, F.G.; Middleton, E.M.; Black, T.A.; Barr, A.G.; Margolis, H.A. A MODIS-derived photochemical reflectance index to detect inter-annual variations in the photosynthetic light-use efficiency of a boreal deciduous forest. *Remote Sens*. *Environ*. **2005**, *98*, 212–224.
57. Goerner, A.; Reichstein, M.; Rambal, S. Tracking seasonal drought effects on ecosystem light use efficiency with satellite-based PRI in a Mediterranean forest. *Remote Sens*. *Environ*. **2009**, *113*, 1101–1111.
58. Rahman, A.F.; Cordova, V.D.; Gamon, J.A.; Schmid, H.P.; Sims, D.A. Potential of MODIS ocean bands for estimating CO_2 flux from terrestrial vegetation: A novel approach. *Geophys*. *Res*. *Lett*. **2004**, *31*, 3–6.
59. Rahman, A.F.; Gamon, J.A.; Fuentes, D.A.; Roberts, D.A.; Prentiss, D. Modeling spatially distributed ecosystem flux of boreal forest using hyperspectral indices from AVIRIS imagery. *J*. *Geophys*. *Res*. **2001**, *106*, 33579–33591.
60. Stagakis, S.; Markos, N.; Sykioti, O.; Kyparissis, A. Tracking seasonal changes of leaf and canopy light use efficiency in a *Phlomis fruticosa* Mediterranean ecosystem using field measurements and multi-angular satellite hyperspectral imagery. *ISPRS J*. *Photogramm*. *Remote Sens*. **2014**, *97*, 138–151.
61. Gamon, J.A.; Field, C.B.; Goulden, M.L.; Griffin, K.L.; Hartley, A.E.; Joel, G.; Peñuelas, J.; Valentini, R. Relationships Between NDVI, canopy structure, and photosynthesis in three Californian vegetation types. *Ecol*. *Appl*. **1995**, *21*, 28–41.
62. Mänd, P.; Hallik, L.; Peñuelas, J.; Nilson, T.; Duce, P.; Emmett, B.A.; Beier, C.; Estiarte, M.; Garadnai, J.; Kalapos, T.; Schmidt, I.K.; Kovács-Láng, E.; Prieto, P.; Tietema, A.; Westerveld, J. W.; Kull, O. Responses of the reflectance indices PRI and NDVI to experimental warming and drought in European shrublands along a north-south climatic gradient. *Remote Sens*. *Environ*. **2010**, *114*, 626–636.
63. Stylinski, C.D.; Gamon, J.A.; Oechel, W.C. Seasonal patterns of reflectance indices, carotenoid pigments and photosynthesis of evergreen chaparral species. *Oecologia* **2002**, *131*, 366–374.
64. Drolet, G.G.; Middleton, E.M.; Huemmrich, K.F.; Hall, F.G.; Amiro, B.D.; Barr, A.G.; Black, T.A.; McCaughey, J.H.; Margolis, H.A. Regional mapping of gross light-use efficiency using MODIS spectral indices. *Remote Sens*. *Environ*. **2008**, *112*, 3064–3078.
65. Peñuelas, J.; Bartrons, M.; Llusià, J.; Filella, I. Sensing the energetic status of plants and ecosystems. *Trends Plant Sci*. **2015**, *20*, 528–530.
66. Song, C.; Dannenberg, M.P.; Hwang, T. Optical remote sensing of terrestrial ecosystem primary productivity. *Prog*. *Phys*. *Geogr*. **2013**, *37*, 834–854.
67. Gamon, J.A.; Berry, J.A. Facultative and constitutive pigment effects on the Photochemical Reflectance Index (PRI) in sun and shade conifer needles. *Isr. J*. *Plant Sci*. **2012**, *60*, 85–95.
68. Hall, F.G.; Hilker, T.; Coops, N.C.; Lyapustin, A.; Huemmrich, K. F.; Middleton, E.; Margolis, H.; Drolet, G.; Black, T.A. Multi-angle remote sensing of forest light use efficiency by observing PRI variation with canopy shadow fraction. *Remote Sens*. *Environ*. **2008**, *112*, 3201–3211.
69. Hernández-Clemente, R.; Navarro-Cerrillo, R.M.; Suárez, L.; Morales, F.; Zarco-Tejada, P.J. Assessing structural effects on PRI for stress detection in conifer forests. *Remote Sens*. *Environ*. **2011**, *115*, 2360–2375.
70. Hilker, T.; Lyapustin, A.; Hall, F.G.; Wang, Y.; Coops, N.C.; Drolet, G.; Black, T.A. An assessment of photosynthetic light use efficiency from space: Modeling the atmospheric and directional impacts on PRI reflectance. *Remote Sens*. *Environ*. **2009**, *113*, 2463–2475.
71. Hilker, T.; Coops, N.C.; Hall, F.G.; Nichol, C.J.; Lyapustin, A.; Black, T.A.; Wulder, M.A.; Leuning, R.; Barr, A.; Hollinger, D.Y.; et al. Inferring terrestrial photosynthetic

light use efficiency of temperate ecosystems from space. *J. Geophys. Res. Biogeosciences* **2011**, *116*, 1–11.

72. Porcar-Castell, A.; Garcia-Plazaola, J.; Ignacio; Nichol, C.J.; Kolari, P.; Olascoaga, B.; Kuusinen, N.; Fernández-Marín, B.; Pulkkinen, M.; Juurola, E.; Nikinmaa, E. Physiology of the seasonal relationship between the photochemical reflectance index and photosynthetic light use efficiency. *Oecologia* **2012**, *170*, 313–323.
73. Suáez, L.; Zarco-Tejada, P.J.; Sepulcre-Cantó, G.; Pérez-Priego, O.; Miller, J.R.; Jiménez-Muñoz, J.C.; Sobrino, J. Assessing canopy PRI for water stress detection with diurnal airborne imagery. *Remote Sens. Environ*. **2008**, *112*, 560–575.
74. Suárez, L.; Zarco-Tejada, P.J.; Berni, J.A.J.; González-Dugo, V.; Fereres, E. Modelling PRI for water stress detection using radiative transfer models. *Remote Sens. Environ*. **2009**, *113*, 730–744.
75. Zarco-Tejada, P.J.; González-Dugo, V.; Williams, L.E.; Suárez, L.; Berni, J.A.J.; Goldhamer, D.; Fereres, E. A PRI-based water stress index combining structural and chlorophyll effects: Assessment using diurnal narrow-band airborne imagery and the CWSI thermal index. *Remote Sens. Environ*. **2013**, *138*, 38–50.
76. Gamon, J.A.; Kovalchuck, O.; Wong, C.Y.S.; Harris, A.; Garrity, S.R. Monitoring seasonal and diurnal changes in photosynthetic pigments with automated PRI and NDVI sensors. *Biogeosciences* **2015**, *12*, 4149–4159.
77. Nakaji, T.; Kosugi, Y.; Takanashi, S.; Niiyama, K.; Noguchi, S.; Tani, M.; Oguma, H.; Nik, A. R.; Kassim, A.R. Estimation of light-use efficiency through a combinational use of the photochemical reflectance index and vapor pressure deficit in an evergreen tropical rainforest at Pasoh, Peninsular Malaysia. *Remote Sens. Environ*. **2014**, *150*, 82–92.
78. Guo, J.M.; Trotter, C.M. Estimating photosynthetic light‐use efficiency using the photochemical reflectance index: the effects of short‐term exposure to elevated CO_2 and low temperature. *Int. J. Remote Sens*. **2006**, *27*, 4677–4684.
79. Goerner, A.; Reichstein, M.; Tomelleri, E.; Hanan, N.; Rambal, S.; Papale, D.; Dragoni, D.; Schmullius, C. Remote sensing of ecosystem light use efficiency with MODIS-based PRI. *Biogeosciences* **2011**, *8*, 189–202.
80. Nakaji, T.; Oguma, H.; Fujinuma, Y. Seasonal changes in the relationship between photochemical reflectance index and photosynthetic light use efficiency of Japanese larch needles. *Int. J. Remote Sens*. **2006**, *27*, 493–509.
81. Cheng, Y. B.; Middleton, E.M.; Zhang, Q.; Huemmrich, K.F.; Campbell, P.K.E.; Corp, L.A.; Cook, B.D.; Kustas, W.P.; Daughtry, C.S. Integrating solar induced fluorescence and the photochemical reflectance index for estimating gross primary production in a cornfield. *Remote Sens*. **2013**, *5*, 6857–6879.
82. Cheng, Y.B.; Middleton, E.M.; Huemmrich, K.F.; Zhang, Q.; Campbell, P.K.E.; Corp, L.A.; Russ, A.L.; Kustas, W.P. Utilizing in situ directional hyperspectral measurements to validate bio-indicator simulations for a corn crop canopy. *Ecol. Inform*. **2010**, *5*, 330–338.
83. Cheng, Y.B.; Middleton, E.M.; Zhang, Q.; Corp, L.A.; Dandois, J.; Kustas, W.P. The photochemical reflectance index from directional cornfield reflectances: Observations and simulations. *Remote Sens. Environ*. **2012**, *124*, 444–453.
84. Gamon, J.A.; Bond, B. Effects of irradiance and photosynthetic downregulation on the photochemical reflectance index in Douglas-fir and ponderosa pine. *Remote Sens. Environ*. **2013**, *135*, 141–149.
85. Harris, A.; Gamon, J.A.; Pastorello, G.Z.; Wong, C.Y.S. Retrieval of the photochemical reflectance index for assessing xanthophyll cycle activity: A comparison of near-surface optical sensors. *Biogeosciences* **2014**, *11*, 6277–6292.
86. Hmimina, G.; Dufrêne, E.; Soudani, K. Relationship between photochemical reflectance index and leaf ecophysiological and biochemical parameters under two different water statuses: Towards a rapid and efficient correction method using real-time measurements. *Plant Cell Environ*. **2014**, *37*, 473–487.
87. Weng, J.H.; Jhaung, L.H.; Lin, R.J.; Chen, H.Y. Relationship between photochemical

efficiency of photosystem II and the photochemical reflectance index of mango tree: Merging data from different illuminations, seasons and leaf colors. *Tree Physiol*. **2010**, *30*, 469–478.

88. Rahimzadeh-Bajgiran, P.; Munehiro, M.; Omasa, K. Relationships between the photochemical reflectance index (PRI) and chlorophyll fluorescence parameters and plant pigment indices at different leaf growth stages. *Photosynth*. *Res*. **2012**, *113*, 261–271.
89. Ibaraki, Y.; Gupta, S.D. Nondestructive evaluation of the photosynthetic properties of micropropagated plantlets by imaging photochemical reflectance index under low light intensity. *In Vitro Cell*. *Dev*. *Biol*. *Plant* **2010**, *46*, 530–536.
90. Sarlikioti, V.; Driever, S.M.; Marcelis, L.F.M. Photochemical reflectance index as a mean of monitoring early water stress. *Ann*. *Appl*. *Biol*. **2010**, *157*, 81–89.
91. Magney, T.S.; Eusden, S.A.; Eitel, J.U.H.; Logan, B.A.; Jiang, J.; Vierling, L.A. Assessing leaf photoprotective mechanisms using terrestrial LiDAR: Towards mapping canopy photosynthetic performance in three dimensions. *New Phytol*. **2014**, *201*, 344–356.
92. Kováč, D.; Malenovský, Z.; Urban, O.; Špunda, V.; Kalina, J.; Ač, A.; Kaplan, V.; Hanuš, J. Response of green reflectance continuum removal index to the xanthophyll de-epoxidation cycle in Norway spruce needles. *J*. *Exp*. *Bot*. **2013**, *64*, 1817–1827.
93. Osório, J.; Osório, M.L.; Romano, A. Reflectance indices as nondestructive indicators of the physiological status of *Ceratonia siliqua* seedlings under varying moisture and temperature regimes. *Funct*. *Plant Biol*. **2012**, *39*, 588–597.
94. Shrestha, S.; Brueck, H.; Asch, F. Chlorophyll index, photochemical reflectance index and chlorophyll fluorescence measurements of rice leaves supplied with different N levels. *J*. *Photochem*. *Photobiol*. *B Biol*. **2012**, *113*, 7–13.
95. Su, Y.; Zhang, Z.; Su, G.; Liu, J.; Liu, C.; Shi, G. Genotypic differences in spectral and photosynthetic response of peanut to iron deficiency. *J*. *Plant Nutr.* **2015**, *38*, 145–160.
96. Rajsnerová, P.; Klem, K.; Holub, P.; Novotná, K.; Večeřová, K.; Kozáčiková, M.; Rivas-Ubach, A.; Sardans, J.; Marek, M.V.; Peñuelas, J.; Urban, O. Morphological, biochemical and physiological traits of upper and lower canopy leaves of European beech tend to converge with increasing altitude. *Tree Physiol*. **2015**, *35*, 47–60.
97. Lv, Z.; Zhang, X.; Liu, L.; Guo, Y.; Fan, Y.; Yang, X.; Li, Y.; Zhang, W. Comparing intraspecific responses of 12 winter wheat cultivars to different doses of ultraviolet-B radiation. *J*. *Photochem*. *Photobiol*. *B Biol*. **2013**, *119*, 1–8.
98. Pallozzi, E.; Fortunati, A.; Marino, G.; Loreto, F.; Agati, G.; Centritto, M. BVOC emission from *Populus* × *canadensis* saplings in response to acute UV-A radiation. *Physiol*. *Plant*. **2013**, *148*, 51–61.
99. Ashourloo, D.; Mobasheri, M.R.; Huete, A. Evaluating the effect of different wheat rust disease symptoms on vegetation indices using hyperspectral measurements. *Remote Sens*. **2014**, *6*, 5107–5123.
100. Ashourloo, D.; Mobasheri, M.R.; Huete, A. Developing two spectral disease indices for detection of wheat leaf rust (*Pucciniatriticina*). *Remote Sens*. **2014**, *6*, 4723–4740.
101. Calderón, R.; Navas-Cortés, J.A.; Lucena, C.; Zarco-Tejada, P.J. High-resolution airborne hyperspectral and thermal imagery for early detection of *Verticillium* wilt of olive using fluorescence, temperature and narrow-band spectral indices. *Remote Sens*. *Environ*. **2013**, *139*, 231–245.
102. Elena, G.; Fernàndez-Martínez, J.; Zacchini, M.; Moret, A.; Fleck, I. Susceptibility to melampsora leaf rust of poplar clones from diverse genetic backgrounds: Effects on photochemistry and water relations. *J*. *Plant Stud*. **2014**, *3*, 1–12.
103. Xue, Z.; Gao, H.; Zhao, S. Effects of cadmium on the photosynthetic activity in mature and young leaves of soybean plants. *Environ*. *Sci*. *Pollut*. *Res*. **2014**, *21*, 4656–4664.
104. Mõttus, M.; Rautiainen, M. Scaling PRI between coniferous canopy structures. *IEEE J*. *Sel*. *Top*. *Appl*. *Earth Obs*. *Remote Sens*. **2013**, *6*, 708–714.
105. Garrity, S.R.; Eitel, J.U.H.; Vierling, L.A.

Disentangling the relationships between plant pigments and the photochemical reflectance index reveals a new approach for remote estimation of carotenoid content. *Remote Sens*. *Environ*. **2011**, *115*, 628–635.
106. Cogliati, S.; Rossini, M.; Julitta, T.; Meroni, M.; Schickling, A.; Burkart, A.; Pinto, F.; Rascher, U.; Colombo, R. Continuous and long-term measurements of reflectance and sun-induced chlorophyll fluorescence by using novel automated field spectroscopy systems. *Remote Sens*. *Environ*. **2015**, *164*, 270–281.
107. Hmimina, G.; Merlier, E.; Dufrêne, E.; Soudani, K. Deconvolution of pigment and physiologically related photochemical reflectance index variability at the canopy scale over an entire growing season. *Plant Cell Environ*. **2015**, *38*, 1578–1590.
108. Damm, A.; Guanter, L.; Verhoef, W.; Schläpfer, D.; Garbari, S.; Schaepman, M.E. Impact of varying irradiance on vegetation indices and chlorophyll fluorescence derived from spectroscopy data. *Remote Sens*. *Environ*. **2015**, *156*, 202–215.
109. Wu, C.; Niu, Z.; Tang, Q.; Huang, W. Revised photochemical reflectance index (PRI) for predicting light use efficiency of wheat in a growth cycle: Validation and comparison. *Int*. *J*. *Remote Sens*. **2010**, *31*, 2911–2924.
110. Liu, L.; Zhang, Y.; Jiao, Q.; Peng, D. Assessing photosynthetic light-use efficiency using a solar-induced chlorophyll fluorescence and photochemical reflectance index. *Int*. *J*. *Remote Sens*. **2013**, *34*, 4264–4280.
111. Zinnert, J.C.; Nelson, J.D.; Hoffman, A.M. Effects of salinity on physiological responses and the photochemical reflectance index in two co-occurring coastal shrubs. *Plant Soil* **2012**, *354*, 45–55.
112. Harris, A.; Owen, S.M.; Sleep, D.; Pereira, M.D. Constitutive changes in pigment concentrations: implications for estimating isoprene emissions using the photochemical reflectance index. *Physiol*. *Plant*. **2016**, *156*, 190–200.
113. Weng, J.H.; Wong, S.L.; Lai, K.M.; Lin, R.J. Relationships between photosystem II efficiency and photochemical reflectance index under different levels of illumination: Comparison among species grown at high- and low elevations through different seasons. *Trees-Struct*. *Funct*. **2012**, *26*, 343–351.
114. Nyongesah, M.J.; Wang, Q.; Li, P. Effectiveness of photochemical reflectance index to trace vertical and seasonal chlorophyll a/b ratio in *Haloxylon ammodendron*. *Acta Physiol*. *Plant*. **2015**, *37*, doi:10.1007/s11738-014-1747-x.
115. Ainsworth, E.A.; Serbin, S.P.; Skoneczka, J.A.; Townsend, P.A. Using leaf optical properties to detect ozone effects on foliar biochemistry. *Photosynth*. *Res*. **2014**, *119*, 65–76.
116. Ghulam, A.; Fishman, J.; Maimaitiyiming, M.; Wilkins, J.L.; Maimaitijiang, M.; Welsh, J.; Bira, B.; Grzovic, M. Characterizing crop responses to background ozone in open-air agricultural field by using reflectance spectroscopy. *IEEE Geosci*. *Remote Sens*. *Lett*. **2015**, *12*, 1307–1311.
117. Hernández-Clemente, R.; Navarro-Cerrillo, R.M.; Zarco-Tejada, P.J. Carotenoid content estimation in a heterogeneous conifer forest using narrow-band indices and PROSPECT + DART simulations. *Remote Sens*. *Environ*. **2012**, *127*, 298–315.
118. Barták, M.; Trnková, K.; Hansen, E.S.; Hazdrová, J.; Skácelová, K.; Hájek, J.; Forbelská, M. Effect of dehydration on spectral reflectance and photosynthetic efficiency in *Umbilicaria arctica* and *U*. *hyperborea*. *Biol*. *Plant*. **2015**, *59*, 357–365.
119. Sun, P.; Wahbi, S.; Tsonev, T.; Haworth, M.; Liu, S.; Centritto, M. On the use of leaf spectral indices to assess water status and photosynthetic limitations in *Olea europaea* L. during water-stress and recovery. *PLoS ONE* **2014**, *9*, e105165.
120. Zarco-Tejada, P.J.; González-Dugo, V.; Berni, J.A.J. Fluorescence, temperature and narrow-band indices acquired from a UAV platform for water stress detection using a micro-hyperspectral imager and a thermal camera. *Remote Sens*. *Environ*. **2012**, *117*, 322–337.
121. Tsonev, T.; Wahbi, S.; Sun, P.; Sorrentino, G.; Centritto, M. Gas exchange, water relations and their relationships with photochemical reflectance index in *Quercus ilex* plants during water stress and recovery. *Int*. *J*. *Agric*. *Biol*. **2014**, *16*, 335–341.

122. Naumann, J.C.; Bissett, S.N.; Young, D.R.; Edwards, J.; Anderson, J.E. Diurnal patterns of photosynthesis, chlorophyll fluorescence, and PRI to evaluate water stress in the invasive species, *Elaeagnus umbellata* Thunb. *Trees-Struct. Funct.* **2010**, *24*, 237–245.
123. Soudani, K.; Hmimina, G.; Dufrêne, E.; Berveiller, D.; Delpierre, N.; Ourcival, J.M.; Rambal, S.; Joffre, R. Relationships between photochemical reflectance index and light-use efficiency in deciduous and evergreen broadleaf forests. *Remote Sens. Environ.* **2014**, *144*, 73–84.
124. Wu, C.; Huang, W.; Yang, Q.; Xie, Q. Improved estimation of light use efficiency by removal of canopy structural effect from the photochemical reflectance index (PRI). *Agric. Ecosyst. Environ.* **2015**, *199*, 333–338.
125. Marino, G.; Pallozzi, E.; Cocozza, C.; Tognetti, R.; Giovannelli, A.; Cantini, C.; Centritto, M. Assessing gas exchange, sap flow and water relations using tree canopy spectral reflectance indices in irrigated and rainfed *Olea europaea* L. *Environ. Exp. Bot.* **2014**, *99*, 43–52.
126. Stagakis, S.; González-Dugo, V.; Cid, P.; Guillén-Climent, M.L.; Zarco-Tejada, P.J. Monitoring water stress and fruit quality in an orange orchard under regulated deficit irrigation using narrow-band structural and physiological remote sensing indices. *ISPRS J. Photogramm. Remote Sens.* **2012**, *71*, 47–61.
127. Gray, S.B.; Dermody, O.; DeLucia, E.H. Spectral reflectance from a soybean canopy exposed to elevated CO_2 and O_3. *J. Exp. Bot.* **2010**, *61*, 4413–4422.
128. Suárez, L.; Zarco-Tejada, P.J.; Gonzáez-Dugo, V.; Berni, J.A.J.; Sagardoy, R.; Morales, F.; Fereres, E. Detecting water stress effects on fruit quality in orchards with time-series PRI airborne imagery. *Remote Sens. Environ.* **2010**, *114*, 286–298.
129. Rossini, M.; Meroni, M.; Migliavacca, M.; Manca, G.; Cogliati, S.; Busetto, L.; Picchi, V.; Cescatti, A.; Seufert, G.; Colombo, R. High resolution field spectroscopy measurements for estimating gross ecosystem production in a rice field. *Agric. For. Meteorol.* **2010**, *150*, 1283–1296.
130. Van Leeuwen, M.; Kremens, R. L.; van Aardt, J. Tracking diurnal variation in photosynthetic down-regulation using low cost spectroscopic instrumentation. *Sensors* **2015**, *15*, 10616–10630.
131. Middleton, E.M.; Huemmrich, K.F.; Cheng, Y.B.; Margolis, H.A. Spectral bioindicators of photosynthetic efficiency and vegetation stress. In *Hyperspectral Remote Sensing of Vegetation*; CRC Press: Boca Raton, United States, 2011; pp. 265–288.
132. Stagakis, S.; Markos, N.; Sykioti, O.; Kyparissis, A. Monitoring canopy biophysical and biochemical parameters in ecosystem scale using satellite hyperspectral imagery: An application on a *Phlomis fruticosa* Mediterranean ecosystem using multiangular CHRIS/PROBA observations. *Remote Sens. Environ.* **2010**, *114*, 977–994.
133. Galvão, L.S.; Breunig, F.M.; dos Santos, J.R.; de Moura, Y.M. View-illumination effects on hyperspectral vegetation indices in the Amazonian tropical forest. *Int. J. Appl. Earth Obs. Geoinf.* **2013**, *21*, 291–300.
134. Sims, D.A.; Rahman, A.F.; Vermote, E.F.; Jiang, Z. Seasonal and inter-annual variation in view angle effects on MODIS vegetation indices at three forest sites. *Remote Sens. Environ.* **2011**, *115*, 3112–3120.
135. Vicca, S.; Balzarolo, M.; Filella, I.; Granier, A.; Herbst, M.; Knohl, A.; Longdoz, B.; Mund, M.; Nagy, Z.; Pintér, K.; et al. Remotely-sensed detection of effects of extreme droughts on gross primary production. *Sci. Rep.* **2016**, *6*, 1–13.
136. Rossini, M.; Cogliati, S.; Meroni, M.; Migliavacca, M.; Galvagno, M.; Busetto, L.; Cremonese, E.; Julitta, T.; Siniscalco, C.; Morra Di Cella, U.; et al. Remote sensing-based estimation of gross primary production in a subalpine grassland. *Biogeosciences* **2012**, *9*, 2565–2584.
137. Drolet, G.; Wade, T.; Nichol, C.J.; MacLellan, C.; Levula, J.; Porcar-Castell, A.; Nikinmaa, E.; Vesala, T. A temperature-controlled spectrometer system for continuous and unattended measurements of canopy spectral radiance and reflectance. *Int. J. Remote Sens.* **2014**, *35*, 1769–1785.
138. Gamon, J.A.; Rahman, A.F.; Dungan, J.L.; Schildhauer, M.; Huemmrich, K.F. Spectral Network (SpecNet)—What is it and why do

we need it? *Remote Sens. Environ.* **2006**, *103*, 227–235.
139. Pacheco-Labrador, J.; Martín, M.P. Nonlinear response in a field portable spectroradiometer: Characterization and effects on output reflectance. *IEEE Trans. Geosci. Remote Sens.* **2014**, *52*, 920–928.
140. Ibaraki, Y.; Matsumura, K.; Dutta Gupta, S. Low-cost photochemical reflectance index measurements of micropropagated plantlets using image analysis. *Comput. Electron. Agric.* **2010**, *71*, 170–175.
141. Peñuelas, J.; Marino, G.; Llusià, J.; Morfopoulos, C.; Farré-Armengol, G.; Filella, I. Photochemical reflectance index as an indirect estimator of foliar isoprenoid emissions at the ecosystem level. *Nat. Commun.* **2013**, *4*, 2604.
142. Stratoulias, D.; Balzter, H.; Zlinszky, A.; Tóth, V.R. Assessment of ecophysiology of lake shore reed vegetation based on chlorophyll fluorescence, field spectroscopy and hyperspectral airborne imagery. *Remote Sens. Environ.* **2015**, *157*, 72–84.
143. Sun, C.X.; Yuan, F.; Zhang, Y.L.; Cui, Z.B.; Chen, Z.H.; Chen, L.J.; Wu, Z.J. Unintended effects of genetic transformation on photosynthetic gas exchange, leaf reflectance and plant growth properties in barley (*Hordeum vulgare* L.). *Photosynthetica* **2013**, *51*, 22–32.
144. Yoshizumi, Y.; Li, M.S.; Akihiro, I. Assessment of photochemical reflectance index as a tool for evaluation of chlorophyll fluorescence parameters in cotton and peanut cultivars under water stress condition. *Agric. Sci. China* **2010**, *9*, 662–670.
145. Šebela, D.; Quiñones, C.; Olejníčková, J.; Jagadish, K.S.V. Temporal chlorophyll fluorescence signals to track changes in optical properties of maturing rice panicles exposed to high night temperature. *F. Crop. Res.* **2015**, *177*, 75–85.
146. Delalieux, S.; Zarco-tejada, P.J.; Somers, B.; Delalieux, S.; Zarco-tejada, P.J.; Tits, L.; Ángel, M.; Bello, J.; Intrigliolo, D.S.; Somers, B. Unmixing-based fusion of hyperspatial and hyperspectral airborne imagery for early detection of vegetation stress. *IEEE J. Sel. Top. Appl. Earth Obs. Remote Sens.* **2014**, *7*, 2571–2582.
147. Rossini, M.; Panigada, C.; Cilia, C.; Meroni, M.; Busetto, L.; Cogliati, S.; Amaducci, S.; Colombo, R. Discriminating irrigated and rainfed maize with diurnal fluorescence and canopy temperature airborne maps. *ISPRS Int. J. Geo-Inf.* **2015**, *4*, 626–646.
148. Panigada, C.; Rossini, M.; Meroni, M.; Cilia, C.; Busetto, L.; Amaducci, S.; Boschetti, M.; Cogliati, S.; Picchi, V.; Pinto, F.; et al. Fluorescence, PRI and canopy temperature for water stress detection in cereal crops. *Int. J. Appl. Earth Obs. Geoinf.* **2014**, *30*, 167–178.
149. Zarco-Tejada, P.J.; Morales, A.; Testi, L.; Villalobos, F.J. Spatio-temporal patterns of chlorophyll fluorescence and physiological and structural indices acquired from hyperspectral imagery as compared with carbon fluxes measured with eddy covariance. *Remote Sens. Environ.* **2013**, *133*, 102–115.
150. Rossini, M.; Fava, F.; Cogliati, S.; Meroni, M.; Marchesi, A.; Panigada, C.; Giardino, C.; Busetto, L.; Migliavacca, M.; Amaducci, S.; et al. Assessing canopy PRI from airborne imagery to map water stress in maize. *ISPRS J. Photogramm. Remote Sens.* **2013**, *86*, 168–177.
151. Hall, F.G.; Hilker, T.; Coops, N.C. PHOTOSYNSAT, photosynthesis from space: Theoretical foundations of a satellite concept and validation from tower and spaceborne data. *Remote Sens. Environ.* **2011**, *115*, 1918–1925.
152. Kefauver, S.C.; Peñuelas, J.; Ustin, S. Using topographic and remotely sensed variables to assess ozone injury to conifers in the Sierra Nevada (USA) and Catalonia (Spain). *Remote Sens. Environ.* **2013**, *139*, 138–148.
153. Balzarolo, M.; Vescovo, L.; Hammerle, A.; Gianelle, D.; Papale, D.; Wohlfahrt, G. On the relationship between ecosystem-scale hyperspectral reflectance and CO_2 exchange in European mountain grasslands. *Biogeosci. Discuss.* **2015**, *11*, 10323–10363.
154. Hilker, T.; Hall, F.G.; Tucker, C.J.; Coops, N.C.; Black, T.A.; Nichol, C.J.; Sellers, P.J.; Barr, A.; Hollinger, D.Y.; Munger, J.W. Data assimilation of photosynthetic light-use efficiency using multi-angular satellite data: II Model implementation and validation. *Remote Sens. Environ.* **2012**, *121*, 287–300.
155. Garrity, S.R.; Vierling, L.A.; Bickford, K. A

simple filtered photodiode instrument for continuous measurement of narrowband NDVI and PRI over vegetated canopies. *Agric*. *For. Meteorol*. **2010**, *150*, 489–496.
156. Roujean, J.L.; Breon, F.M. Estimating PAR absorbed by vegetation from bidirectional reflectance measurements. *Remote Sens*. *Environ*. **1995**, *51*, 375–384.
157. Meroni, M.; Rossini, M.; Guanter, L.; Alonso, L.; Rascher, U.; Colombo, R.; Moreno, J. Remote sensing of solar-induced chlorophyll fluorescence: Review of methods and applications. *Remote Sens*. *Environ*. **2009**, *113*, 2037–2051.
158. Porcar-Castell, A.; Tyystjärvi, E.; Atherton, J.; Van Der Tol, C.; Flexas, J.; Pfündel, E.E.; Moreno, J.; Frankenberg, C.; Berry, J.A. Linking chlorophyll a fluorescence to photosynthesis for remote sensing applications: Mechanisms and challenges. *J*. *Exp*. *Bot*. **2014**, *65*, 4065–4095.
159. Brugnoli, E.; Björkman, O. Chloroplast movements in leaves: influence on chlorophyll fluorescence and measurements of light-induced absorbance changes related to ΔpH and zeaxanthin formation. *Photosynth*. *Res*. **1992**, *32*, 23–35.
160. Gago, J.; Douthe, C.; Coopman, R.E.; Gallego, P.P.; Ribas-Carbo, M.; Flexas, J.; Escalona, J.; Medrano, H. UAVs challenge to assess water stress for sustainable agriculture. *Agric*. *Water Manag*. **2015**, *153*, 9–19.
161. Sentinel Online—ESA. Available online: https://sentinel.esa.int/web/sentinel/home (accessed on 23 June 2016).
162. EnMAP. Available online: www.enmap.org (accessed on 23 June 2016).
163. WMO OSCAR—Space-Based Capabilities—Instruments: DESIS. Available online: https://www.wmo-sat.info/oscar/instruments/view/1082 (accessed on 23 June 2016).
164. HyspIRI Mission Study Website. Available online: https://hyspiri.jpl.nasa.gov (accessed on 23 June 2016).
165. Turtle, E.P.; McEwen, A.S.; Collins, G.C.; Fletcher, L.; Hansen, C.J.; Hayes, A.G.; Hurford, T.A.; Kirk, R.L.; Mlinar, A.C.B.; Nimmo, F.; et al. The europa imaging system (EIS): High-resolution imaging and topography to investigate Europa's geology, ice shell, and potential for current activity. *Lunar Planet*. *Sci*. *Conf*. **2016**, *47*, 1626.
166. Fluxnet. Available online: https://fluxnet.ornl.gov (accessed on 23 June 2016).

Block II. PRI assessment of the photosynthetic dynamics of evergreen species in response to water and temperature stresses. Leaf level.

Chapter 2. Optical cues reveal the photosynthetic spring recovery in Scots pine needles

Chao Zhang, Jon Atherton, Josep Peñuelas, Iolanda Filella, Pasi Kolari, Juho Aalto, Hanna Ruhanen, Jaana Bäck and Albert Porcar-Castell

This chapter is under review in ***New Phytologist***.

Abstract

The spring recovery of photosynthesis in evergreen trees generates multiple optical cues that can be measured from a distance. A few studies have previously assessed seasonal relationships between optical signals and photosynthesis, but no study has so far considered the seasonal dynamics between leaf spectral fluorescence and photosynthesis. We conducted a high temporal resolution measurement campaign to explore the efficacy of spectral fluorescence and other optical signals in detecting photosynthetic seasonality during the spring recovery of boreal Scots pine under field conditions.

We measured both PAM and spectral chlorophyll fluorescence, photochemical reflectance (PRI), water index (WI), normalized difference vegetation index (NDVI), modified NDVI ($NDVI_{705}$), photosynthetic efficiency, water content (WC), and chlorophyll and carotenoid contents over boreal evergreen conifer needles during spring recovery .

All wavelengths of the leaf-level fluorescence spectra, from 670 to 800 nm were strongly correlated with photosynthetic seasonality. In addition, PRI and WI significantly captured the photosynthetic reactivation in Scots pine needles.

The mechanisms regulating the above relationships were different, NPQ controlled spectral fluorescence, carotenoid content regulated PRI, and the WI tracked WC. We suggest that the combination of different indices that simultaneously capture multiple physiological processes provides a robust and multi-faceted method to track photosynthesis dynamics.

Key words: spring recovery, photosynthesis, spectral fluorescence, photochemical reflectance index (PRI), water index (WI), carotenoid, seasonality

1. Introduction

The seasonality of photosynthesis plays a key role in regulating climate-vegetation-carbon cycle feedbacks (Forkel *et al*., 2016). Over the past few decades, climate change associated shifts towards earlier timing of spring recovery of photosynthesis (Peñuelas & Filella, 2001) have been detected both in continental Europe (Menzel & Fabian, 1999; Fu *et al*., 2014) and at more northerly latitudes (Buermann *et al*., 2013; Wang *et al*., 2015) which may have important consequences for the afore mentioned feedback cycle.

In boreal regions, increasing temperatures during the winter to spring transition period stimulate the intrinsic photosynthetic apparatus and trigger seasonal photosynthetic reactivation (Öquist & Huner, 2003; Ensminger *et al*., 2004, 2008; Verhoeven, 2014). However unlike deciduous trees, spring development of photosynthetic activity in evergreen vegetation, which accounts for c.16% of the whole land surface (Bartholomé & Belward, 2005), is difficult to detect at large spatial scales. Consequently quantifying the photosynthetic reactivation of boreal evergreen ecosystems during spring, and in response to ongoing climate fluctuations, remains a challenging issue for ecophysiology, climate change and global biogeochemical research.

Vegetation indices (VIs) such as normalized difference vegetation index (NDVI), have been extensively applied for detecting vegetation green biomass, and utilised to estimate photosynthetic carbon assimilation dynamics at the ecosystem, landscape and regional levels (Bannari *et al*., 1995; Huete *et al*., 2002; Buermann *et al*., 2013). These VIs generally exploit the contrast between chlorophyll absorption in the red and foliar structure scattering in the near-infrared (Tucker, 1979). However, due to the fact that the NDVI is a rather (spectrally) insensitive proxy for broadband light absorption by chlorophyll, this index is a poor indicator of photosynthetic dynamics caused by the rapid alterations taking place in the photosynthetic machinery during seasonal transition periods (Garbulsky *et al*., 2011).

An alternative VI, the photochemical reflectance index (PRI, Gamon *et al*., 1992; Peñuelas *et al*., 1995), has been shown to correlate with the rapid adjustments in photosynthetic performance across a wide range of species and scales, including boreal evergreens (Garbulsky *et al*., 2011; Porcar-Castell *et al*., 2012; Wong & Gamon, 2015a; Zhang *et al*., 2016; Ulsig *et al*., 2017). The PRI is a good indicator of the short- (Gamon

et al., 1992; Peñuelas *et al*., 1995) and long-term (Garbulsky *et al*., 2008; Nyongesah *et al*., 2016) changes of photosynthetic radiation-use efficiency (RUE), and responses to carotenoid/chlorophyll ratio (Filella *et al*., 2009; Porcar-Castell *et al*., 2012; Wong & Gamon, 2015b) and xanthophyll pigments (Gamon *et al*., 1992; Peñuelas *et al*., 1994; Filella *et al*., 2009; Porcar-Castell *et al*., 2012). It is xanthophyll pigments that participate in the thermal dissipation of excess light (a process known as non-photochemical quenching, NPQ), and also act as scavengers of reactive oxygen species (Demmig-Adams & Adams, 2006; Jahns & Holzwarth, 2012).

Temporal dynamics in the concentration of carotenoids, particularly xanthophyll pigments, are tightly coupled to photosynthetic dynamics (Demmig-Adams & Adams, 2006), especially in overwintering evergreens (Öquist & Huner, 2003; Verhoeven, 2014; Wong & Gamon, 2015a,b). Seasonal changes of pigment pool sizes also strongly influence spectral reflectance dynamics captured by PRI (Busch *et al*., 2009; Zhang *et al*., 2016), and have been recently demonstrated to be the driving factor of PRI long-term variations in evergreen conifers (Porcar-Castell *et al*., 2012; Wong & Gamon, 2015a,b). The PRI can therefore provide a potential optical window into the seasonal dynamics of photosynthesis (Garbulsky *et al*., 2011; Zhang *et al*., 2016).

In contrast to VIs, which are largely related to foliage pigment contents, the emission of chlorophyll *a* fluorescence (ChlF) is controlled both by the amount of foliar chlorophyll as well as by the instantaneous photosynthetic performance of the leaves (see review by (Porcar-Castell *et al*., 2014). ChlF is therefore a highly sensitive optical measure of photosynthetic activity and have been extensively used in plant science to study the structural, functioning and environmental regulation of the photosynthetic apparatus (Krause & Weis, 1991; Govindjee, 1995; Ensminger *et al*., 2006; Porcar-Castell *et al*., 2014). The technique is now being widely adopted by the remote sensing community via measuring passive solar-induced chlorophyll fluorescence (SIF) from towers, drones, aircraft and satellites in an attempt to obtain remote information on photosynthesis dynamics (Guanter *et al*., 2012, 2014; Zarco-Tejada *et al*., 2013; Drolet *et al*., 2014; Porcar-Castell *et al*., 2015). Despite the small contribution of the fluorescence emission to the total radiation reflected from vegetation, SIF can be measured using the Fraunhofer Line Depth technique, where fluorescence is retrieved within narrow, dark and discrete bands generated by solar or telluric absorption (Meroni *et al*., 2009).

Importantly, and in contrast to the traditional pulse-amplitude modulated (PAM) fluorescence which is registered over a broad spectral range, SIF is acquired within narrow and discrete bands and therefore the information content might differ depending on wavelengths. For example, red/far-red ChlF ratios (e.g. F_{690}/F_{735} or F_{690}/F_{740}) have been used as a non-destructive proxy to assess changes in chlorophyll content of leaves (Hák *et al*., 1990; Lichtenthaler *et al*., 1990; D'Ambrosio *et al*., 1992; Buschmann & Lichtenthaler, 1998; Buschmann, 2007), given that increasing chlorophyll contents result in enhanced reabsorption of red ChlF within the leaf relative to far-red fluorescence.

Evidence that supports the use of SIF as a remote proxy of vegetation photosynthetic dynamics is rapidly accumulating (Frankenberg *et al*., 2011; Zarco-Tejada *et al*., 2013; Guanter *et al*., 2014; Pinto *et al*., 2016; Verrelst *et al*., 2016), including the case of boreal evergreens (Walther *et al*., 2016). However the relationship between the leaf spectral properties of the fluorescence signal and photosynthesis, and the physiological processes that underline this relationship have not yet been characterized at the seasonal scale for evergreen vegetation. The intensity and spectral properties of the fluorescence emission are expected to respond to changes in pigment contents, photosystem I (PSI) and PSII stoichiometry, and the overall seasonal regulation of photosynthesis (Buschmann & Lichtenthaler, 1998; Porcar-Castell *et al*., 2014; Van Wittenberghe *et al*., 2015; Atherton *et al*., 2016). This raises the questions: are all fluorescence wavelengths equally capable of conveying the seasonal signal of the spring recovery of photosynthesis? Are there any seasonal processes interfering with these relationships at the leaf level and for a particular wavelength? The spring photosynthetic recovery is the ideal time to investigate these issues, during which the evergreen plants progress from the winter down-regulated state to the photosynthetically active summer state.

During the spring recovery, increases in water loss can occur due to the reopening of stomata, which were previously closed during winter to mitigate water deficit during freezing conditions (Tranquillini, 1982). Hence foliage water availability further affects the photosynthetic regulation of overwintering evergreen (Öquist & Huner, 2003). One of the optical indices that can quantify plant water content (WC) is the water index (WI), which is based on the near infra-red water absorption at 970 nm waveband (Peñuelas *et al*., 1993). The WI has been found to be highly correlated with WC, leaf water potential and stomatal conductance (Peñuelas *et al*., 1993, 1997; Serrano *et al*., 2010; Osório *et al*.,

2012; Marino *et al*., 2014). Since the water status affects photosynthetic capacity, recent studies have indirectly estimated photosynthesis using canopy WI in rice (Inoue *et al*., 2008) and an olive orchard (Marino *et al*., 2014). In boreal evergreens, however, the applicability of WI for assessing plant water status and the seasonality of the leaf-scale WI in conjunction to photosynthesis are poorly understood.

Seasonal changes in photosynthetic capacity of evergreen foliage typically result from the interplay of multiple and concomitant biochemical, structural and physiological adjustments operating at the photosystem, leaf and whole-plant level, such as changes in the membrane fluidity (Vogg *et al*., 1998; Los *et al*., 2013), structural rearrangement of the light harvesting antennae (Ottander *et al*., 1995; Öquist & Huner, 2003; Verhoeven, 2014), changes in the contents of photosynthetic and photoprotective pigments (Öquist & Huner, 2003; Ensminger *et al*., 2004; Porcar-Castell *et al*., 2008), or the reactivation of plant water relations (Tranquillini, 1982; Treydte *et al*., 2014; Vanhatalo *et al*., 2015). Furthermore, the relative role of each of the above processes might depend on the environmental conditions, type of stresses, or species. Assessing the performance of different optical proxies and dissecting the processes that control the relationships calls for comprehensive and high temporal resolution measurements.

The goal of this study was to characterize the optical cues of the spring recovery of photosynthesis in boreal Scots pine needles with an emphasis on spectral fluorescence. We combined long-term and *in situ* monitoring measurements with high frequency laboratory measurements to compare the seasonal relationships between NDVI, $NDVI_{705}$, PRI, WI, PAM fluorescence, spectral fluorescence, and photosynthesis; and to identify and discuss the underlying mechanisms. In particular, we investigated the information content of different fluorescence wavelengths for tracking dynamics of foliar photosynthetic seasonality.

2. Materials and methods

2.1. Study site and field sampling protocol

Measurements were conducted at SMEAR-II (Station for Measuring Forest Ecosystem-Atmosphere Relations, Hari & Kulmala, 2005), Hyytiälä Forestry Field Station of the

University of Helsinki (61°51´N, 24°17´E) at 181 m a. s. l. on southern Finland. The dominant stand is a 52-year old (in 2015) Scots pine (*Pinus sylvestris* L.).

The measurements were carried out between 24 February and 20 July 2015 in five Scots pine trees. Five top branches per tree were selected and accessed using scaffolding towers. Last cohort of needles (developed in summer 2014) were used in the study. Needles were collected before 10 AM and immediately frozen in liquid nitrogen or brought to the nearby lab for measurements. Measurements took place at variable frequency (from 2-3 days for the critical recovery period (March 3 to May 21), to 3 weeks for the reference winter (February 24) and summer periods (May 26 to July 20)). We measured a total of 30 points in time. One set of needles was used for biochemical analysis. Another set was separated into two portions and used for reflectance, maximum photochemical efficiency of PSII (F_V/F_M), spectral fluorescence (F_λ, λ is the wavelength in nanometres) and leaf water content (WC) measurements. In each sampling day we also measured the F_V/F_M under field conditions using same fluorometer with laboratory measurement. In addition, chlorophyll fluorescence (ChlF) and shoot-level photosynthetic gas exchange were continuously measured in a few of the same pine trees in towers. For a schematic of the sampling and measurement protocol see Figure 1.

2.2. Environmental and gas exchange monitoring

Air temperature (°C) (Pt100 sensor) at treetop height and photosynthetically active radiation (PAR, μmol m^{-2} s^{-1}) (Li-190SZ quantum sensor, Li-Cor Inc., Lincoln, NE, USA) above the forest were monitored at 1 min intervals from sensors placed in a tall mast. The CO_2 exchange of the shoots was measured in unshaded conditions at the top of the canopy with a dynamic chamber system (Li-840, Li-Cor Inc., Lincoln, NE, USA) that was operated automatically (see e.g. Aalto *et al*., 2014) for a detailed description of the system) and closed intermittently 30-60 times a day with a record of every 5 seconds. The chambers were opened most of the time exposing the studied shoots to the ambient conditions. The fluxes were calculated from the gas concentration change in the chambers during the first 40 s of the closure (Kolari *et al*., 2012). The shoots were debudded prior to chamber installation to prevent new growth during the study period. Only one needle age class (2014 cohort) was installed inside the chambers; after completing the measurements, the needles areas were measured. Maximum four chambers were in use simultaneously during the study period from February 24 to July 20 in 2015.

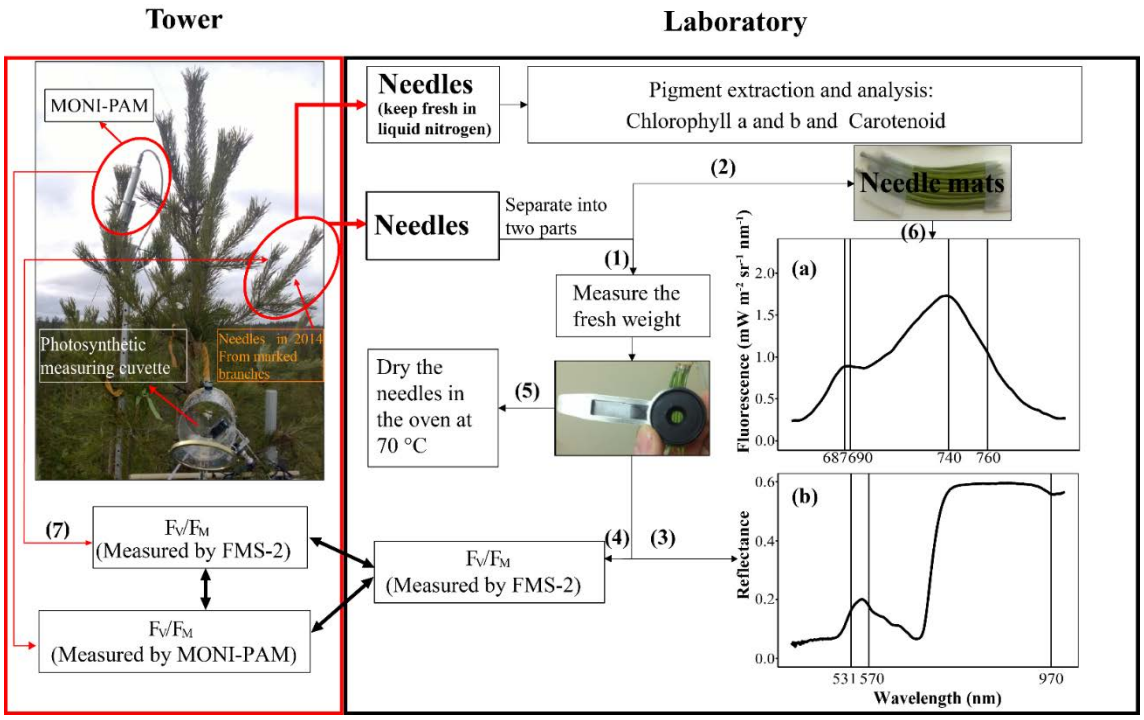

Figure 1. Scheme of the sampling protocol. One set of needles sampled from the tower was synchronously put into the liquid nitrogen container within the cryotubes to keep needles fresh and was used for further biochemical measurements. Another set was separated in two in the laboratory, one portion was immediately used to measure fresh weight for later water content estimation, followed by reflectance and dark acclimation for 1 hour prior to measurements of maximum photochemical efficiency of PSII (F_V/F_M), and then dry weight was measured. The other was used to construct a mat of needles and dark acclimated for at least 1 hour in order to measure spectral fluorescence. Before collecting needles, we also clipped the needles for dark acclimation for at least 1 h in the same branches in the tower (field) to further measure F_V/F_M under field conditions using FMS-2. Examples of the averaged fluorescence spectrum between 660 and 800 nm (a) and reflectance (b) from five trees are shown in the figure panels which were measured on May 18 in 2015. The numbers in the brackets indicate the order of measurements in time.

Two photosynthetic parameters were estimated in 3-day time window: (1) β (m s^{-1}), the photosynthetic efficiency in the optimal stomatal control model (Hari *et al*., 1986; see also Kolari *et al*., 2007). The parameter is essentially the rate of light-saturated

photosynthesis per unit inter-cellular CO_2 concentration. The model also incorporates responses of stomatal control and photosynthesis to temperature, CO_2 and vapour pressure deficit; (2) α (µmol CO_2/µmol PAR), the slope of linear function fitted to the photosynthetic light response with low incident PAR (<300 µmol m^{-2} s^{-1}) before noon (Kolari *et al*., 2014). For statistical analyses we normalized the time series of β and α for each studied shoot with the respective parameter values between May 3 and 24 when the data were available from all chambers and then rescaled using maximum summer values. The rescaled normalized β and α were later denoted P_p (the proxy of the photosynthetic efficiency) and RUE_p (the proxy of the radiation-use efficiency (RUE)) respectively.

2.3. Leaf spectral reflectance measurements

Leaf spectral reflectance was measured using a handheld VIS-NIR field spectroradiometer (FieldSpec, ASD-Panalytical, Boulder, CO). The spectroradiometer covered the spectral range between 325 and 1075 nm at a sampling interval of 1 nm and FWHM of 3.5nm (see Porcar-Castell *et al*., 2012; Olascoaga *et al*., 2014 for further details). A dark current and subsequent white reference was firstly registered using a calibrated Spectralon reference panel (Labsphere, North Sutton, NH). Integration times were 544 ms, recording time for each sample was no less than 10 s, and ten replicate spectra were recorded for each sample (five to seven needles were arranged in a tight row). The photochemical reflectance index (PRI) was calculated as (R531-R570)/(R531+R570) according to Gamon *et al*. (1992) and Peñuelas *et al*. (1995), where R indicates the reflectance and the numbers mean the wavelength in nanometres. The normalized difference vegetation index (NDVI = (R900-R680)/(R900+R680); Tucker, 1979), modified NDVI ($NDVI_{705}$ = (R750-R705)/(R750+R705); Gitelson & Merzlyak, 1994) and WI (R900/R970; Peñuelas *et al*., 1993) were also calculated.

2.4. Leaf Spectral fluorescence Measurements

Leaf F_λ (mW m^{-2} sr^{-1} nm^{-1}) was measured using a FluoWat Clip (Image Processing Laboratory, University of Valencia, Spain) coupled to the above described spectrometer (See Atherton *et al*., 2017 for further details). The fibre optic was positioned in the nadir direction 1 cm above the sample center. A white-light LED (MJ-858, Magicshine, UK) was used as light source which provided a PAR level of c. 1200 µmol at the leaf surface as estimated with a LiCor quantum sensor (Licor LI150-A, Li-Cor Inc., Lincoln, NE, USA). The incidence angle of the light beam was 45°. A Barium Sulphate Lambertian

panel (Gigahertz-Optik GmbH, Türkenfeld, Germany) approximately 1 mm thick was firstly placed in the FluoWat clip and ten reference spectra were recorded. The emitted ChlF from fully dark-acclimated needles (arranged as a needle mat see Figure 1) was excited using the LED light source, where the red to near-infrared contribution to incident light spectrum was negated with a 650 nm short-pass filter (Edmund Optics Ltd, UK). The filter had an optical depth of 4 (transmittance of 0.01%) and we neglected the transmitted component in the rejection zone. Integration times were 136 ms and 275 spectra were recorded to ensure that we reached the steady state. The last ten spectra were averaged and used to estimate steady state F_λ between 650 nm and 850 nm ($F_{650\text{-}850}$). To further reduce noise, the average $F_{650\text{-}850}$ spectrum was smoothed using a Savitzky-Golay filter (Filter order was 2 and averaging interval was 15). Two 1 nm bands around fluorescence emission peaks of red and far-red bands (F_{690} and F_{740}) and their ratio (F_{690}/F_{740}) were utilized in the analysis as proxy for red and far-red fluorescence, respectively.

2.5. PAM fluorescence measurements

F_V/F_M was measured in the field using a fluorescence monitoring PAM (pulse-amplitude modulated) system (MONI-PAM, Walz GmbH, and Germany) (Porcar-Castell *et al*., 2008; Porcar-Castell, 2011). The MONI-PAM system was composed of 5 independent PAM fluorometers installed in three of the five pine trees measured in the study. The system recorded the instantaneous fluorescence yield, the maximal fluorescence yield (F_M), incoming PAR, and temperature every 30 minutes. The MONI-PAM uses a blue LED to provide both measuring light and saturating pulses (>4000 μmol PAR of 0.8 s duration) to the needles. The parameter F_V/F_M was then calculated after Genty *et al*. (1989) using the night fluorescence (F_o) and F_M data. We also measured F_V/F_M both in the field and in the lab with a portable fluorometer (FMS-2, Hansatech Instruments Ltd., Norfolk, UK) to facilitate the intercomparison of field and lab measurements. Dark acclimation was always more than 1 hour. The Hansatech fluorometer uses an amber LED light to provide measuring light to the sample and an halogen lamp for providing the saturating pulses (>6000μmol PAR of 0.8 s duration). Note that differences in the measuring light color between Hansatech and MONI-PAM instruments mean that F_V/F_M values between instruments should not be compared in absolute units since amber light penetrates deeper into the leaf than blue light (Vogelmann, 1993; Vogelmann & Evans, 2002), yielding a

different measurement footprint.

2.6. Pigment analysis

Pigment extraction and analysis followed Wellburn (Wellburn, 1994) and dimethyl sulfoxide (DMSO; VWR Chemicals, 23500.322) were used as extractant. Between 75 to 100 mg of frozen needle samples were homogenized using bead mill (TissueLyser II Qiagen, Germany), 4 mm stainless steel beads and 2 ml microtubes for 2 minutes at 30 Hz. 1800 µl DMSO were added to homogenate and the mixture was homogenized again for 1 minute at 30 Hz. All samples were extracted in 40°C for 4 hours. Chlorophyll a and b and carotenoid content were measured by spectrophotometer (Shimadzu UV- 2401 PC) at wavelengths 480.0, 649.1 and 665.1 nm.

2.7. Leaf water content

Fresh weight (FW) of needles was measured with a precision scale immediately upon arriving to the laboratory. When the reflectance and F_V/F_M measurements were finished, the needles were dried in an oven at 70 °C for 48h before measuring dry weight (DW). WC was thus calculated as: WC = (FW-DW)/FW.

2.8. Statistical analyses

Linear regression models and simple Pearson's correlation analyses were used to assess the relationships between optical signals and photosynthetic parameters, and the relationships between PRI, F_λ and F_V/F_M, and to explore the influences of pigment parameters and water content on photosynthetic efficiency and optical signals during spring recovery period. The significance of the statistical models was tested at probability levels $p<0.05$, $p<0.01$, and $p<0.001$. We also used Principal Component Analysis (PCA) to evaluate the temporal variability and (wavelength) correlation occurring in the spectral measurements. We ran PCA separately on time series of (1) the reflectance data-set and (2) the F_λ data-set using R function 'prcomp'. Spectral data were centred and the noisy spectral ends clipped prior to the analyses. All the analyses were conducted with R version 3.2.2 (R Core Development Team, 2015) and MatLab version R2014a (MathWorks Inc. 2014).

3. Results

3.1. Seasonal patterns in environmental data and photosynthesis

Both temperature and photosynthetically active radiation (PAR) increased gradually from winter to summer (Figure 2). Daily mean temperatures in February (-1.7 °C) and March (0.6 °C) were higher by 6 and 4 °C, respectively, compared to the average for the period 1981-2010 (Pirinen *et al*., 2012). Despite the relatively mild winter we registered a cold spell on March 22 with temperatures reaching a minimum of -11.4 °C and daily mean temperature of -5.7 °C (Figure 2). The cold spell helped us investigate the responses of optical indices and photosynthesis to a sudden decrease in temperature. Both the parameter P_p, a measure of maximum photosynthetic rate, estimated from the continuous gas exchange measurements in the field, and the parameter RUE_p, a measure of maximum photosynthetic radiation-use efficiency, increased over the study period with similar seasonal patterns (Figure 3). Both parameters were rather stable at the start of the measuring campaign but rapidly decreased twice during March. The first decrease affected both P_p and RUE_p and occurred along with a sudden increase in daily noon PAR with temperatures around zero degrees. The second decrease affected predominantly P_p and took place during 23 March, one day after the drastic decrease in temperature.

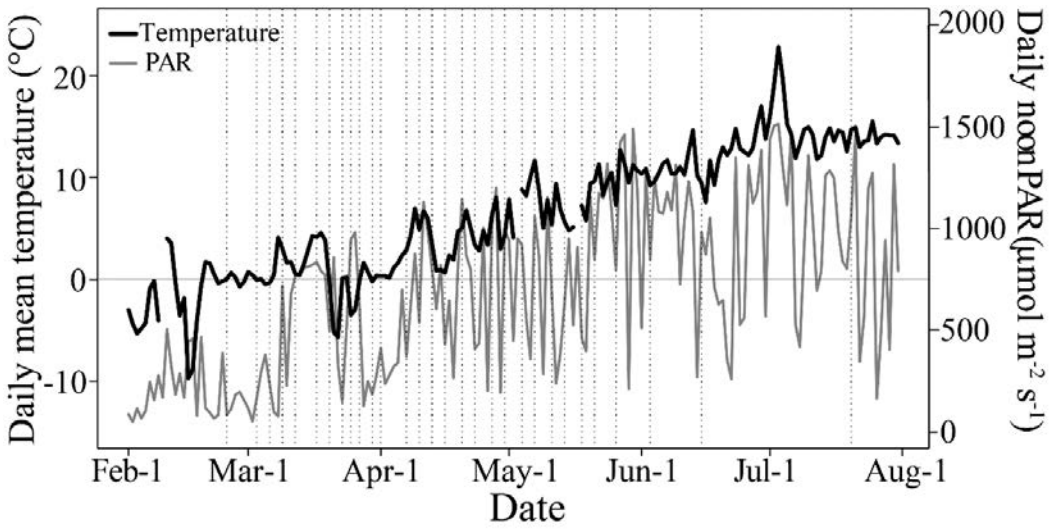

Figure 2. Seasonal variation in daily noon photosynthetically active radiation (PAR) (*grey line*) and daily mean temperature (*black line*) during the course of the campaign in 2015. Sampling dates are marked with vertical dotted lines.

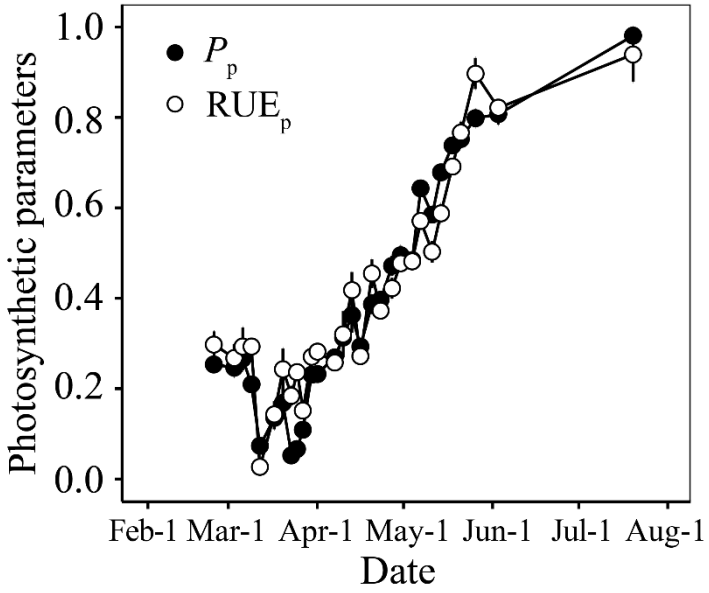

Figure 3. Seasonal variation in rescaled normalized daily photosynthetic efficiency (P_p, closed symbols) and rescaled normalized slope of linear function fitted to photosynthetic light response with low incident PAR before noon (RUE_p, open symbols) estimated from the continuous gas exchange data in the field. Points represent means of four shoots (n = 4). Error bars represent the standard error (SE, shown only when larger than symbols).

3.2. Seasonal patterns in optical indices

Leaf spectral fluorescence (F_λ) and maximum photochemical efficiency of PSII (F_V/F_M) exhibited seasonal variability coincident with temperature and photosynthesis (Figure 4a, b). Both F_{690} and F_{740} were relatively flat at the beginning of the campaign and started to gradually increase from early May (Figure 4a). The fluorescence ratio (F_{690}/F_{740}) only showed a decrease during the cold episode but exhibited no clear seasonal patterns (Figure S1). F_V/F_M trends (Figure 4b), measured either in the field or in the lab, followed the gradual increase in daily mean temperature and tracked remarkably well the development of photosynthetic capacity as expressed by P_p and RUE_p (Figure 3). All F_V/F_M decreased on March 23 one day after the cold spell. The F_V/F_M values obtained with the MONI-PAM system where consistently lower than those obtained with the Hansatech system.

Seasonal changes in the photochemical reflectance index (PRI) (Figure 4c) were consistent with photosynthesis, F_λ, and F_V/F_M (Figure 3 and Figure 4a, b). PRI values gradually increased from winter, through spring to summer, accompanied by slight increase from -0.1 to -0.04 during the period of February 24 to May 4 and an abrupt increase from -0.06 in May 4 to -0.02 in May 7. In contrast, the normalized difference

vegetation index (NDVI) and modified NDVI ($NDVI_{705}$) had no clear seasonal patterns (Figure 4d, e) but values suddenly decreased in March and April. The water index (WI) presented a gradual decreasing trend throughout the study period (Figure 4f).

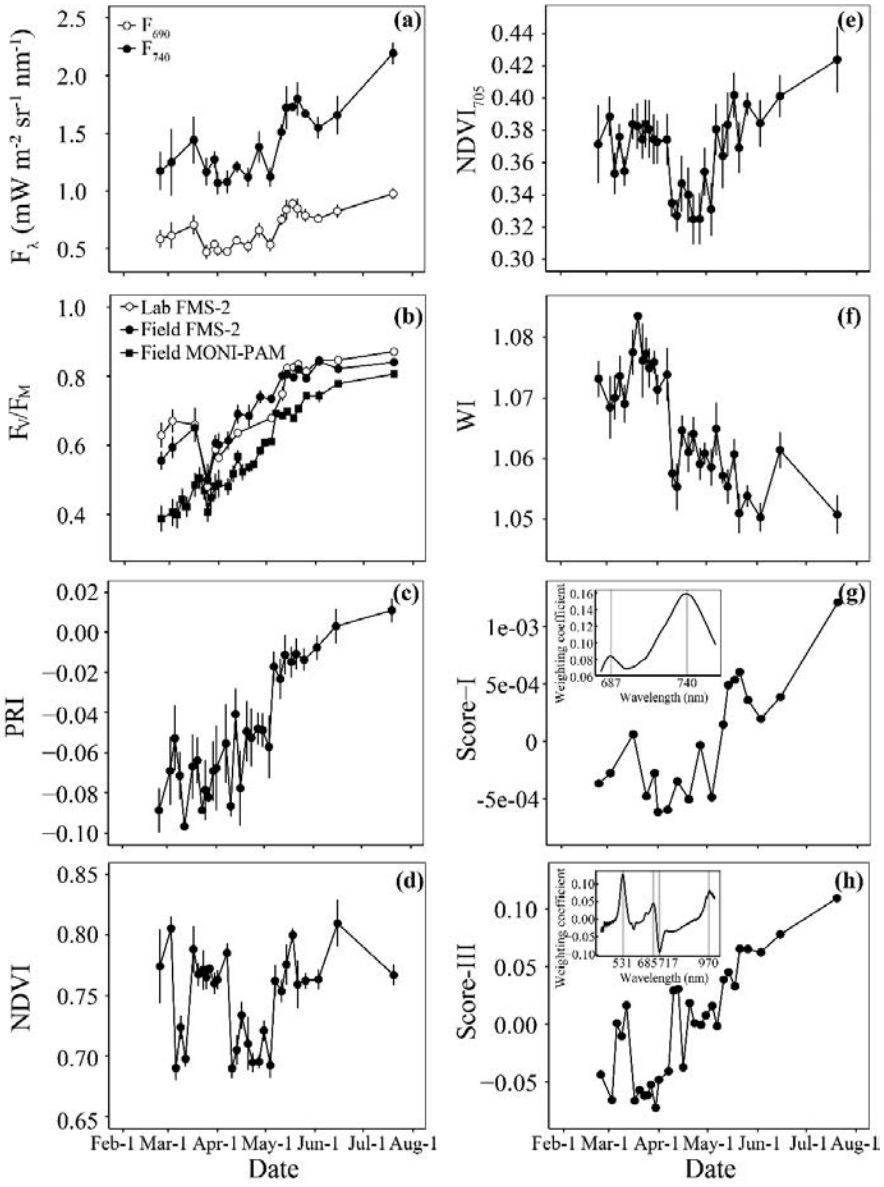

Figure 4. Seasonal variations in (a) spectral fluorescence (F_λ) at 690 and 740 nm, (b) maximum photochemical efficiency (F_V/F_M) measured in the field using MONI-PAM and in laboratory using FMS-2 of Scots pine shoots, (c) photochemical reflectance index (PRI), (d) normalized difference vegetation index (NDVI), (e) modified NDVI ($NDVI_{705}$), (f) water index (WI), and PC analysis of the spectral variance (g) in fluorescence emitting wavelength from FluoWat (680-760nm) and (h) in visible and near infrared (400-1000nm) from the Probe. Points represent means of five biological replicates (n = 5) and error bars represent the standard error (SE, shown only when larger than symbols).

The F_λ and reflectance data were also analysed using Principle Component Analysis (PCA) to detect spectral variance over the spring recovery season. In PC analysis for F_λ (Figure S2 and Figure 4g), PC-1 explained 98.9% variance of spectra, and only those scores were consistent with seasonal changes in F_{740} and F_{690}. All the fluorescence emitting bands contributed weighting coefficients from 0.065 to 0.159 to PC-1 with two peaks in red (~687 nm) and far-red (~740) wavelengths (Figure S2e and Figure 4g). In PC analysis for reflectance (Figure S3 and Figure 4h), PC-1 and PC-2 explained 87.1% and 10.5% spectral variance respectively, and PC-3 explained just 1.03% variance. However, only the scores in PC-3 (Figure S3c and Figure 4h) exhibited similar seasonal patterns to photosynthetic parameters highlighted by significant decreases in both PC-3 and P_p during March (Figure 3). The strongest wavelength contributions to PC-3 occurred at the PRI detection band (~531 nm), the red-edge band of 685 nm and 717 nm and the WI detection band (~970 nm) (Figure S3g and Figure 4h), emphasizing that this PC carried most of the physiological information content.

3.3. Relationships of optical indices with photosynthesis

Both F_{690} and F_{740}, F_V/F_M and PRI showed highly significant correlations with photosynthetic parameters across the entire study period (Figure 5 and Figure S4). Particularly, F_{690}, F_{740} and F_V/F_M explained 71-89% variation of P_p and 62-84% variation of RUE_p. The fluorescence ratio (F_{690}/F_{740}) was uncorrelated with photosynthesis during this critical spring recovery season (F_{690}/F_{740} vs P_p: n=18, p=0.16; F_{690}/F_{740} vs RUE_p: n=18, p=0.36; Figure S5). The PRI also demonstrated strong relationships with P_p (Figure 5c) and RUE_p (Figure S4c). However, the photosynthetic reactivation during winter-spring transition failed to be detected by the commonly used indices NDVI and $NDVI_{705}$ analysed in this study (NDVI vs P_p: n=29, p=0.62; NDVI vs RUE_p: n=29, p=0.50; $NDVI_{705}$ vs P_p: n=29, p=0.15; $NDVI_{705}$ vs RUE_p: n=29, p=0.08; Figure 5d, e). Interestingly, the WI significantly and inversely correlated with photosynthesis ($R^2>0.66$; Figure 5f and Figure S4f). In PC analysis, the score-I for F_λ and score-III for reflectance were also strongly correlated with photosynthesis ($R^2>0.63$; Figure 5g, h and Figure S4g, h). Importantly, all F_λ across the range 670-800 nm were strongly correlated with photosynthetic parameters (P_p and RUE_p) ($R^2 > 0.5$; Figure 6) with maximum correlations obtained in the red (675-690nm) and far-red (730-770) regions.

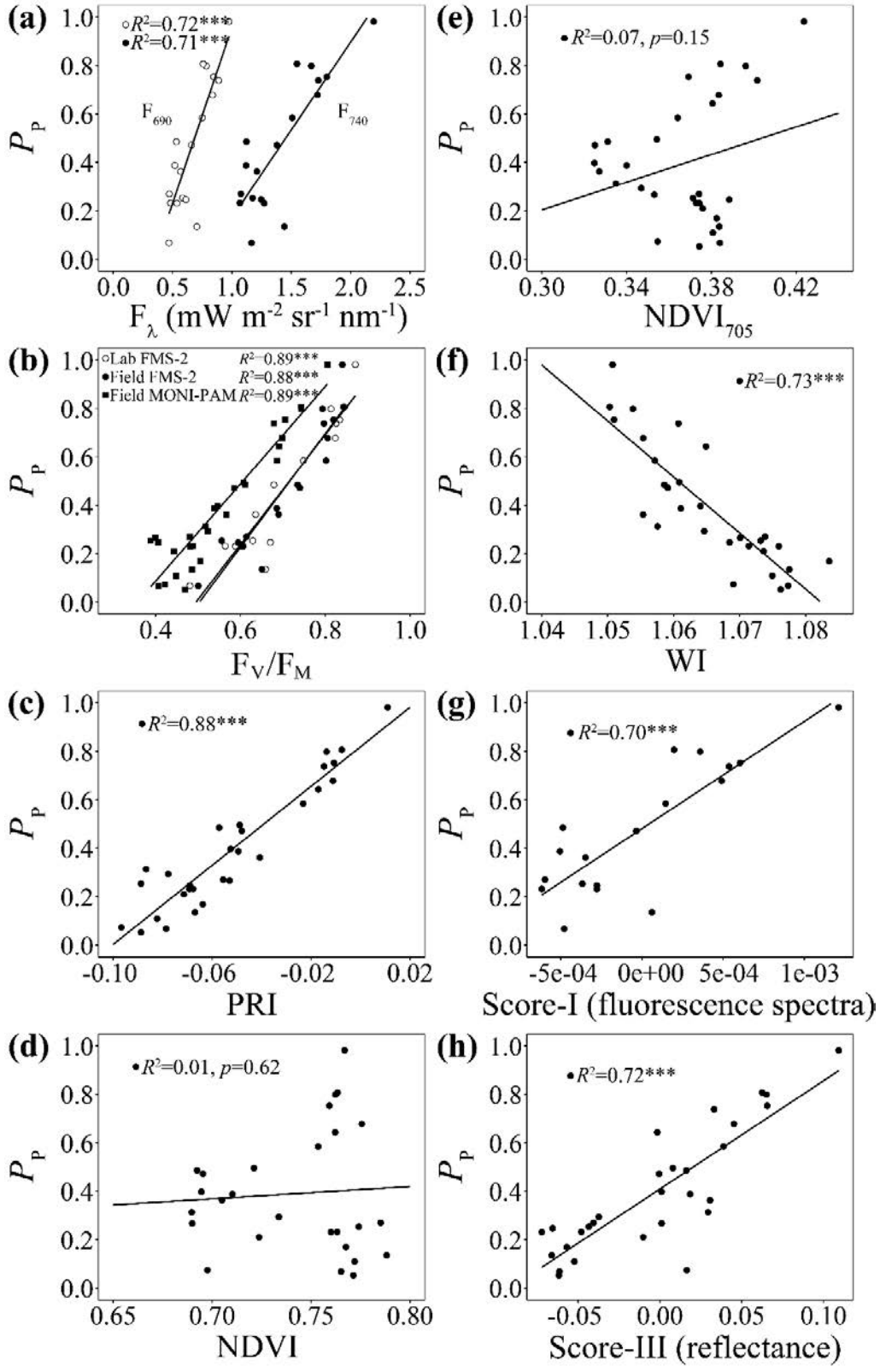

Figure 5. The relationships of optical indices in Figure 4 with rescaled normalized photosynthetic efficiency (P_p). Points represent means of five biological replicates (n = 5). ***p<0.001.

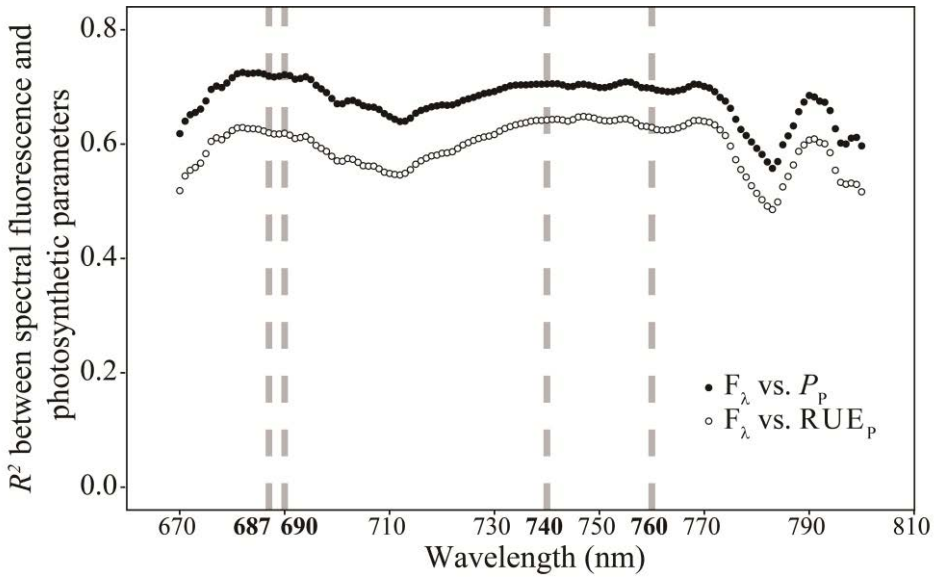

Figure 6. The relationships between all spectral fluorescence (F_λ) from 670 to 800 nm and rescaled normalized photosynthetic parameters (P_p and RUE_p).

Both F_{690} and F_{740} were significantly correlated with F_V/F_M across the entire study period (Figure 7a-c), and presented similar relationships with F_V/F_M measured under natural conditions using two different fluorometers. The two main optical indices F_λ and PRI were strongly correlated with each other (Figure 7d). The PRI explained more than 85% variance of F_V/F_M measured both in the laboratory and field conditions (Figure 7e-g). However, the relationships of NDVI and $NDVI_{705}$ with F_V/F_M were not significant (NDVI vs F_V/F_M (lab FMS-2): n=16, p=0.36; NDVI vs F_V/F_M (field FMS-2): n=19, p=0.86; NDVI vs F_V/F_M (field MONI-PAM): n=30, p=0.31; $NDVI_{705}$ vs F_V/F_M (lab FMS-2): n=16, p=0.08; $NDVI_{705}$ vs F_V/F_M (field FMS-2): n=16, p=0.36; $NDVI_{705}$ vs F_V/F_M (Lab FMS-2): n=30, p=0.10;). The F_V/F_M measured in the laboratory and in the field were strongly correlated (Figure 7h) demonstrating that needles measured in the lab had similar physiological status to those in the field.

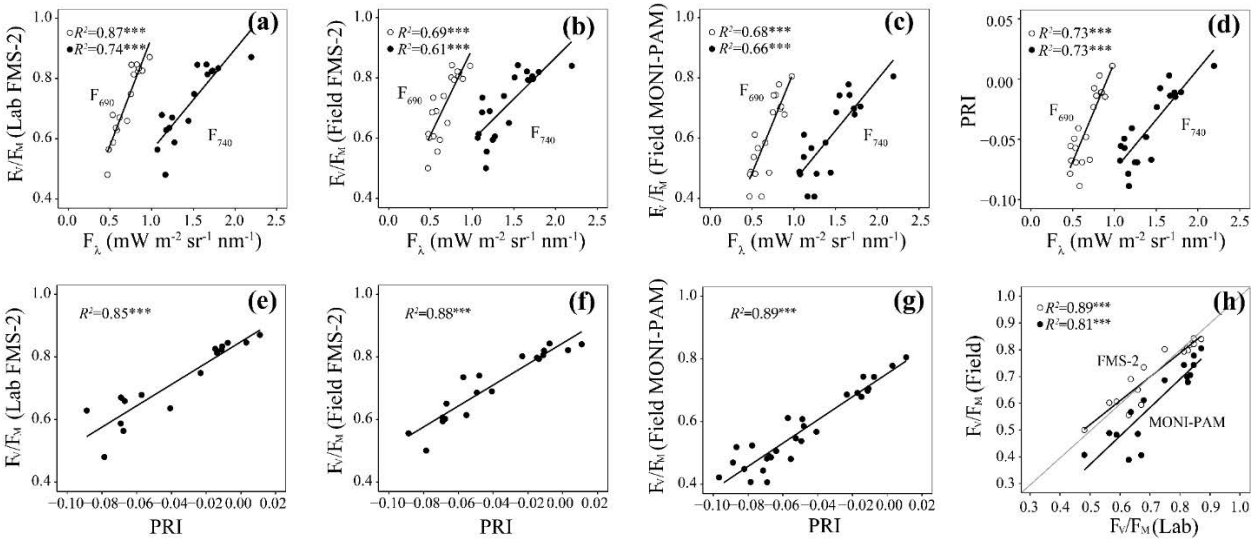

Figure 7. The relationships of spectral fluorescence (F_λ), maximum photochemical efficiency (F_V/F_M) and photochemical reflectance index (PRI). In panel h, the grey line is the 1:1 line. Points represent means of five biological replicates (n = 5). ***p<0.001.

3.4. Dynamics of leaf pigment contents and correlation with photosynthesis and optical data

Total chlorophyll (Chl) contents remained quite stable between 1.4-1.6 µg $mgDW^{-1}$ throughout the study period and registered only a slight and gradual decrease until mid-May (Figure 8a). The Chl a/b ratio was stable until mid-April and then started to increase reaching a maximum in early June (Figure 8b). In contrast, the dynamics of total carotenoid (Car) contents and Car/Chl ratio were different (Figure 8c, d). The Car contents increased slightly during early spring, reaching a maximum on March 23 during the cold spell, which was also when minimum values of P_p occurred. This was followed by a gradual decrease in Car from mid-April until the end of the measuring campaign in summer (Figure 8c). The fluctuations in the Car/Chl ratio were somewhat muted by the slight adjustments in Chl contents and remained rather constant from mid-March to May, when values started to gradually decrease.

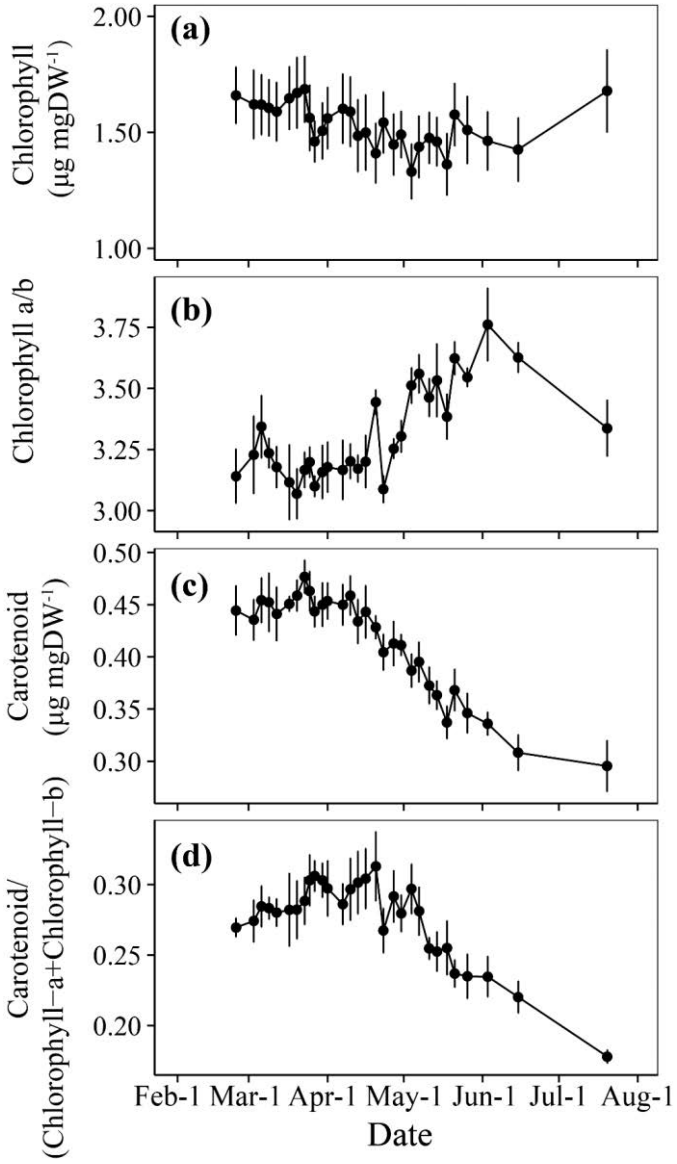

Figure 8. Seasonal variations in (a) total chlorophyll (a+b) content, (b) chlorophyll a/b ratio, (c) total carotenoid content, and (d) carotenoid/chlorophyll (a+b) ration of Scots pine needles. Points represent means of five biological replicates (n=5) and error bars represent the standard error (SE, shown only when larger than symbols).

During the entire study period, the relationships of the photosynthetic parameters (P_p and RUE_p), F_λ and PRI with Car parameters (Car and Car/Chl) were highly significant and stronger than with Chl parameters (total Chl and Chl a/b) (Table 1). The WI also showed significant relationships with pigments, but these correlations were smaller in magnitude than F_λ and PRI with pigments. Interestingly, both PRI and photosynthesis were found to correlate best with Car content. Additionally, total Chl showed the lowest correlations with all the parameters.

Table 1. Seasonal correlation coefficients (*r*) of photosynthetic parameters, spectral fluorescence (F_{690} and F_{740}), F_{690}/F_{740}, photochemical reflectance index (PRI), normalized difference vegetation index (NDVI), modified NDVI ($NDVI_{705}$) and water index (WI) with pigments.

	Chlorophyll (μg $mgDW^{-1}$)	Chlorophyll a/b	Carotenoid (μg $mgDW^{-1}$)	Carotenoid/ (Chlorophyll-a+Chlorophyll-b)
P_p	-0.39*	0.78***	-0.95***	-0.78***
RUE_p	N.S.	0.78***	-0.92***	-0.77***
F_{690}	N.S.	0.56*	-0.87***	-0.88***
F_{740}	N.S.	0.50*	-0.85***	-0.90***
F_{690}/F_{740}	N.S.	N.S.	N.S.	N.S.
PRI	-0.38*	0.78***	-0.91***	-0.77***
NDVI	N.S.	N.S.	N.S.	-0.39*
$NDVI_{705}$	N.S.	N.S.	-0.42*	-0.61***
WI	0.46*	-0.71***	0.76***	0.55**

3.5. Dynamics of leaf water content and correlation with photosynthesis and optical data

Foliar water content (WC) decreased gradually from the beginning of the study period until mid-May (Figure 9a). When compared with the seasonality of photosynthesis, the dynamics of WC were inversely correlated with the increase of P_p and RUE_p (Figure 9b). The WI was found to be strongly correlated with foliar WC (Figure 9c). Further, all the optical indices except NDVI and $NDVI_{705}$ had significant relationships with WC, especially PRI (data not shown).

3.6. Principal component analysis

In the PC analysis, the score-I for F_λ significantly correlated with photosynthesis and F_λ but not with F_{690}/F_{740} (Table 2). The F_{690}/F_{740} ratio was inversely correlated with score-II. Additionally, score-I also had significant inverse relationships with Car and Car/Chl ratios and was correlated with Chl a/b but uncorrelated with Chl. Importantly, the score-I and II in the PC analysis for seasonal reflectance changes were not correlated with P_p, WI, Chl a/b, Chl and Car contents, but strongly and inversely correlated with NDVI and $NDVI_{705}$ (Table 3). Score-II was slightly and inversely correlated with RUE_p and PRI and affected by Car/Chl. Only score-III showed the significant relationships with photosynthesis, PRI, WI and pigments.

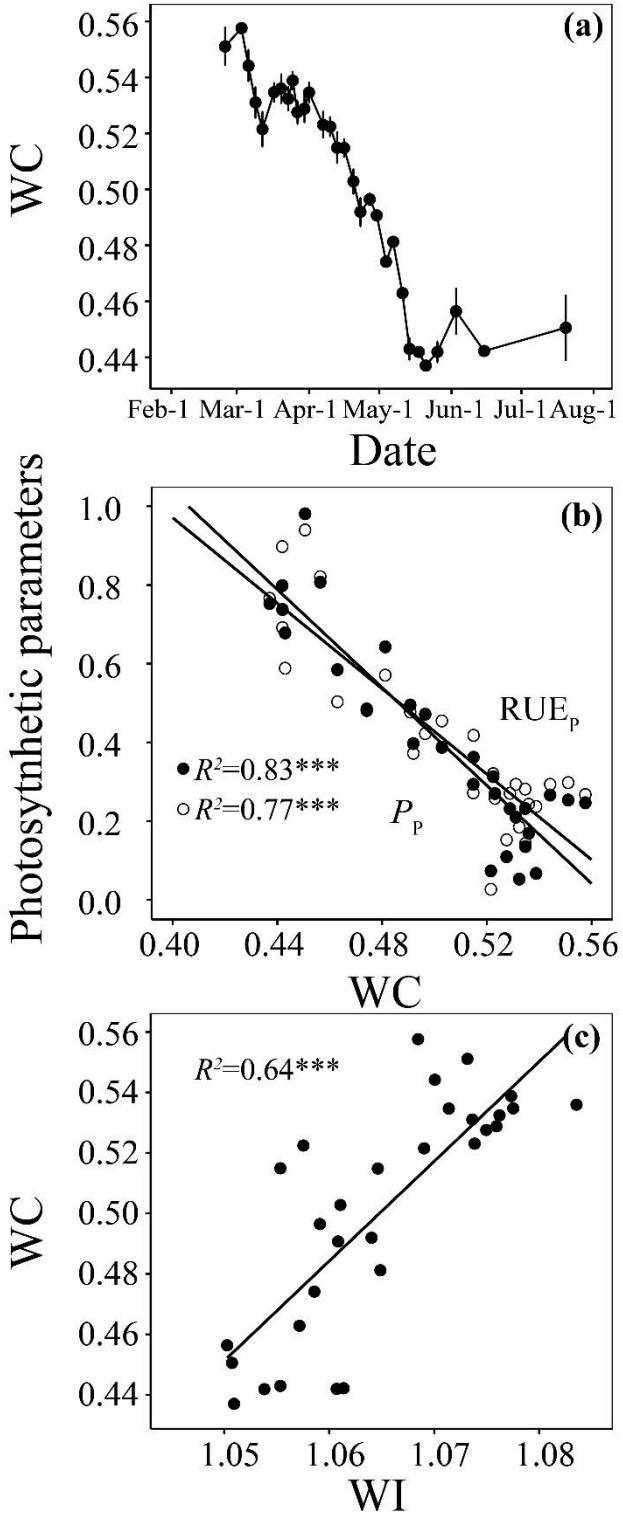

Figure 9. Seasonal variations in water content (WC) for Scots pine needles (a), and the relationships of WC with rescaled normalized photosynthetic parameters (P_p and RUE_p) (b) and water index (WI) (c). Points represent means of five biological replicates (n = 5), standard error (SE; shown only when larger than symbols) is shown in (a). ***p<0.001

Table 2. Seasonal correlation coefficients (*r*) of photosynthetic parameters, spectral fluorescence (F_{690} and F_{740}), F_{690}/F_{740} and pigments with the first three PC scores of fluorescence spectra.

	Score-I	Score-II	Score-III
P_p	0.84***	N.S.	N.S.
RUE_p	0.79***	N.S.	N.S.
F_{690}	0.98***	N.S.	N.S.
F_{740}	1.00***	N.S.	N.S.
F_{690}/F_{740}	N.S.	-0.90***	N.S.
Chlorophyll (μg $mgDW^{-1}$)	N.S.	N.S.	N.S.
Chlorophyll a/b	0.50***	N.S.	0.59***
Carotenoid (μg $mgDW^{-1}$)	-0.85***	N.S.	N.S.
Carotenoid/(Chlorophyll-a+Chlorophyll-b)	-0.89***	N.S.	N.S.

Table 3. Seasonal correlation coefficients (*r*) of photosynthetic parameters, normalized difference vegetation index (NDVI), modified NDVI ($NDVI_{705}$), water index (WI) and pigments with the first three PC scores of reflectance.

	Score-I	Score-II	Score-III
P_p	N.S.	N.S.	0.85***
RUE_p	N.S.	-0.38*	0.82***
PRI	N.S.	-0.39*	0.79***
NDVI	-0.73***	-0.64***	N.S.
$NDVI_{705}$	-0.47**	-0.82***	N.S.
WI	N.S.	N.S.	-0.88***
Chlorophyll (μg $mgDW^{-1}$)	N.S.	N.S.	N.S.
Chlorophyll a/b	N.S.	N.S.	0.72***
Carotenoid (μg $mgDW^{-1}$)	N.S.	N.S.	-0.84***
Carotenoid/(Chlorophyll-a+Chlorophyll-b)	N.S.	0.49**	-0.73***

4. Discussion

4.1. Spectral fluorescence tracks the spring recovery of photosynthesis

Leaf-level fluorescence yields are known to increase during the spring recovery of photosynthesis in evergreen foliage (Ottander *et al*., 1995; Ensminger *et al*., 2004; Porcar-Castell *et al*., 2008; Soukupová *et al*., 2008; Porcar-Castell, 2011). Previous studies have been based on pulse-amplitude modulated (PAM) methods which register the fluorescence in a broad spectral range, typically from 700 to 760 nm, depending on instrument design. In contrast, proximal and remote sensing of chlorophyll fluorescence (ChlF) is based on retrievals within very narrow spectral bands located in either the red or far-red regions of the fluorescence emission spectra (F_λ) (Figure 1a). Importantly, a number of seasonal processes such as changes in chlorophyll (Chl) contents, sustained forms of non-photochemical quenching (NPQ), or conformational changes in the photosystems could interfere with the spectral properties of the leaf-level fluorescence signal, which could erode the relationship between fluorescence and photosynthesis for some spectral regions. We asked whether these processes exert a significant effect on the seasonal correlation between solar-induced chlorophyll fluorescence (SIF) and photosynthesis, i.e., are all wavelengths equally correlated with the photosynthetic recovery process? (Porcar-Castell *et al*., 2014; Ač *et al*., 2015).

Firstly, seasonal changes in leaf Chl contents potentially affect the overall absorption of photosynthetically active radiation as well as the reabsorption of ChlF particularly in the red bands causing a spectral effect (Buschmann & Lichtenthaler, 1998). This phenomenon has been used by the red/far-red ChlF ratio F_{690}/F_{740}, to track leaf Chl contents, where the ratio decreases with increasing Chl contents (Lichtenthaler & Rinderle, 1988; Hák *et al*., 1990; Lichtenthaler *et al*., 1990; D'Ambrosio *et al*., 1992; Agati *et al*., 1996, 2000). Here, seasonal Chl contents remained rather constant (Figure 8a), and so did the ratio F_{690}/F_{740} (Figure S1), which was accordingly a poor indicator of photosynthetic recovery (Figure S5). We therefore conclude that changes in leaf chlorophyll content of evergreen vegetation are not likely to interact with the relationship between F_λ and photosynthesis during spring recovery period.

Secondly, although reversible forms of NPQ are known to quench photosystem II (PSII) fluorescence, they have no apparent effect on the far-red fluorescence contribution

from PSI (Genty *et al*., 1990). If the same holds true for sustained forms of NPQ (see e.g. Verhoeven, 2014) we would expect the red fluorescence range to be more sensitive to sustained NPQ (and by extension to the seasonality of photosynthesis) than the far-red. Although more work is needed to elucidate whether sustained forms of NPQ operate in PSI in a similar fashion as they do in PSII, the fact that the fluorescence ratio F_{690}/F_{740} remained rather constant (Figure S1) and did not follow the recovery of photosynthesis would support this hypothesis.

Overall, we found that all F_λ from F_{670} to F_{800} were capable of tracking the spring recovery of photosynthesis in boreal evergreen foliage (Figure 6). This finding suggests that the above described processes do not significantly disrupt the correlation between SIF and photosynthesis across the spectral range. This also means that, *a priori*, all the telluric or Fraunhofer lines used for SIF retrievals share similar intrinsic potential to track the leaf-level seasonality of photosynthesis. Obviously, when measuring at spatial scales larger than a few needles, as we did in the present study, physical factors such as canopy structure and wavelength dependent reabsorption (van der Tol *et al*., 2009; Fournier *et al*., 2012; Verrelst *et al*., 2015; Rossini *et al*., 2016; Migliavacca *et al*., 2017), and canopy multi-layer heterogeneity or atmospheric absorption and scattering (Guanter *et al*., 2010; Damm *et al*., 2014) will also contribute to the seasonal SIF dynamics and possibly impact on the seasonal correlation between different SIF wavelengths and photosynthesis.

4.2. F_V/F_M and the seasonal dynamics of photosynthesis

Winter levels of maximum photochemical efficiency of PSII (F_V/F_M) measured by MONI-PAM were higher than those registered in previous years for the same site (Porcar-Castell *et al*., 2008; Porcar-Castell, 2011). This was consistent with the relatively mild winter we experienced during the campaign compared to previous years. Low F_V/F_M levels observed during winter (Figure 4b) are known to reflect mainly the accumulation of sustained forms of NPQ (Demmig-Adams & Adams, 2006; Porcar-Castell *et al*., 2008; Porcar-Castell, 2011; Verhoeven, 2014). Accordingly, the correlation between steady state F_λ and photosynthesis (Figure 5a) or F_V/F_M (Figure 7a-c) supports the statement that seasonal dynamics in F_λ are mainly controlled by NPQ at the leaf level. It is important to note that while F_V/F_M is related to the sustained component of NPQ alone, F_λ was also affected by the reversible pH-dependent forms of NPQ upon illumination during our spectral measurements, complicating the relationship between F_λ and F_V/F_M. In addition,

photochemical quenching and photoinhibition of reaction centres might also add to the decoupling between F_λ and F_V/F_M. In turn, chlorophyll content dynamics did not have any significant impact on F_λ dynamics as reflected by the lack of correlation with score-I in the principle component analysis (PCA; Table 2).

4.3. PRI but not NDVI or $NDVI_{705}$ tracks the spring recovery of photosynthesis

The photochemical reflectance index (PRI) significantly tracked the photosynthetic reactivation of boreal Scots pine needles (Figure 5c and Figure S4c). Seasonal changes in leaf-level PRI have been shown to be strongly controlled by the carotenoid/chlorophyll (Car/Chl) ratio (Filella *et al*., 2009) both during the spring recovery (Porcar-Castell *et al*., 2012; Wong & Gamon, 2015a,b), as well as during the autumn downregulation of photosynthesis (Fréchette *et al*., 2016). Interestingly, we observed a slightly better correlation between PRI and total Car compared to the Car/Chl ratio (Table 1). In addition, we had 30 measuring points concentrated during the spring recovery period whereas the measurements in the studies by Porcar-Castell *et al*. (2012) and Wong and Gamon (2015a,b) expanded throughout the year with a much lower temporal resolution. Accordingly, differences in the temporal patterns of Chl and Car contents between spring and autumn could explain these contrasting results, emphasizing also the importance and trade-off between temporal range and resolution in field studies.

Accumulation of Car during winter and early spring (Figure 8c) provides sustained photoprotection contributing to sustained forms of NPQ (Ottander *et al*., 1995; Öquist & Huner, 2003; Busch *et al*., 2009; Porcar-Castell *et al*., 2012; Verhoeven, 2014). As temperature increases, sustained NPQ gradually decreases until the photochemical machinery is fully recovered (Öquist & Huner, 2003; Busch *et al*., 2009; Porcar-Castell, 2011). This close seasonal relationship between Car and NPQ sets the relationship between PRI and F_λ (Figure 7d) or F_V/F_M (Figure 7e-g) (Porcar-Castell *et al*., 2012).

In contrast to PRI, the normalized difference vegetation index (NDVI) and the modified NDVI ($NDVI_{705}$) failed to track the spring recovery of photosynthesis in Scots pine needles (Figure 5d, e and Figure S4d, e). This is because the seasonality of photosynthesis was decoupled from Chl content but was significantly reflected in Car changes that were involved in the rapid physiological variations of plant under stress conditions, which was not detectable by NDVI or $NDVI_{750}$ (Huete *et al*., 2002; Garbulsky *et al*., 2011).

4.4. WI tracks the spring recovery of photosynthesis

Our results indicated that the WI was not only correlated with foliar water content (WC) (Figure 9c) but was also strongly correlated with seasonal photosynthetic dynamics (Figure 5f), indicating the applicability of WI in tracking photosynthetic dynamics. Plant water status (e.g. water potential and foliar water content), stomatal conductance and leaf transpiration have been successfully detected using the water index (WI) under water stress conditions for crops and Mediterranean trees at the leaf, canopy and landscape scales (Peñuelas *et al*., 1996, 1997; Peñuelas & Inoue, 1999; Marino *et al*., 2014; Sun *et al*., 2014). PRI was significantly correlated with WC (data not shown), indicating that PRI can be used for detecting rapid foliar WC changes. Similar results were also found in previous studies for monitoring changes in WC or relative water content for trees subjected to water stress (Sun *et al*., 2008, 2014; Osório *et al*., 2012; Rossini *et al*., 2013) .

Water transport dynamics play a key role in the photosynthetic spring recovery of evergreen trees, and are modulated by a number of stress related processes that include increased evaporative demand and reduced water transport capacity due to xylem embolism, limited osmotic potential, higher viscosity and excess sugar loading (Nikinmaa *et al*., 2013; Lintunen *et al*., 2014). Over the course of our measurements we observed gradual decreases in foliar WC (Figure 9a) and WI, which were concomitant with the simultaneous restoration of photosynthetic capacity and transpiration (Kolari *et al*., 2007). However, intuitively we may expect foliar WC and photosynthesis to be positively correlated, whereas we found the opposite to be true (Figure 9b). Similar high values in winter, with subsequent declines through spring, have been found for moisture levels and sugar content of boreal conifer needles, mainly due to spring reactivation of photosynthesis (Van Wagner, 1967; Little, 1970; Jolly *et al*., 2014). Therefore the changes in foliage water content that we measured could reflect the temporal dynamics of sugar content.

Further to the above, diurnal fluctuations in WC of needles are likely related to transpiration dynamics i.e. water content decreases towards noon in summer but not in winter this may explain the lack of recovery we observed in Figure 9a. In summary the negative relationship that we observed could reflect the fact that the relationship between WC and photosynthesis is not direct, but an indirect effect due to latent factors, and could be any one, or a combination, of the following: transpiration dynamics, sugar contents,

soil water content (Wu *et al*., 2011, 2012) or unrelated diurnal variation in foliar WC. Further work is needed to elucidate the specific mechanism(s) that cause the spring recovery dynamics of WC/WI.

4.5. Summary of the principal component analysis

The PC analysis provided a useful summary of the wavelength dependent information content of both F_λ and reflectance datasets during the study period. For example PC-3 from the reflectance dataset tracked the photosynthetic spring recovery (Figure 5h and Figure S4h), and the wavelengths that contributed most to PC-3 were the PRI detection band (531 nm), the red edge (close to 685 and 717 nm) and the WI detection band, 970 nm.

The largest fractions of variation in the reflectance dataset were explained by PC-1 and PC-2 which were both correlated with NDVI and $NDVI_{705}$, and neither which tracked the spring recovery (Table 3). We suggest that this variation, and resulting correlation with NDVI, was likely an artefact of our measurements. Measuring the optical properties of needles is notoriously difficult (Olascoaga *et al*., 2016), and although we tried to standardise our measurements as best we could it is likely that slight differences in needle mat structure (see Figure 1) during the measurement period were the main cause for this variation. For F_λ, in contrast to reflectance, the largest proportion of variation as represented by PC-1, did track the spring recovery (Figure 5g and Figure S4g). This suggests that F_λ is a robust and potentially less error prone method for measuring photosynthetic dynamics than spectral reflectance.

5. Concluding remarks

We reported for the first time that all ChlF emission wavelengths could be used to assess photosynthetic seasonality of boreal evergreen needles. Additionally, the changes in PRI revealed photoprotective activity and the WI provided a measure of foliar water content during the re-adjustment of photosynthesis that occurs during the spring summer transition period. Therefore we suggest that the combination of different optical indices is preferable for maximising physiological information content retrieval, and can provide

a non-destructive and robust approach to track photosynthetic dynamics during complex winter-spring transitions.

In boreal evergreen conifers, the summer-autumn transition under fluctuating temperature and daylength elicits changes in physiological processes along with changes in NPQ, de-epoxidation state, carotenoid and chlorophyll contents, and foliar water content etc., which differ from winter-spring-summer transition studied here (Öquist & Huner, 2003; Busch *et al*., 2007; Fréchette *et al*., 2016). Further work could be used to test the applicability of optical signals in revealing photosynthetic activity over summer-autumn transition period for Scots pine. Our results also could be applied to evaluate vegetation productivity shift response to ongoing climate change during critical seasonal transitions. Additionally, more work is now needed to explore the efficacy of the main fluorescence emission wavebands and the seasonal mechanisms controlling ChlF and PRI (Atherton *et al*., 2017) for different species (e.g. broadleaf and herbaceous), especially at longer timescales and larger spatial levels. Our results support the assertion that the increasing use of unmanned aerial vehicles (UAVs; Gago *et al*., 2015) and ongoing and forthcoming satellite missions such as GOME (Global Ozone Monitoring Experiment; Guanter *et al*., 2014), OCO-2 (Orbiting Carbon Observatory-2; Frankenberg *et al*., 2014) and FLEX (FLuorescence EXplorer mission; Kraft *et al*., 2013), will provide improved spatial-temporal assessment of terrestrial photosynthetic activity using SIF, PRI and potentially WI.

References

Aalto J, Kolari P, Hari P, Kerminen VM, Schiestl-Aalto P, Aaltonen H, Levula J, Siivola E, Kulmala M, Bäck J. 2014. New foliage growth is a significant, unaccounted source for volatiles in boreal evergreen forests. *Biogeosciences* **11**: 1331–1344.

Ač A, Malenovský Z, Olejníčková J, Gallé A, Rascher U, Mohammed G. 2015. Meta-analysis assessing potential of steady-state chlorophyll fluorescence for remote sensing detection of plant water, temperature and nitrogen stress. *Remote sensing of environment* **168**: 420–436.

Agati G, Cerovic ZG, Moya I. 2000. The effect of decreasing temperature up to chilling values on the in vivo F685/F735 chlorophyll fluorescence ratio in *Phaseolus vulgaris* and *Pisum sativum*: the role of the photosystem I contribution to the 735 nm fluorescence band. *Photochemistry and Photobiology* **72**: 75–84.

Agati G, Mazzinghi P, Lipucci di Paola M, Fusi F, Cecchi G. 1996. The F685/F730 chlorophyll fluorescence ratio as indicator of chilling stress in plants. *Journal of Plant Physiology* **148**: 384–390.

Atherton J, Nichol CJ, Porcar-Castell A. 2016. Using spectral chlorophyll fluorescence and the photochemical reflectance index to predict physiological dynamics. *Remote Sensing of Environment* **176**: 17–30.

Atherton J, Olascoaga B, Alonso L, Porcar-Castell A. 2017. Spatial variation of leaf optical properties in a boreal forest is influenced by species and light environment. *Frontiers in Plant Science* **8**.

Bannari A, Morin D, Bonn F, Huete AR. 1995. A review of vegetation indices. *Remote Sensing Reviews* **13**: 95–120.

Bartholomé E, Belward A. 2005. GLC2000: a new approach to global land cover mapping from Earth observation data. *International Journal of Remote Sensing* **26**: 1959–1977.

Buermann W, Bikash PR, Jung M, Burn DH, Reichstein M. 2013. Earlier springs decrease peak summer productivity in North American boreal forests. *Environmental Research Letters* **8**: 24027.

Busch F, Hüner NPA, Ensminger I. 2007. Increased air temperature during simulated autumn conditions does not increase photosynthetic carbon gain but affects the dissipation of excess energy in aeedlings of the evergreen conifer Jack pine. *Plant Physiology* **143**: 1242–1251.

Busch F, Hüner NPA, Ensminger I. 2009. Biochemical constrains limit the potential of the photochemical reflectance index as a predictor of effective quantum efficiency of photosynthesis during the winter spring transition in Jack pine seedlings. *Functional Plant Biology* **36**: 1016–1026.

Buschmann C. 2007. Variability and application of the chlorophyll fluorescence emission ratio red/far-red of leaves. *Photosynthesis Research* **92**: 261–271.

Buschmann C, Lichtenthaler HK. 1998. Principles and characteristics of multi-colour fluorescence imaging of plants. *Journal of Plant Physiology* **152**: 297–314.

D'Ambrosio N, Szabo K, Lichtenthaler HK. 1992. Increase of the chlorophyll fluorescence ratio F690/F735 during the autumnal chlorophyll breakdown. *Radiation and Environmental Biophysics* **31**: 51–62.

Damm A, Guanter L, Laurent VCE, Schaepman ME, Schickling A, Rascher U. 2014. FLD-based retrieval of sun-induced chlorophyll fluorescence from medium spectral resolution airborne spectroscopy data. *Remote Sensing of Environment* **147**: 256–266.

Demmig-Adams B, Adams WW. 2006. Photoprotection in an ecological context: the remarkable complexity of thermal energy dissipation. *New Phytologist* **172**: 11–21.

Drolet G, Wade T, Nichol CJ, MacLellan C, Levula J, Porcar-Castell A, Nikinmaa E, Vesala T. 2014. A temperature-controlled spectrometer system for continuous and unattended measurements of canopy spectral radiance and reflectance. *International Journal of Remote Sensing* **35**: 1769–1785.

Ensminger I, Busch F, Huner NPA. 2006. Photostasis and cold acclimation: sensing low temperature through photosynthesis. *Physiologia Plantarum* **126**: 28–44.

Ensminger I, Schmidt L, Lloyd J. 2008. Soil temperature and intermittent frost modulate the rate of recovery of photosynthesis in Scots pine under simulated spring conditions. *New Phytologist* **177**: 428–442.

Ensminger I, Sveshnikov D, Campbell DA, Funk C, Jansson S, Lloyd J, Shibistova O, Öquist G. 2004. Intermittent low temperatures constrain spring recovery of photosynthesis in

boreal Scots pine forests. *Global Change Biology* **10**: 995–1008.

Filella I, Porcar-Castell A, Munné-Bosch S, Bäck J, Garbulsky MF, Peñuelas J. **2009**. PRI assessment of long-term changes in carotenoids/chlorophyll ratio and short-term changes in de-epoxidation state of the xanthophyll cycle. *International Journal of Remote Sensing* **30**: 4443–4455.

Forkel M, Carvalhais N, Rödenbeck C, Keeling R, Heimann M, Thonicke K, Zaehle S, Reichstein M. **2016**. Enhanced seasonal CO_2 exchange caused by amplified plant productivity in northern ecosystems. *Science* **4971**: 1–9.

Fournier A, Daumard F, Champagne S, Ounis A, Goulas Y, Moya I. **2012**. Effect of canopy structure on sun-induced chlorophyll fluorescence. *ISPRS Journal of Photogrammetry and Remote Sensing* **68**: 112–120.

Frankenberg C, Fisher JB, Worden J, Badgley G, Saatchi SS, Lee JE, Toon GC, Butz A, Jung M, Kuze A, e*t al*. **2011**. New global observations of the terrestrial carbon cycle from GOSAT: Patterns of plant fluorescence with gross primary productivity. *Geophysical Research Letters* **38**: 1–6.

Frankenberg C, O'Dell C, Berry J, Guanter L, Joiner J, Köhler P, Pollock R, Taylor TE. **2014**. Prospects for chlorophyll fluorescence remote sensing from the Orbiting Carbon Observatory-2. *Remote Sensing of Environment* **147**: 1–12.

Fréchette E, Chang CY-Y, Ensminger I. **2016**. Photoperiod and temperature constraints on the relationship between the photochemical reflectance index and the light use efficiency of photosynthesis in *Pinus strobus*. *Tree Physiology* **36**: 311–324.

Fu YH, Piao S, Op de Beeck M, Cong N, Zhao H, Zhang Y, Menzel A, Janssens IA. **2014**. Recent spring phenology shifts in western Central Europe based on multiscale observations. *Global Ecology and Biogeography* **23**: 1255–1263.

Gago J, Douthe C, Coopman RE, Gallego PP, Ribas-Carbo M, Flexas J, Escalona J, Medrano H. **2015**. UAVs challenge to assess water stress for sustainable agriculture. *Agricultural Water Management* **153**: 9–19.

Gamon JA, Peñuelas J, Field CB. **1992**. A narrow-waveband spectral index that tracks diurnal changes in photosynthetic efficiency. *Remote Sensing of Environment* **41**: 35–44.

Garbulsky MF, Peñuelas J, Gamon J, Inoue Y, Filella I. **2011**. The photochemical reflectance index (PRI) and the remote sensing of leaf, canopy and ecosystem radiation use efficiencies. A review and meta-analysis. *Remote Sensing of Environment* **115**: 281–297.

Garbulsky MF, Peñuelas J, Papale D, Filella I. **2008**. Remote estimation of carbon dioxide uptake by a Mediterranean forest. *Global Change Biology* **14**: 2860–2867.

Genty B, Briantais J-M, Baker NR. **1989**. The relationship between the quantum yield of photosynthetic electron transport and quenching of chlorophyll fluorescence. *Biochimica et Biophysica Acta (BBA) - General Subjects* **990**: 87–92.

Genty B, Wonders J, Baker NR. **1990**. Non-photochemical quenching of F_o in leaves is emission wavelength dependent: consequences for quenching analysis and its interpretation. *Photosynthesis Research* **26**: 133–139.

Gitelson A, Merzlyak MN. **1994**. Spectral reflectance changes associated with autumn senescence of *Aesculus hippocastanum* L. and *Acer platanoides* L. leaves. Spectral features and relation to chlorophyll estimation. *Journal of Plant Physiology* **143**: 286–292.

Govindjee. **1995**. Sixty-three years since Kautsky: chlorophyll a fluorescence. *Australian Journal of Plant Physiology* **22**: 131–160.

Guanter L, Alonso L, Gómez-Chova L, Meroni M, Preusker R, Fischer J, Moreno J. **2010**. Developments for vegetation fluorescence retrieval from spaceborne high-resolution spectrometry in the O_2-A and O_2-B absorption bands. *Journal of Geophysical Research Atmospheres* **115**: 1–16.

Guanter L, Frankenberg C, Dudhia A, Lewis PE, Gómez-Dans J, Kuze A, Suto H, Grainger RG. **2012**. Retrieval and global assessment of terrestrial chlorophyll fluorescence from GOSAT space measurements. *Remote Sensing of Environment* **121**: 236–251.

Guanter L, Zhang Y, Jung M, Joiner J, Voigt M, Berry J a, Frankenberg C, Huete AR, Zarco-Tejada P, Lee J-E, e*t al*. **2014**. Global and time-resolved monitoring of crop photosynthesis with chlorophyll fluorescence. *Proceedings of the National Academy of Sciences of the United States of America* **111**: E1327-33.

Hák R, Lichtenthaler HK, Rinderle U. **1990**. Decrease of the chlorophyll fluorescence ratio F690/F730 during greening and development of leaves. *Radiation and Environmental Biophysics* **29**: 329–336.

Hari P, Kulmala M. **2005**. Station for measuring ecosystem-atmophere relations (SMEAR II). *Boreal Environment Research* **10**: 351–322.

Hari P, Mäkelä A, Korpilahti E, Holmberg M. **1986**. Optimal control of gas exchange. *Tree Physiology* **2**: 169–175.

Huete A, Didan K, Miura T, Rodriguez EP, Gao X, Ferreira LG. **2002**. Overview of the radiometric and biophysical performance of the MODIS vegetation indices. *Remote Sensing of Environment* **83**: 195–213.

Inoue Y, Peñuelas J, Miyata A, Mano M. **2008**. Normalized difference spectral indices for estimating photosynthetic efficiency and capacity at a canopy scale derived from hyperspectral and CO_2 flux measurements in rice. *Remote Sensing of Environment* **112**: 156–172.

Jahns P, Holzwarth AR. **2012**. The role of the xanthophyll cycle and of lutein in photoprotection of photosystem II. *Biochimica et Biophysica Acta - Bioenergetics* **1817**: 182–193.

Jolly WM, Hintz J, Kropp RC, Conrad ET. **2014**. Physiological drivers of the live foliar moisture content 'spring dip' in *Pinus resinosa* and *Pinus banksiana* and their relationship to foliar flammability. *Advances in forest fire research*: 401–408.

Kolari P, Bäck J, Taipale R, Ruuskanen TM, Kajos MK, Rinne J, Kulmala M, Hari P. **2012**. Evaluation of accuracy in measurements of VOC emissions with dynamic chamber system. *Atmospheric Environment* **62**: 344–351.

Kolari P, Lappalainen HK, Hänninen H, Hari P. **2007**. Relationship between temperature and the seasonal course of photosynthesis in Scots pine at northern timberline and in southern boreal zone. *Tellus, Series B: Chemical and Physical Meteorology* **59**: 542–552.

Kraft S, Bézy J-L, Del Bello U, Berlich R, Drusch M, Franco R, Gabriele A, Harnisch B, Meynart R, Silvestrin P. **2013**. FLORIS: phase A status of the fluorescence imaging spectrometer of the Earth Explorer mission candidate FLEX. **8889**: 88890T.

Krause G, Weis E. **1991**. Chlorophyll fluorescence and photosynthesis: the basics. *Annual Review of Plant Physiology and Plant Molecular Biology* **42**: 313–349.

Lichtenthaler HK, Hak R, Rinderle U. **1990**. The chlorophyll fluorescence ratio F690/F730 in leaves of different chlorophyll content. *Photosynthesis Research* **25**: 295–298.

Lichtenthaler HK, Rinderle U. **1988**. The role of chlorophyll fluorescence in the detection of stress conditions in plants. *CRC Critical Reviews in Analytical Chemistry* **19**: S29–S85.

Lintunen A, Lindfors L, Kolari P, Juurola E, Nikinmaa E, Hölttä T. **2014**. Bursts of CO_2 released during freezing offer a new perspective on avoidance of winter embolism in trees. *Annals of Botany* **114**: 1711–1718.

Little C. **1970**. Seasonal changes in carbohydrate and moisture content in needles of balsam fir (*Abies balsamea*). *Canadian Journal of Botany* **48**: 2021–2028.

Los DA, Mironov KS, Allakhverdiev SI. **2013**. Regulatory role of membrane fluidity in gene expression and physiological functions. *Photosynthesis Research* **116**: 489–509.

Marino G, Pallozzi E, Cocozza C, Tognetti R, Giovannelli A, Cantini C, Centritto M. **2014**. Assessing gas exchange, sap flow and water relations using tree canopy spectral reflectance indices in irrigated and rainfed *Olea europaea* L. *Environmental and Experimental Botany* **99**: 43–52.

Menzel A, Fabian P. **1999**. Growing season extended in Europe. *Nature* **397**: 659.

Meroni M, Rossini M, Guanter L, Alonso L, Rascher U, Colombo R, Moreno J. **2009**. Remote sensing of solar-induced chlorophyll fluorescence: review of methods and applications. *Remote Sensing of Environment* **113**: 2037–2051.

Migliavacca M, Perez-Priego O, Rossini M, El-Madany TS, Moreno G, van der Tol C, Rascher U, Berninger A, Bessenbacher V, Burkart A, e*t al*. **2017**. Plant functional traits and canopy structure control the relationship between photosynthetic CO_2 uptake and far-red sun-induced fluorescence in a Mediterranean grassland under different nutrient availability. *New Phytologist* **214**: 1078–1091.

Nikinmaa E, Hölttä T, Hari P, Kolari P, Mäkelä A, Sevanto S, Vesala T. **2013**. Assimilate transport in phloem sets conditions for leaf gas exchange. *Plant, Cell and Environment* **36**: 655–669.

Nyongesah MJ, Wang Q, Xu L. **2016**. Remote sensing of assimilating branch light use efficiency using the photochemical reflectance index in *Haloxylon ammodendron* forest. *Journal of Applied Remote Sensing* **10**: 25013.

Olascoaga B, Mac Arthur A, Atherton J, Porcar-Castell A. **2016**. A comparison of methods to estimate photosynthetic light absorption in leaves with contrasting morphology. *Tree Physiology* **36**: 368–379.

Olascoaga B, Juurola E, Pinho P, Lukeš P, Halonen L, Nikinmaa E, Bäck J, Porcar-Castell A. **2014**. Seasonal variation in the reflectance of photosynthetically active radiation

from epicuticular waxes of Scots pine (*Pinus sylvestris*) needles. *Boreal Environment Research* **19**: 132–141.

Öquist G, Huner NPA. 2003. Photosynthesis of overwintering evergreen plants. *Annual Review of Plant Biology* **54**: 329–355.

Osório J, Osório ML, Romano A. 2012. Reflectance indices as nondestructive indicators of the physiological status of *Ceratonia siliqua* seedlings under varying moisture and temperature regimes. *Functional Plant Biology* **39**: 588–597.

Ottander C, Campbell D, Öquist G. 1995. Seasonal changes in photosystem II organisation and pigment composition in *Pinus sylvestris*. *Planta* **197**: 176–183.

Peñuelas J, Filella I, Biel C, Serrano L, Savé R. 1993. The reflectance at the 950-970nm region as an indicator of plant water status. *International Journal of Remote Sensing* **14**: 1887–1905.

Peñuelas J, Gamon J, Freeden A, Merino J, Field C. 1994. Reflectance indices associated with physiological changes in nitrogen- and water-limited sunflower leaves. *Remote Sensing of Environment* **48**:135–146.

Peñuelas J, Filella I, Gamon JA. 1995. Assessment of photosynthetic radiation use efficiency with spectral reflectance. *New Phytologist* **131**: 291–296.

Peñuelas J, Filella I, Serrano L, Savé R. 1996. Cell wall elasticity and Water Index (R970 nm/R900 nm) in wheat under different nitrogen availabilities. *International Journal of Remote Sensing* **17**: 373–382.

Peñuelas J, Inoue Y. 1999. Reflectance indices indicative of changes in water and pigment contents of peanut and wheat leaves. *Photosynthetica* **36**: 355–360.

Peñuelas J, Pinol J, Ogaya R, Filella I. 1997. Estimation of plant water concentration by the reflectance Water Index WI (R900/R970). *International Journal of Remote Sensing* **18**: 2869–2875.

Pinto F, Damm A, Schickling A, Panigada C, Cogliati S, Müller-Linow M, Balvora A, Rascher U. 2016. Sun-induced chlorophyll fluorescence from high-resolution imaging spectroscopy data to quantify spatio-temporal patterns of photosynthetic function in crop canopies. *Plant, Cell & Environment* **39**: 1500–1512.

Pirinen P, Simola H, Aalto J, Kaukoranta J-P, Karlsson P, Ruuhela R. 2012. Tilastoja suomen ilmastosta 1981-2010. (Climatological statistics of Finland 1981–2010). *Finnish Meteorological Institute, Helsinki*.

Porcar-Castell A. 2011. A high-resolution portrait of the annual dynamics of photochemical and non-photochemical quenching in needles of *Pinus sylvestris*. *Physiologia Plantarum* **143**: 139–153.

Porcar-Castell A, Mac Arthur A, Rossini M, Eklundh L, Pacheco-Labrador J, Anderson K, Balzarolo M, Martín MP, Jin H, Tomelleri E, e*t al*. **2015**. EUROSPEC: At the interface between remote-sensing and ecosystem CO_2 flux measurements in Europe. *Biogeosciences* **12**: 6103–6124.

Porcar-Castell A, Garcia-Plazaola JI, Nichol CJ, Kolari P, Olascoaga B, Kuusinen N, Fernández-Marín B, Pulkkinen M, Juurola E, Nikinmaa E. 2012. Physiology of the seasonal relationship between the photochemical reflectance index and photosynthetic light use efficiency. *Oecologia* **170**: 313–323.

Porcar-Castell A, Pfündel E, Korhonen JFJ, Juurola E. 2008. A new monitoring PAM fluorometer (MONI-PAM) to study the short- and long-term acclimation of photosystem II in field conditions. *Photosynthesis Research* **96**: 173–179.

Porcar-Castell A, Tyystjärvi E, Atherton J, Van Der Tol C, Flexas J, Pfündel EE, Moreno J, Frankenberg C, Berry JA. 2014. Linking chlorophyll a fluorescence to photosynthesis for remote sensing applications: mechanisms and challenges. *Journal of Experimental Botany* **65**: 4065–4095.

Rossini M, Fava F, Cogliati S, Meroni M, Marchesi A, Panigada C, Giardino C, Busetto L, Migliavacca M, Amaducci S, e*t al*. **2013**. Assessing canopy PRI from airborne imagery to map water stress in maize. *ISPRS Journal of Photogrammetry and Remote Sensing* **86**: 168–177.

Rossini M, Meroni M, Celesti M, Cogliati S, Julitta T, Panigada C, Rascher U, van der Tol C, Colombo R. 2016. Analysis of red and far-red sun-induced chlorophyll fluorescence and their ratio in different canopies based on observed and modeled data. *Remote Sensing* **8**: 412.

Serrano L, González-Flor C, Gorchs G. 2010. Assessing vineyard water status using the reflectance based Water Index. *Agriculture, Ecosystems and Environment* **139**: 490–499.

Soukupová J, Cséfalvay L, Urban O, Košvancová M, Marek M, Rascher U, Nedbal L. 2008. Annual variation of the steady-state

chlorophyll fluorescence emission of evergreen plants in temperate zone. *Functional Plant Biology* **35**: 63–76.

Sun P, Grignetti A, Liu S, Casacchia R, Salvatori R, Pietrini F, Loreto F, Centritto M. **2008**. Associated changes in physiological parameters and spectral reflectance indices in olive (*Olea europaea* L.) leaves in response to different levels of water stress. *International Journal of Remote Sensing* **29**: 1725–1743.

Sun P, Wahbi S, Tsonev T, Haworth M, Liu S, Centritto M. **2014**. On the use of leaf spectral indices to assess water status and photosynthetic limitations in *Olea europaea* L. during water-stress and recovery. *PLOS ONE* **9**.

van der Tol C, Verhoef W, Rosema A. **2009**. A model for chlorophyll fluorescence and photosynthesis at leaf scale. *Agricultural and Forest Meteorology* **149**: 96–105.

Tranquillini W. **1982**. Frost-drought and its ecological significance. In: Physiological Plant Ecology II. 379–400.

Treydte K, Boda S, Graf Pannatier E, Fonti P, Frank D, Ullrich B, Saurer M, Siegwolf R, Battipaglia G, Werner W, e*t al*. **2014**. Seasonal transfer of oxygen isotopes from precipitation and soil to the tree ring: source water versus needle water enrichment. *New Phytologist* **202**: 772–783.

Tucker CJ. **1979**. Red and photographic infared linear combinations for monitoring vegetation. *Remote Sensing of Environment* **8**: 127–150.

Ulsig L, Nichol C, Huemmrich K, Landis D, Middleton E, Lyapustin A, Mammarella I, Levula J, Porcar-Castell A. **2017**. Detecting inter-annual variations in the phenology of evergreen conifers using long-term MODIS vegetation index time series. *Remote Sensing* **9**: 49.

Vanhatalo A, Chan T, Aalto J, Korhonen JF, Kolari P, Hölttä T, Nikinmaa E, Bäck J. **2015**. Tree water relations can trigger monoterpene emissions from Scots pine stems during spring recovery. *Biogeosciences* **12**: 5353–5363.

Verhoeven A. **2014**. Sustained energy dissipation in winter evergreens. *New Phytologist* **201**: 57–65.

Verrelst J, Rivera JP, Van Der Tol C, Magnani F, Mohammed G, Moreno J. **2015**. Global sensitivity analysis of the SCOPE model: what drives simulated canopy-leaving sun-induced fluorescence? *Remote Sensing of Environment* **166**: 8–21.

Verrelst J, van der Tol C, Magnani F, Sabater N, Rivera JP, Mohammed G, Moreno J. **2016**. Evaluating the predictive power of sun-induced chlorophyll fluorescence to estimate net photosynthesis of vegetation canopies: a SCOPE modeling study. *Remote Sensing of Environment* **176**: 139–151.

Vogelmann TC. **1993**. Plant tissue optics. *Annual Review of Plant Physiology and Plant Molecular Biology* **44**: 231–251.

Vogelmann TC, Evans JR. **2002**. Profiles of light absorption and chlorophyll within spinach leaces from chlorophyll fluorescence. *Plant, Cell & Environment* **25**: 1313–1323.

Vogg G, Heim R, Gotschy B, Beck E, Hansen J. **1998**. Frost hardening and photosynthetic performance of Scots pine (*Pinus sylvestris* L.). II. Seasonal changes in the fluidity of thylakoid membranes. *Planta* **204**: 201–206.

van Wagner C. **1967**. Seasonal variation in moisture content of eastern Canadian tree foliage and the possible effect on crown fires. *Canada Department of Forestry and Rural Development, Forestry Branch, Departmental Publication*: 1–15.

Walther S, Voigt M, Thum T, Gonsamo A, Zhang Y, Köhler P, Jung M, Varlagin A, Guanter L. **2016**. Satellite chlorophyll fluorescence measurements reveal large-scale decoupling of photosynthesis and greenness dynamics in boreal evergreen forests. *Global Change Biology* **22**: 2979–2996.

Wang X, Piao S, Xu X, Ciais P, Macbean N, Myneni RB, Li L. **2015**. Has the advancing onset of spring vegetation green-up slowed down or changed abruptly over the last three decades? *Global Ecology and Biogeography* **24**: 621–631.

Wellburn AR. **1994**. The spectral determination of chlorophylls a and b, as well as total carotenoids, using various solvents with spectrophotometers of different resolution. *Journal of Plant Physiology* **144**: 307–313.

Van Wittenberghe S, Alonso L, Verrelst J, Moreno J, Samson R. **2015**. Bidirectional sun-induced chlorophyll fluorescence emission is influenced by leaf structure and light scattering properties - a bottom-up approach. *Remote Sensing of Environment* **158**: 169–179.

Wong CYS, Gamon JA. **2015a**. The photochemical reflectance index provides an optical indicator of spring photosynthetic activation in evergreen conifers. *New Phytologist* **206**: 196–208.

Wong CYS, Gamon JA. **2015b**. Three causes of variation in the photochemical reflectance index (PRI) in evergreen conifers. *New Phytologist* **206**:

187–195.

Wu SH, Jansson PE, Kolari P. **2011**. Modeling seasonal course of carbon fluxes and evapotranspiration in response to low temperature and moisture in a boreal Scots pine ecosystem. *Ecological Modelling* **222**: 3103–3119.

Wu SH, Jansson PE, Kolari P. **2012**. The role of air and soil temperature in the seasonality of photosynthesis and transpiration in a boreal Scots pine ecosystem. *Agricultural and Forest Meteorology* **156**: 85–103.

Zarco-Tejada PJ, Catalina A, González MR, Martín P. **2013**. Relationships between net photosynthesis and steady-state chlorophyll fluorescence retrieved from airborne hyperspectral imagery. *Remote Sensing of Environment* **136**: 247–258.

Zhang C, Filella I, Garbulsky M, Peñuelas J. **2016**. Affecting factors and recent improvements of the photochemical reflectance index (PRI) for remotely sensing foliar, canopy and ecosystemic radiation-use efficiencies. *Remote Sensing* **8**: 677.

Chapter 3. PRI and passive ChlF (R690/R630) assessment of the photosynthetic activity response to enhanced drought stress and recovery in Mediterranean evergreen leaves

Chao Zhang, Catherine Preece, Iolanda Filella, Gerard Farré-Armengol, Josep Peñuelas

This chapter was submitted to ***Forests***.

Abstract

Monitoring Mediterranean summer drought is highly important because of its increasing frequency of occurrence and its effects on ecosystem functioning. The photochemical reflectance index (PRI) and passive chlorophyll fluorescence (ChlF) are known to be sensitive to plant physiological processes, and through measurement of these optical signals it is possible to use non-invasive remote sensing to monitor the plant photosynthetic status in response to environmental stresses such as drought. Here we explored whether PRI and passive ChlF are sensitive enough to assess not only drought but also recovery after drought. It is also important to explore the feasibility of using passive ChlF obtained from simple reflectance ratios such as R690/R630 in assessing photosynthetic phenology. We thus conducted a greenhouse experiment using *Quercus ilex*, a Mediterranean evergreen oak species, to investigate the links between leaf-level PRI and R690/R630 with CO_2 assimilation rates (A), and photochemical efficiency (F_V/F_M and Yield) in response to a gradient of mild to extreme drought treatments (9 progressively enhanced drought levels) and corresponding recovery. PRI and R690/R630 both decreased under enhanced drought stress, and had significant correlations with A, F_V/F_M and Yield. The differential values between recovery and drought treatments of PRI ($\Delta PRI_{recovery}$) and R690/R630 ($\Delta R690/R630_{recovery}$) increased with the enhanced drought levels, and significantly correlated with the increases of $\Delta A_{recovery}$, $\Delta F_V/F_{Mrecovery}$ and $\Delta Yield_{recovery}$. We concluded that both PRI and R690/R630 were not only sensitive to enhanced drought stresses but also highly sensitive to photosynthetic recovery. Our study makes important progress for remotely monitoring the effect of drought and recovery on photosynthetic regulation using the simple physiological indices of PRI and passive ChlF.

Keywords: chlorophyll fluorescence (ChlF), drought, Mediterranean, photochemical reflectance index (PRI), photosynthesis, R690/R630, recovery

1. Introduction

The increasing occurrence of drought in the Mediterranean region is widely reported (Giorgi & Lionello, 2008; Nicault *et al*., 2008; Hoerling *et al*., 2012) and during the last twenty years observations show that drought has affected ecosystem functioning and structure (Liu *et al*., 2016; Peñuelas *et al*., 2017), decreased plant growth (Granda *et al*., 2013) and primary production (Liu *et al*., 2015; Vicca *et al*., 2016), and triggered vegetation mortality (Barbeta *et al*., 2013). The increase of drought has also enhanced the water scarcity (Iglesias *et al*., 2007), and elicited ecological damage (Lloret *et al*., 2004) and crop failures (Turner, 2004). Faced with these negative impacts, monitoring the timing of drought onset and the extent of the effects on vegetation ecosystems is being increasingly warranted.

Summer drought, one of key constraints of Mediterranean ecosystems (Peñuelas *et al*., 2017), elicit a water deficit in the leaf tissue that can down-regulate photosynthesis (Farquhar & Sharkey, 1982). This reduction in photosynthesis for Mediterranean species such as *Quercus ilex* L. is generally caused by stomatal closure in response to drought stress (Peñuelas *et al*., 1998; Peña-Rojas *et al*., 2004; Ogaya *et al*., 2014). *Quercus ilex* is a broadleaved evergreen tree or shrub that is widely distributed from semi-arid to humid areas of Mediterranean region (de Rigo & Caudullo, 2016). The sclerophyllous characteristics of *Q*. *ilex* make it possible to reduce its transpiration and to withstand the effect of long summer drought. *Quercus ilex* also has the ability to reactivate its photosynthetic machinery and increase photosynthesis rates when the soil water content (SWC) is high enough to again support water transport through the plant (Vaz *et al*., 2010).

When plants suffer water stress, the reducing power from photosynthesis becomes excessive, but then the increases in zeaxanthin pigments from xanthophyll de-epoxidation can safely dissipate excessive energy and prevent the photosystems from potential damage by accumulating excitation energy (Adams & Demmig-Adams, 1994;

Demmig-Adams & Adams, 1996). The photochemical reflectance index (PRI) was firstly defined based on changes in zeaxanthin at the wavelength of 531 nm to assess the efficiency of absorbed photosynthetic active radiation (APAR) for photosynthesis (radiation use efficiency; RUE) (Gamon *et al*., 1992; Peñuelas *et al*., 1995). A great number of studies have found that PRI is able to track RUE changes at diurnal and seasonal scales from leaf, canopy to ecosystem levels (Peñuelas *et al* 2011; Garbulsky *et al*., 2011; Zhang *et al*., 2016), because apart from xanthophyll pigments, PRI was also associated with changes of carotenoid/chlorophyll ratios (Peñuelas *et al*., 1994; Garbulsky *et al*., 2010; Porcar-Castell *et al*., 2012; Wong & Gamon, 2015) which play a key role in long-term dynamics of photosynthesis (Adams & Demmig-Adams, 1994; Frank & Cogdell, 1996). Increasing attention has been focused on using PRI to detect the effect of environmental stress (e.g. intense irradiance, water shortage, nutrition deficit, and high and low temperature stresses) on photosynthetic changes (Filella *et al*., 1996; Peñuelas *et al*., 1997, 1998; Dobrowski *et al*., 2005; Moreno *et al*., 2012; Guarini *et al*., 2014; Sun *et al*., 2014; Vicca *et al*., 2016).

The changes in photosynthesis are synchronously accompanied by the emission of chlorophyll *a* fluorescence (ChlF), which competes with photochemical conversion and heat dissipation of excitation energy to use the absorbed light (Krause & Weis, 1991). The contribution of the ChlF emission is only a small part of the total radiation reflected from vegetation, however, ChlF is highly sensitive to the variability of plant physiological processes in response to various environmental conditions, and can provide a direct approach to detect the functional status of photosynthetic machinery (Lichtenthaler & Miehe, 1997; Porcar-Castell *et al*., 2014). The range of the ChlF emission spectrum is from the red to near-infrared regions, with two peaks at ca. 690 and 740 nm (Lichtenthaler & Miehe, 1997). Both the active (obtained from pulse-amplitude modulated (PAM) fluorometer) and passive (solar-induced fluorescence (SIF) obtained from Fraunhofer Line Depth technique) ChlF are extensively used for monitoring the photosynthetic apparatus at leaf, canopy, ecosystem, regional and global levels using PAM and spectroradiometers that are ground-based or carried on drones,

aircrafts and satellites (Carter *et al*., 1996; Freedman *et al*., 2002; Dobrowski *et al*., 2005; Guanter *et al*., 2014; Zarco-Tejada *et al*., 2016).

The ChlF can also be simply retrieved by reflectance ratios in the bands affected by ChlF emission (mainly bands at two peaks) normalized by bands not affected by ChlF, to remove the spectral information related to the reflectance (Meroni *et al*., 2009), because the ChlF signal is superimposed on the leaf reflectance (Lichtenthaler & Miehe, 1997; Buschmann & Lichtenthaler, 1998). Although this method only provides the relative values of ChlF and not real estimates with physical units, the reflectance ratios such as R690/R600, R690/R630, R690/R655, and R740/R800 have been shown to track the changes in fluorescence, photochemical efficiency and carbon assimilation rates for healthy and stressed plants (Zarco-Tejada *et al*., 2000a,b, 2009; Dobrowski *et al*., 2005; Ač *et al*., 2008, 2009; Furuuchi *et al*., 2013; Ni *et al*., 2015).

Numerous studies had shown that PRI is sensitive to water stress (Zarco-Tejada *et al*., 2009, 2013; Moreno *et al*., 2012; Rossini *et al*., 2013; Panigada *et al*., 2014), but no studies have illustrated that PRI was sensitive enough to track recovery after drought stress, at least to the best of our knowledge. Few studies so far have either exploited the applicability of the reflectance ratio based on ChlF for detecting the photosynthetic response to water stress (Zarco-Tejada *et al*., 2000b, 2009; Dobrowski *et al*., 2005). Only the study by Dobrowski et al. (2005) monitored photosynthetic response to water stress and recovery with only a 4-days long experiment.

Along with the increasing occurrence of drought, it is important to find an easy, non-destructive and efficient method to monitor both the effect of drought on plant physiological and functional variability and subsequent recovery of the photosynthetic machinery. This is particularly important for regions confronted with progressively more extreme summer droughts such as the Mediterranean basin. Based on the previous studies, PRI and ChlF are thus promising methods to test such photosynthetic responses. In this study, we conducted a two-month long greenhouse experiment using the typical Mediterranean species *Q*. *ilex*, by exposing the plants to 9 different progressive drought

treatments through controlling the soil water content (SWC) and then re-watering for 5 weeks to explore the levels of plant recovery. We simultaneously measured foliar reflectance to obtain PRI and reflectance ratio based ChlF (R690/R630), PAM ChlF to get maximum (F_V/F_M) and actual (Yield) photochemical efficiency, and CO_2 assimilation rates (*A*). We hypothesized that both PRI and R690/R630 would be sensitive to the progressively increasing drought, and could therefore be used to monitor photosynthetic dynamics. We also hypothesized that both PRI and R690/R630 would detect the photosynthetic recovery after experiencing different levels of drought stresses.

2. Material and methods

2.1. Experimental design

Three-year old *Quercus ilex* saplings of ca. 60 cm height were obtained in May 2015 (Forestal Catalana, Barcelona, Spain) and were re-potted in 3.5 l pots, with a substrate consisting of 45% sand, 45% autoclaved peat, and 10% natural soil inoculum. The soil was collected from a natural holm oak forest on a south-facing slope (25% slope) in the Prades Mountains in north-eastern Spain (41°13′N, 0°55′E). There were 162 saplings in total, divided into 6 blocks, and plants were grown in the greenhouse of the Autonomous University of Barcelona (Barcelona, Spain) with a 6-week period of adequate watering, to allow them to acclimate to greenhouse conditions. The saplings were then exposed to water stress by withholding water for 9 different drought treatments with 18 plants each. The length of time withholding water ranged from 0 to 21 days. At the end of each treatment, the foliar photochemical efficiency and the reflectance were synchronously measured on half of the pots (nine per drought level) inside the greenhouse under clear skies within one hour of solar noon (12:00 to 14:00h). These pots were then harvested to obtain plant biomass for a related study. The remaining pots then had five weeks of recovery, which involved re-watering at optimal levels, and then identical leaf measurements were collected for these plants.

The water content of the substrate was determined in each pot at the start of the study and at the end of its drought period, and recovery period if relevant, (using ML3

Theta Probe connected to a HH2 Moisture Meter from Delta-T Devices, Cambridge, UK). Mean soil moisture at the start of the experiment was 22.6% and it decreased exponentially to 0.3% at the end of the most extreme drought treatment. Soil moisture recovered quickly to ca. 20% within one week of re-watering and was 24.7% on average during the recovery phase. The differential SWC ($\Delta SWC_{recovery}$) was calculated by subtracting the 9 different drought treatments values from corresponding recovery treatments.

2.2. Leaf photosynthesis measurements

In the greenhouse, the CO_2 assimilation rates (*A*) of leaves were measured using an ADC pro (LCpro1Portable Photosynthesis System; ADC BioScientific Ltd., Hoddesdon, Herts, EN11 0DB) gas exchange system. The measurements were conducted under a quantum flux density of 1000 μmol m^{-2} s^{-1} and ambient CO_2 concentration of 385 μmol mol^{-1}. Five measurements were recorded for each plant. After each measurement, the leaf area that was enclosed in the cuvette was marked on the leaves; leaves were later photographed and the leaf areas for which *A* was measured were estimated using ImageJ 1.46r (NIH, Bethesda, USA) to standardize all *A* measurements. The differential *A* ($\Delta A_{recovery}$) was calculated by subtracting the 9 different drought treatments values from corresponding recovery treatments.

2.3. Chlorophyll fluorescence measurements

Chlorophyll fluorescence measurements were performed by a pulse-amplitude-modulated photosynthesis yield analyser (PAM-2000; Walz, Effeltrich, Germany). The measurements were conducted on three healthy and mature leaves at the top of each plant. A saturating light pulse (SP) was applied to dark-adapted (at least 20 mins) leaves for the determination of minimum (F_o) and maximum (F_M) fluorescence. The maximum photochemical efficiency of photosystem II (PSII) (F_V/F_M) was then calculated according to Genty et al. (1989):

$$F_V/F_M = (F_M-F_o)/F_M \quad (1)$$

In parallel with Fv/Fm, the actual photochemical efficiency of PSII (Yield) was also calculated based on the measurements of steady-state (F_S) and the maximal (F_M')

fluorescence yield during fully closing of PSII center in light adapted leaves:

$$Yield = (F_M'-F_S)/F_M' \quad (2)$$

The differential F_V/F_M ($\Delta F_V/F_{Mrecovery}$) and Yield ($\Delta Yield_{recovery}$) between the 9 different drought treatments values and recovery treatments were also calculated.

2.4. Reflectance measurements

Leaf spectral reflectance measurements were collected using a broad range mini spectroradiometer (LR1; ASEQ, Vancouver, Canada). The instrument measures spectral reflectance between 300 and 1000 nm with a sampling interval of less than 1 nm. To reduce atmospheric condition changes, the spectroradiometer was calibrated using a white Spectralon reference panel (Labsphere, North Sutton, NH, USA), which can be regarded as a Lambertian reflector. Incident solar irradiance was determined using the same white reference panel. All spectral measurements were carried out at a nadir view angle above the leaf. In each plant, we measured three different leaves at the top of the canopy as replicates. The photochemical reflectance index (PRI, Gamon et al., 1992; Peñuelas et al., 1995) was calculated from the reflectance data (Rx implies reflectance at x nm) as:

$$PRI = (R531-R570)/(R531+R570) \quad (3)$$

Additionally, we also retrieved the red chlorophyll fluorescence signal based on the reflectance ratio R690/R630, because in the red reflectance region both PSI and PSII fluorescence emission have effects on leaf reflectance and the reflectance at 630 nm is less or not sensitive to fluorescence emission (Zarco-Tejada *et al*., 2000a).

The differential PRI ($\Delta PRI_{recovery}$) and R690/R630 ($\Delta R690/R630_{recovery}$) were obtained through 9 different drought treatments values subtracted from corresponding recovery treatments.

2.5. Statistical analysis

Differences of soil water content, CO_2 assimilation rate, photochemical efficiency, and reflectance indices between the 9 drought levels and corresponding plant recovery were analyzed using repeated-measures analyses of variance (ANOVAs). The differences were considered statistically significant at $P<0.05$. The applicability of PRI and

R690/R630 for assessing CO_2 assimilation, photochemical efficiency responses to drought stress and recovery were analyzed using standardized major-axis regression to identify correlations between the variables. All analyses were conducted with R version 3.3.2 (R Core Development Team, 2016).

3. Results

3.1. Responses to enhanced drought stress

In our experiment, the *Q. ilex* seedlings were treated by witholding watering from 0 to 21 days in 9 different drought levels treatments. Along with the increasing days of drought and decreasing soil water content (i.e. enhanced drought stress), CO_2 assimilation rates (A) and maximum (F_V/F_M) and actual (Yield) photochemical efficiency decreased from highest values at the beginning of the experiment to lowest values in severe drought condition (Figure 1). The physiological indices of the photochemical reflectance index (PRI) (Figure 1a) and red chlorophyll fluorescence obtained from reflectance ratio ($ChlF_{red}$, R690/R630) (Figure 1b) also decreased gradually. Both changes in PRI and R690/R630 were highly consistent with the decreases in soil water content (SWC), A, F_V/F_M and Yield. However, in the last three extreme drought level treatments, PRI did not change too much.

3.2. Relationships of PRI and R690/R630 with A, F_V/F_M, and Yield under enhanced drought stress

PRI and R690/R630 were used to assess the photosynthetic response to drought stress. Both PRI (Figure 2a) and R690/R630 (Figure 2b) were significantly correlated with A and explained 72% and 86% of variance of A, respectively. PRI had strong relationships with F_V/F_M and Yield ($R^2 \geq 0.85$ and $P<0.001$ for both, Figure 2c). Similar significant correlations were found between R690/R630 and F_V/F_M and Yield ($R^2=0.89$ and $P<0.001$ for both, Figure 2d).

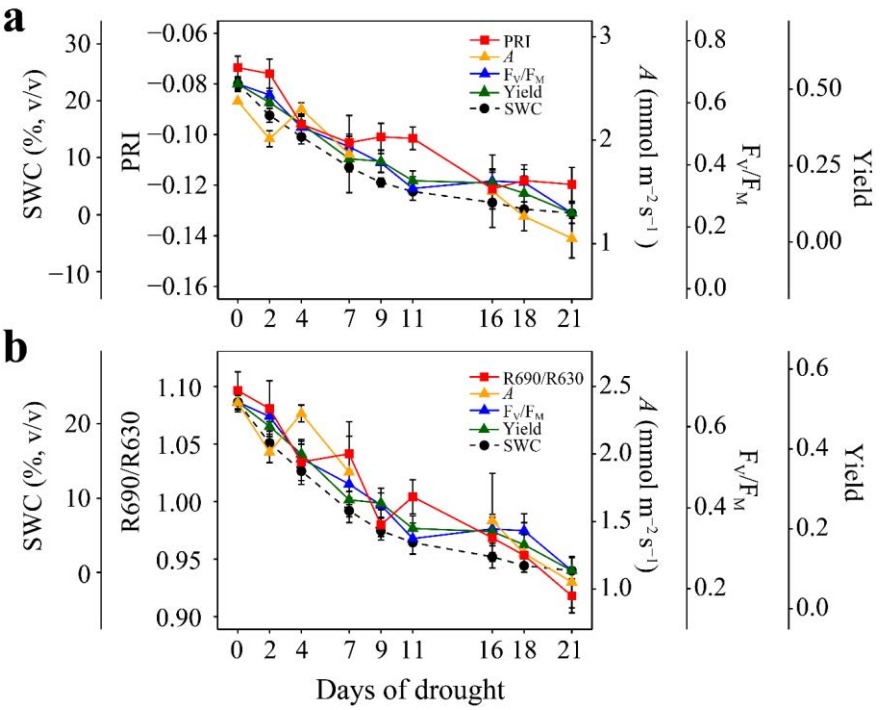

Figure 1. Changes in CO_2 assimilation rates (A), maximum (F_V/F_M) and actual (Yield) photochemical efficiency of PSII, and soil water content (SWC) with the photochemical reflectance index (PRI) (a) and with red fluorescence obtained from reflectance (R690/R630) in response to nine different drought levels treatment for *Quercus ilex*. Error bars denote the standard errors of the mean (n=9).

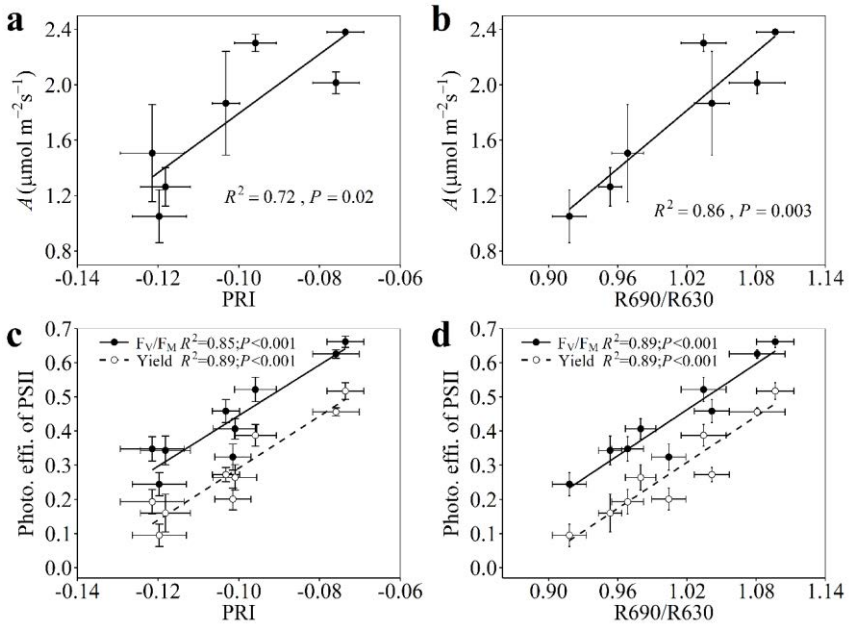

Figure 2. Relationships of A with PRI (a) and R690/R630 (b), photochemical efficiency of PSII (F_V/F_M and Yield) and PRI (c) and R690/R630 (d) for *Quercus ilex*. All the values are from Figure 1.

3.3. Responses to recovery

The SWC (Figure 3a) clearly recovered to the pre-drought condition in all drought treatments after five-weeks re-watering. They all reached identically high values, significantly higher than in the drought treatments from the 4-days drought level treatment onwards (P<0.001). A (Figure 3b) was higher and remained similar in the recovery treatment, particularly in the last three severe drought treatments. All F_V/F_M values (Figure 3c) in the recovery treatment reached up to ca. 0.70 which were similar to the 0-day drought treatment. The mean of F_V/F_M in the 2-days drought level treatment was not different to the mean of the 0-day treatment after five-weeks re-watering. The recovery of F_V/F_M significantly increased from 7-days drought level treatment (P<0.001). Yield (Figure 3d) presented analogous changes with SWC, A, and F_V/F_M, and strongly increased from 9-days drought level treatment (P<0.001). Both PRI (Figure 3e) and R690/R630 (Figure 3f) had no significant difference in first four drought treatments with corresponding recovery treatments, but significantly increased from the recovery treatment of 9-days drought level.

The differential values of variables by subtracting 9 drought levels treatments from corresponding recovery treatments were calculated to assess the changes of photosynthesis after one-month re-watering the plants of the drought treatment and to evaluate the applicability of PRI and R690/R630 in detecting the recovery of that. The values of $\Delta A_{recovery}$, $\Delta F_V/F_{Mrecovery}$, and $\Delta Yield_{recovery}$ increased in conjunction with increasing ΔSWC and increasing drought levels (Figure 4). Both $\Delta F_V/F_{Mrecovery}$ and $\Delta Yield_{recovery}$ increased slowly in the last three drought levels. Changes in $\Delta PRI_{recovery}$ (Figure 4a) were consistent with $\Delta A_{recovery}$, $\Delta F_V/F_{Mrecovery}$, and $\Delta Yield_{recovery}$. $\Delta R690/R630_{recovery}$ (Figure 4b) also showed a gradual increase as with the other variables, with a high value in the 9-days drought level treatment.

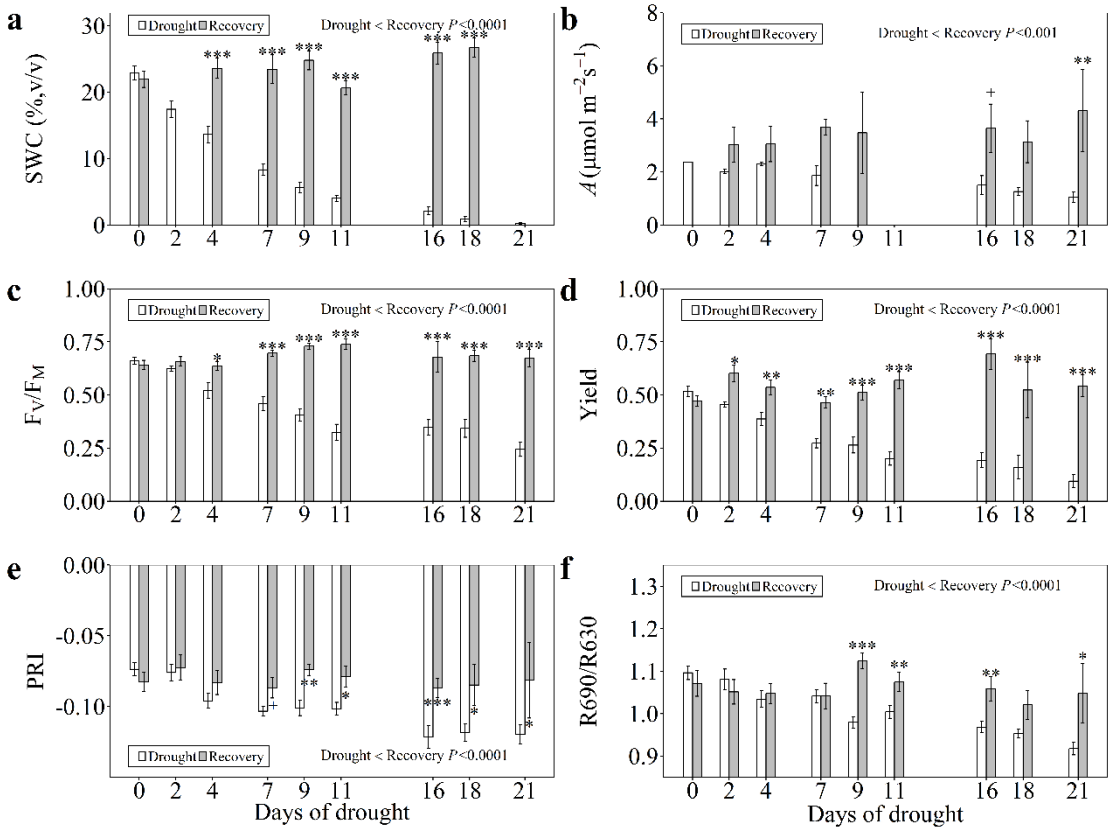

Figure 3. Changes in SWC (a), *A* (b), F_V/F_M (c), Yield (d), PRI (e) and R690/R630 (f) in response to nine different drought levels and corresponding recovery treatments for *Quercus ilex*. The significances were denoted as $^{+}p<0.1$, $*p<0.05$, $**p<0.01$ and $***p<0.001$.

3.4. Relationships of $\Delta PRI_{recovery}$ and $\Delta R690/R630_{recovery}$ with $\Delta A_{recovery}$, $\Delta F_V/F_{Mrecovery}$, and $\Delta Yield_{recovery}$

Both $\Delta PRI_{recovery}$ and $\Delta R690/R630_{recovery}$ accounted for large proportions of the variability of $\Delta A_{recovery}$ ($R^2 \geq 0.70$ and $P<0.05$ for both, Figure 5a, b). $\Delta PRI_{recovery}$ was highly significantly correlated with $\Delta F_V/F_{Mrecovery}$ and $\Delta Yield_{recovery}$ ($R^2 \geq 0.85$ and $P<0.001$ for both, Figure 5c). The relationships of $\Delta R690/R630_{recovery}$ with $\Delta F_V/F_{Mrecovery}$ and $\Delta Yield_{recovery}$ were also significant, but they were not as good as those of $\Delta PRI_{recovery}$ with $\Delta F_V/F_{Mrecovery}$ and $\Delta Yield_{recovery}$ (Figure 5d).

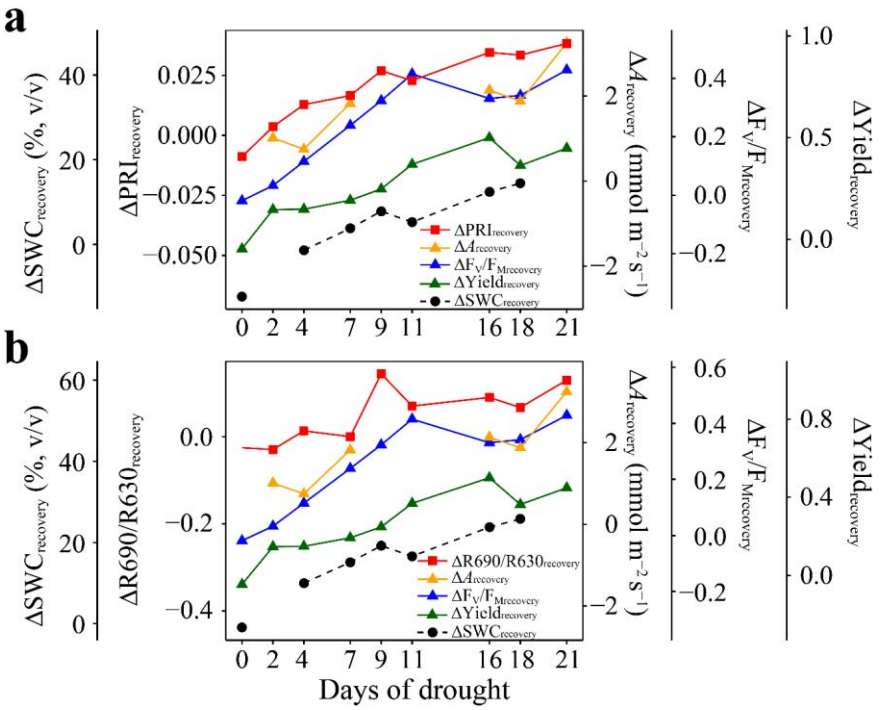

Figure 4. Changes in differential *A* (Δ*A*), $\Delta F_V/F_M$, ΔYield, and ΔSWC with ΔPRI (a) and with ΔR690/R630 in response to nine different drought levels for *Quercus ilex*. The differential values of variables calculated by subtracting the mean of 9 drought levels treatment from corresponding mean of recovery treatments in Figure 3.

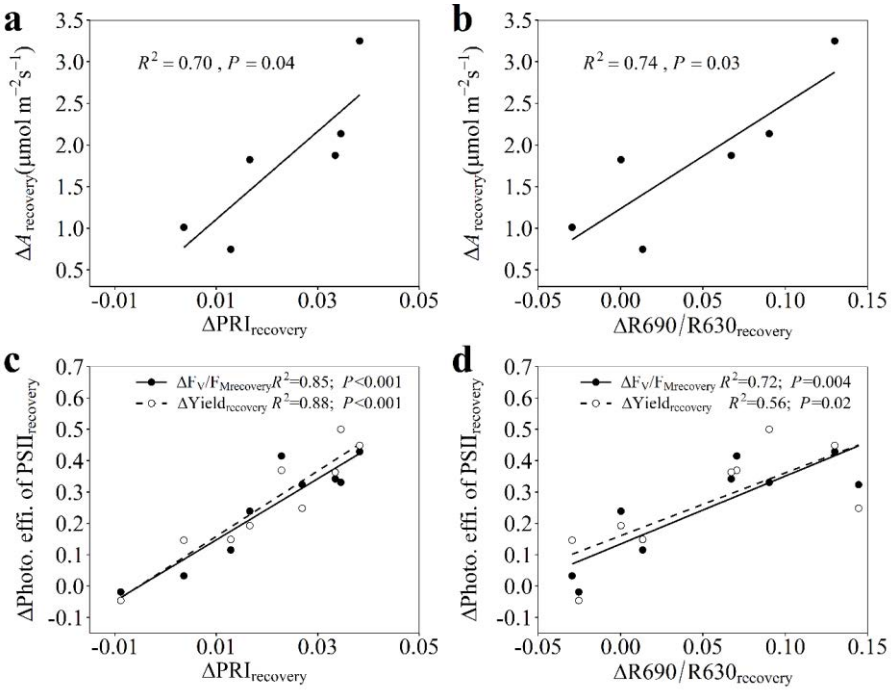

Figure 5. Relationships of differential PRI (ΔPRI) and R690/R630 (ΔR690/R630) with differential *A* (Δ *A*) and photochemical efficiency ($\Delta F_V/F_M$ and ΔYield) for *Quercus ilex*. All the differential values are from Figure 4

4. Discussion

4.1. PRI and R690/R630 tracked the photosynthetic changes under enhanced drought levels

The enhanced levels of drought caused reductions in CO_2 assimilation rates (*A*) and photochemical efficiency (F_V/F_M and Yield) in Mediterranean evergreen leaves (Figure 1). Similar trends were also recorded for the photochemical reflectance index (PRI, Figure 1a) and the reflectance ratio based on chlorophyll fluorescence (ChlF) (R690/R630, Figure 1b), indicating the sensitivity of PRI and R690/R630 to gradually increased drought stress. The close correspondence of PRI and R690/R630 with photosynthetic activity (Figure 3a) and photochemical efficiency (Figure 3b) demonstrated the promise of pigment- or red ChlF-based approaches to remotely monitoring of evergreen photosynthetic activity under gradually enhanced drought.

PRI, is used to reveal the facultative xanthophyll cycle activity at short-term scale (hours to few days) (Gamon *et al*., 1992; Peñuelas *et al*., 1994, 1995) but also to estimate the changes in the constitutive pigment pool size at long-term scale (weeks to months) (Filella *et al*., 2009; Gamon & Berry, 2012; Porcar-Castell *et al*., 2012; Wong & Gamon, 2015). In our study, PRI showed promise as an index of photosynthetic down-regulation and illustrated the activation of photoprotective carotenoid pigments under photosynthetic down-regulation in response to gradually enhanced drought stress. During the summer drying period, leaves in evergreen vegetation of semi-arid Mediterranean region experience decreases in pigment contents and increases in carotenoids/chlorophyll (Car/Chl) ratio (Baquedano & Castillo, 2006). This change in Car/Chl ratios play a key role in photosynthetic down-regulation, and is associated with variability in PRI (Filella *et al*., 2009; Porcar-Castell *et al*., 2012). PRI thus detected the effect of the progressive drought on photosynthesis, consistent with many previous studies that demonstrated PRI was correlated with photosynthesis and Yield under water stress conditions (Peñuelas *et al*., 1997, 1998).

Additionally, PRI was quite stable in the last three extreme drought level treatments (plants without water for 16-21 days), unlike the slight decrease of *A*, F_V/F_M,

Yield, and R690/R630, reflecting the insensitivity of PRI to severe drought, at intensities where there is observable leaf fall. Previous leaf level studies have reported that PRI was unable to assess the negative radiation-use efficiency (RUE) of severely damaged plants (Peñuelas *et al*., 1997). At canopy level, changes in structure, heterogeneity in irradiance, and differences in sun angles within crown hindered PRI interpretation and assessment of RUE (Zhang *et al*., 2016). At larger spatial scales, satellite-based (Moderate Resolution Imaging Spectroradiometer, MODIS) PRI has tracked ecosystem RUE even during severe water limitation of summer time for *Q*. *ilex* (Goerner *et al*., 2009). The normalized PRI by absorbed light detected the drought effect on gross primary production (GPP) in a deciduous forest and an evergreen broadleaf forest in France, but did not capture the reduction of GPP in a semi-arid grassland in Hungary (Vicca *et al*., 2016). Guarini et al. (2014) demonstrated that MODIS-based PRI should be used with care under severe water stress, because the disturbances from canopy structure, illumination and viewing angles etc. could increase the uncertainty of PRI in tracking RUE. These studies presented the complications of the applicability of PRI under severe drought conditions at different spatial scales, and other factors, such as soil backgrounds, vegetation functional types, atmospheric interference and instrument characteristics can also complicate the applications of PRI in assessing RUE (Zhang *et al*., 2016). However, the strong correlations between PRI and *A* and photosynthetic efficiency (F_V/F_M and Yield,) under enhanced drought levels demonstrate that PRI can be applied to detect the effect of continuously increased drought on photosynthesis for Mediterranean evergreen sclerophylls which generally experience summer drought.

The recent progress in canopy, regional and global studies of SIF (Meroni *et al*., 2009; Porcar-Castell *et al*., 2014; Ač *et al*., 2015) support the use of leaf-level passive ChlF as a non-invasive method of assessing photosynthetic activity. Interestingly, the reflectance ratio based ChlF, R690/R630 obtained from leaf spectra presented highly significant correlations with *A*, F_V/F_M, and Yield, and efficiently tracked the photosynthetic changes in response to enhanced drought levels (Figure 2b,d). Our study

not only made progress on the assessment of photosynthesis of leaf-level passive ChlF, but also provided a simple method of obtaining passive ChlF using apparent reflectance.

R690/R630 was defined to obtain red ChlF because of the superimposed ChlF emission at red reflectance. The reference band (R630) was chosen due to its insensitivity to ChlF and sensitivity to chlorophyll pigments (Zarco-Tejada *et al*., 2000a). Thus the R690/R630 can give a potential estimation of relative ChlF. It should be noted that the reabsorption of red ChlF (particularly at ChlF emission peak near 690 nm) by chlorophyll pigments can affect the measurement of passive ChlF (Buschmann & Lichtenthaler, 1998). However, in our study, the chlorophyll contents should have been rather constant due to the characteristics of evergreen species, which probably contributed to estimating ChlF and tracking photosynthetic changes of R690/R630. Further studies of the reflectance ratio based ChlF should be focused on plants with obvious changes in chlorophyll contents.

Additionally, the down-regulation of maximum photochemical efficiency (F_V/F_M) is associated with changes of non-photochemical quenching (NPQ) under environmental stress (Demmig-Adams & Adams, 2006; Porcar-Castell, 2011; Verhoeven, 2014). The significant correlation of R690/R630 with F_V/F_M in this and previous diurnal studies (Zarco-Tejada *et al*., 2000a,b) indicated that NPQ probably plays a key role in linking R690/R630 with changes in photosynthetic activity. Although PRI was also highly correlated with F_V/F_M, the rather constant PRI in the extreme drought conditions (the last three drought treatments) was decoupled with the strong depression of F_V/F_M. Such decoupling of PRI with RUE and NPQ was also found in early spring when Scots pine needles confronted deep down-regulation due to the effect of severe stress (Porcar-Castell *et al*., 2012). In contrast, in our study R690/R630 presented consistent changes with F_V/F_M, Yield and *A* even under extreme water stress conditions.

4.2. PRI and R690/R630 tracked the photosynthetic recovery from progressively

enhanced drought stresses

The CO_2 assimilation rates and photochemical efficiency of *Q*. *ilex* were rapidly recovered to normal values through five weeks of re-watering (Figure 3). The values of PRI and R690/R630 were increased to similar values after re-watering, indicating that both PRI and R690/R630 were also sensitive to the recovery of plant. The significant correlations of differential PRI ($\Delta PRI_{recovery}$) and R690/R630 ($\Delta R690/R630_{recovery}$) with $\Delta A_{recovery}$, $\Delta F_V/F_{Mrecovery}$ and $\Delta Yield_{recovery}$ (Figure 5) illustrated their potential to monitor photosynthetic recovery response to drought stress.

PRI was originally defined to detect the variability of zeaxanthin changes at 531 nm (Gamon *et al*., 1992; Peñuelas et al 1005). However, it should be noted that 531 nm was the band associated with carotenoid pigment changes, including zeaxanthin and also other carotenoid pigments such as lutein and neoxanthin (Gitelson *et al*., 2002). These carotenoids both play key roles in energy dissipation of photosynthetic down- and up-regulation (Ruban *et al*., 2007; Jahns & Holzwarth, 2012). However, studies had demonstrated that constitutive long-term changes of PRI were greatly attributable to carotenoid pigment pool sizes (Filella *et al*., 2009; Gamon & Berry, 2012; Porcar-Castell *et al*., 2012; Wong & Gamon, 2015).Thus, the mechanism of PRI detecting photosynthetic recovery probably was due to the carotenoid pigments acting on the photochemical process. Also during water stress and recovery, PRI was significantly correlated with carotenoid pigments in olive saplings (Sun *et al*., 2014).

In contrast with PRI, ChlF is the energy of absorbed photosynthetically active radiation (APAR) that is lost during the first steps of photosynthesis which involves the emission of red to far-red light (ca. 660 to 800 nm) (Porcar-Castell *et al*., 2014). ChlF is therefore associated with the fraction of APAR and also with radiation-use efficiency (RUE), giving the possibility of using R690/R630 to monitor the photosynthetic recovery after experiencing different drought stresses. Additionally, ChlF is mainly emitted from photosystem II (PSII), so the recovery of photochemistry could increase the ChlF emission, particularly in red wavelengths close to 690 nm which is the absorption peak of the pigment of PSII (Buschmann & Lichtenthaler, 1998; Porcar-

Castell *et al*., 2014). Consequently, R690/R630 is a good indicator of photosynthetic recovery in response to progressive drought stress for evergreen leaves.

5. Conclusions and final remarks

This study makes significant progress in assessing mild to extreme drought stresses in Mediterranean evergreen species using PRI and passive ChlF. Both PRI and red ChlF obtained from the reflectance ratio R690/R630 were not only sensitive to progressive drought but also to plant recovery. Both PRI and R690/R630 significantly tracked the photosynthetic response to enhanced drought levels and also detected the photosynthetic recovery after five-weeks of re-watering. Both PRI and R690/R630 can be used for remotely monitoring the effect of drought on the carbon uptake and productivity of the Mediterranean species.

Our work also promotes the possibility of parameterizing RUE models based on the PRI, SIF and normalized difference vegetation index (NDVI). This is because of links between NDVI with greenness changes in annual and deciduous vegetation, PRI with short and rapid changes in xanthophyll pigments and long-term shifts in pigment pools, and SIF with the fraction of absorbed photosynthetically active radiation and radiation-use efficiency (Gamon, 2015). Increasing use of hyperspectral spectraradiometers carried on unmanned aerial vehicles (UAVs) (Gago *et al*., 2015) and satellites (such as Metop and Sentinel series) provides the possibility of testing the RUE model using PRI, SIF and NDVI for multiple vegetation types and at different spatiotemporal scales.

References

Ač A, Malenovský Z, Hanuš J, Tomášková I, Urban O, Marek M V. 2009. Near-distance imaging spectroscopy investigating chlorophyll fluorescence and photosynthetic activity of grassland in the daily course. *Functional Plant Biology* **36**: 1006–1015.

Ač A, Malenovský Z, Olejníčková J, Gallé A, Rascher U, Mohammed G. 2015. Meta-analysis assessing potential of steady-state chlorophyll fluorescence for remote sensing detection of plant water, temperature and nitrogen stress. *Remote sensing of environment* **168**: 420–436.

Ač A, Olejníčková J, Mishra KB, Malenovský Z, Hanuš J, Trtílek M, Nedbal L, Marek M V. 2008. Towards remote sensing of vegetation processes. In: Proceedings Workshop Sensing a Changing World. 19–23.

Adams WW, Demmig-Adams B. 1994. Carotenoid composition and down regulation of photosystem II in three conifer species during the winter. *Physiologia Plantarum* **92**: 451–458.

Baquedano FJ, Castillo FJ. 2006. Comparative ecophysiological effects of drought on seedlings of the Mediterranean water-saver *Pinus halepensis* and water-spenders *Quercus coccifera* and *Quercus ilex*. *Trees - Structure and Function* **20**: 689–700.

Barbeta A, Ogaya R, Peñuelas J. 2013. Dampening effects of long-term experimental drought on growth and mortality rates of a Holm oak forest. *Global Change Biology* **19**: 3133–3144.

Buschmann C, Lichtenthaler HK. 1998. Principles and characteristics of multi-colour fluorescence imaging of plants. *Journal of Plant Physiology* **152**: 297–314.

Carter GA, Jones JH, Mitchell RJ, Brewer CH. 1996. Detection of solar-excited chlorophyll a fluorescence and leaf photosynthetic capacity using a Fraunhofer Line Radiometer. *Remote Sensing of Environment* **55**: 89–92.

Demmig-Adams B, Adams WW. 1996. The role of xanthophyll cycle carotenoids in the protection of photosynthesis. *Trends in Plant Science* **1**: 21–26.

Demmig-Adams B, Adams WW. 2006. Photoprotection in an ecological context: the remarkable complexity of thermal energy dissipation. *New Phytologist* **172**: 11–21.

Dobrowski SZ, Pushnik JC, Zarco-Tejada PJ, Ustin SL. 2005. Simple reflectance indices track heat and water stress-induced changes in steady-state chlorophyll fluorescence at the canopy scale. *Remote Sensing of Environment* **97**: 403–414.

Farquhar GD, Sharkey TD. 1982. Stomatal conductance and photosynthesis. *Annual review of plant physiology* **33**: 317–345.

Filella I, Amaro T, Araus JL, Peñuelas J. 1996. Relationship between photosynthetic radiation-use efficiency of barley canopies and the photochemical reflectance index (PRI). *Physiologia Plantarum* **96**: 211–216.

Filella I, Porcar-Castell A, Munné-Bosch S, Bäck J, Garbulsky MF, Peñuelas J. 2009. PRI assessment of long-term changes in carotenoids/chlorophyll ratio and short-term changes in de-epoxidation state of the xanthophyll cycle. *International Journal of Remote Sensing* **30**: 4443–4455.

Frank HA, Cogdell RJ. 1996. Carotenoids in photosynthesis. *Photochemistry and Photobiology* **63**: 257–264.

Freedman A, Cavender-Bares J, Kebabian PL, Bhaskar R, Scott H, Bazzaz FA. 2002. Remote sensing of solar-excited plant fluorescence as a measure of photosynthetic rate. *Photosynthetica* **40**: 127–132.

Furuuchi H, Jenkins MW, Senock RS, Houpis JLJ, Pushnik JC. 2013. Estimating plant crown transpiration and water use efficiency by vegetative reflectance indices associated with chlorophyll fluorescence. *Open Journal of Ecology* **3**: 122–132.

Gago J, Douthe C, Coopman RE, Gallego PP, Ribas-Carbo M, Flexas J, Escalona J, Medrano H. 2015. UAVs challenge to assess water stress for sustainable agriculture. *Agricultural Water Management* **153**: 9–19.

Gamon JA. 2015. Reviews and Syntheses: optical sampling of the flux tower footprint. *Biogeosciences* **12**: 4509–4523.

Gamon JA, Berry JA. 2012. Facultative and constitutive pigment effects on the photochemical reflectance index (PRI) in sun and shade conifer needles. *Israel Journal of Plant Sciences* **60**: 85–95.

Gamon JA, Peñuelas J, Field C. 1992. A narrow-waveband spectral index that tracks diurnal changes in photosunthetic efficiency. *Remote Sensing of Environment* **41**: 35–44.

Garbulsky MF, Peñuelas J, Gamon J, Inoue Y, Filella I. 2011. The photochemical reflectance index (PRI) and the remote sensing of leaf, canopy and ecosystem radiation use efficiencies. A review and meta-analysis. *Remote Sensing of Environment* **115**: 281–297.

Garbulsky MF, Peñuelas J, Papale D, Ardö J, Goulden ML, Kiely G, Richardson AD, Rotenberg E, Veenendaal EM, Filella I. 2010. Patterns and controls of the variability of radiation use efficiency and primary productivity across terrestrial ecosystems. *Global Ecology and*

Biogeography **19**: 253–267.

Genty B, Briantais J-M, Baker NR. **1989**. The relationship between the quantum yield of photosynthetic electron transport and quenching of chlorophyll fluorescence. *Biochimica et Biophysica Acta (BBA) - General Subjects* **990**: 87–92.

Giorgi F, Lionello P. **2008**. Climate change projections for the Mediterranean region. *Global and Planetary Change* **63**: 90–104.

Gitelson AA, Zur Y, Chivkunova OB, Merzlyak MN. **2002**. Assessing carotenoid content in plant leaves with reflectance spectroscopy. *Photochemistry and Photobiology* **75**: 272–281.

Goerner A, Reichstein M, Rambal S. **2009**. Tracking seasonal drought effects on ecosystem light use efficiency with satellite-based PRI in a Mediterranean forest. *Remote Sensing of Environment* **113**: 1101–1111.

Granda E, Camarero JJ, Gimeno TE, Martínez-Fernández J, Valladares F. **2013**. Intensity and timing of warming and drought differentially affect growth patterns of co-occurring Mediterranean tree species. *European Journal of Forest Research* **132**: 469–480.

Guanter L, Zhang Y, Jung M, Joiner J, Voigt M, Berry JA, Frankenberg C, Huete AR, Zarco-Tejada P, Lee J-E, e*t al*. **2014**. Global and time-resolved monitoring of crop photosynthesis with chlorophyll fluorescence. *Proceedings of the National Academy of Sciences of the United States of America* **111**: E1327-33.

Guarini R, Nichol C, Clement R, Loizzo R, Grace J, Borghetti M. **2014**. The utility of MODIS-sPRI for investigating the photosynthetic light-use efficiency in a Mediterranean deciduous forest. *International Journal of Remote Sensing* **35**: 6157–6172.

Hoerling M, Eischeid J, Perlwitz J, Quan X, Zhang T, Pegion P. **2012**. On the increased frequency of Mediterranean drought. *Journal of Climate* **25**: 2146–2161.

Iglesias A, Garrote L, Flores F, Moneo M. **2007**. Challenges to manage the risk of water scarcity and climate change in the Mediterranean. *Water Resources Management* **21**: 775–788.

Jahns P, Holzwarth AR. **2012**. The role of the xanthophyll cycle and of lutein in photoprotection of photosystem II. *Biochimica et Biophysica Acta - Bioenergetics* **1817**: 182–193.

Krause G, Weis E. **1991**. Chlorophyll fluorescence and photosynthesis: the basics. *Annual Review of Plant Physiology and Plant Molecular Biology* **42**: 313–349.

Lichtenthaler HK, Miehe J a. 1997. Fluorescence imaging as a diagnostic tool for plant stress. *Trends in plant sciece* **2**: 316–320.

Liu D, Llusià J, Ogaya R, Estiarte M, Llorens L, Yang X, Peñuelas J. **2016**. Physiological adjustments of a Mediterranean shrub to long-term experimental warming and drought treatments. *Plant Science* **252**: 53–61.

Liu D, Ogaya R, Barbeta A, Yang X, Peñuelas J. **2015**. Contrasting impacts of continuous moderate drought and episodic severe droughts on the aboveground-biomass increment and litterfall of three coexisting Mediterranean woody species. *Global Change Biology* **21**: 4196–4209.

Lloret F, Siscart D, Dalmases C. **2004**. Canopy recovery after drought dieback in holm-oak Mediterranean forests of Catalonia (NE Spain). *Global Change Biology* **10**: 2092–2099.

Meroni M, Rossini M, Guanter L, Alonso L, Rascher U, Colombo R, Moreno J. **2009**. Remote sensing of solar-induced chlorophyll fluorescence: review of methods and applications. *Remote Sensing of Environment* **113**: 2037–2051.

Moreno A, Maselli F, Gilabert MA, Chiesi M, Martínez B, Seufert G. **2012**. Assessment of MODIS imagery to track light-use efficiency in a water-limited Mediterranean pine forest. *Remote Sensing of Environment* **123**: 359–367.

Ni ZY, Liu ZG, Li ZL, Nerry F, Huo HY, Li XW. **2015**. Estimation of solar-induced fluorescence using the canopy reflectance index. *International Journal of Remote Sensing* **36**: 5239–5256.

Nicault A, Alleaume S, Brewer S, Carrer M, Nola P, Guiot J. **2008**. Mediterranean drought fluctuation during the last 500 years based on tree-ring data. *Climate Dynamics* **31**: 227–245.

Ogaya R, Llusià J, Barbeta A, Asensio D, Liu D, Alessio GA, Peñuelas J. **2014**. Foliar CO2 in a holm oak forest subjected to 15 years of climate change simulation. *Plant Science* **226**: 101–107.

Panigada C, Rossini M, Meroni M, Cilia C, Busetto L, Amaducci S, Boschetti M, Cogliati S, Picchi V, Pinto F, e*t al*. **2014**. Fluorescence, PRI and canopy temperature for water stress detection in cereal crops. *International Journal of Applied Earth Observation and Geoinformation* **30**: 167–178.

Peña-Rojas K, Aranda X, Fleck I. **2004**. Stomatal limitation to CO2 assimilation and down-regulation of photosynthesis in *Quercus ilex* resprouts in response to slowly imposed drought. *Tree physiology* **24**: 813–22.

Peñuelas J, Filella I, Gamon JA. **1995**. Assessment of photosynthetic radiation use efficiency with spectral reflectance. *New Phytologist* **131**: 291–296.

Peñuelas J, Filella I, Llusià J, Siscart D, Pinol J. **1998**. Comparative field study of spring and summer leaf gas exchange and photobiology of the mediterranean trees *Quercus ilex* and *Phillyrea latifolia*. *Journal of Experimental Botany* **49**: 229–238.

Peñuelas J, Garbulsky MF, Filella I. 2011. Photochemical reflectance index (PRI) and

remote sensing of plant CO_2 uptake. *New Phytologist* **191**(3): 596–599.

Peñuelas J, Gamon JA, Fredeen AL, Merino J, Field CB. **1994**. Reflectance indices associated with physiological changes in nitrogen- and water-limited sunflower leaves. *Remote Sensing of Environment* **48**: 135–146.

Peñuelas J, Llusià J, Pinol J, Filella I, Peñuelas J, Llusià J, Pinol J, Filella I. **1997**. Photochemical reflectance index and leaf photosynthetic radiation-use-efficiency assessment in Mediterranean trees. *International Journal of Remote Sensing* **18**: 2863–2868.

Peñuelas J, Sardans J, Filella I, Estiarte M, Llusià J, Ogaya R, Carnicer J, Bartrons M, Rivas-Ubach A, Grau O, e*t al*. **2017**. Assessment of the impacts of climate change on Mediterranean terrestrial ecosystems based on data from field experiments and long-term monitored field gradients in Catalonia. *Environmental and Experimental Botany*.

Porcar-Castell A. **2011**. A high-resolution portrait of the annual dynamics of photochemical and non-photochemical quenching in needles of *Pinus sylvestris*. *Physiologia Plantarum* **143**: 139–153.

Porcar-Castell A, Garcia-Plazaola JI, Nichol CJ, Kolari P, Olascoaga B, Kuusinen N, Fernández-Marín B, Pulkkinen M, Juurola E, Nikinmaa E. **2012**. Physiology of the seasonal relationship between the photochemical reflectance index and photosynthetic light use efficiency. *Oecologia* **170**: 313–323.

Porcar-Castell A, Tyystjärvi E, Atherton J, Van Der Tol C, Flexas J, Pfündel EE, Moreno J, Frankenberg C, Berry JA. **2014**. Linking chlorophyll a fluorescence to photosynthesis for remote sensing applications: mechanisms and challenges. *Journal of Experimental Botany* **65**: 4065–4095.

de Rigo D, Caudullo G. **2016**. *Quercus ilex* in Europe: distribution, habitat, usage and threats. In: European Atlas of Forest Tree Species, Publ. Off. EU, Luxembourg. 130–131.

Rossini M, Fava F, Cogliati S, Meroni M, Marchesi A, Panigada C, Giardino C, Busetto L, Migliavacca M, Amaducci S, e*t al*. **2013**. Assessing canopy PRI from airborne imagery to map water stress in maize. *ISPRS Journal of Photogrammetry and Remote Sensing* **86**: 168–177.

Ruban A V., Berera R, Ilioaia C, van Stokkum IHM, Kennis JTM, Pascal A a, van Amerongen H, Robert B, Horton P, van Grondelle R. **2007**. Identification of a mechanism of photoprotective energy dissipation in higher plants. *Nature* **450**: 575–578.

Sun P, Wahbi S, Tsonev T, Haworth M, Liu S, Centritto M. **2014**. On the use of leaf spectral indices to assess water status and photosynthetic limitations in *Olea europaea* L. during water-stress and recovery. *PLOS ONE* **9**.

Turner NC. **2004**. Sustainable production of crops and pastures under drought in a Mediterranean environment. *Annals of Applied Biology* **144**: 139–147.

Vaz M, Pereira JS, Gazarini LC, David TS, David JS, Rodrigues A, Maroco J, Chaves MM. **2010**. Drought-induced photosynthetic inhibition and autumn recovery in two Mediterranean oak species (*Quercus ilex* and *Quercus suber*). *Tree Physiology* **30**: 946–956.

Verhoeven A. **2014**. Sustained energy dissipation in winter evergreens. *New Phytologist* **201**: 57–65.

Vicca S, Balzarolo M, Filella I, Granier A, Herbst M, Knohl A, Longdoz B, Mund M, Nagy Z, Pintér K, e*t al*. **2016**. Remotely-sensed detection of effects of extreme droughts on gross primary production. *Scientific Reports* **6**: 28269.

Wong CYS, Gamon JA. **2015**. Three causes of variation in the photochemical reflectance index (PRI) in evergreen conifers. *New Phytologist* **206**: 187–195.

Zarco-Tejada PJ, Berni JAJ, Suárez L, Sepulcre-Cantó G, Morales F, Miller JR. **2009**. Imaging chlorophyll fluorescence with an airborne narrow-band multispectral camera for vegetation stress detection. *Remote Sensing of Environment* **113**: 1262–1275.

Zarco-Tejada PJ, González-Dugo M V., Fereres E. **2016**. Seasonal stability of chlorophyll fluorescence quantified from airborne hyperspectral imagery as an indicator of net photosynthesis in the context of precision agriculture. *Remote Sensing of Environment* **179**: 89–103.

Zarco-Tejada PJ, González-Dugo V, Williams LE, Suárez L, Berni JAJ, Goldhamer D, Fereres E. **2013**. A PRI-based water stress index combining structural and chlorophyll effects: assessment using diurnal narrow-band airborne imagery and the CWSI thermal index. *Remote Sensing of Environment* **138**: 38–50.

Zarco-Tejada PJ, Miller JR, Mohammed GH, Nolan TL. **2000a**. Chlorophyll fluoresence effects on vegetation apparent reflectanc: I. Leaf-level measurements and model simulation. *Remote Sensing of Environment* **74**: 582–592.

Zarco-Tejada PJ, Miller JR, Mohammed GH, Noland TL, Sampson PH. **2000b**. Chlorophyll fluorescence effects on vegetation apparent reflectance: II. Laboratory and Airborne canopy-level measurements with hyperspectral data. *Remote Sensing of Environment* **74**: 596–608.

Zhang C, Filella I, Garbulsky M, Peñuelas J. **2016**. Affecting factors and recent improvements of the photochemical reflectance index (PRI) for remotely sensing foliar, canopy and ecosystemic radiation-use efficiencies. *Remote Sensing* **8**: 67

Chapter 4. Photochemical reflectance index (PRI) for detecting responses of diurnal and seasonal photosynthetic activity to experimental drought and warming in a Mediterranean shrubland

Chao Zhang, Iolanda Filella, Daijun Liu, Joan Llusià, Dolores Asensio and Josep Peñuelas

This chapter is under review in ***Remote Sensing of Environment.***

Abstract

Climatic warming and drying are having profound impacts on terrestrial carbon cycling by altering plant physiological traits and photosynthetic processes, particularly for the species in the semi-arid Mediterranean ecosystems. More effective methods of remote sensing are needed to accurately assess the physiological responses and the seasonal photosynthetic activities of evergreen species to climate change. We evaluated the stand reflectance in parallel to the diurnal and seasonal changes in gas exchange, fluorescence and water contents of leaves and soil for a Mediterranean evergreen shrub, *Erica multiflora*, submitted to long-term experimental warming and drought. We also calculated a differential photochemical reflectance index (ΔPRI, morning PRI subtracted from midday PRI) to assess the diurnal responses of photosynthesis (Δ*A*) to warming and drought. The results indicated that the PRI, but not the normalized difference vegetation index (NDVI), was able to assess the seasonal changes of photosynthesis. Changes in water index (WI) were consistent with seasonal foliar water content (WC). In the warming treatment, Δ*A* value was higher than control in winter but was significantly lower in both summer and autumn, demonstrating the positive effect of the warming on the photosynthesis in winter and the negative effect in summer and autumn, i.e., increased photosynthetic midday depression in summer and autumn. Drought treatment increased the midday depression of photosynthesis in spring and summer. Importantly, ΔPRI was significantly correlated with Δ*A* both under warming and drought, indicating the applicability of ΔPRI for tracking the midday depression of photosynthetic processes. Using PRI and ΔPRI to monitor the variability in photosynthesis could provide a simple method to remotely sense photosynthetic seasonality and midday depression in response to ongoing and future environmental stresses.

Keywords: drought; evergreen; midday depression; photochemical reflectance index (PRI); photosynthesis; remote sensing; warming; water index (WI)

1. Introduction

Droughts have occurred frequently under global warming around the world (Dai, 2011; Vicente-Serrano et al., 2014), prominently disturbing terrestrial ecosystemic services and functioning, such as water cycles (Sheffield *et al*., 2012), terrestrial production (Ciais *et al*., 2005; Yuan *et al*., 2016), ecosystemic respiration (Ciais *et al*., 2005), biodiversity (Bertrand *et al*., 2016) and plant survival and mortality (Carnicer *et al*., 2011; McDowell *et al*., 2008). Increases in climatic warming and drought projected by some global models (Dai, 2011; Sheffield and Wood, 2008) could profoundly affect Mediterranean ecosystems (Giorgi and Lionello, 2008; Nardini *et al*., 2014; Peñuelas *et al*., 2013; Peñuelas *et al*., in press), regions highly susceptible to climate change due to the interaction between heat and aridity. Higher temperatures and lower precipitation in the coming decades (Cook *et al*., 2016; Giorgi and Lionello, 2008) are expected to change community structure (Liu *et al*., 2017) and decrease photosynthesis (Liu *et al*., 2016; Wu *et al*., 2011) and plant growth (Barbeta *et al*., 2013; Granda *et al*., 2013; Liu *et al*., 2015) in Mediterranean ecosystems and thus to affect carbon uptake by terrestrial vegetation and to alter regional carbon balances (Ciais, *et al*., 2005; Powell *et al*., 2013).

Plants respond to warmer and drier conditions mainly by downregulating photosynthesis due to stomatal limitation and lack of soil water (Asensio *et al*., 2007; Farquhar and Sharkey, 1982; Liu *et al*., 2016; McDowell *et al*., 2008; Ogaya *et al*., 2014; Powell *et al*., 2013) or to electron-transport limitation and Rubisco (ribulose 1,5-bisphosphate carboxylase/oxygenase) deactivation (Crafts-Brandner and Salvucci, 2000; Llorens *et al*., 2003b; Sharkey, 2005). Such decreases in photosynthesis are accompanied by decreases in the maximum photochemical efficiency of photosystem II (PSII, F_V/F_M) (Gallé *et al*., 2007; Oliveira and Peñuelas, 2005). When the sinks of reducing power decrease and photosynthesis is downregulated, the increase in the dissipation of excess energy can be estimated by quantifying the de-epoxidation state of the xanthophyll-cycle pigments (violaxanthin, antheraxanthin and zeaxanthin) (Gallé *et al*., 2007; Nogués *et al*., 2012), in which violaxanthin is converted to zeaxanthin via the intermediate antheraxanthin accompanied by a decrease in the pH of the thylakoid lumen (Demmig-Adams and Adams, 2006; Porcar-Castell *et al*., 2014). The increase in zeaxanthin associated with reversible non-photochemical quenching (NPQ) (Demmig-Adams and Adams, 2006) can thus be detected by the photochemical reflectance index (PRI; Gamon

et al., 1992; Peñuelas *et al*., 1995b) at an absorption band of 531 nm in the vegetation spectrum. PRI tracks the rapid physiological changes that are generally difficult to follow in evergreen species using indices of greenness and canopy structure, such as the normalized difference vegetation index (NDVI) (Garbulsky *et al*., 2011; Peñuelas *et al*., 2011; Stylinski *et al*., 2002).

PRI is a good indicator of the photosynthetic apparatus across functional types and spatiotemporal scales (Garbulsky *et al*., 2011; Zhang *et al*., 2016) and has detected the reactivation of photosynthesis from winter stress in evergreen species (Wong and Gamon, 2015a, 2015b; Gamon *et al*., 2016). The effects of seasonal drought on the photosynthetic apparatus have also been detected by satellite-based PRI (Goerner *et al*., 2009; Vicca *et al*., 2016). Maximum CO_2 assimilation has been efficiently estimated by PRI under severe drought conditions (Ripullone *et al*., 2011), and Rossini *et al*. (2013) demonstrated that changes in PRI were correlated with water stress in maize. Photosynthetic variability induced by heat and drought is simultaneously accompanied by complex physiological and biochemical processes, which could constrain the PRI-based estimation of the photosynthetic apparatus. Carotenoid and chlorophyll pigments and structural changes to canopies have strong effects at the canopy level and seasonal scale (Filella *et al*., 2009; Garbulsky *et al*., 2011; Stylinski *et al*., 2002; Wong and Gamon, 2015a; Zhang *et al*., 2016). Many studies have focused on improving PRI to decrease the influences of pigment-pool size and canopy structural change on the seasonal detection of photosynthesis using PRI (Zhang *et al*., 2016). Long-term studies of PRI at ecosystemic levels have increased during the last six years (e.g. Garbulsky *et al*., 2011; Zhang *et al*., 2016).

The use of PRI to assess the effects of warming and drought on photosynthetic activity, however, has received little attention. Filella *et al*. (2004) reported that a low-canopy leaf area index (LAI) at the early stage of experimental warming and drought was associated with the ability of PRI to detect photosynthesis. Mänd *et al*. (2010) detected the impact of experimental warming and drought on the photosynthetic apparatus based on the canopy PRI. Importantly, the differential PRI, ΔPRI, obtained by subtracting dark-state PRI from light-exposed PRI (Gamon and Berry, 2012; Gamon and Surfus, 1999; Hmimina *et al*., 2014; Soudani *et al*., 2014) or by subtracting predawn PRI from midday PRI (Magney *et al*., 2016; Wong and Gamon, 2015b), can eliminate the impacts of canopy structure and foliar pigments on interpretations of PRI. Additionally, the midday

depression or downregulation of photosynthesis can affect the global carbon budget (Arora *et al*., 2009). Gamon *et al*. (2013) reported that the PRI depression was associated with photosynthetic downregulation in evergreen trees. These studies led to our hypothesis that a ΔPRI obtained by subtracting morning PRI from midday PRI could be used to detect midday photosynthetic depression.

We examined the seasonality and diurnal responses of photosynthesis to long-term experimental warming and drought in an evergreen Mediterranean shrub. The optical signals of PRI and fluorescence were measured in parallel with the photosynthetic rates and water contents of leaves and soil. The primary purpose of this study was to determine the utility of canopy PRI and ΔPRI for assessing the seasonal and diurnal photosynthetic performance. We also assessed the influences of simulated climatic warming and drought on the photosynthetic activity in a long-term experimental system.

2. Materials and methods

2.1. Study site and plant species

The study was conducted in Garraf Natural Park on the central coast of Catalonia, Spain (41°18′N, 1°49′E; 210 m a.s.l.), on a south-facing hill (13° slope). The test species, *Erica multiflora* L., is a common evergreen, short-leaved, sclerophyllous and resprouting shrub that typically grows on calcareous soils in the western Mediterranean Basin. The vegetation coverage in Garraf is ca. 70% and is dominated by *E. multiflora* and *Globularia alypum* L., each ca. 1 m high, accompanied by other Mediterranean coastal shrubs (e.g. *Dorycnium pentaphyllum* L., *Rosmarinus officinalis* L., *Ulex parviflorus* L. and *Pistacia lentiscus* L.). *E. multiflora* re-sprouts abundantly after disturbance removal of aboveground biomass from the temporary extensive stump or from external roots near the stump (Llorens *et al*., 2003a). Dry conditions, however, can greatly decrease the productivity of *E. multiflora* (Llorens *et al*., 2003a).

2.2. Experimental design and field sampling

Our experiment was part of an experimental system established in 1999 and consisted of nine 20-m^2 plots. Six of the plots were treatments representing climate change: three drought plots and three warming plots. The remaining three were untreated control plots. The drought treatment decreased the input of rainwater in spring and autumn using a

transparent plastic covering the vegetation canopy operated automatically based on the rainfall (<0.3 mm) and wind (<10 m s^{-1}), decreasing the amount of soil water by 20% (Liu *et al*., 2016). The warming treatment increased the nocturnal temperature by ca. 0.6 °C and decreased the loss of heat by 64% using a reflective aluminum curtain (Liu *et al*., 2016), depending on the season. The curtain was retracted automatically to avoid hydrological effects during rains. See Peñuelas *et al*. (2007) for details of the experimental sites and treatments.

The study site has a typical Mediterranean climate characterized by a pronounced three-month summer drought, a wet spring and autumn and a cool winter. The annual precipitation in the study year was 510.2 mm, and the average monthly temperature was 15.8 °C.

Two randomly chosen *E*. *multiflora* plants in each plot were concurrently monitored for gas exchange, parameters of chlorophyll fluorescence and optical signals. Measurements were obtained on 12-14 February, 1-3 May, 23-25 July and 29 October-1 November 2014, i.e. one sampling for each season. Measurements were conducted on sunny days in the morning (8:00-10:30, solar time) and at midday (11:30-14:30, solar time). The start times were chosen based on the changes in solar irradiance during the year. Soil water content and temperature were also measured in the morning and at midday. Foliar water content was obtained by sampling branches of *E*. *multiflora* in the morning.

2.3. *Environmental and gas-exchange monitoring*

The air temperature and precipitation were continuously monitored at an automatic meteorological station installed at the study site in 1998. The CO_2 assimilation rate (*A*) and stomatal conductance (g_s) were measured using a Li-Cor LI-6400XT Portable Photosynthesis System equipped with a LI-6400-40 Leaf Chamber Fluorometer (Li-Cor, Inc., Lincoln, USA) at 25 °C and a light intensity of 1000 μmol m^{-2} s^{-1}. Three measurements were recorded for each plant to reduce measurement error. Total leaf area for each branch was obtained from small leaves pasted together and was then estimated from a photograph of all leaves using ImageJ 1.46r (NIH, Bethesda, USA). The diurnal change of photosynthesis (Δ*A*) was expressed as morning *A* subtracted from midday *A*.

2.4. *Soil water content and temperature*

Soil water content was measured using an HH2 moisture meter with an ML2x soil-moisture sensor (Delta-T Devices Ltd, Cambridge, England). The measurements were

obtained by inserting the sensor's stainless-steel cylindrical rods into the soil to a depth of 10 cm at three randomly selected locations within each plot. Soil temperature was also measured at 10 cm using a digital soil thermometer (TO 15, Jules Richard instruments, Argenteuil, France) (Asensio *et al*., 2008).

2.5. Foliar water content

Five branches were sampled as replicates to analyze foliar water content (WC) and retained freshness in each plot using a portable crisper. The fresh weight (FW) of the leaves was determined immediately after transport to the laboratory. The leaves were then dried in an oven at 70 °C for two days to a constant weight (dry weight, DW). WC (Eq. (1)) was then calculated as:

$$WC = (FW-DW)/FW \quad (1)$$

2.6. Chlorophyll fluorescence

The maximum photochemical efficiency of PSII (F_V/F_M) was estimated based on measurements of minimum (F_0) and maximum (F_M) fluorescence by a portable miniaturized pulse-amplitude-modulated photosynthesis yield analyser (MINI-PAM, Walz, Effeltrich, Germany) with a leaf-clip holder. The leaves were dark-adapted for at least 20 min with the leaf clips.

The actual photochemical efficiency of PSII (Yield, Eq. (2)) was estimated based on the measured fluorescence parameters as:

$$Yield = (F_M'-F_S)/ F_M' \quad (2)$$

where F_S and F_M' are the steady-state yield of fluorescence and the maximum fluorescence yield, respectively, during full closure of the PSII center obtained by the fluorometer from light-adapted samples.

The diurnal change of Yield (ΔYield) was calculated by subtracting morning Yield from midday Yield.

2.7. Canopy reflectance

Ground-based canopy spectra were measured *in situ* using a portable field spectroradiometer (GER1500, Geophysical & Environmental Research, Spectra Vista Corp., Poughkeepsie, USA). The instrument measures spectral reflectance between 268 and 1095 nm with a sampling interval from 1.5 to 2.1 nm and a 25° field of view. The

reflectance was calculated after standardization by canopy irradiance using a reference spectral panel (Spectralon, Labsphere, North Sutton, USA) serving as a Lambertian reflector. All spectral measurements were from a nadir view angle approximately 0.5 m above the canopy to minimize atmospheric and directional effects. The area measured was thus a circle with a diameter of ca. 0.58 m on the top of the canopy. Three scans were quickly recorded in different positions for each plant as replicates after measuring the white standard spectrum. The vegetation eco-physiological indices used were PRI (Eq. (3), Gamon *et al*., 1992; Peñuelas *et al*., 1995b), NDVI (Eq. (4), Tucker, 1979), water index (WI, Eq. (5), Peñuelas *et al*., 1993), normalized difference chlorophyll index (NDCI, Eq. (6), Gitelson and Merzlyak, 1994) and structure-insensitive pigment index (SIPI, Eq. (7), Peñuelas *et al*., 1995a) calculated from the reflectance data and expressed as:

$$PRI = (R531-R570)/(R531+R570) \quad (3)$$

$$NDVI = (R900-R680)/(R900+R680) \quad (4)$$

$$WI = R900/R970 \quad (5)$$

$$NDCI = (R750-R705)/(R750+R705) \quad (6)$$

$$SIPI = (R445-R800)/(R680-R800) \quad (7)$$

where Rx is reflectance at x nm.

ΔPRI was also calculated by subtracting early morning PRI from midday PRI.

2.8. Statistical analysis

The seasonal variations of gas exchange, F_V/F_M, Yield and the vegetation indices were determined using one mean per stand. One mean per plot was used for soil water content and temperature and for foliar WC. We used repeated-measures analyses of variance to detect the seasonal changes of all variables and to determine the impacts of the treatments and the water status of both leaves and soil on photosynthetic seasonality. The responses of the vegetation indices to photosynthetic seasonality and the applicability of WI for assessing WC were analyzed using standardized major-axis regression to identify correlations between the variables. We compared the fitted bivariate slopes between treatments using 95% confidence intervals and the smart R package. All analyses were conducted with R version 3.2.2 (R Core Development Team, 2015).

3. Results

3.1. Climate and soil and foliar water statuses

The seasonal mean temperatures in 2014 (Figure 1) ranged between 9.7 °C in winter and 22.4 °C in summer. The summer was wet, with a total precipitation of 161.7 mm, considerably higher than in winter (66.2 mm) and spring (79.6 mm). Soil water content and temperature clearly varied seasonally. Soil water content (Figure 2a) was higher in winter than the other seasons for all treatments. Soil temperature (Figure 2b) was lowest in winter and highest in summer and was higher at midday for each season. Foliar WC (Figure 3) differed significantly (p<0.001) between seasons and decreased from winter to spring and then recovered in summer and autumn. The treatments, however, had no impacts on WC.

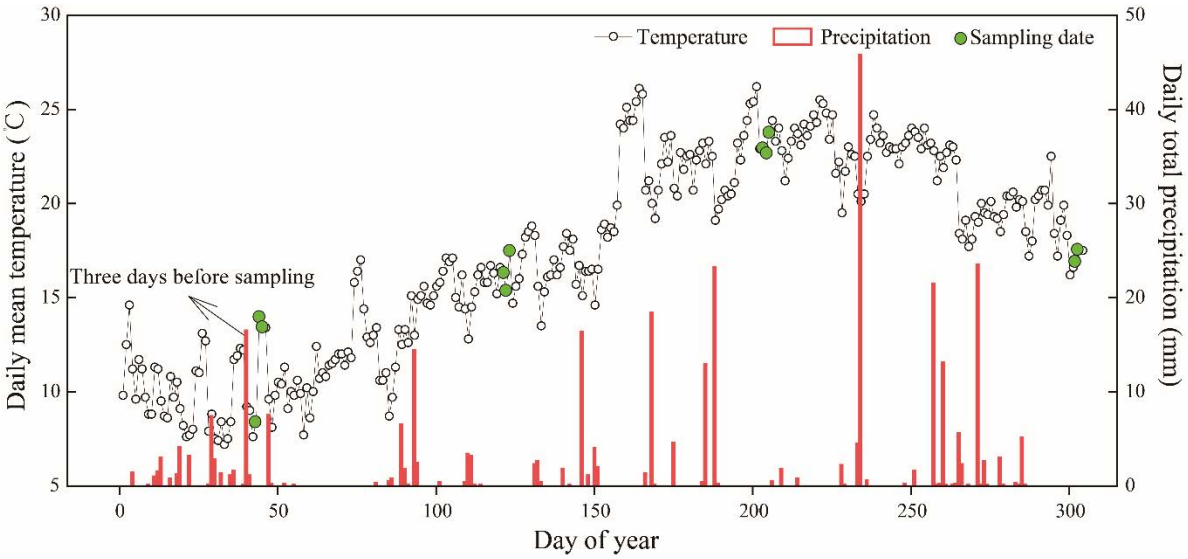

Figure 1. Daily mean temperature and daily total precipitation in Garraf Natural Park in 2014. Total precipitation was 66.2 mm in winter (January-March), 79.6 mm in spring (April-June), 161.7 mm in summer (July-September) and 202.3 mm in autumn (October-December). Seasonal mean temperatures were 9.7 °C (winter), 17.5 °C (spring), 22.4 °C (summer) and 13.5 °C (autumn).

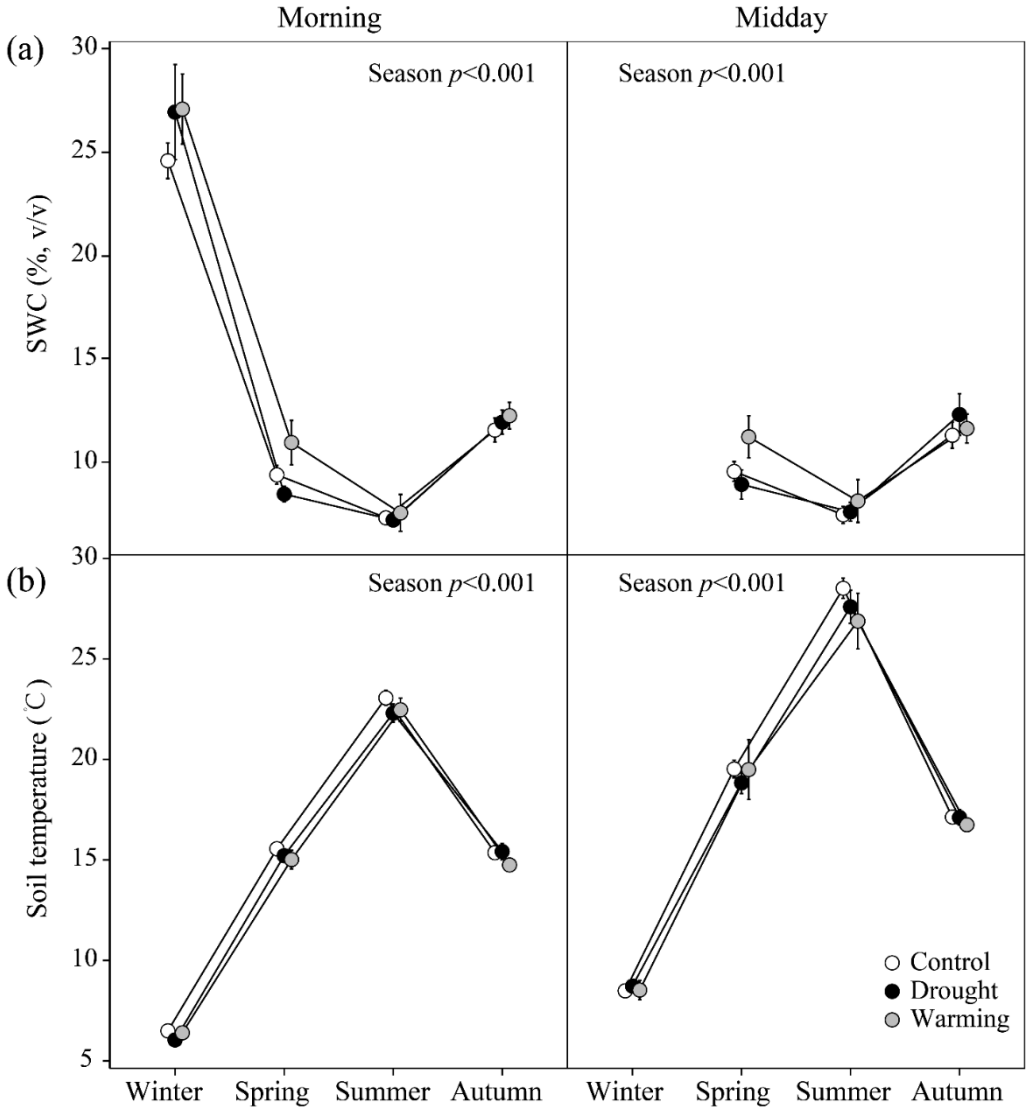

Figure 2. Seasonal variation of soil water content (SWC) (a) and temperature (b) in Garraf Natural Park in 2014. Error bars are standard errors of the mean (n=9 for the drought and warming treatments, and n=18 for the control treatment). The significances of the repeated-measures ANOVAs are depicted.

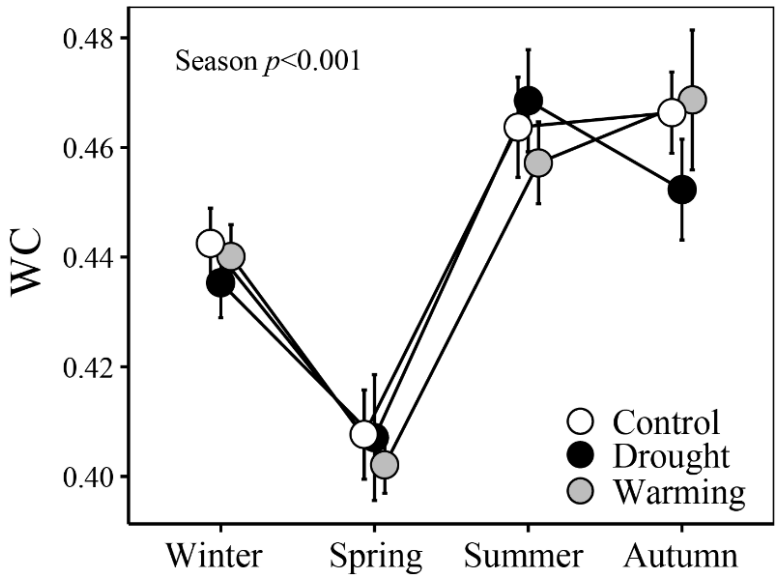

Figure 3. Seasonal variation of foliar water content (WC) for *Erica multiflora* in 2014. Error bars are standard errors of the mean (n=6 for the drought and warming treatments, and n=12 for the control treatment). The significances of overall repeated-measures ANOVAs are depicted.

3.2. Seasonal patterns of gas exchange, fluorescence and vegetation indices

The rate of CO_2 assimilation (*A*) (Figure 4a) was significantly lower in winter (ca. 2 μmol m^{-2} s^{-1}) than autumn (ca. 8 μmol m^{-2} s^{-1}) for both the morning and midday measurements. Morning *A* was significantly lower in the warming than the other treatments in spring (p<0.05). Midday photosynthesis was significantly lower in the drought than the control treatment throughout the year (drought < control, p=0.03), particularly in autumn (p<0.05). Morning stomatal conductance (g_S) (Figure 4b) was slightly lower in summer than spring. Midday g_S was significantly lower in both the drought and warming treatments, particularly in summer (p<0.05 for both).

F_V/F_M (Figure 5a) increased throughout the year in the morning and at midday, in parallel with the seasonal patterns in *A* (Figure 4a). Morning F_V/F_M was significantly lower in the drought treatment, particularly in winter (p<0.01). Yield (Figure 5b) had similar seasonal patterns as F_V/F_M, but was slightly lower in autumn than summer in the morning. Midday Yield was significantly lower in the drought and warming treatments, particularly in spring and autumn.

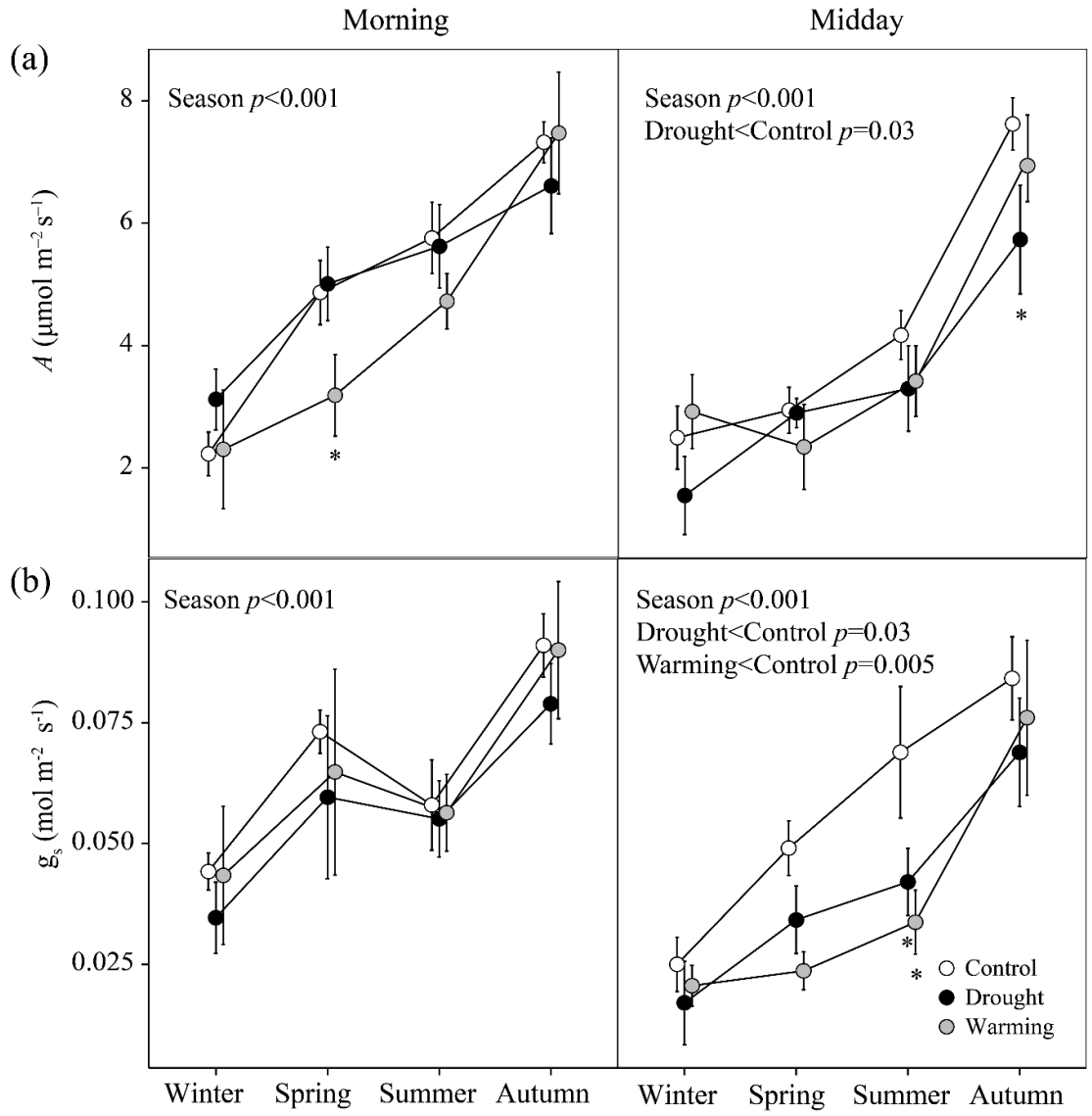

Figure 4. Seasonal variation of CO_2 assimilation rate (*A*) (a) and stomatal conductance (gS) (b) for *Erica multiflora* in 2014. Error bars are standard errors of the mean (n=6 for the drought and warming treatments, and n=12 for the control treatment). The significances of overall repeated-measures ANOVAs are depicted. *p<0.05 between treatments for each seasonal measurement.

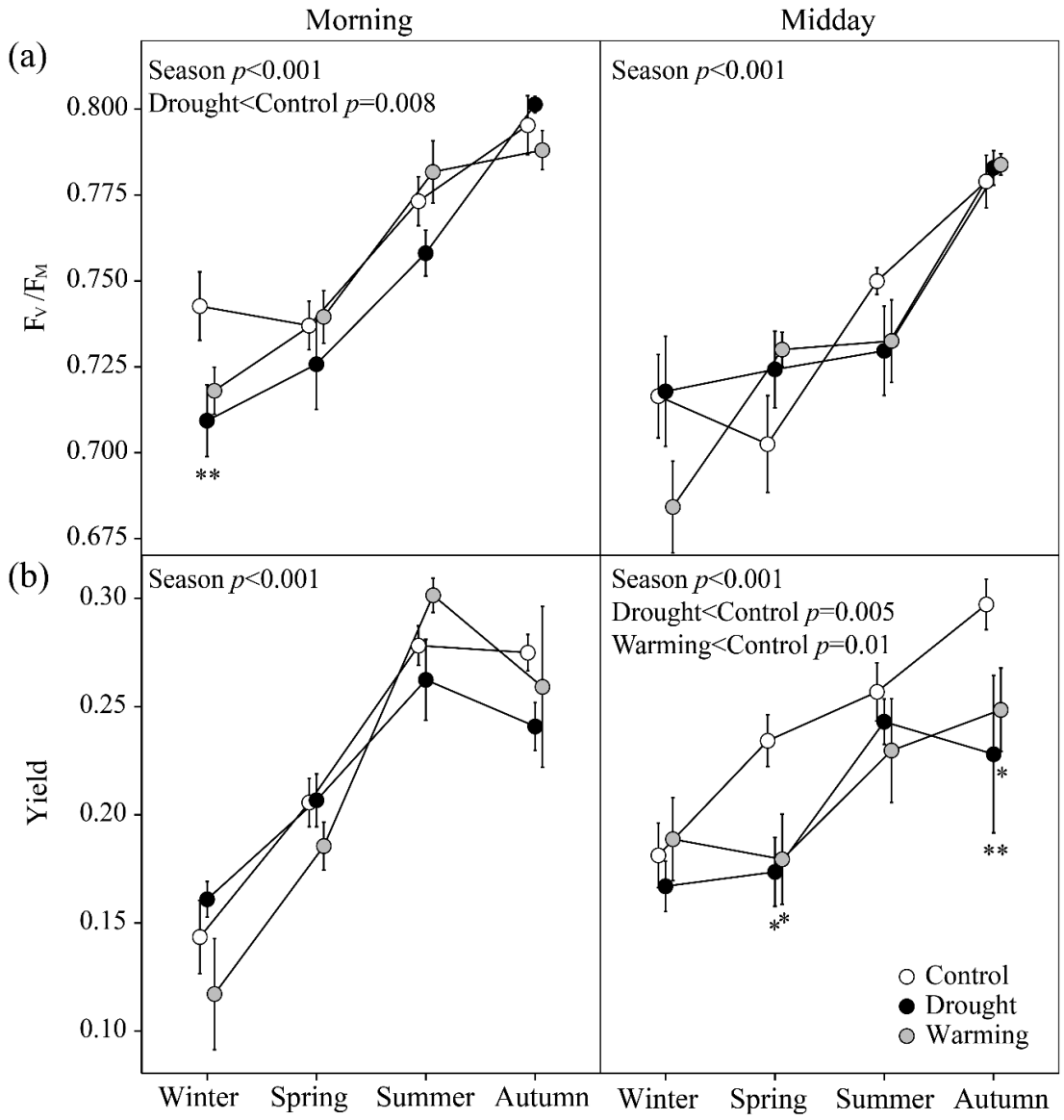

Figure 5. Seasonal variation of foliar maximum (F_V/F_M) (a) and actual (Yield) (b) photochemical efficiency for *Erica multiflora* in 2014. Error bars are standard errors of the mean (n=6 for the drought and warming treatments, and n=12 for the control treatment). The significances of overall repeated-measures ANOVAs are depicted. *p<0.05, **p<0.01 between treatments for each seasonal measurement.

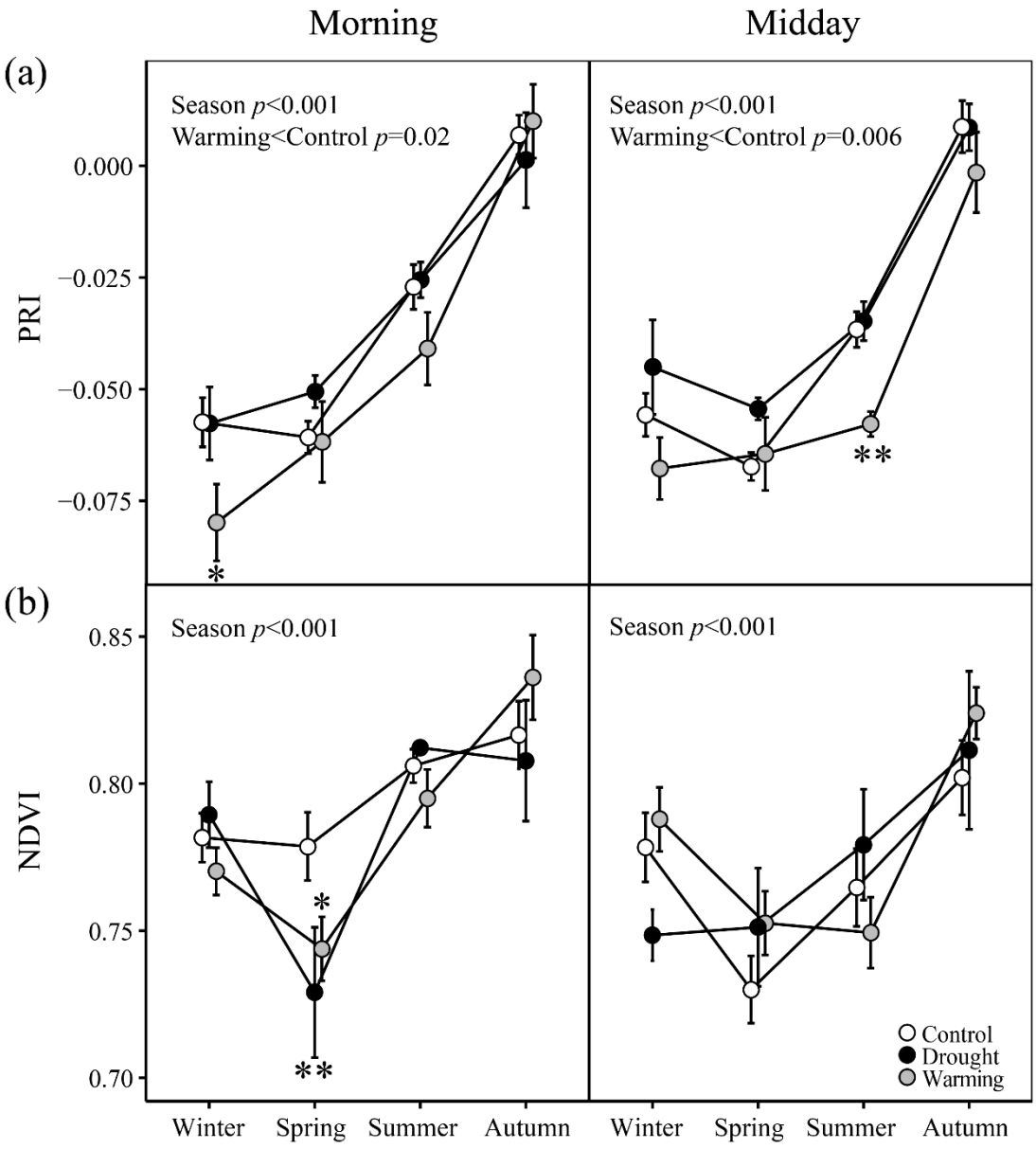

Figure 6. Seasonal variation of the photochemical reflectance index (PRI) (a) and normalized difference vegetation index (NDVI) (b) for *Erica multiflora* in 2014. Error bars are standard errors of the mean (n=6 for the drought and warming treatments, and n=12 for the control treatment). The significances of overall repeated-measures ANOVAs are depicted. *p<0.05, **p<0.01 between treatments for each seasonal measurement.

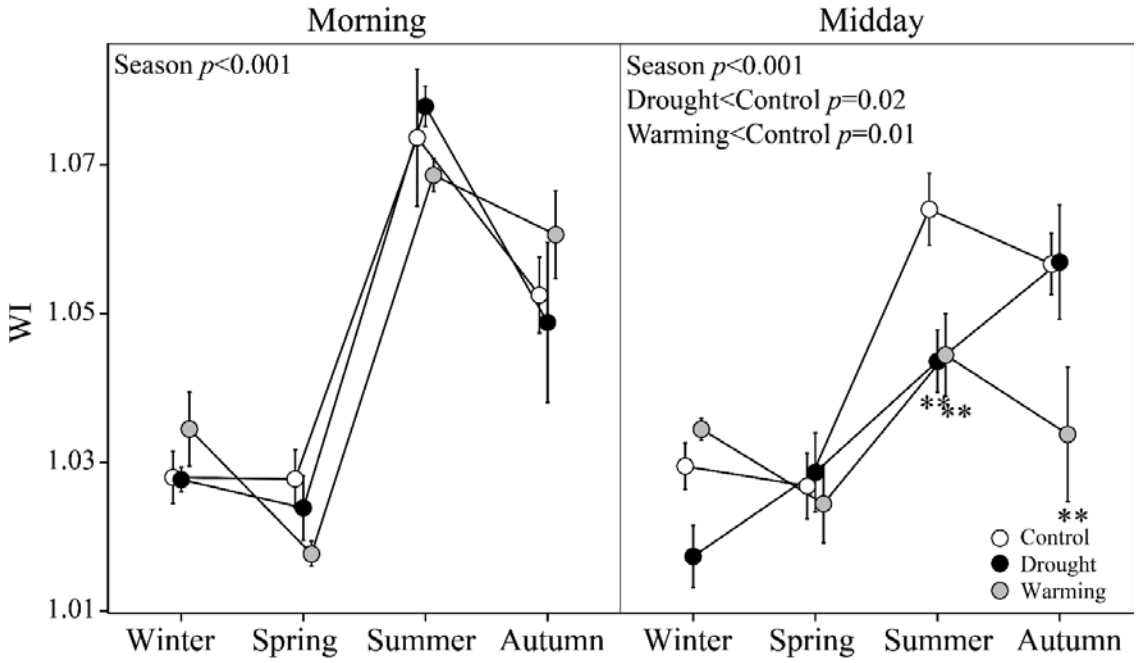

Figure 7. Seasonal variation of the water index (WI) for *Erica multiflora* in 2014. Error bars are standard errors of the mean (n=6 for the drought and warming treatments, and n=12 for the control treatment). The significances of overall repeated-measures ANOVAs are depicted. ** $p<0.01$ between treatments for each seasonal measurement.

The seasonality of PRI (Figure 6a) was similar to that of A and F_V/F_M. PRI was significantly lower in the warming treatment both in the morning and at midday, particularly in the morning in winter ($p<0.05$) and at midday in summer ($p<0.01$). NDVI (Figure 6b) was lowest in spring and similar in winter and summer but did not differ significantly between the treatments, both in the morning and at midday. Interestingly, morning WI (Figure 7) varied similarly to WC (Figure 3) throughout the year. Midday WI, however, was significantly lower in the drought and warming treatments, particularly in summer ($p<0.01$ for both) and autumn ($p<0.01$ for the warming treatment). NDCI (higher values indicate higher chlorophyll contents) (Figure S1a) was stable from winter to summer but increased rapidly in autumn. NDCI was lower in the warming and drought treatments both in the morning and at midday. SIPI (an estimator of the carotenoids/chlorophyll relationship; higher values indicate higher carotenoid/chlorophyll ratios) (Figure S1b) increased from winter to spring and then decreased to minimum values in autumn.

3.3. Relationships of A with PRI, WC, fluorescence and the other vegetation indices

PRI and *A* were significantly correlated in the treatments and over time (Figure 8a). NDVI only poorly tracked the photosynthetic changes (Figure 8b). The indicators of foliar water status, WC (Figure S2a) and WI (Figure S2b), however, were not correlated with the seasonality of photosynthesis. F_V/F_M and Yield had significant relationships with *A* (Figure S3) but more weakly than PRI. In particular, Yield and *A* were only marginally correlated at midday in the drought and warming treatments ($p<0.1$, Figure S3b). NDCI also tracked photosynthetic seasonality less well than PRI, with an R^2 range of 0.22-0.77 in the treatments (Figure S4a). SIPI was only weakly correlated with *A* (Figure S4b), unlike PRI and NDCI. In the warming treatment, however, 47 and 42% of the variability of *A* in the morning and at midday, respectively, were explained by SIPI.

3.4. Relationships between WC and WI

WI varied similarly to WC in the treatments in the morning but decoupled at midday in the drought treatment (Figure 9). WI accounted for 77% of the variance of morning WC in the warming treatment, 25% higher than in the control treatment. Midday WI and WC relationship, however, were similar in the warming and control treatments.

3.5. Relationships of PRI with the fluorescence parameters and indices of vegetation pigments

PRI was correlated significantly with F_V/F_M (Figure 10a, R^2 of 0.63-0.82 in the morning and 0.59-0.69 at midday) but weakly with Yield (Figure 10b). Interestingly, PRI was strongly correlated with NDCI (Figure S5a, $R^2>0.58$ and $p<0.001$ for all treatments), particularly in the warming treatment ($R^2=0.81$ and 0.88 for the morning and midday measurements, respectively). The correlation between PRI and SIPI was also strong, with a clearly higher R^2 at midday (Figure S5b).

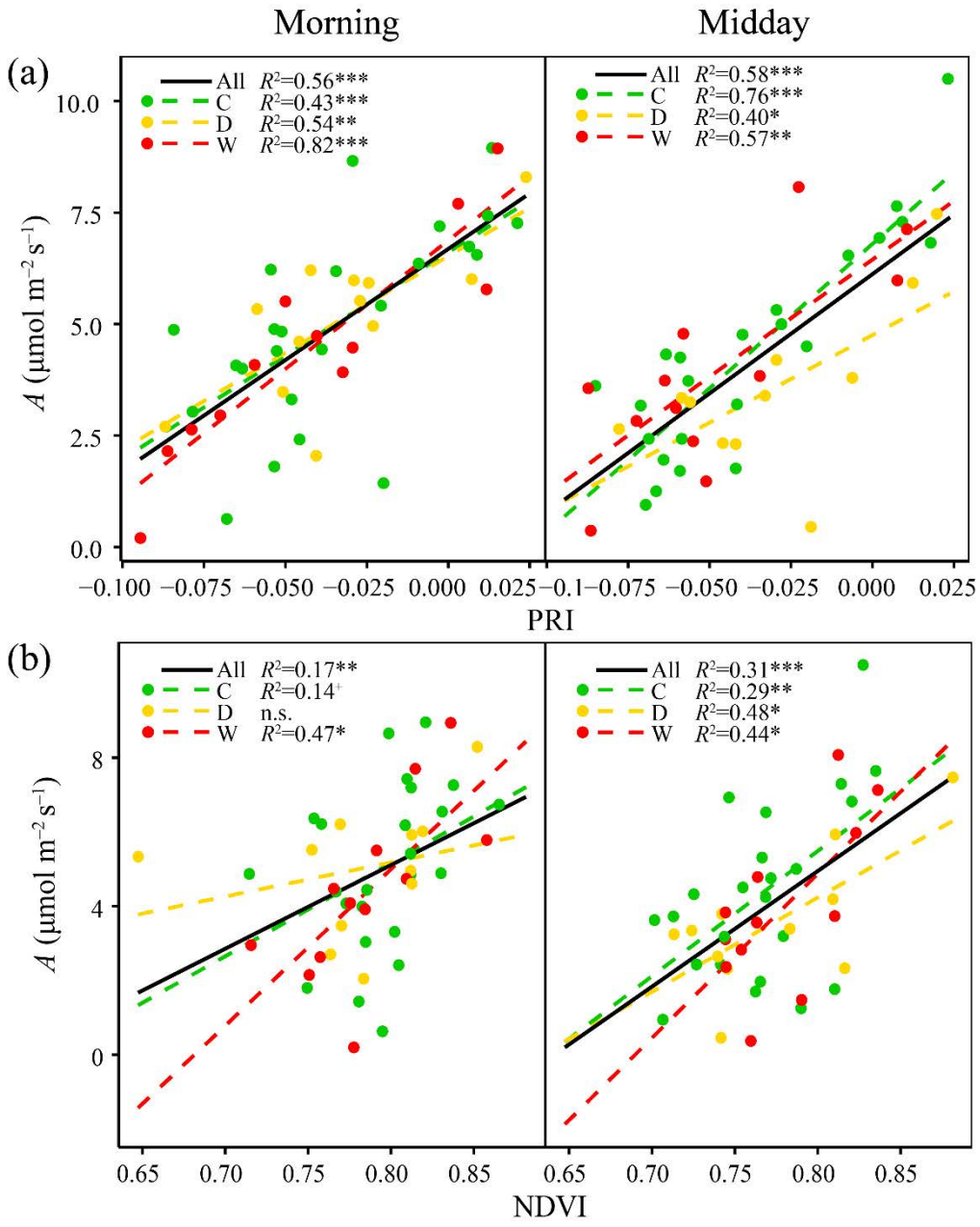

Figure 8. Relationships of CO_2 assimilation rate (A) with the photochemical reflectance index (PRI) (a) and normalized difference vegetation index (NDVI) (b) for *Erica multiflora* in 2014. The black lines represent the linear relationships over all three treatments. n.s. $p>0.1$, $^{+}p<0.1$, $*p<0.05$, $**p<0.01$ and $***p<0.001$ between variables. C, D and W indicate the control, drought and warming treatments, respectively.

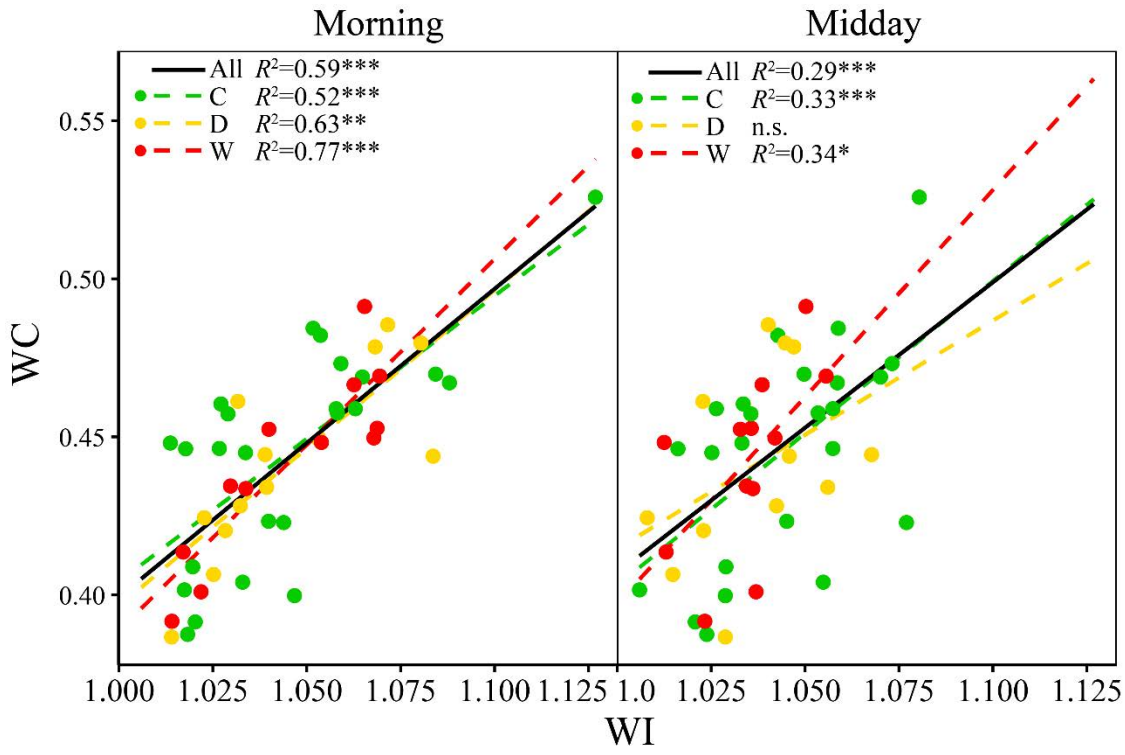

Figure 9. Relationships between water content (WC) and the water index (WI) for *Erica multiflora* in 2014. The black lines represent the linear relationships over all three treatments. n.s. $p>0.1$, *$p<0.5$, **$p<0.01$ and ***$p<0.001$ between variables. C, D and W indicate the control, drought and warming treatments, respectively.

3.6. Responses of ΔPRI to ΔA and ΔYield

PRI varied diurnally similarly with *A* and Yield in all treatments throughout the year, particularly in the warming treatment (Figure 11). Δ*A*, ΔYield and ΔPRI varied from high winter values (near or >0) to low summer values (<0) and then slightly increased in autumn (Figure 11). These changes indicated that photosynthesis and PRI were mostly lowest at midday in summer. ΔYield (Figure 11b) was significantly higher ($p<0.05$) in the control than the drought and warming treatments that had low negative values from spring to autumn, i.e. midday Yield was much lower in the drought and warming treatments. Δ*A* and ΔYield were strongly correlated with ΔPRI (Figure 12, >50% of the variability was explained by ΔPRI for all treatments combined), particularly for the drought (R^2=0.82 and $p<0.1$ for Δ*A*, R^2=0.95 and $p<0.05$ for ΔYield) and warming (R^2=0.98 and $p<0.05$ for both) treatments. The slopes of these relationships were not different among treatments except the slope between ΔYield and ΔPRI that was lower in the drought than in the warming treatment.

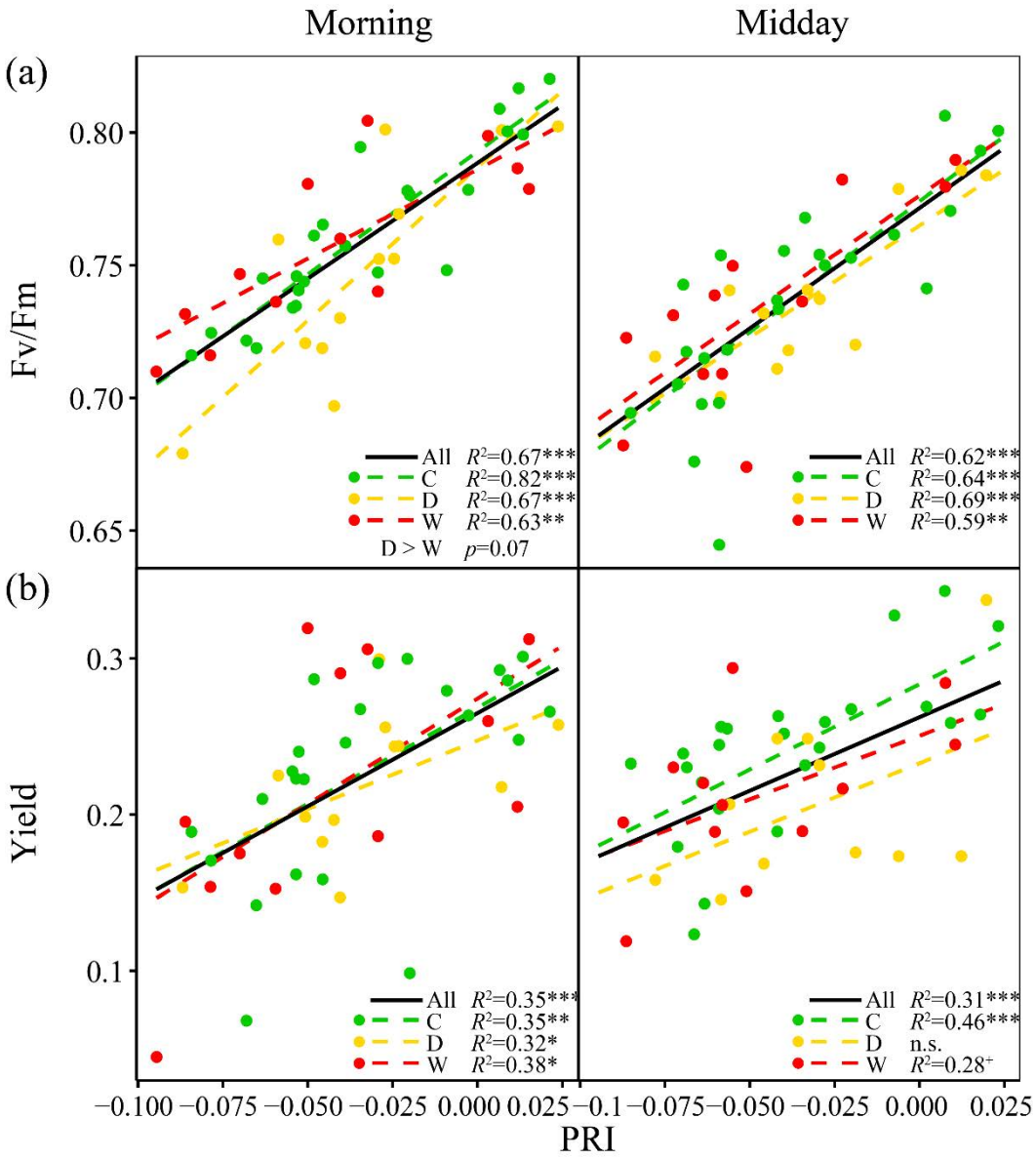

Figure 10. Relationships of maximum (F_V/F_M) (a) and actual (Yield) (b) photochemical efficiency of PSII with the photochemical reflectance index (PRI) for *Erica multiflora* in 2014. The black lines represent the linear relationships over all three treatments. n.s. $p>0.1$, $^{+}p<0.1$, $*p<0.05$, $**p<0.01$ and $***p<0.001$ between variables. C, D and W indicate the control, drought and warming treatments, respectively.

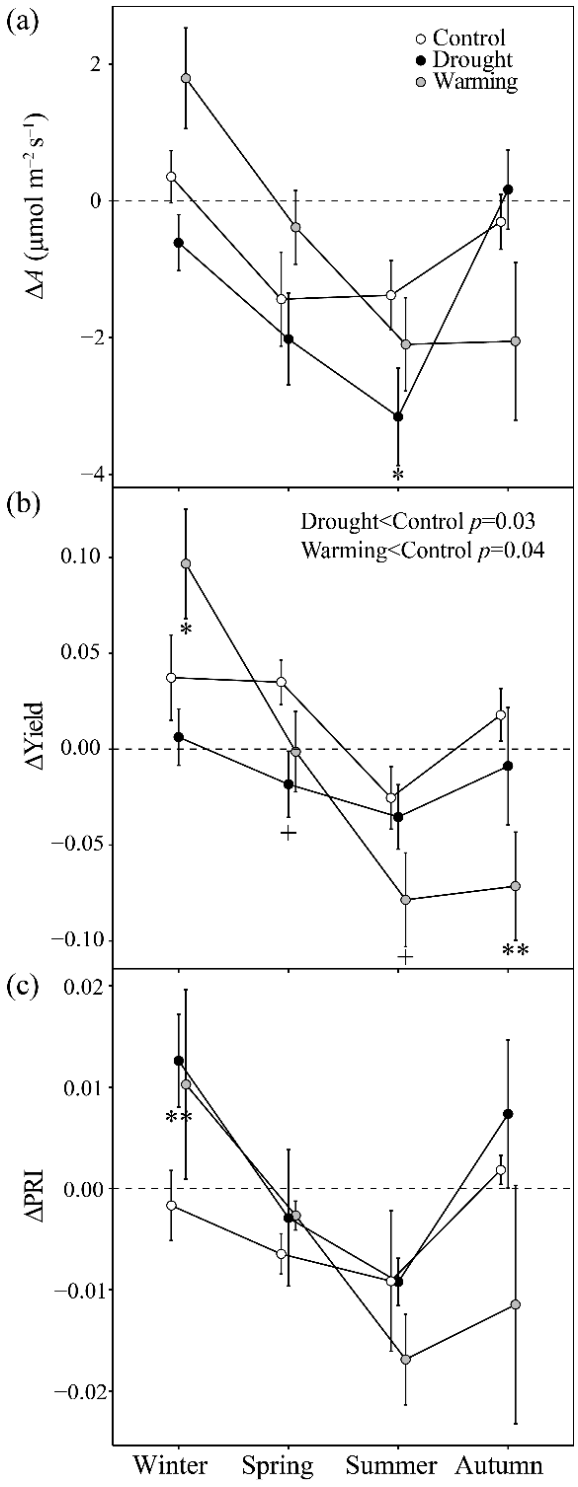

Figure 11. Seasonal variation of differential CO_2 assimilation rate (ΔA) (a), actual photochemical efficiency (ΔYield) (b) and photochemical reflectance index (ΔPRI) (c) between midday and early morning measurements for *Erica multiflora* in 2014. Error bars are standard errors of the mean (n=6 for the drought and warming treatments, and n=12 for the control treatment). The significances of overall repeated-measures ANOVAs are depicted. $^{+}p<0.1$, $*p<0.05$, $**p<0.01$ between treatments for each seasonal measurement.

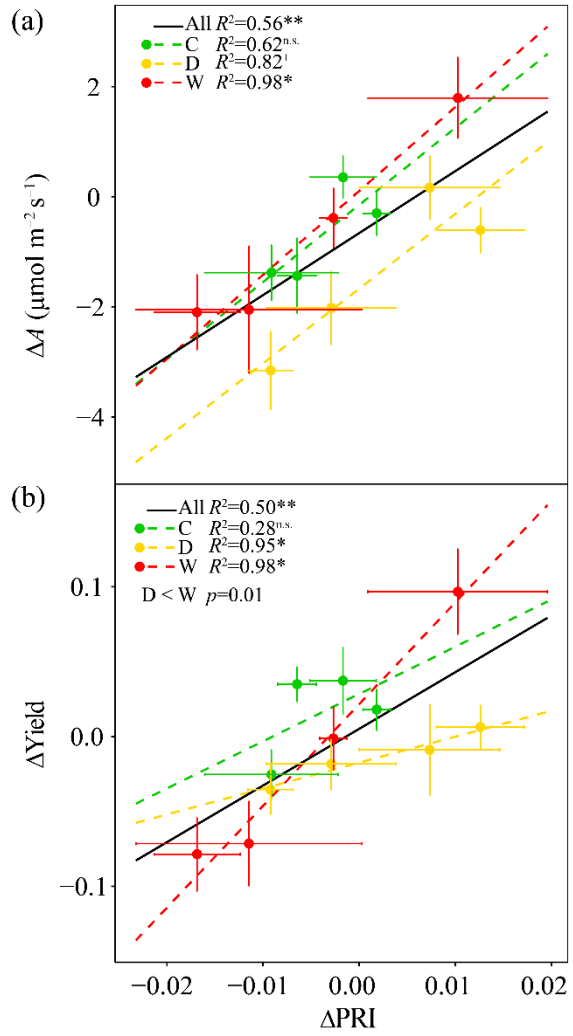

Figure 12. Relationships of differential CO_2 assimilation rate (ΔA) (a) and actual photochemical efficiency of PSII (ΔYield) between midday and early morning measurements (b) with the differential photochemical reflectance index (ΔPRI) (c) for *Erica multiflora* in 2014. The black lines represent the linear relationships over all three treatments. n.s. p>0.1, ^{+}p<0.1, *p<0.05 and **p<0.01 between variables. C, D and W indicate the control, drought and warming treatments, respectively.

4. Discussion

Our results showed that PRI but not NDVI efficiently tracked the photosynthetic seasonality of mature evergreen plants under experimental warming and drought conditions. PRI also tracked photosynthetic activity better than NDCI and SIPI. WI was a good indicator of the seasonal variability of foliar WC in this drought-tolerant evergreen shrub. Importantly, ΔPRI detected the midday depression in photosynthesis in response

to the warming and drought conditions, which are generally accompanied by multiple physiological processes (e.g. lower midday g_S in this study) and are not readily detectable.

4.1. PRI assessment of seasonal photosynthesis under long-term drought and warming conditions

The study site, a typical Mediterranean region, has been generally characterized by low precipitation and high temperatures in previous summers (Vicente-Serrano *et al*., 2014) and in future climatic projections (Giorgi and Lionello, 2008). The summer was wetter and the spring was drier in 2014 than previous years because of the higher summer precipitation (82.1 mm more than in spring) (Figure 1) and a considerably lower spring soil water content (Figure 2a; Liu *et al*., 2016; Nogués *et al*., 2012). *A* consequently increased seasonally from winter to autumn, and F_V/F_M increased from spring to summer, in contrast to the significant decrease in previous studies (Llorens *et al*., 2003a, 2003b). These seasonal increases in *A* and F_V/F_M were efficiently tracked by PRI, with strong correlations in all treatments (Figure 8a), which were stronger than in previous years in this experimental system (Filella *et al*., 2004).

Midday *A*, g_S and Yield and morning F_V/F_M were significantly lower in the drought treatment throughout the study year, likely due to the effect of the water stress (Figures. 4, 5). Midday g_S and Yield were also lower in the warming treatment. It has been reported that drought and warming can advance the spring growing season, affect reproductive performance and decrease plant productivity of *E. multiflora* (del Cacho *et al*., 2013; Prieto *et al*., 2009c). The drier and warmer conditions projected for the future could affect diversity, decrease biomass and increase mortality in Mediterranean ecosystems (Liu *et al*., 2015, 2016; Nardini *et al*., 2014; Prieto *et al*., 2009a). Our results demonstrated the negative effects of water deficit with or without warming on seasonal photosynthetic dynamics, which would further affect plant growth in Mediterranean ecosystems. PRI provided a simple method to non-destructively assess such long-term effects for drought-tolerant plants. NDVI, however, was only weakly correlated with midday *A* (Figure 8b), in contrast to a higher correlation of previous study (Filella *et al*., 2004). NDCI was also strongly seasonally correlated with *A* (Figure S4a), and SIPI was weakly and negatively correlated with *A* (Figure S4b), but neither was as strongly correlated as PRI. PRI was not only sensitive to long-term carotenoid/chlorophyll changes, but also to short-term xanthophyll pigment conversion (Filella *et al*., 2009; Gamon and Berry, 2012; Porcar-Castell *et al*., 2012). The strong correlations of PRI with NDCI and SIPI (Figure S5)

supported the importance of pigments in using PRI to monitor the photosynthetic apparatus at seasonal timescales (Filella *et al*., 2009), because NDCI is an index of chlorophyll changes (Gamon and Surfus, 1999; Gitelson and Merzlyak, 1994) and SIPI is associated with carotenoid and chlorophyll ratios (Peñuelas *et al*., 1995a). PRI and NDCI were much lower in the warming than the control treatment, further demonstrating the regulation of de-epoxidation state of the xanthophyll cycle in plants confronted by heat stress, which affected the changes of the photosynthetic pigments. Our results also indicated that these indices were sensitive to decreases in foliar gas exchange and photochemical efficiency induced by warming.

Seasonal changes of the pools of carotenoid pigments, including xanthophyll pigments but also lutein, neoxanthin and β-carotenoid, play an important role in preventing photosynthetic inhibition and downregulation (Demmig-Adams *et al*., 1996; Gamon *et al*., 2016; Niyogi, 1999). A previous study at our site found large seasonal changes of carotenoids in *E. multiflora* (Nogués *et al*., 2012). Our study did not find pigment changes, but the strong interactions of the indices associated with pigments (PRI, NDCI and SIPI) with photosynthesis indirectly illustrated the role of the pigments in the seasonality of photosynthetic regulation.

Variations in canopy structure such as shadows and plant architecture generally also have large effects on the seasonality of PRI. Filella *et al*. (2004) proposed that PRI could be a better indicator of photosynthetic activity than NDVI, under increased vegetation coverage or LAI during the early successional stages of the *E. multiflora* canopy. Our study supported this proposal, with NDVIs near saturation (Figure 6b), but PRI increased synchronously with CO_2 assimilation rate (Figures. 4a, 6a). Additionally, NDVI did not detect the disturbances to plant functionality due to drought or warming. Many reports have demonstrated that NDVI is readily saturated in dense canopies and/or at high LAIs, which could lead to poor or failed assessments of photosynthetic activity and plant biomass (Garbulsky *et al*., 2011; Mänd *et al*., 2010; Stylinski *et al*., 2002; Zarco-Tejada *et al*., 2013b).

PRI has also been used to track variability in *A* in mature olive trees in response to seasonal water stress (Marino *et al*., 2014). The prolonged summer-drought limited radiation-use efficiency (RUE) was assessed by satellite-based PRI (Moreno *et al*., 2012). Our study confirmed the ability of PRI to detect the effects of seasonal water deficits on photosynthesis and demonstrated the potential of PRI to assess the impacts of climatic

warming on plant photosynthesis.

4.2 WI tracked the seasonal changes of foliar WC

Water availability plays a key role in photosynthetic regulation in *E*. *multiflora* (Llorens *et al*., 2003b). Many reports have demonstrated that WI can be a non-destructive proxy of plant water content for identifying water stress and predicting crop yield (Claudio *et al*., 2006; Peñuelas *et al*., 1993, 1997; Peñuelas and Inoue, 1999; Rischbeck *et al*., 2016). Our results also showed that the WI clearly detected changes in WC, particularly in the morning measurements, probably because the measuring time of WI in the morning was closer to the WC measurement and the relative water content in *E*. *multiflora* is lower at midday than predawn (close to our morning measurement time) in dry summer season (Catoni *et al*. 2013), which is also consistent with WI in our study being lower at midday summer particularly in the warming and drought treatments (Figure 7). However, neither WC nor WI were highly correlated with CO_2 assimilation rate (Figure S2a, b). This decoupling of foliar water status and photosynthesis in *E*. *multiflora* was probably caused by the large role played by soil water availability in photosynthetic adjustment in Mediterranean ecosystems, which generally encounter drought stress (Asensio *et al*., 2007; Liu *et al*., 2016; Ogaya *et al*., 2014; Prieto *et al*., 2009b).

4.3. *PRI assessment of midday depressions of photosynthesis under long-term drought and warming*

The low negative values of foliar Δ*A* and ΔYield in summer at the diurnal scale (Figure 11a, b) identified the midday depression of photosynthesis, which has been previously reported for the same site by Llorens *et al*. (2003a). The higher winter Δ*A* and ΔYield in the warming than the control treatment indicated that warming was beneficial to winter photosynthetic activity. In contrast, the lower negative summer and autumn Δ*A* and ΔYield in the warming than the control treatment demonstrated that warming increased photosynthetic midday depression in these two seasons. The drought treatment, however, increased spring and summer midday depression of photosynthesis and had no effect on winter and autumn photosynthetic depression. These results demonstrated that plant photosynthesis in summer season was highly sensitive to climatic warming and drought, and indicated that future climate change could enhance photosynthetic midday depression, decrease vegetation production and disturb carbon budget for Mediterranean ecosystems. Interestingly, the patterns of ΔPRI with midday depression of photosynthesis were similar

in the warming and drought treatments. The results present here, together with the strong correlations of ΔPRI with Δ*A* and ΔYield (Figure 12), illustrated that ΔPRI was sensitive to midday photoinhibition under experimental warming and drought and was a good indicator of reduced carbon assimilation.

The midday depression of photosynthesis in Mediterranean summers can be caused to a large extent by the excessive noon irradiance and high temperature (Damesin and Rambal, 1995), which can profoundly influence diurnal PRI patterns and decrease midday PRIs (Gamon and Bond, 2013). Short-term changes of PRI have been associated with rapid conversion of xanthophyll pigments that protect the photosystem from photoinhibition at high midday irradiances (Gamon and Bond, 2013; Peñuelas *et al*., 1995b) and downregulate PSII photochemical efficiency (Figure 11b; Damesin and Rambal, 1995; Demmig-Adams *et al*., 1989). The regulation of photosynthetic midday depression aids plant survival when environmental conditions are unfavorable but decreases RUE and plant productivity (Gamon and Bond, 2013). Models have demonstrated that photosynthetic downregulation reduces carbon uptake and affects the carbon budget (Arora *et al*., 2009). Our study introduces a simple method to detect the photosynthetic midday depression. Gamon and Bond (2013) reported that PRI was sensitive to illumination and photosynthetic downregulation in a short-term study, which supports the potential utility of ΔPRI for monitoring the seasonal midday depression of photosynthesis in the present study.

The midday depression of photochemical activity was also due to the significantly lower soil water content and g_S and higher soil temperature relative to the morning measurements (Figures. 2, 4b). The availability of soil water may have been a key constraint regulating photosynthesis in previous studies at the same site (Liu *et al*., 2016; Llorens *et al*., 2003a, 2003b) and in a Mediterranean forest (Asensio *et al*., 2007). Lower g_S in *E*. *multiflora* generally co-occur with lower transpiration rates and higher vapor-pressure deficits (Liu *et al*., 2016; Llorens *et al*., 2003a). Lower g_S can also decrease midday transpiration rates and prevent or control the decrease in foliar water potential (Farquhar and Sharkey, 1982; van der Molen *et al*., 2011), eliciting lower midday rates of carbon assimilation.

He *et al*. (2016) recently demonstrated that MODIS-based PRI was sensitive to RUE constrained by water stress due to low soil water content. Magney *et al*. (2016) also reported that ΔPRI was more sensitive to water and nutrient limitation but less sensitive

to LAI and chlorophyll content throughout the wheat growing season, which enabled ΔPRI to deconvolve the diurnal component from seasonal changes. Together with these previous reports, our study further supported the ability of ΔPRI to detect the responses of photosynthetic midday depression to environmental stresses.

5. Final remarks

Ongoing global warming in the Mediterranean region, where the frequency of summer drought has been increasing, is having a critical impact on the functioning of terrestrial ecosystems and on plant physiological processes (Giorgi and Lionello, 2008; Liu *et al*., 2016; Nardini *et al*., 2014). Remote sensing can potentially assess plant functional adjustments and carbon assimilation at various temporal and spatial scales in response to stress. PRI has been used to detect the impacts of water deficit on the photosynthetic apparatus in Mediterranean species (Marino *et al*., 2014; Stylinski *et al*., 2002; Tsonev *et al*., 2014; Zarco-Tejada *et al*., 2013a). We used PRI to detect the seasonality of photosynthesis in *E. multiflora* under long-term drought and warming conditions (Figure 10). WI also provided a simple method for non-destructively detecting changes in plant water content in this drought-tolerant shrub. Strong photosynthetic downregulation under severe stress, however, can also be caused by other biochemical mechanisms and probably be prevented by other photoprotective processes (Demmig-Adams and Adams, 2006; Takahashi and Badger, 2011). For example, PRI was decoupled from NPQ in *Ceratonia siliqua* seedlings subjected to water stress (Osório *et al*., 2012) and in boreal evergreen needles during the transition from a cold winter to a warm spring (Porcar-Castell *et al*., 2012) by non-regulated quenching other than thermal dissipation mediated by xanthophyll for protecting the photosynthetic machinery. Our study also indicated that warming was beneficial to winter photosynthetic activity and instead that warming and drought increased summer midday depression of photosynthesis for semi-arid Mediterranean evergreen shrub. ΔPRI provided a simple method for detecting this midday depression or downregulation of photosynthesis response to climate change.

It should be noted that we measured photosynthesis under constant light conditions that can represent RUE at a given light intensity. Further study should test the utility of PRI and ΔPRI as indicators of plant photosynthetic dynamics and midday depression

under natural illumination in evergreen shrubs and other functional types. Importantly, assessments of PRI should be adjusted based on the effects of canopy structure, pigments, view angle and irradiance etc. (Damm *et al*., 2015; Hilker *et al*., 2010; Magney *et al*., 2016; Moreno *et al*., 2012; Soudani *et al*., 2014), to facilitate its applicability in interpreting photosynthetic activity and in the large-scale monitoring of carbon uptake. Increasingly used unmanned aerial vehicles (UAVs) with various optical sensors provide an exciting opportunity to monitor multiple optical signals (e.g. PRI and WI) with high spatiotemporal resolution (Gago *et al*., 2015). MODIS (Moderate Resolution Imaging Spectroradiometer) aboard the Terra and Aqua satellites provides the possibility of retrieving PRI or CCI (chlorophyll/carotenoid index, Gamon *et al*., 2016) both in the morning and at midday, which can be further applied to test the diurnal changes of PRI or CCI and the utility of assessing carbon budget under ongoing and future climate change at larger spatial and longer temporal scales. GOME-2 (Global Ozone Monitoring Experiment-2) spectrometer, aboard the Metop satellite with a high spectral (0.2-0.4nm in ultraviolet and visible spectrum) and temporal resolution (enables scanning the earth surface within 1.5 day), also provides the possibility of calculation of PRI to detect changes in carbon uptake at high spatiotemporal scales.

Our ground-based study could provide basic information for validating the airborne or satellite-based inferences of photosynthesis using PRI in response to environmental stresses and the ongoing changes to climate, particularly, in regions dominated by evergreen species where photosynthetic capacity is mainly constrained by stomatal adjustment and water availability both in soil and leaves due to the effects of summer drought and low precipitation, such as our study site. Remotely sensing pigment activity to assess the seasonality of photosynthesis is a basic but vital step toward the ultimate assessment of the global carbon budget.

References

Arora, V. K., Boer, G. J., Christian, J. R., Curry, C. L., Denman, K. L., Zahariev, K., Flato, G. M., Scinocca, J. F., Merryfield, W. J. Lee, W. G., 2009. The effect of terrestrial photosynthesis down regulation on the twentieth-century carbon budget simulated with the CCCma earth system model. Journal of Climate, 22(22), 6066-6088.

Asensio, D., Peñuelas, J., Ogaya, R., Llusià, J., 2007. Seasonal soil and leaf CO_2 exchange rates in a Mediterranean holm oak forest and their responses to drought conditions. Atmospheric Environment, 41(11), 2447–2455.

Asensio, D., Peñuelas, J., Prieto, P., Estiarte, M., Filella, I., Llusià, J., 2008. Interannual and seasonal changes in the soil exchange rates of monoterpenes and other VOCs in a Mediterranean shrubland. European Journal of Soil Science, 59(5), 878–891.

Barbeta, A., Ogaya, R., Peñuelas, J., 2013. Dampening effects of long-term experimental drought on growth and mortality rates of a holm oak forest. Global Change Biology, 19(10), 3133–3144.

Bertrand, R., Riofrío-Dillon, G., Lenoir, J., Drapier, J., de Ruffray, P., Gégout, J.-C., Loreau, M., 2016. Ecological constraints increase the climatic debt in forests. Nature Communications, 7, 12643.

Carnicer, J., Coll, M., Ninyerola, M., Pons, X., Sánchez, G., Peñuelas, J., 2011. Widespread crown condition decline, food web disruption, and amplified tree mortality with increased climate change-type drought. Proceedings of the National Academy of Sciences of the United States of America, 108(4), 1474–8.

Catoni, R., Varone, L. Gratani, L., 2013. Variations in leaf respiration across different seasons for Mediterranean evergreen species. Photosynthetica, 51(2), 295-304.

Ciais, P., Reichstein, M., Viovy, N., Granier, A., Ogée, J., Allard, V., Aubinet, M., Buchmann, N., Bernhofer, C., Carrara, A., Chevallier, F., de Noblet, N., Friend, A. D., Friedlingstein, P., Grünwald, T., Heinesch, B., Keronen, P., Knohl, A., Krinner, G., Loustau, D., Manca, G., Matteucci, G., Miglietta, F., Ourcival, J. M., Papale, D., Pilegaard, K., Rambal, S., Seufert, G., Soussana, J. F., Sanz, M. J., Schulze, E. D., Vesala, T., Valentini, R., 2005. Europe-wide reduction in primary productivity caused by the heat and drought in 2003. Nature, 437(7058), 529–533.

Claudio, H. C., Cheng, Y., Fuentes, D. A., Gamon, J. A., Luo, H., Oechel, W., Qiu, H. L., Rahman, A. F., Sims, D. A., 2006. Monitoring drought effects on vegetation water content and fluxes in chaparral with the 970 nm water band index. Remote Sensing of Environment, 103(3), 304–311.

Cook, B. I., Anchukaitis, K. J., Touchan, R., Meko, D. M., Cook, E. R., 2016. Spatiotemporal drought variability in the Mediterranean over the last 900 years. Journal of Geophysical Research: Atmospheres, 121(5), 2060–2074.

Crafts-Brandner, S. J., Salvucci, M. E., 2000. Rubisco activase constrains the photosynthetic potential of leaves at high temperature and CO_2. Proceedings of the National Academy of Sciences of the United States of America, 97(24), 13430–13435.

Dai, A., 2011. Drought under global warming: a review. Wiley Interdisciplinary Reviews: Climate Change, 2(1), 45–65.

Damesin, C., Rambal, S., 1995. Field study of leaf photosynthetic performance by a Mediterranean deciduous oak tree (*Quercus pubescens*) during a severe summer drought. New Phytologist, 131(2), 159–167.

Damm, A., Guanter, L., Verhoef, W., Schläpfer, D., Garbari, S., Schaepman, M. E., 2015. Impact of varying irradiance on vegetation indices and chlorophyll fluorescence derived from spectroscopy data. Remote Sensing of Environment, 156, 202–215.

del Cacho, M., Peñuelas, J., Lloret, F., 2013. Reproductive output in Mediterranean shrubs under climate change experimentally induced by drought and warming. Perspectives in Plant Ecology, Evolution and Systematics, 15(6), 319–327.

Demmig-Adams, B., Adams, W. W., 1996. The role of xanthophyll cycle carotenoids in the protection of photosynthesis. Trends in Plant Science, 1(1), 21–26.

Demmig-Adams, B., Adams, W. W., 2006. Photoprotection in an ecological context: the remarkable complexity of thermal energy dissipation. New Phytologist, 172(1), 11–21.

Demmig-Adams, B., Adams, W. W., Winter, K., Meyer, A., Schreiber, U., Pereira, J.S., Krüger, A., Czygan, F. C., Lange, O. L., 1989. Photochemical efficiency of photosystem II, photon yield of O_2 evolution, photosynthetic capacity, and carotenoid composition during the

midday depression of net CO_2 uptake in *Arbutus unedo* growing in Portugal. Planta, 177(3), 377–387.

Farquhar, G. D., Sharkey, T. D., 1982. Stomatal conductance and photosynthesis. Annual review of plant physiology, 33(1), 317–345.

Filella, I., Peñuelas, J., Llorens, L., Estiarte, M., 2004. Reflectance assessment of seasonal and annual changes in biomass and CO_2 uptake of a Mediterranean shrubland submitted to experimental warming and drought. Remote Sensing of Environment, 90(3), 308–318.

Filella, I., Porcar-Castell, A., Munné-Bosch, S., Bäck, J., Garbulsky, M. F., Peñuelas, J., 2009. PRI assessment of long-term changes in carotenoids/chlorophyll ratio and short-term changes in de-epoxidation state of the xanthophyll cycle. International Journal of Remote Sensing, 30(17), 4443–4455.

Gago, J., Douthe, C., Coopman, R., Gallego, P., Ribas-Carbo, M., Flexas, J., Escalona, J., Medrano, H., 2015. UAVs challenge to assess water stress for sustainable agriculture. Agricultural water management, 153, 9–19.

Gallé, A., Haldimann, P., Feller, U., 2007. Photosynthetic performance and water relations in young pubescent oak (*Quercus pubescens*) trees during drought stress and recovery. New Phytologist, 174(4), 799–810.

Gamon, J. A., Berry, J. A., 2012. Facultative and constitutive pigment effects on the photochemical reflectance index (PRI) in sun and shade conifer needles. Israel Journal of Plant Sciences, 60(1-2), 85–95.

Gamon, J.A., Bond, B., 2013. Effects of irradiance and photosynthetic downregulation on the photochemical reflectance index in Douglas-fir and ponderosa pine. Remote Sensing of Environment, 135, 141–49.

Gamon, J. A., Huemmrich, K. F., Wong, C. Y. S., Ensminger, I., Garrity, S., Hollinger, D. Y., Noormets, A., Peñuelas, J., 2016. A remotely sensed pigment index reveals photosynthetic phenology in evergreen conifers. Proceedings of the National Academy of Sciences of the United States of America, 113(46), 13087–13092.

Gamon, J. A., Peñuelas, J., Field, C. B., 1992. A narrow-waveband spectral index that tracks diurnal changes in photosynthetic efficiency. Remote Sensing of Environment, 41(1), 35–44.

Gamon, J. A., Surfus, J. S., 1999. Assessing leaf pigment content and activity with a reflectometer. New Phytologist, 143(1), 105–117.

Garbulsky, M. F., Peñuelas, J., Gamon, J. A., Inoue, Y., Filella, I., 2011. The photochemical reflectance index (PRI) and the remote sensing of leaf, canopy and ecosystem radiation use efficiencies: a review and meta-analysis. Remote Sensing of Environment, 115(2), 281–297.

Giorgi, F., Lionello, P., 2008. Climate change projections for the Mediterranean region. Global and Planetary Change, 63(2–3), 90–104.

Gitelson, A., Merzlyak, M.N., 1994. Spectral reflectance changes associated with autumn senescence of *Aesculus hippocastanum* L. and *Acer platanoides* L. leaves. Spectral features and relation to chlorophyll estimation. Journal of Plant Physiology, 143(3), 286-292.

Goerner, A., Reichstein, M., Rambal, S., 2009. Tracking seasonal drought effects on ecosystem light use efficiency with satellite-based PRI in a Mediterranean forest. Remote Sensing of Environment, 113(5), 1101–1111.

Granda, E., Camarero, J. J., Gimeno, T. E., Martínez-Fernández, J., Valladares, F., 2013. Intensity and timing of warming and drought differentially affect growth patterns of co-occurring Mediterranean tree species. European Journal of Forest Research, 132(3), 469–480.

He, M., Kimball, J.S., Running, S., Ballantyne, A., Guan, K., Huemmrich, F., 2016. Satellite detection of soil moisture related water stress impacts on ecosystem productivity using the MODIS-based photochemical reflectance index. Remote Sensing of Environment, 186, 173-183.

Hilker, T., Hall, F. G., Coops, N. C., Lyapustin, A., Wang, Y., Nesic, Z., Grant, N., Black, T.A., Wulder, M. A., Kljun, N., Hopkinson, C., Chasmer, L., 2010. Remote sensing of photosynthetic light-use efficiency across two forested biomes: spatial scaling. Remote Sensing of Environment, 114(12), 2863–2874.

Hmimina, G., Dufrêne, E., Soudani, K., 2014. Relationship between photochemical reflectance index and leaf ecophysiological and biochemical parameters under two different water statuses: towards a rapid and efficient correction method using real-time measurements. Plant, cell & environment, 37(2), 473-487.

Liu, D., Llusià, J., Ogaya, R., Estiarte, M., Llorens, L., Yang, X., Peñuelas, J., 2016. Physiological adjustments of a Mediterranean shrub to long-term experimental warming and drought treatments. Plant Science, 252, 53–61.

Liu, D., Estiarte, M., Ogaya, R., Yang, X., Peñuelas, J., 2017. Shift in community structure in an early-successional Mediterranean shrubland driven by long-term experimental warming and drought and natural extreme

droughts. Global Change Biology, 1–13.

Liu, D., Ogaya, R., Barbeta, A., Yang, X., Peñuelas, J., 2015. Contrasting impacts of continuous moderate drought and episodic severe droughts on the aboveground-biomass increment and litterfall of three coexisting Mediterranean woody species. Global Change Biology, 21(11), 4196–4209.

Llorens, L., Peñuelas, J., Estiarte, M., 2003a. Ecophysiological responses of two Mediterranean shrubs, *Erica multiflora* and *Globularia alypum*, to experimentally drier and warmer conditiions. Physiologia Plantarum, 119(2), 231–243.

Llorens, L., Peñuelas, J., Filella, I., 2003b. Diurnal and seasonal variations in the photosynthetic performance and water relations of two co-occurring Mediterranean shrubs, *Erica multiflora* and *Globularia alypum*. Physiologia Plantarum, 118, 84–95.

Magney, T. S., Vierling, L. A., Eitel, J. U. H., Huggins, D. R., Garrity, S. R., 2016. Remote sensing of environment response of high frequency photochemical reflectance index (PRI) measurements to environmental conditions in wheat. Remote Sensing of Environment, 173, 84–97.

Mänd, P., Hallik, L., Peñuelas, J., Nilson, T., Duce, P., Emmett, B. A., Beier, C., Estiarte, M., Garadnai, J., Kalapos, T., Schmidt, I. K., Kovács-Láng, E., Prieto, P., Tietema, A., Westerveld, J. W., Kull, O., 2010. Responses of the reflectance indices PRI and NDVI to experimental warming and drought in European shrublands along a north-south climatic gradient. Remote Sensing of Environment, 114(3), 626–636.

Marino, G., Pallozzi, E., Cocozza, C., Tognetti, R., Giovannelli, A., Cantini, C., Centritto, M., 2014. Assessing gas exchange, sap flow and water relations using tree canopy spectral reflectance indices in irrigated and rainfed *Olea europaea* L. Environmental and Experimental Botany, 99, 43–52.

McDowell, N., Pockman, W. T., Allen, C. D., Breshears, D. D., Cobb, N., Kolb, T., Plaut, J., Sperry, J., West, A., Williams, D. G., Yepez, E. A., 2008. Mechanisms of plant survival and mortality during drought: why do some plants survive while others succumb to drought? New Phytologist, 178(4), 719–739.

Moreno, A., Maselli, F., Gilabert, M. A., Chiesi, M., Martínez, B., Seufert, G., 2012. Assessment of MODIS imagery to track light-use efficiency in a water-limited Mediterranean pine forest. Remote Sensing of Environment, 123, 359–367.

Nardini, A., Lo Gullo, M. A., Trifilò, P., Salleo, S., 2014. The challenge of the Mediterranean climate to plant hydraulics: Responses and adaptations. Environmental and Experimental Botany, 103, 68–79.

Niyogi, K., 1999. Photoprotection revisited: genetic and molecular approaches. Annual review of plant biology, 50(1), 333–359.

Nogués, I., Peñuelas, J., Llusià, J., Estiarte, M., Munné-Bosch, S., Sardans, J., Loreto, F., 2012. Physiological and antioxidant responses of *Erica multiflora* to drought and warming through different seasons. Plant Ecology, 213(4), 649–661.

Ogaya, R., Llusià, J., Barbeta, A., Asensio, D., Liu, D., Alessio, G. A., Peñuelas, J., 2014. Foliar CO_2 in a holm oak forest subjected to 15 years of climate change simulation. Plant Science, 226, 101–107.

Oliveira, G., Peñuelas, J., 2005. Effects of winter cold stress on photosynthesis and photochemical efficiency of PSII of the Mediterranean *Cistus albidus* L. and *Quercus ilex* L. Plant Ecology, 175(2), 179–191.

Osório, J., Osório, M. L., Romano, A., 2012. Reflectance indices as nondestructive indicators of the physiological status of *Ceratonia siliqua* seedlings under varying moisture and temperature regimes. Functional Plant Biology, 39(7), 588–597.

Peñuelas, J., Baret, F., Filella, I., 1995a. Semi-empirical indexes to assess carotenoids chlorophyll-a ratio from leaf spectral reflectance. Photosynthetica, 31(2), 221–230.

Peñuelas, J., Filella, I., Biel, C., Serrano, L. Savé, R., 1993. The reflectance at the 950-970nm region as an indicator of plant water status. International Journal of Remote Sensing, 14(10), 1887–1905.

Peñuelas, J., Filella, I., Gamon, J. A., 1995b. Assessment of photosynthetic radiation use efficiency with spectral reflectance. New Phytologist, 131, 291–296.

Peñuelas, J., Garbulsky, M.F., Filella, I., 2011. Photochemical reflectance index (PRI) and remote sensing of plant CO_2 uptake. New Phytologist, 191(3), 596-599.

Peñuelas, J., Inoue, Y., 1999. Reflectance indices indicative of changes in water and pigment contents of peanut and wheat leaves. Photosynthetica, 36(3), 355–360.

Peñuelas, J., Prieto, P., Beier, C., Cesaraccio, C., de Angelis, P., de Dato, G., Emmett, B. A., Estiarte, M., Garadnai, J., Gorissen, A., Láng, E.

K., Kroel-Dulay, G., Llorens, L., Pellizzaro, G., Riis-Nielsen, T., Schmidt, I. K., Sirca, C., Sowerby, A., Spano, D., Tietema, A., 2007. Response of plant species richness and primary productivity in shrublands along a north-south gradient in Europe to seven years of experimental warming and drought: reductions in primary productivity in the heat and drought year of 2003. Global Change Biology, 13(12), 2563–2581.

Peñuelas, J., Pinol, J., Ogaya, R., Filella, I., 1997. Estimation of plant water concentration by the reflectance water index WI (R900/R970). International Journal of Remote Sensing, 18(13), 2869-2875.

Peñuelas, J., Sardans, J., Estiarte, M., Ogaya, R., Carnicer, J., Coll, M., Barbeta, A., Rivas-Ubach, A., Llusià, J., Garbulsky, M., Filella, I., 2013. Evidence of current impact of climate change on life: a walk from genes to the biosphere. Global change biology, 19(8), 2303-2338.

Peñuelas, J., Sardans, J., Filella, I., Estiarte, M., Llusià, J., Ogaya, R., Carnicer, J., Bartrons M., Rivas-Ubach, A., Grau O., Peguero, G., Margalef,. O, Pla-Rabés, S., Stefanescu, C., Asensio, L., Preece, C., Liu L., Verger, A., Rico, L., Barbeta, A., Achotegui-Castells, A., Gargallo-Garriga, A., Sperlich, D., Farré-Armengol, G., Fernández-Martínez, M., Liu, D., Zhang, C., Urbina, I., Camino, M., Vives, M., Nadal-Sala. D., Sabaté, S., Gracia. C., Terradas, J., 2017. Assessment of the impacts of climate change on Mediterranean terrestrial ecosystems based on data from field experiments and long-term monitored field gradients in Catalonia. Environmental and Experimental Botany. (*in press*).

Porcar-Castell, A., Garcia-Plazaola, J. J. I., Nichol, C. J., Kolari, P., Olascoaga, B. B., Kuusinen, N., Fernández-Marín, B., Pulkkinen, M., Juurola, E., Nikinmaa, E., 2012. Physiology of the seasonal relationship between the photochemical reflectance index and photosynthetic light use efficiency. Oecologia, 170(2), 313–323.

Porcar-Castell, A., Tyystjärvi, E., Atherton, J., van der Tol, C., Flexas, J., Pfündel, E. E., Moreno, J., Frankenberg, C., Berry, J. A., 2014. Linking chlorophyll a fluorescence to photosynthesis for remote sensing applications: mechanisms and challenges. Journal of Experimental Botany, 65(15), 4065–4095.

Powell, T. L., Galbraith, D. R., Christoffersen, B. O., Harper, A., Imbuzeiro, H. M. A., Rowland, L., Almeida, S., Brando, P. M., Costa, A. C. L., Costa, M. H., Levine, N. M., Malhi, Y., Saleska, S. R., Sotta, E., Williams, M., Meir, P., Moorcroft, P. R., 2013. Confronting model predictions of carbon fluxes with measurements of Amazon forests subjected to experimental drought. New Phytologist, 200(2), 350–365.

Prieto, P., Peñuelas, J., Lloret, F., Llorens, L., Estiarte, M., 2009a. Experimental drought and warming decrease diversity and slow down post-fire succession in a Mediterranean shrubland. Ecography, 32(4), 623–636.

Prieto, P., Peñuelas, J., Llusià, J., Asensio, D., Estiarte, M., 2009b. Effects of long-term experimental night-time warming and drought on photosynthesis, Fv/Fm and stomatal conductance in the dominant species of a Mediterranean shrubland. Acta Physiologiae Plantarum, 31(4), 729–739.

Prieto, P., Peñuelas, J., Niinemets, Ü., Ogaya, R., Schmidt, I. K., Beier, C., Tietema, A., Sowerby, A., Emmett, B.A., Láng, E.K., Kröel-Dulay, G., Lhotsky, B., Cesaraccio, C., Pellizzaro, G., de Dato, G., Sirca, C., Estiarte, M., 2009c. Changes in the onset of spring growth in shrubland species in response to experimental warming along a north-south gradient in Europe. Global Ecology and Biogeography, 18(4), 473–484.

Ripullone, F., Rivelli, A. R., Baraldi, R., Guarini, R., Guerrieri, R., Magnani, F., Peñuelas, J., Raddi, S., Borghetti, M., 2011. Effectiveness of the photochemical reflectance index to track photosynthetic activity over a range of forest tree species and plant water statuses. Functional Plant Biology, 38(3), 177–186.

Rischbeck, P., Elsayed, S., Mistele, B., Barmeier, G., Heil, K., Schmidhalter, U., 2016. Data fusion of spectral, thermal and canopy height parameters for improved yield prediction of drought stressed spring barley. European Journal of Agronomy, 78, 44–59.

Rossini, M., Fava, F., Cogliati, S., Meroni, M., Marchesi, A., Panigada, C., Giardino, C., Busetto, L., Migliavacca, M., Amaducci, S., Colombo, R., 2013. Assessing canopy PRI from airborne imagery to map water stress in maize. ISPRS Journal of Photogrammetry and Remote Sensing, 86, 168–177.

Sharkey, T. D., 2005. Effects of moderate heat stress on photosynthesis: importance of thylakoid reactions, rubisco deactivation, reactive oxygen species, and thermotolerance provided by isoprene. Plant, Cell and Environment, 28(3), 269–277.

Sheffield, J., Wood, E. F., 2008. Projected changes in drought occurrence under future global warming from multi-model, multi-scenario, IPCC AR4 simulations. Climate Dynamics, 31(1), 79–105.

Sheffield, J., Wood, E. F., Roderick, M. L., 2012. Little change in global drought over the past 60 years. Nature, 491(7424), 435–438.

Soudani, K., Hmimina, G., Dufrêne, E., Berveiller, D., Delpierre, N., Ourcival, J. M., J.M., Rambal, S., Joffre, R., 2014. Relationships between photochemical reflectance index and light-use efficiency in deciduous and evergreen broadleaf forests. Remote Sensing of Environment, 144, 73–84.

Stylinski, C. D., Gamon, J. A., Oechel, W. C., 2002. Seasonal patterns of reflectance indices, carotenoid pigments and photosynthesis of evergreen chaparral species. Oecologia, 131(3), 366–374.

Takahashi, S., Badger, M. R., 2011. Photoprotection in plants: a new light on photosystem II damage. Trends in Plant Science, 16(1), 53–60.

Tsonev, T., Wahbi, S., Sun, P., Sorrentino, G., Centritto, M., 2014. Gas exchange, water relations and their relationships with photochemical reflectance index in *Quercus ilex* plants during water stress and recovery. International Journal of Agriculture and Biology, 16(2), 335–341.

Tucker, C. J., 1979. Red and photographic infared linear combinations for monitoring vegetation. Remote Sensing of Environment, 8(2), 127–150.

van der Molen, M. K., Dolman, A. J., Ciais, P., Eglin, T., Gobron, N., Law, B. E., B.E., Meir, P., Peters, W., Phillips, O.L., Reichstein, M., Chen, T., Dekker, S. C., Doubková, M., Friedl, M. A. M., Jung, M., van den Hurk, B.J.J.M., de Jeua, R.A.M., Kruijt, B., Ohta, T., Rebel, K. T., Plummer, S., Seneviratne, S. I., Sitchg, S., Teuling, A.J., van der Werf, G.R., Wang, G., 2011. Drought and ecosystem carbon cycling. Agricultural and Forest Meteorology, 151(7), 765–773.

Vicca, S., Balzarolo, M., Filella, I., Granier, A., Herbst, M., Knohl, A., Longdoz, B., Mund, M., Nagy, Z., Pintér, K., Rambal, S., Verbesselt, J., Verger, A., Zeileis, A., Zhang, C., Peñuelas, J., 2016. Remotely-sensed detection of effects of extreme droughts on gross primary production. Scientific Reports, 6, 28269.

Vicente-Serrano, S. M., Lopez-Moreno, J.-I., Beguería, S., Lorenzo-Lacruz, J., Sanchez-Lorenzo, A., García-Ruiz, J. M., Azorin-Molina, C., Morán-Tejeda, E., Revuelto, J., Trigo, R., Coelho, F., Espejo, F., 2014. Evidence of increasing drought severity caused by temperature rise in southern Europe. Environmental Research Letters, 9(4), 44001.

Wong, C. Y. S., Gamon, J. A., 2015a. The photochemical reflectance index provides an optical indicator of spring photosynthetic activation in evergreen conifers. New Phytologist, 206(1), 196–208.

Wong, C. Y. S., Gamon, J. A., 2015b. Three causes of variation in the photochemical reflectance index (PRI) in evergreen conifers. New Phytologist, 206(1), 187–195.

Wu, Z., Dijkstra, P., Koch, G. W., Peñuelas, J., Hungate, B. A., 2011. Responses of terrestrial ecosystems to temperature and precipitation change: a meta-analysis of experimental manipulation. Global Change Biology, 17(2), 927–942.

Yuan, W., Cai, W., Chen, Y., Liu, S. S., Dong, W., Zhang, H., Yu, G., Chen, Z., He, H., Guo, W., Liu, D., Liu, S., Xiang, W., Xie, Z., Zhao, Z., Zhou, G., 2016. Severe summer heatwave and drought strongly reduced carbon uptake in Southern China. Scientific Reports, 6, 18813.

Zarco-Tejada, P. J., González-Dugo, V., Williams, L. E., Suárez, L., Berni, J. A. J., Goldhamer, D., Fereres, E., 2013a. A PRI-based water stress index combining structural and chlorophyll effects: assessment using diurnal narrow-band airborne imagery and the CWSI thermal index. Remote Sensing of Environment, 138, 38–50.

Zarco-Tejada, P. J., Morales, A., Testi, L., Villalobos, F. J., 2013b. Spatio-temporal patterns of chlorophyll fluorescence and physiological and structural indices acquired from hyperspectral imagery as compared with carbon fluxes measured with eddy covariance. Remote Sensing of Environment, 133, 102–115.

Zhang, C., Filella, I., Garbulsky, M., Peñuelas, J., 2016. Affecting factors and recent improvements of the photochemical reflectance index (PRI) for remotely sensing foliar, canopy and ecosystemic radiation-use efficiencies. Remote Sensing, 8(9), 677.

Block III. MODIS PRI assessing the effect of extreme drought on GPP and isoprenoid emissions. Ecosystem level.

Chapter 5. Remotely-sensed detection of effects of extreme droughts on gross primary production

Sara Vicca, Manuela Balzarolo, Iolanda Filella, André Granier, Mathias Herbst, Alexander Knohl, Bernard Longdoz, Martina Mund, Zoltan Nagy, Krisztina Pintér, Serge Rambal, Jan Verbesselt, Aleixandre Verger, Achim Zeileis, Chao Zhang and Josep Peñuelas

This chapter was published in ***Scientific Reports,*** 2016 (28269).

Abstract

Severe droughts strongly impact photosynthesis (GPP), and satellite imagery has yet to demonstrate its ability to detect drought effects. Especially changes in vegetation functioning when vegetation state remains unaltered (no browning or defoliation) pose a challenge to satellite-derived indicators. We evaluated the performance of different satellite indicators to detect strong drought effects on GPP in a beech forest in France (Hesse), where vegetation state remained largely unaffected while GPP decreased substantially. We compared the results with three additional sites: a Mediterranean holm oak forest (Puéchabon), a temperate beech forest (Hainich), and a semi-arid grassland (Bugacpuszta). In Hesse, a three-year reduction in GPP following drought was detected only by the Enhanced Vegetation Index (EVI). The Photochemical Reflectance Index (PRI) also detected this drought effect, but only after normalization for absorbed light. In Puéchabon normalized PRI outperformed the other indicators, while the short-term drought effect in Hainich was not detected by any tested indicator. In contrast, most indicators, but not PRI, captured the drought effects in Bugacpuszta. Hence, PRI improved detection of drought effects on GPP in forests and we propose that PRI normalized for absorbed light is considered in future algorithms to estimate GPP from space.

1. Introduction

Increased frequency and intensity of drought events is among the prospects that we are facing due to climate change. How ecosystems cope with and respond to extreme droughts will be crucial in the terrestrial feedback to climate change[1]. Severe and recurrent droughts can reduce the terrestrial carbon sink[2], eliciting a positive feedback on climate change. Ecosystem responses to drought, however, are highly variable in time and space[3–5]. Our knowledge of these responses is still very limited, in part because research on the effects of extreme droughts began only relatively recently and because extreme events occur only rarely in nature. The tools best suited for large-scale, long-term, and continuous high-frequency monitoring of terrestrial ecosystems, i.e. remote sensing imagery, though, have yet to demonstrate their ability to capture the effects of extreme droughts on carbon cycling in natural ecosystems.

To use satellite data for detecting and quantifying the effects of drought at a global scale, we need products that can reliably capture the variation in vegetation state (e.g. defoliation or browning) and in vegetation functioning (e.g. decreases in photosynthesis). Both can change in response to drought, but drought effects may also be restricted to changes in vegetation functioning, for example when trees that already reached peak leaf area experience a drought event, close their stomata and thereby strongly reduce photosynthetic CO_2 uptake. When drought severity remains below the level where leaves turn brown, vegetation state remains largely unaltered whereas vegetation functioning is altered and gross primary production (GPP) is decreased considerably.

Although commonly used remote sensing indicators such as the Normalized Difference Vegetation Index (NDVI) detect green biomass and generally detect changes in vegetation state (greening, mortality or defoliation)[6,7], these indicators often fail to reflect drought-induced decreases in plant activity. This failure can be due to absence of structural changes, to early saturation at high leaf area index masking moderate structural changes, or to particularly complex structural changes[8,9]. A recent comparison of commonly used remote sensing indicators with field observational data accordingly indicated a modest performance of these indicators in capturing the interannual variability in GPP[10]. Whereas for grasslands and evergreen broadleaved forests, NDVI and the Enhanced Vegetation Index (EVI) capture interannual variability in GPP relatively well, the relationships between the relative anomalies in annual GPP (estimated from eddy

covariance measurements) and the corresponding anomalies for the remote sensing indicators was very poor for deciduous broadleaved and evergreen needleleaved forests[10].

The GPP derived from Moderate Resolution Imaging Spectroradiometer (MODIS) product (modGPP) is an advanced satellite product for estimating the uptake of carbon by plants. The modGPP has been compared to field estimates of GPP in various studies, which typically suggest that this product is reliable at large spatial and temporal scales, but is more erratic at fine temporal and spatial resolution[10–13]. The modGPP is calculated as a function of FAPAR (fraction of absorbed photosynthetically active radiation), temperature, vapor pressure deficit (VPD), light (all three derived from a global dataset[14]) and an estimate of maximum radiation-use efficiency (RUE). It thus includes important abiotic variables that enable short-term fluctuations in this indicator that are not detected in commonly used remote sensing indicators such as FAPAR. Field conditions, however, may deviate from those suggested by these abiotic variables, which may lead to substantial differences between modGPP and field-based GPP estimates during drought periods (see e.g.11). The VPD obtained from the global dataset in particular may not well represent water availability. For example, a drought-induced decline in GPP may last much longer than the increase in VPD, which could lead to an underestimation of the drought effect by modGPP if FAPAR is unaltered. Moreover, RUE is here expressed as a biome-specific constant at its potential maximum that may not be representative of the seasonally variable RUE of an ecosystem. Hence, resulting GPP estimates often do not scale with field observations[15].

It has been suggested that RUE can be estimated remotely from the Photochemical Reflectance Index (PRI)[16]. The PRI is linked to the de-epoxidation status of the xanthophyll cycle pigments, which is one of the components of the non-photochemical de-excitation pathway[16]. PRI can capture the temporal dynamics in RUE via variations in the xanthophyll cycle pigments and the relative ratio of carotenoids to chlorophyll. It is a promising tool to better represent plant functioning through spectral measurements[15,17,18]. However, a valid remotely-based RUE estimate across different plant functional types and wide range of conditions has not yet been identified[15,19]. Accordingly, the performance of PRI in detecting drought effects on plant activity is still debated. A study by Peguero-Pina et al.[20] demonstrated that ground-based PRI can be a reliable index for detecting drought-induced reductions in plant activity (or more specifically, plant stress indicators such as chlorophyll fluorescence), but drought detection using PRI derived

from satellite data may be more problematic[19]. Although PRI can capture changes in the xanthophyll cycle, indicative of stress[21,22], these changes can be obscured by the much stronger signals of seasonal variation in the pigment pool of the leaves (e.g. chlorophyls)[21], and by seasonal changes in illumination[23]. Recent insights from ground-based remote sensing suggest that a normalization for absorbed light may overcome many of these problems[24]. This promising approach of normalizing PRI for absorbed light remains to be evaluated for satellite-based PRI.

The aim of this study was to test if commonly used remote sensing indicators and PRI calculated with MODIS bands could detect effects of extreme drought on GPP. We hypothesized that commonly used remote sensing indicators, except for modGPP, detect drought effects only when vegetation state is affected. We expected PRI to capture drought effects on GPP in case of physiological changes and in particular, we anticipated a substantial improvement of drought detection by PRI when normalized for absorbed light. To test our hypotheses, we selected a beech forest in Hesse, France where long-term monitoring revealed a strong reduction of GPP during the European heatwave[25] that was associated with a drought event that lasted from 2003 until 2005 in this forest, but hardly affected vegetation state (leaf area index, tree mortality). To further test the generalizability of our findings, this ideal test case was further complemented with three long-term monitoring sites that had experienced a severe drought. These three additional sites - which were the only ones that met the necessary criteria (see Methods) - are an uneven-aged and unmanaged beech forest in Hainich, Germany; an evergreen broadleaved holm oak forest in Puéchabon, France; and a semi-arid grassland in Bugacpuszta, Hungary (see Supplementary Table S1 for general site information). We used the following remote sensing indicators in our study: NDVI, EVI, EVI2, FAPAR, absorbed photosynthetically active radiation (APAR), Leaf Area Index (LAI), Simple Ratio (SR), Global Environmental Monitoring Index (GEMI), Normalized Difference Water Index (NDWI), modGPP and PRI (see Methods and Supplementary Table S2 for calculations).

2. Methods

2.1. Site description

The key site in this study was a beech forest in Hesse, northeastern France. The

monitoring site was installed in a 0.6-ha fenced experimental plot in the central part of the forest. The forest was naturally regenerated and contained 95% European beech (*Fagus sylvatica* L.) trees averaging 40 years of age in 2005. The young forest has been managed traditionally by the French forest service (ONF) and was thinned just before the start of the monitoring (end of 1995, no data available), in spring 1999, at the end of 2004, and at the beginning of 2010. Stem density was reduced by 24.4, 17.7 and 10.5%, whereas LAI decreased by 35.1, 33.3 and 22.9%, in 1999, 2004 and 2010, respectively (Figure 1b). More information about this forest is provided in Supplementary Table S1 and in Bréda et al.[46] and Granier et al.[29].

We further searched the FLUXNET and European fluxes databases for sites to test the robustness of the results obtained for Hesse. These sites, as for Hesse, had to meet the following criteria:

1. Time series of GPP covering at least five consecutive years
2. Homogenous vegetation at 1 km resolution
3. Drought event that is detected in GPP

The first criterion is a prerequisite for analyzing time series. The effect of a drought on GPP and its detection by remote sensing imagery can only be tested with sufficiently long time series that (1) enable comparison of drought and non-drought periods, and (2) enable detection of potential lagged and/or carry-over effects. The second criterion ensures reliable comparisons between field data and remote sensing indicators, as it avoids contradictory flux measurements that depend on wind direction and footprint extent. The third criterion is necessary for testing the use of satellite data for detecting the effects of drought. We selected only those sites where GPP was significantly affected during a drought based on a breakpoint-detection technique and for which the site investigators confirmed that the reduction in GPP during the drought could indeed be attributed to water stress. These three criteria excluded the vast majority of sites, especially because drought events were often not reflected in GPP measurements (e.g. because trees had access to deep soil water), or because simultaneous management activities confounded the drought response of GPP. The remaining sites provided datasets of high quality, which was essential for this study. These three additional sites were: an uneven-aged and unmanaged beech forest in Hainich, Germany; an evergreen broadleaved holm oak forest in Puéchabon, France; and a semi-arid grassland in Bugacpuszta, Hungary.

2.2. Drought episodes

We calculated the Standardized Precipitation Evapotranspiration Index (SPEI) using the SPEI-package in R47. SPEI is a meteorological drought indicator based on a monthly climatic water balance (precipitation – potential evapotranspiration), which is adjusted using a three-parameter log-logistic distribution. We then accumulated the values at a timescale of 12 months, and this SPEI12 indicates for each moment in time the meteorological dryness (or wetness) of the previous 12 months as compared to historical observations. The choice of this timescale was arbitrary but of minor importance for this study, because it only served to identify the occurrence and timing of a severe drought. Moreover, the patterns in SPEI were similar for all timescales between six and 18 months (data not shown). SPEI values between 1 and −1 are considered normal, whereas values <-1 indicate drought and values <-1.5 indicate severe drought[47]. We defined a drought as a period where SPEI12 decreased to ≤ -1.5.

Because we were interested in evaluating the use of globally available products, we extracted the necessary long-term precipitation and potential evapotranspiration data from EC-JRC-MARS (a dataset based on ECMWF model outputs and a reanalysis of ERA-Interim; see http://spirits.jrc.ec.europa.eu/), based on the geographic location of each site. This dataset provides a finer spatial resolution (0.25°) than the CRU data set (0.5°) used by Vicente Serrano et al.[47]. The period covered by the JRC-MARS dataset was 1989–2012. Potential evapotranspiration estimates in this dataset are calculated using the Penman-Monteith equation[48].

Although SPEI is a useful and convenient metric for detecting meteorological drought, with good spatial and temporal coverage, it does not necessarily indicate field conditions well. Plants experience a given reduction in precipitation quite differently between sites (e.g., because of differences in soil texture)[40], and periods of drought are therefore best identified using site-specific data. For that reason, we computed for the selected sites relative extractable water (REW) based on a water balance model[49] (see details in Supplementary Notes S1). REW represents soil moisture as a fraction of maximum soil water across the rooting zone and is thus a type of agricultural drought index50. Below REW=0.4, plants can be considered drought stressed[29].

Because the necessary data for calculation of REW were not available for Bugacpuszta, soil water content (SWC) was used instead as an indicator of the water status of the site. These data suggested a strong drought in 2009, when SPEI12 remained

only slightly above −1.5. Therefore, 2009 was also considered as a dry year in the analyses. In addition, we computed for Puéchabon the water stress index (WSI), which incorporates not only soil measurements but also predawn leaf water potential measurements and is therefore an even better indicator of plant drought stress than REW. We consider WSI≤−250MPa day to be indicative of moderate to severe drought (see Supplementary Notes S1 for details).

2.3. Flux data

We extracted half-hourly data from the European fluxes database (http://www.europe-fluxdata. eu), and complemented these with the most recent data available (provided by the PI). We then calculated daily means from the half-hourly data. Gaps in the data due to sensor malfunctions or less than ideal turbulence conditions[51] were filled using marginal distribution sampling described by Reichstein et al.[52]. We used only days when both daily meteorological and flux data contained less than 20% gapfilled half-hourly data. Gross primary production was estimated using flux partitioning, based on the extrapolation of nighttime flux observations corrected for temperature differences with temperature-dependency relationships[52]. We further refer to this GPP estimate as 'tower GPP' to distinguish from MODIS' GPP product (modGPP; see below).

2.4. Satellite data

We used MODIS subset data (collection 5) provided by ORNL DAAC (http://daac.ornl. gov/cgi-bin/MODIS/GR_col5_1/mod_viz.html, col. 5) for deriving the commonly used indicators (Table S2). The MOD09A1 ASCII subset dataset contains surface reflectance data of MODIS bands ranging from 620 nm to 2155 nm at 500 m spatial resolution and eight-day synthesis period. For comparison with the other satellite indicators at 1-km spatial sampling, the 500 m reflectance data were re-sampled to 1-km spatial resolution by simple aggregation of the 2×2 pixels centered at the flux tower. Only high quality data were included and images affected by clouds or snow cover were removed according to the quality flag associated with MOD09A1 data. The reflectances at 1 km spatial resolution were used to compute the standard MODIS indicators presented in Table S2 (NDVI, EVI, EVI2, SR, GEMI, NDWI). We also gathered FAPAR and LAI from MOD15A253 at 8 days and 1 km and GPP data from MOD17 at 8 days and 500 m, aggregated at 1 km; http://www.ntsg.umt.edu/project/ mod17[28]. Finally, APAR (absorbed photosynthetically active radiation) was calculated from the MODIS FAPAR data, and

global radiation was calculated from EC-MARS-JRC data (0.25° spatial resolution; one-day interval). We assumed a constant fraction of PAR in global radiation: global radiation was divided by 43 to obtain an estimate of the photosynthetically active radiation (PAR; this relationship was derived from a comparison with field observations of PAR; Figure S3). This method removed gaps in the field data of PAR and was especially relevant for the current study where the aim was to determine how drought effects observed in the field could be detected using global databases. Note that we did not gapfill MODIS data because the interpolations that are used for gapfilling could create important artefacts that can influence drought detection.

Calculations of PRI were based on MOD21KM daily-calibrated radiance data (see http://ladsweb.nascom. nasa.gov). These images were georeferenced using MOD3 geolocation information and the Swath MODIS Tool available from LP DAAC (https://lpdaac.usgs.gov/tools/modis_reprojection_tool_swath). The pixel area of 1×1 km corresponding to the flux tower position was extracted and PRI was calculated as suggested by its developers[16,54] (see Supplementary Table S2) and later also applied by, for example, Drolet et al.17, Garbulsky et al.[42], Goerner et al.[44], Guarini et al.[55].

Dates when clouds were detected (using the MODIS MOD35 cloud algorithm and visual inspection) were discarded. The maximum value of PRI was calculated from a daily time series over an eight-day window to correspond to the temporal resolution of MOD09 and MOD15A2. Because corrected reflectances for applying an atmospheric correction are currently not available, we used the uncorrected PRI. Earlier studies reported that atmospheric correction did not improve the estimation of RUE[17,42,44], and therefore MODIS PRI without atmospheric correction was assumed to be an accurate indicator of RUE in different ecosystem types[17,42,55]. The temporal consistency observed in the PRI profiles presented in our study supports the reliability of the estimates.

To ensure positive values that are better comparable to commonly used remote sensing indicators such as NDVI, PRI values were standardized as by Rahman et al.[56] and Goerner et al.[57]:

$$sPRI = (1 + PRI)/2 \quad (1)$$

Because the relationship between PRI and RUE varies over the seasons[24], along with the dynamics in green biomass that absorbs the incoming radiation, we calculated a standardized PRI (PRIn), which is normalized for APAR (absorbed PAR; see[24] for rationale). This normalization allows to focus on the part of PRI explaining RUE and

photosynthetic performance because it removes the part linked to pigments and structure. PRIn was calculated by:

$$PRIn = PRI – RI0 \quad (2)$$

with PRI0 the intercept of PRI vs APAR for a two-month window. This window size was the best compromise between having sufficient data for a reliable fit (eight data points if none are missing), and an informative relationship between PRI and APAR. The latter changes over time[24], so the smaller the window, the better APAR represents the structure of the vegetation. Finally, we standardized PRIn to obtain only positive values analogous to sPRI:

$$sPRIn = (1 + PRIn)/2 \quad (3)$$

sPRIn is an indicator of the excess energy not photosynthetically processed; when plants are stressed, their RUE decreases as more energy is lost through heat dissipation. An increase in sPRIn should thus indicate an increase in foliar photosynthetic activity.

2.5. Analyses

To test whether drought effects on tower GPP are detected by any of the remote sensing indicators under test, we first calculated for each site the average seasonal pattern over the entire time series, using a 1-month moving window (thus providing for each day the average value across the time series). The anomalies from this average season were then computed and used for further analyses, except in the case of sPRIn, which showed no seasonality (Supplementary Figure S4). We then removed for all sites data for October-April (thus leaving only May-September) to study only the season when plants have leaves and are active. This elimination was necessary to avoid artifacts in the remote sensing indicators caused by sensing soil instead of leaves.

In order to test if tower GPP and the remote sensing indicators were significantly different during the drought period(s) as compared to the rest of the time series, we compared a linear model with and without a drought term (which indicates the pre-defined drought periods visualized as grey areas in Figs 1–7) using ANOVA. In addition, we ran a test for structural changes58 considering only the pre-defined drought period and the year before. As the data were all seasonally adjusted prior to this analysis, a simple piecewise constant model was used. Hence, whereas the ANOVA considers all drought periods within a time series at once, the test for structural changes considers the individual drought periods.

Responses in remote sensing indicators may lag behind the responses observed in

the field - for example when physiological changes reduce tower GPP while vegetation state (LAI for example) is unaltered -, and full recovery from drought may be (long) after precipitation ends the meteorological drought. These inconsistent responses complicate robust detection of drought effects and are best analyzed with a flexible technique, such as breakpoint analysis. Breakpoint analysis is a technique developed for detecting breaks based on structural changes in the time series[59]. This analysis is related to the test for structural changes indicated above, but does not presume any periods where breaks would occur (i.e., no pre-defined drought periods are considered). A simple piecewise constant model with unknown number and location of breakpoints was adopted. Given a certain number of breaks, their location is chosen to minimize the residual sum of squares across the corresponding segments subject to a minimal segment size of 12 observations (about three months of observations). The number of breaks was then chosen to optimize the Bayesian information criterion (BIC). The result for each site and anomaly series is a piecewise constant fit with the BIC-optimal number/location of breaks/segments. See Zeileis et al.[60] for more details.

All analyses were performed in MATLAB R2014b (The MathWorks Inc., Natick, USA), except for the breakpoint analysis and the test for structural change, which both used the strucchange package in R[58].

3. Results

In Hesse, the 2003 heatwave is clearly visible in the Standardized Precipitation Evapotranspiration Index (accumulated over 12 months; SPEI12; see Methods); SPEI12 decreased below −1.5 and did not return to zero until 2006 (Figure 1a; for temperature and precipitation data, see Supplementary Figure S1). This corresponds well with patterns for relative extractable soil water (REW; calculated from ground data of soil moisture) which reached a minimum in 2003 and remained low in 2004 and 2005. No other droughts were visible in SPEI12 or REW for the rest of the observation period (Figure 1a). The strong and lengthy drought had little effect on ground-based leaf area index (LAI) estimates, which varied between 5.8 and 8.7 and reached a minimum in 2005, after the thinning of autumn 2004 (Figure 1b). In contrast to LAI, tower GPP was substantially reduced during 2003–2005 (Tables 1 and 2) and returned to pre-2003 levels only in 2006 (Figure 1c). The strong reduction in tower GPP due to the 2003–2005 drought was clearly

captured by the test for structural change (Table 1) and by the breakpoint-detection technique (Figure 1d).

Table 1. For each site and each variable the P values of ANOVA analysis comparing a model with and without drought term and P values resulting from the test for structural changes (SC) for the indicated period (i.e., the drought episode + the year before). P values in bold indicate robust reductions during the drought period (i.e. the structural change test corresponds to the results of the breakpoint analysis presented in Figs 2–7 and in SI). NA indicates that too few data were available to run the test for structural changes.

	Hesse		Hainich			Puéchabon			Bugacpuszta			
	ANOVA	SC (2002–2006)	ANOVA	SC (2002–2003)	SC (2002–2004)	ANOVA	SC (2004–2006)	SC (2008–2011)	ANOVA	SC (2002–2003)	SC (2006–2007)	SC (2008–2009)
GPP	<0.01	**<0.01**	<0.01	**<0.01**	**<0.01**	<0.01	**<0.01**	**0.03**	<0.01	**<0.01**	**<0.01**	**<0.01**
modGPP	<0.01	0.05	0.01	0.15	0.37	<0.01	**<0.01**	0.07	<0.01	0.15	**<0.01**	**<0.01**
EVI	<0.01	**<0.01**	0.74	0.99	<0.01	<0.01	**<0.01**	**<0.01**	<0.01	NA	**<0.01**	**<0.01**
sPRIn	0.03	**<0.01**	0.21	0.12	0.36	<0.01	**<0.01**	**<0.01**	0.10	0.99	NA	0.01
APAR	0.90	0.30	0.76	0.44	0.48	0.04	**0.02**	0.52	<0.01	**0.03**	0.07	**<0.01**
EVI2	0.08	0.77	0.63	0.21	0.79	0.08	0.90	0.10	0.02	0.74	**<0.01**	**0.02**
FAPAR	0.53	0.48	0.52	0.63	0.45	<0.01	0.38	1.00	<0.01	<0.01	**<0.01**	**0.01**
GEMI	0.05	0.27	0.22	0.98	**0.01**	0.02	0.15	<0.01	<0.01	NA	**<0.01**	**<0.01**
LAI	0.07	<0.01	0.53	0.32	0.10	<0.01	**<0.01**	0.99	<0.01	<0.01	**<0.01**	**<0.01**
NDVI	0.90	0.90	0.26	0.78	0.90	<0.01	**<0.01**	0.05	<0.01	NA	**<0.01**	**<0.01**
NDWI	0.62	0.06	0.41	0.97	0.97	<0.01	**<0.01**	0.01	<0.01	NA	**<0.01**	**<0.01**
sPRI	0.25	0.37	0.19	0.78	0.57	0.25	0.41	0.12	<0.01	0.03	0.69	0.99
SR	0.04	**<0.01**	0.94	1.00	0.67	<0.01	**<0.01**	0.04	<0.01	NA	**<0.01**	**<0.01**

Table 2. For each site and each variable the mean and standard deviation (in brackets) of the anomalies from the average season for the periods without drought (white areas in Figs 1–6), for the drought periods (grey areas in Figs 1–6) and for the period preceding the first drought. For sPRIn for which the absolute values are presented. For sPRI and sPRIn, values are multiplied by 100 for visualization purposes. Bold numbers indicate significant differences between drought and non-drought periods (corresponding p values are in Table 1, in columns with header 'ANOVA').

	Hesse			Hainich			Puéchabon			Bugacpuszta		
	No drought	Pre-drought	Drought	No drought	Pre-drought	Drought	No drought	Pre-drought	Drought	No drought	Pre-drought	Drought
GPP	0.72 (1.31)	0.88 (1.32)	**−1.65 (1.57)**	0.46 (1.04)	0.99 (1)	**−0.74 (1.33)**	0.42 (1.13)	0.36 (1.17)	**−0.48 (1.12)**	0.73 (1.74)	−0.53 (2.17)	**−1.3 (1.41)**
modGPP	0.08 (0.72)	−0.18 (0.73)	**−0.07 (0.6)**	0.11 (0.75)	−0.08 (0.69)	**−0.29 (0.7)**	0.17 (0.72)	0.03 (0.69)	**−0.15 (0.68)**	0.27 (0.66)	−0.01 (0.62)	**−0.31 (0.64)**
EVI	0.02 (0.06)	0.02 (0.05)	**−0.03 (0.05)**	0.01 (0.08)	0 (0.09)	0.02 (0.04)	0.01 (0.03)	0.01 (0.03)	**−0.01 (0.03)**	0.03 (0.07)	−0.04 (0.06)	**−0.05 (0.08)**
sPRIn*100	50.05 (0.52)	50.14 (0.59)	**49.86 (0.48)**	49.89 (0.56)	49.81 (0.6)	49.64 (0.67)	50.16 (0.55)	50.07 (0.55)	**49.88 (0.38)**	50.02 (0.34)	50.1 (0.23)	50.17 (0.29)
APAR	−0.35 (94.32)	−3.98 (91.73)	−4.91 (105.97)	−4.38 (63.88)	−2.04 (71.65)	−2.39 (81.01)	−2.57 (49.04)	−0.77 (48.41)	**1.41 (49.1)**	14.54 (48.49)	−11.25 (42.17)	**−19.28 (46.15)**
EVI2	0 (0.06)	0.01 (0.06)	0.03 (0.06)	0.01 (0.06)	0.01 (0.06)	0.02 (0.08)	0.01 (0.06)	0.02 (0.06)	0.01 (0.06)	0.02 (0.06)	0.04 (0.07)	**0.01 (0.08)**
FAPAR	−0.03 (0.21)	−0.04 (0.22)	−0.06 (0.21)	−0.02 (0.12)	−0.02 (0.13)	−0.05 (0.15)	−0.01 (0.05)	−0.02 (0.05)	**−0.02 (0.05)**	0.03 (0.1)	−0.03 (0.09)	**−0.08 (0.11)**
GEMI	0.01 (0.06)	0.01 (0.05)	−0.02 (0.05)	0 (0.08)	−0.01 (0.08)	−0.09 (0.14)	0.01 (0.04)	0.01 (0.04)	**−0.01 (0.03)**	0.03 (0.06)	−0.03 (0.05)	**−0.04 (0.07)**
LAI	0.98 (1.91)	1.03 (2)	**0.29 (1.45)**	−0.23 (1.08)	−0.14 (1.22)	−0.51 (1.38)	−0.01 (1.06)	−0.08 (1.01)	**−0.24 (1.03)**	0.1 (0.32)	−0.09 (0.27)	**−0.21 (0.26)**
NDVI	−0.04 (0.12)	−0.03 (0.12)	−0.03 (0.1)	−0.03 (0.15)	−0.03 (0.17)	−0.2 (0.28)	0.01 (0.03)	0.01 (0.03)	**−0.01 (0.03)**	0.05 (0.1)	−0.04 (0.09)	**−0.09 (0.12)**
NDWI	−0.01 (0.07)	−0.01 (0.06)	−0.02 (0.05)	−0.02 (0.1)	−0.02 (0.11)	−0.11 (0.18)	0.01 (0.05)	0 (0.05)	**−0.01 (0.04)**	0.05 (0.14)	−0.12 (0.11)	**−0.1 (0.13)**
sPRI*100	0 (0.35)	−0.05 (0.42)	−0.08 (0.36)	−0.01 (0.37)	−0.08 (0.43)	−0.07 (0.31)	−0.03 (0.27)	−0.04 (0.29)	−0.02 (0.23)	−0.06 (0.26)	−0.06 (0.29)	**0.14 (0.23)**
SR	0.27 (2.9)	1.2 (2.19)	**−0.15 (1.97)**	−0.63 (7.52)	−0.58 (8.34)	−3.2 (8.2)	0.16 (0.55)	0.15 (0.63)	**−0.17 (0.55)**	0.54 (1.21)	−0.35 (0.94)	**−0.71 (1.14)**

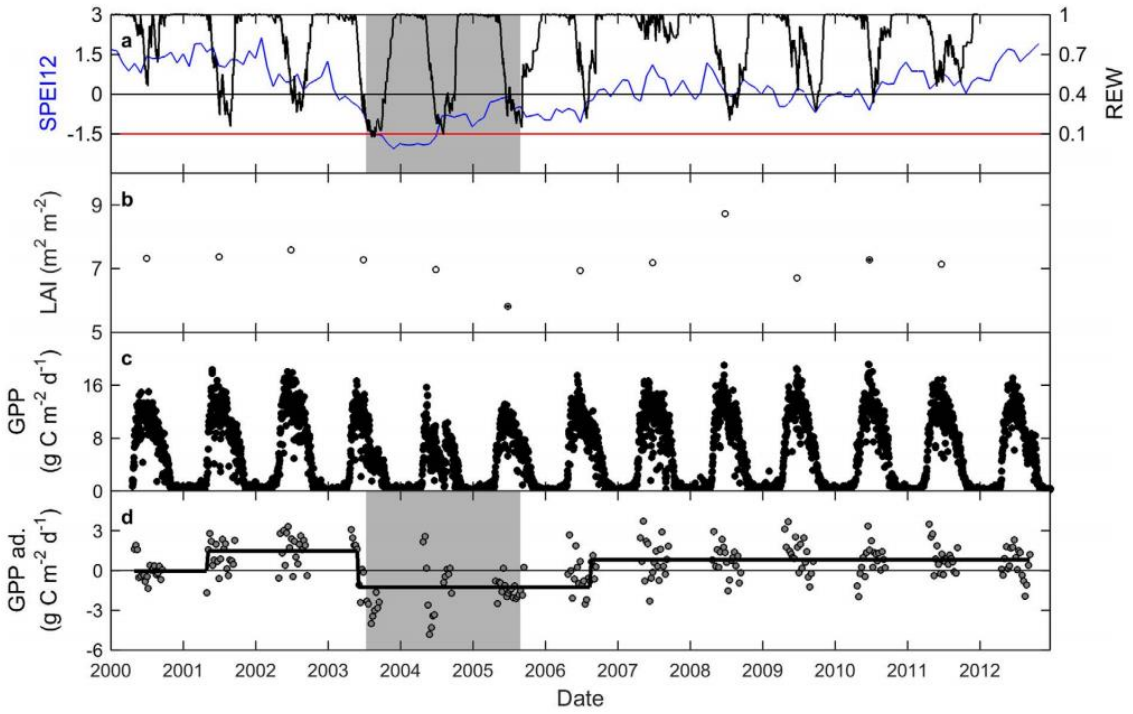

Figure 1. Time series of ground data and of the SPEI12 for the beech forest in Hesse. (a) SPEI12 and relative extractable water (REW); (b) leaf area index (LAI; determined from trapped litter; see29); (c) daily values for tower GPP; and (d) the results of the breakpoint analysis for GPP (with 8-day values). In (a), the blue line corresponds to SPEI12 and the black line to REW. The red line indicates the SPEI12 threshold of −1.5 (indicative of severe drought). Black symbols for LAI indicate the year after thinning. No thinning occurred in the years with open symbols for LAI. In (d), the seasonally adjusted data (abbreviated as 'ad.' in axis labels) are shown and the black line indicates the results of the breakpoint analysis. The grey area indicates the drought episode that is focused on in this study.

The GPP product of MODIS did not reproduce the pattern observed for tower GPP. Although the test for structural change indicated a significant difference between drought and non-drought periods (Tables 1 and 2) and a minor break was detected at the end of the drought period, modGPP could obviously not reproduce the field observations; modGPP during drought was even higher than pre-drought modGPP (Figure 2a, Table 2). Another commonly used reflectance index, NDVI, did not change throughout the time series (Figure 2b, Table 1). EVI, in contrast, decreased significantly during the drought, as did the simple ratio (SR; for calculation see Table S2), albeit only for 2004–2006 (Figure 3e, Tables 1 and 2). None of the other commonly used remote sensing indicators

decreased during the 2003–2005 drought episode (Figs 2 and 3). We suspected an important role for the blue band in the successful detection of the drought effect with EVI, so we tested if EVI2 (which does not cover the dynamics in the blue band) could detect the drought effect on tower GPP. EVI2 did not decrease during the 2003–2005 drought (Figure 2d, Tables 1 and 2), supporting the postulated importance of the blue band in EVI.

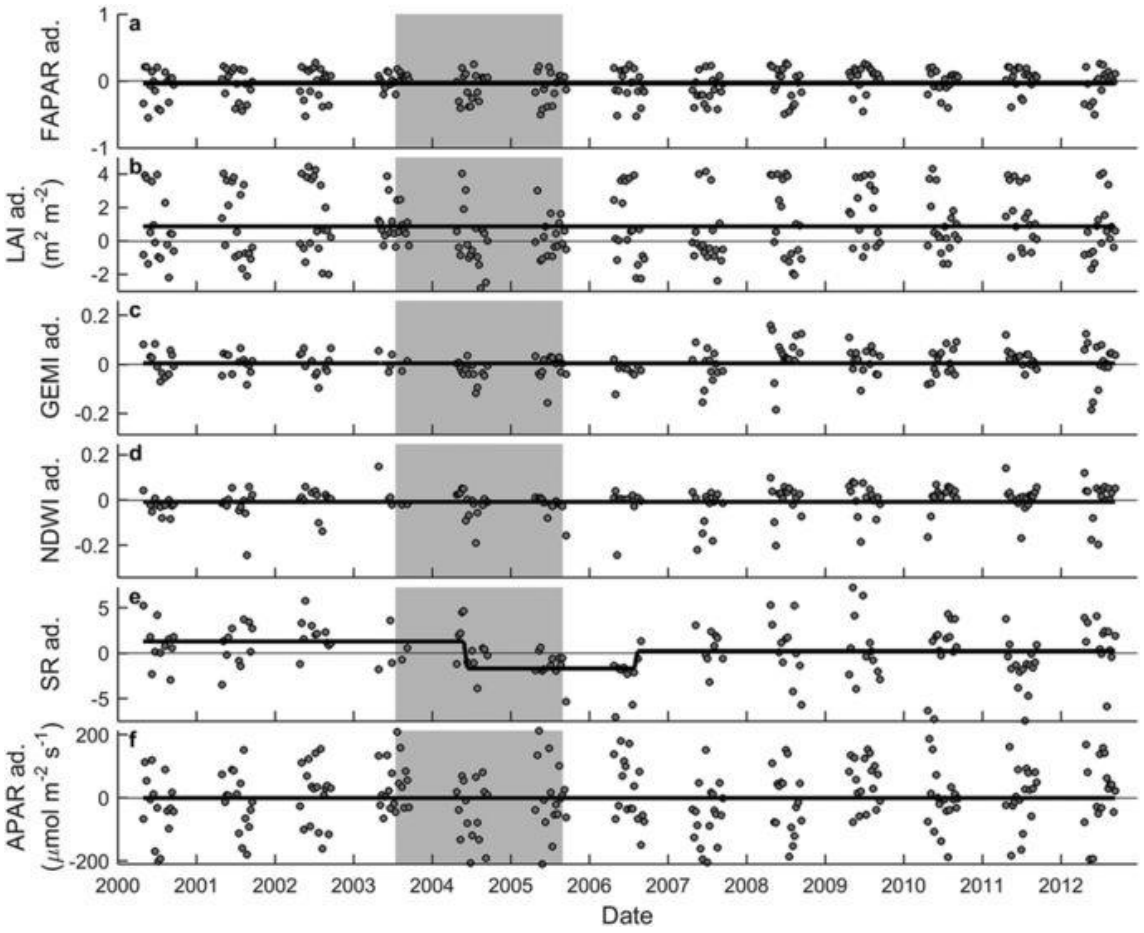

Figure 2. Results of the breakpoint analysis for Hesse. Seasonally adjusted data (abbreviated as 'ad.' in axis labels) are shown for the 8-day products of (a) MODIS GPP product (modGPP), (b) NDVI, (c) EVI, (d) EVI2, and (e) standardized Photochemical Reflectance Index (sPRI). For sPRI normalized for APAR (sPRIn; panel f), the absolute values are shown because no seasonal pattern was detected by sPRIn (see SI). The grey area indicates the drought episode. The black lines indicate the results of the breakpoint analysis.

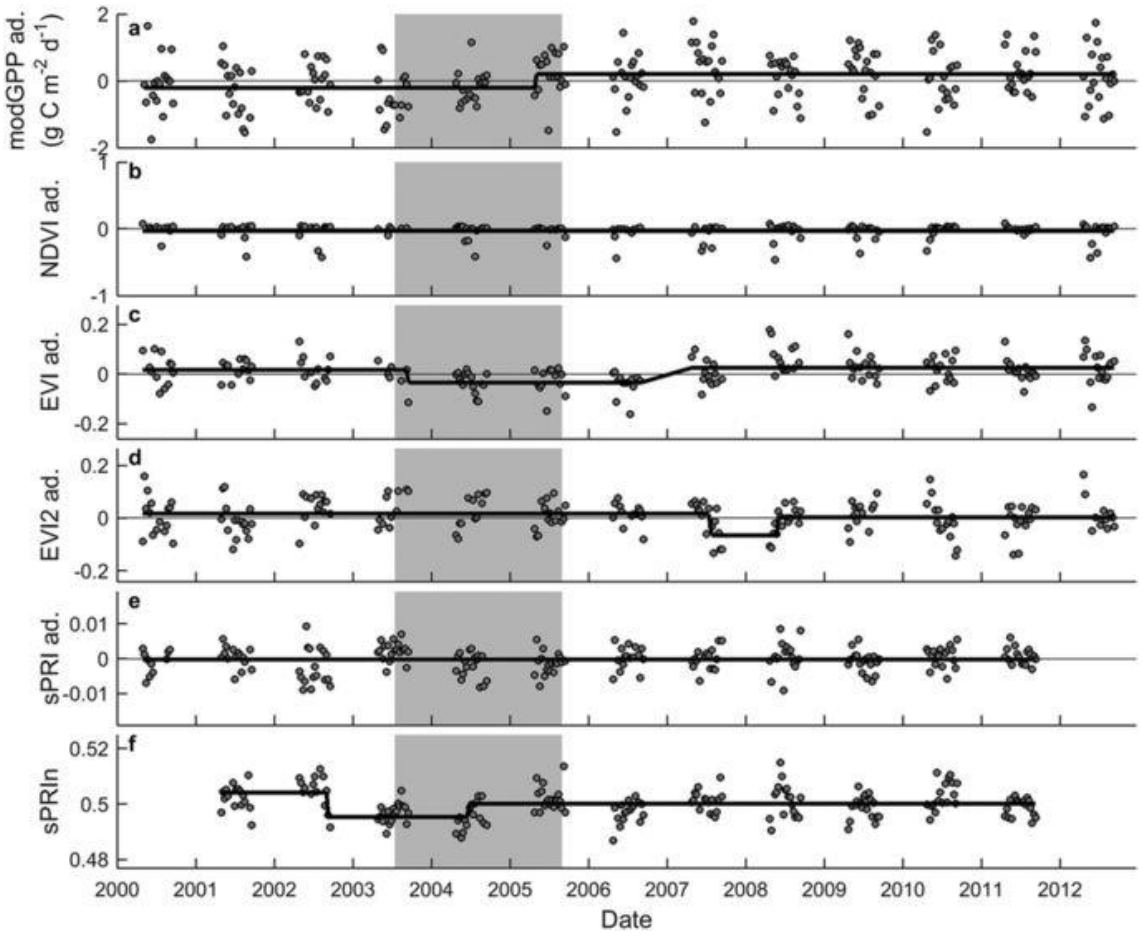

Figure 3. Results of the breakpoint analysis for Hesse. Seasonally adjusted data (abbreviated as 'ad.' in axis labels) are shown for the 8-day products of (a) FAPAR, (b) LAI, (c) GEMI, (d) NDWI, (e) SR, and (f) APAR. The grey area indicates the drought episode. The black line indicates the results of the breakpoint analysis.

We further tested if and how the drought effect was reflected in standardized PRI (sPRI; see Eq. 1) and in sPRI normalized for absorbed light (sPRIn; see Eqs 2 and 3). Whereas sPRI showed no significant response to drought, sPRIn decreased significantly in 2003 and 2004 (Figure 2e,f, Tables 1 and 2). In 2005, i.e., prior to GPP recovery, sPRIn returned to a level similar to pre-2003.

We also tested the performance of the remote sensing indicators at the three other sites where drought had decreased GPP. The first site, Hainich, is an unmanaged beech forest in Germany. Similar to Hesse, SPEI12, REW and GPP in Hainich decreased during the 2003 drought, but this effect was much less pronounced, and soil water was obviously replenished in Hainich in 2004, when REW never decreased below the common stress threshold of 0.4 (Figure 4). Whereas the reduction in tower GPP at the end of the 2003

growing season can be considered drought-induced, the slightly reduced tower GPP in 2004 as compared to other years most likely resulted from an extraordinary cold and rainy spring and massive fruit production (masting) that was associated with the displacement of leaf buds and thus a lower foliar production in 2004 (Supplementary Table S3).

Similar to Hesse, the modGPP data for Hainich did not match the observations in the field well (Figure 4). The reason for the lower modGPP in 2001–2003 compared to other years is unclear, but we presume it was related to artifacts in the algorithm, because neither FAPAR (included in the modGPP algorithm) nor any of the other remote sensing indicators showed this pattern. Interestingly, the 2003 drought was not captured by any of the remote sensing indicators (see also Figure S5). Also, sPRIn did not detect the reduction in photosynthetic activity (Figure 4e; Tables 1 and 2). On the other hand, the reduction in GPP (associated with a reduction in plant area index; Supplementary Table S3) was somewhat reflected in EVI (Table 1; but detection was not robust across methods and only the test for structural changes comparing 2002–2004 against the rest of the time series revealed an effect) and in GEMI (Global Environmental Monitoring Index; detected in the breakpoint analysis; Table 1 and Supplementary Figure S5).

In contrast to Hesse, the Mediterranean forest in Puéchabon is exposed to a dry period every year (see REW in Supplementary Figure S2), causing a decrease in tower GPP every summer, followed by an increase in autumn (Figure 5b). This typical seasonality is not reflected in SPEI12, which indicates the anomalies of the historical mean season. In 2005, however, SPEI12 decreased below −1.5, indicating a more extreme drought than usual. SPEI12 further suggests a milder drought in 2009. In contrast to Hesse, the 2003 heatwave was not obvious in SPEI12 for Puéchabon. This pattern in SPEI12 corresponded somewhat to the field measurements of predawn leaf water potential, detected by the water stress index (WSI), but contained some important differences. First, according to the WSI, the severest drought occurred in 2006, not 2005 (Figure 5a). Second, in contrast to SPEI12, WSI did not quickly recover after the drought in 2009 but remained low until 2011. The substantial decrease in WSI in 2005–2006 and the less severe decrease in 2009–2011 were associated with lower GPP (Figure 5, Table 1). WSI was not extremely low in 2003, but GPP decreased substantially (Figure 5b) due to the extremely high temperatures (Supplementary Figure S1). Most commonly used remote-sensing indicators captured the reduction in 2005–2006, but the reduction in GPP

associated with the dry period of 2009–2011 was captured only by EVI (Figure 5d, Table 1). sPRIn decreased for each drought where tower GPP decreased (and also during the 2003 heatwave). sPRIn therefore outcompeted all other indicators.

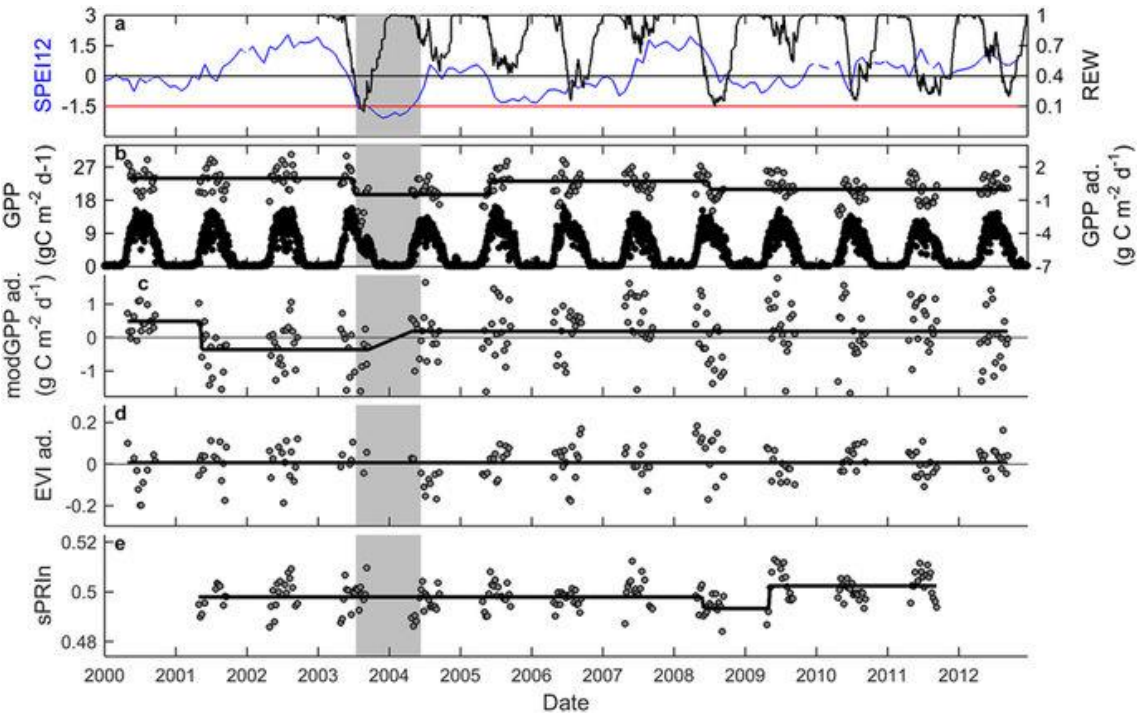

Figure 4. Time series of tower GPP, of remote sensing indicators, and of SPEI12 for the beech forest in Hainich. (a) SPEI12 (blue line) and relative extractable water (REW, black line). The red line indicates the SPEI12 threshold of −1.5 (indicative of severe drought); (b) daily values of tower GPP, and the results of the breakpoint analysis for 8-day GPP and 8-day products of (c) MODIS GPP product (modPP), (d) EVI, and (e) sPRIn. For tower GPP, black symbols represent the flux measurements, while grey symbols are the data for May-September that were adjusted for the seasonal pattern (abbreviated as 'ad.' in axis labels). This adjustment was also made for modGPP and EVI. The grey area indicates the drought episode. The black lines in b-f indicate the result of the breakpoint analysis.

Last, we tested drought detection in Bugacpuszta, a semi-arid grassland in Hungary. Similar to Puéchabon, this grassland experiences drought stress every summer, and GPP consequently peaks first in spring and then in late summer, interspersed by a reduction in the dry summer months (Figure 6). Bugacpuszta experienced extremely dry summers in 2003, 2007, and 2009, as indicated by SPEI12 and supported also by soil moisture

measurements. GPP decreased significantly during each of these droughts (Figure 6b, Tables 1 and 2). The modGPP captured the droughts in 2007 and 2009 but not the 2003 drought. Other commonly used remote sensing indicators such as NDVI and EVI also detected the drought effects of 2007 and 2009 (Table 1 and Supplementary Figure S5). Interestingly, sPRIn did not show any robust changes throughout the time series (Tables 1 and 2).

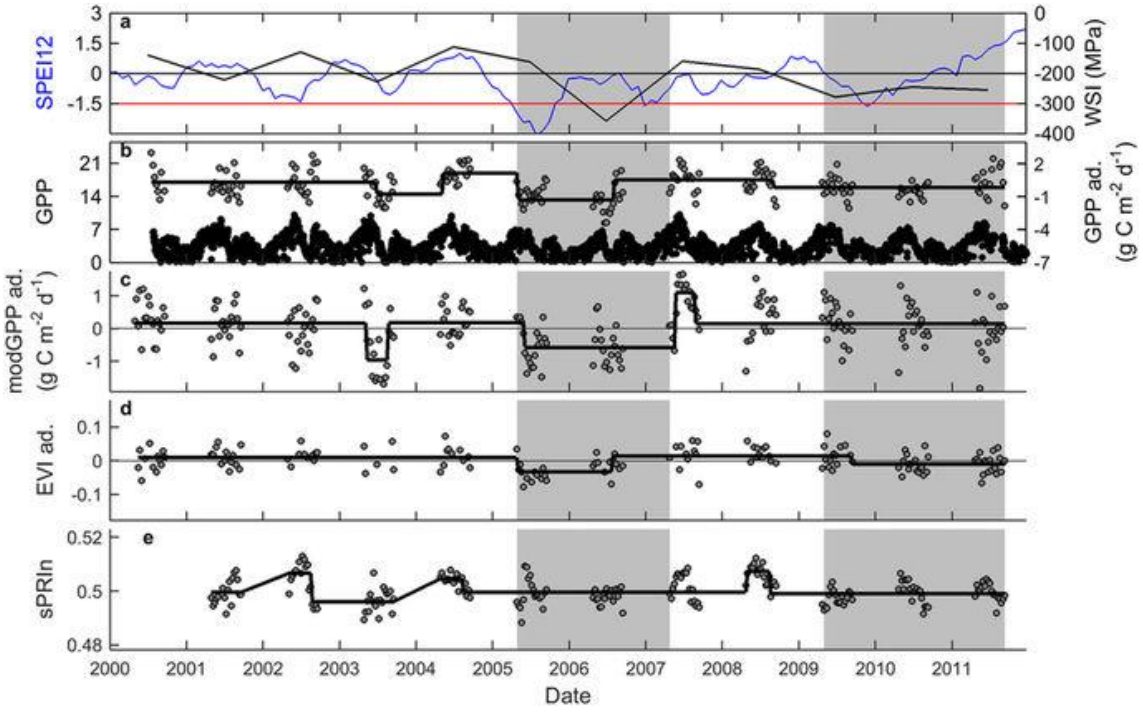

Figure 5. Time series of tower GPP, of remote sensing indicators, and of SPEI12 for the holm oak forest in Puéchabon. (a) SPEI12 (blue line) and annual values of the water stress integral (WSI in MPa day, black line). The red line indicates the SPEI12 threshold of −1.5 (indicative of severe drought); (b) daily values of tower GPP, and the results of the breakpoint analysis for 8-day GPP and 8-day products of (c) MODIS GPP product (modPP), (d) EVI, and (e) sPRIn. For tower GPP, black symbols represent the flux measurements, while grey symbols are the data for May-September that were adjusted for the seasonal pattern (abbreviated as 'ad.' in axis labels). This adjustment was also made for modGPP and EVI. The grey area indicates the drought episode. The black lines in b-f indicate the result of the breakpoint analysis.

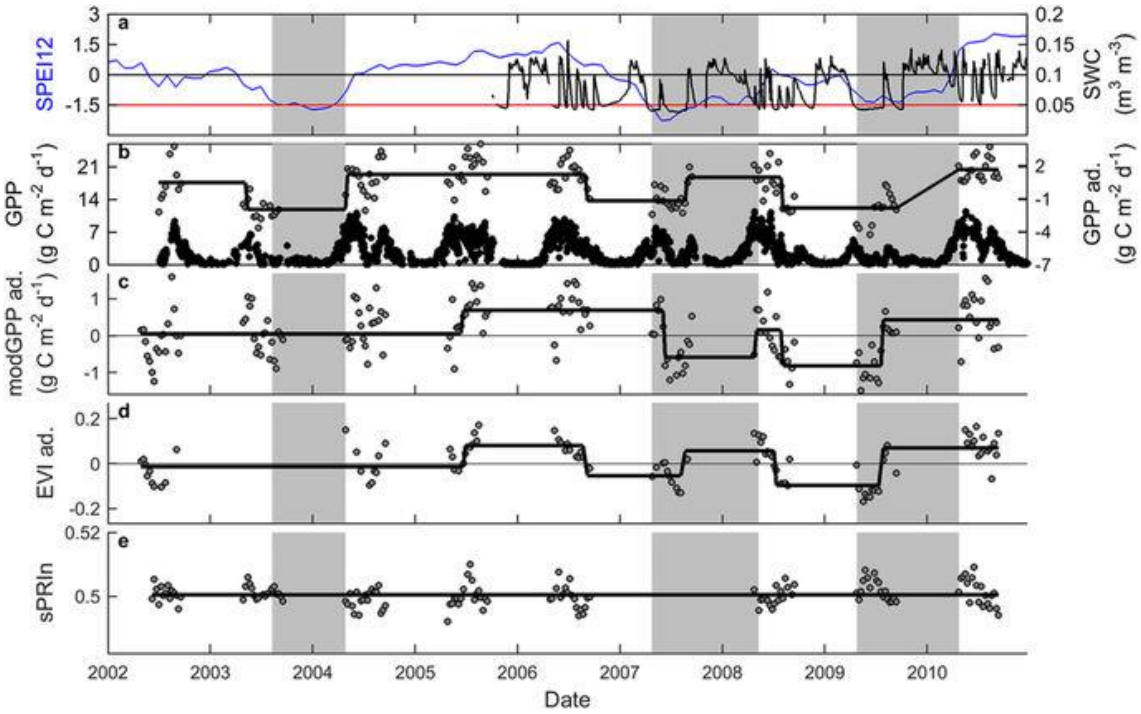

Figure 6. Time series of tower GPP, of remote sensing indicators, and of SPEI12 for the semi-arid grassland in Bugacpuszta. (a) SPEI12 (blue line) and soil water content (SWC, black line). The red line indicates the SPEI12 threshold of −1.5 (indicative of severe drought); (b) daily values of tower GPP, and the results of the breakpoint analysis for 8-day GPP and 8-day products of (c) MODIS GPP product (modGPP), (d) EVI, and (e) sPRIn. For tower GPP, black symbols represent the flux measurements, while grey symbols are the data for May-September that were adjusted for the seasonal pattern (abbreviated as 'ad.' in axis labels). This adjustment was also made for modGPP and EVI. The grey area indicates the drought episode. The black lines in b-f indicate the result of the breakpoint analysis.

4. Discussion

The European heatwave of 2003 substantially reduced water availability in Hesse, and also 2004 and 2005 were dry. Despite the lack of a drought response in LAI, tower GPP obviously decreased. Foliar physiology was thus affected by the drought, but massive defoliation or mortality did not occur. The breakpoint detection technique further revealed that the drought effect on tower GPP lasted until end of 2006, even though water levels had returned to pre-drought levels in that year. This illustrates the value of the breakpoint detection technique, which does not require a predefined drought period and is

particularly useful to detect and characterize drought impacts and climate-related dynamics[26]. We suggest that the application of this method (previously applied to remote sensing data; e.g. in[27)] to time series of flux data can provide deeper insight into ecosystem responses to drought.

As expected, most commonly used indicators did not change throughout the time series. The lack of response of NDVI, FAPAR, and other of these commonly used indicators corresponded to the lack of response of LAI. Moreover, the signals are quickly saturated in forests with high LAI (such as Hesse), making these indicators insensitive to small changes in foliar biomass. Surprisingly, however, modGPP did not decrease in response to the severe drought. Given that the algorithm for this product includes temperature and VPD[28], and both increased in Hesse during the 2003 heatwave[29], modGPP was expected to detect at least a small decrease in 2003. These results indicate that modGPP cannot reliably estimate the tower GPP response to drought for the beech forest in Hesse.

Of the commonly used remote sensing indicators tested, only EVI and simple ratio (SR) decreased significantly during the drought period. Both indicators are less prone to saturation problems[30]. Because the reduction in SR lagged behind the reduction in tower GPP and was not noticeable before 2005, we presume that the reduction in SR mainly detected the thinning effect on LAI and not the drought response of tower GPP. EVI, on the other hand, had already decreased in 2004, and did not even respond to the thinning event of 2005. EVI thus captured the drought-induced reduction in GPP in the absence of a change in LAI.

EVI was the only commonly used indicator under test that includes the blue band, which was included in EVI to reduce the effect of atmospheric aerosols but could also provide additional information on foliar carotenoid contents. Carotenoid absorption peaks between 400 and 500 nm (covered by the blue band)[31], and the carotenoid:chlorophyll ratio usually increases in response to environmental stresses[32], which results in a decrease in EVI. The fact that EVI2 (which is related to EVI but does not include blue band reflectance) remained unaffected by the 2003–2005 drought episode, supports our postulation that the reduction in EVI was related to an increase in foliar carotenoid: chlorophyll ratio that was captured by the blue band.

sPRI did not change throughout the time series for Hesse. When normalized for absorbed light, however, sPRIn did show a decrease in 2003 and this reduction persisted

during 2004. The importance of the normalization for detecting the drought effect can be explained as follows: sPRI can capture changes in the xanthophyll cycle (which responds quickly to environmental stresses), but these changes are obscured by the much stronger signals of seasonal variation in the whole pool of pigments in the leaves[21], and by seasonal changes in illumination[23]. Normalization is therefore necessary to remove the signal of seasonality in pigment pool and foliar structure to clarify the signal of the xanthophyll cycle[24]. PRI was normalized for absorbed light to remove (most of) the signal caused by changes in the pigment pool and illumination, and the resulting sPRIn should thus reflect changes in the xanthophyll cycle. Water limitation was somewhat alleviated in 2005, and sPRIn returned to pre-2003 levels. In contrast to EVI and SR, sPRIn seemed thus unaffected by the thinning in 2005, further confirming its performance in representing the functioning, but not the state, of the vegetation.

Hainich, a mixed beech forest in Germany, also experienced a drought in 2003, but unlike the case for Hesse, this event was brief; soil water was fully replenished during the winter of 2003–2004. Leaf physiology was probably affected only briefly, which poses a challenge on drought detection from satellite data. Indeed, the drought-induced reduction in tower GPP in autumn 2003 was not detected by any of the remote-sensing indicators evaluated (we did not consider modGPP, which obviously did not well reproduce the field observations for previous years) and this example thus indicates the limits of drought detection from satellite imagery. The timing of the drought at the end of the season may have complicated the detection of its effects, with relatively few data points available during the brief drought, and the regular leaf senescence may have obscured drought detection even further.

Interestingly, a reduction in GPP in 2004, related most likely to reduced foliar biomass production caused by an extraordinarily cold and rainy spring (Supplementary Figure S1) and masting in 2004[33], was detected to some extent by EVI and especially by GEMI (Supplementary Figure S5), but not by sPRIn. This illustrates the added value of sPRIn, as EVI and GEMI alone could be taken to suggest a carry-over effect of the drought, whereas the lack of a change in sPRIn indicates that this change in GPP was due to a structural change, not to a change in leaf functioning.

The evergreen broadleaved forest in Puéchabon experienced recurrent droughts during the study period. GPP decreased most strongly during the 2005–2006 drought, which was clearly detected by most remote-sensing indicators. Neither LAI, nor foliar

production decreased in 2006[34], whereas decreases in GPP are directly controlled by water limitation[35]. On the other hand, sPRIn was the only indicator that detected the less pronounced drought in 2009–2011 and the reduction of tower GPP during the 2003 heatwave. The inability of modGPP to detect the drought effects on tower GPP in 2009–2011 may be related to the meteorological data, which in our case differed from field observations.

Lastly, GPP in the Hungarian grassland decreased during each of the three drought events, and these decreases were well detected in many commonly used remote sensing indicators, but not in sPRIn. The contrasting performance of different remote sensing indicators between the grassland and forests studied here could be related to the earlier observations that grasslands respond differently to drought than forests. Whereas trees close their stomata and thus reduce tower GPP when soil moisture decreases below the comfortable level, thereby maintaining leaf water potential above a critical threshold and avoiding cavitation, grasses are not conservative in their water use and tend to remain active until moisture levels drop below the wilting point[36]. Grasses subsequently turn brown and die. Grasslands may thus respond to drought in a way that is more easily detected by remote sensing indicators such as NDVI that reflect green biomass. The quick transition of grasslands from active to dead vegetation may complicate detection by eight-day PRI indicators. The performance of PRI has also been suggested to depend highly on the density of the vegetation[37]. View angle had very little effect on PRI for dense forests, but may confound PRI for sparser vegetation due to the increased importance of background reflectance[37].

In summary, evaluation of sPRIn and commonly used remote sensing indicators against four sites where a severe drought event reduced GPP revealed (1) that commonly used remote sensing indicators, including modGPP are likely to leave drought effects on GPP in forests undetected, (2) that sPRIn is a promising indicator that allows drought detection from space and provides useful information about vegetation functioning that is not captured by the other remote sensing indicators under test, and (3) that GPP responses in a seasonally dry grassland are best detected by greenness indicators such as NDVI, whereas the utility of sPRIn is limited. The fact that drought effects on GPP were in several cases not detected by modGPP contrasts somewhat with Reichstein et al.[38], who found a strong reduction in modGPP across Europe during the 2003 heatwave. This apparent discrepancy can be clarified by the difference in spatial resolution and scale.

While Reichstein et al.[38] reported changes across Europe, using 10× 10 km pixel resolution, we zoom in on just a few 1× 1 km pixels in Europe. Given that for example the forest in Hesse is relatively small and surrounded by cropland and grassland, the difference between our studies highlights the importance of choice of resolution: use of small pixels is essential for a more mechanistic understanding, whereas large pixels facilitate estimation of large-scale impacts, although following our study, the latter might underestimate the drought impact on GPP.

A global product for estimating GPP from space would obviously be of great value for understanding and predicting terrestrial carbon cycling. However, the most advanced product currently available - modGPP - can not explain substantial spatial and temporal variation in GPP[10] and often fails to accurately capture pronounced drought effects on GPP39. This illustrates the broader problem that modGPP (and other commonly used remote sensing indicators) reflect primarily changes in vegetation state and leave important changes in vegetation functioning undetected. The drought response of modGPP is modeled on meteorological data (temperature and VPD), and these may not represent the drought as experienced by the biota, which depends not only on incoming water, but also on soil characteristics and rooting depth[40]. Obviously, if modGPP cannot capture strong drought effects, it is unlikely to capture even more subtle changes with possible important implications for the terrestrial carbon cycle. Remote sensing products targeting drought responses but based solely on greenness indicators and meteorological data (e.g. the Vegetation Drought Response Index[41]) may be prone to similar problems as modGPP. We suggest that remote sensing products to estimate GPP be based on a combination of indicators of vegetation state (e.g. FAPAR) and functioning (e.g. sPRIn).

The PRI has been successfully incorporated in remote sensing algorithms to estimate GPP of a specific site from space[42], and this GPP estimate was more accurate than modGPP for the Mediterranean forest under test (Castelporziano, Italy). Until now, however, a key limitation of PRI is that its relationship with plant physiological variables such as RUE varies spatially and temporally[43,44], complicating its incorporation in remote sensing algorithms for wider application. Possibly, sPRIn has more robust spatiotemporal patterns because at least part of the complicating factors typical for PRI are excluded through the normalization that removes the influence of variation in pigments and illumination. A thorough evaluation of the overall spatiotemporal performance of sPRIn should enable further improvement of the algorithms for estimating GPP from space and

future studies need to evaluate such product against modGPP and alternatives as e.g. provided by[39].

Direct assessment of photosynthetic activity and RUE with PRI remains thus an area of ongoing research, requiring a careful consideration of the spatial and temporal factors affecting the PRI components, and a thorough evaluation of sPRIn. Different ecosystems having contrasting constraints on carbon fluxes should also have contrasting optical properties reflected in PRI and NDVI dynamics[45]. It is not likely that any single parameterization will apply equally well across all ecosystems, biomes and/or seasons due to the contrasting controls on physiology and structure, but this is an open question that needs further consideration in the immediate future.

References

1 Frank, D. A. *et al*. Effects of climate extremes on the terrestrial carbon cycle: concepts, processes and potential future impacts. *Global Change Biol*. **21**, 2861-2880 (2015).

2 Granier, A. *et al*. Evidence for soil water control on carbon and water dynamics in European forests during the extremely dry year: 2003. *Agr*. *Forest Meteorol*. **143**, 123-145 (2007).

3 Reichstein, M. *et al*. Climate extremes and the carbon cycle. *Nature* **500**, 287-295 (2013).

4 van der Molen, M. K. *et al*. Drought and ecosystem carbon cycling. *Agr*. *Forest Meteorol*. **151**, 765-773 (2011).

5 Vicca, S. *et al*. Can current moisture responses predict soil CO2 efflux under altered precipitation regimes? A synthesis of manipulation experiments. *Biogeosc*. **11**, 2991-3013 (2014).

6 Dardel, C. *et al*. Re-greening Sahel: 30 years of remote sensing data and field observations (Mali, Niger). *Remote Sens*. *Environ*. **140**, 350-364 (2014).

7 Sangüesa-Barreda, G., Camarero, J. J., Garcia-Martin, A., Hernandez, R. & de la Riva, J. Remote sensing and tree-ring based characterization of forest defoliation and growth loss due to the Mediterranean pine processionary moth. *Forest Ecol*. *Manag*. **320**, 171-181 (2014).

8 Maselli, F., Papale, D., Puletti, N., Chirici, G. & Corona, P. Combining remote sensing and ancillary data to monitor the gross productivity of water-limited forest ecosystems. *Remote Sens*. *Environ*. **113**, 657-667 (2009).

9 Anderson, L. O. Biome-Scale Forest Properties in Amazonia Based on Field and Satellite Observations. *Remote Sens*. **4**, 1245-1271 (2012).

10 Verma, M. *et al*. Remote sensing of annual terrestrial gross primary productivity from MODIS: an assessment using the FLUXNET La Thuile data set. *Biogeosci*. **11**, 2185-2200 (2014).

11 Zhao, M., Running, S. W. & Nemani, R. R. Sensitivity of Moderate Resolution Imaging Spectroradiometer (MODIS) terrestrial primary production to the accuracy of meteorological reanalyses. *J*. *Geophys*. *Res*.-*Biogeo*. **111** (2006).

12 Peñuelas, J., Garbulsky, M. F. & Filella, I. Photochemical reflectance index (PRI) and remote sensing of plant CO2 uptake. *New Phytol*. **191**, 596-599 (2011).

13 Gamon, J. A., Peñuelas, J. & Field, C. B. A narrow-waveband spectral index that tracks diurnal changes in photosynthetic activity. *Remote Sens*. *Environ*. **41**, 35-44 (1992).

14 Drolet, G. G. *et al*. A MODIS-derived photochemical reflectance index to detect inter-annual variations in the photosynthetic light-use efficiency of a boreal deciduous forest. *Remote Sens*. *Environ*. **98**, 212-224 (2005).

15 Rossini, M. *et al*. Remote sensing-based estimation of gross primary production in a subalpine grassland. *Biogeosci*. **9**, 2565-2584 (2012).

16 Moreno, A. *et al*. Assessment of MODIS imagery to track light-use efficiency in a water-limited Mediterranean pine forest. *Remote Sens*. *Environ*. **123**, 359-367 (2012).

17 Peguero-Pina, J. J., Morales, F., Flexas, J., Gil-Pelegrin, E. & Moya, I. Photochemistry, remotely sensed physiological reflectance index and de-epoxidation state of the xanthophyll cycle in Quercus coccifera under intense drought. *Oecologia* **156**, 1-11 (2008).

18 Wong, C. Y. S. & Gamon, J. A. Three causes of variation in the photochemical reflectance index (PRI) in evergreen conifers. *New Phytol*. **206**, 187-195 (2015).

19 Peñuelas, J., Gamon, J. A., Fredeen, A. L., Merino, J. & Field, C. B. Reflectance indices associated with physiological changes in nitrogen- and water-limited sunflower leaves. *Remote Sens*. *Environ*. **48**, 135-146 (1994).

20 Gamon, J. A. & Bond, B. Effects of irradiance and photosynthetic downregulation on the photochemical reflectance index in Douglas-fir and ponderosa pine. *Remote Sens*. *Environ*. **135**, 141-149 (2013).

21 Soudani, K. *et al*. Relationships between photochemical reflectance index and light-use efficiency in deciduous and evergreen broadleaf forests. *Remote Sens*. *Environ*. **144**, 73-84 (2014).

22 Ciais, P. *et al*. Europe-wide reduction in primary productivity caused by the heat and drought in 2003. *Nature* **437**, 529-533 (2005).

23 Verbesselt, J., Zeileis, A. & Herold, M. Near real-time disturbance detection using satellite image time series. *Remote Sens*. *Environ*. **123**, 98-108 (2012).

24 Saatchi, S. *et al*. Persistent effects of a severe drought on Amazonian forest canopy. *P*. *Natl*. *A*. *Sci*. *USA* **110**, 565-570 (2013).

25 Running, S. W. *et al*. A continuous satellite-derived measure of global terrestrial primary production. *Biosci*. **54**, 547-560 (2004).

26 Granier, A., Breda, N., Longdoz, B., Gross, P. & Ngao, J. Ten years of fluxes and stand growth in a young beech forest at Hesse, North-eastern France. *Ann*. *For*. *Sci*. **65**, 704 (2008).

27 Huete, A. *et al*. Overview of the radiometric and biophysical performance of the MODIS vegetation indices. *Remote Sens*. *Environ*. **83**, 195-213 (2002).

28 Sims, D. A. & Gamon, J. A. Relationships between leaf pigment content and spectral reflectanceacross a wide range of species, leaf structures and developmental stages. *Remote Sens*. *Environ*.
81, 337-354 (2002).

29 Baquedano, F. J. & Castillo, F. J. Comparative ecophysiological effects of drought on seedlings of the Mediterranean water-saver Pinus

halepensis and water-spenders Quercus coccifera and Quercus ilex. *Trees* **20**, 689-700 (2006).
30 Liu, C. *et al*. Effect of drought on pigments, osmotic adjustment and antioxidant enzymes in six woody plant species in karst habitats of southwestern China. *Environ*. *Exp*. *Bot*. **71**, 174-183
(2011).
31 Mund, M. *et al*. The influence of climate and fructification on the inter-annual variability of stem growth and net primary productivity in an old-growth, mixed beech forest. *Tree Physiol*. **30**, 689- 704 (2010).
32 Rambal, S. *et al*. How drought severity constrains gross primary production (GPP) and its partitioning among carbon pools in a Quercus ilex coppice? *Biogeosci*. **11**, 6855-6869 (2014)
33 Rambal, S. *et al*. Drought controls over conductance and assimilation of a Mediterranean evergreen ecosystem: scaling from leaf to canopy. *Global Change Biol*. **9**, 1813-1824 (2003).
34 Baldocchi, D. D., Xu, L. & Kiang, N. How plant functional-type, weather, seasonal drought, and soil physical properties alter water and energy fluxes of an oak–grass savanna and an annual grassland. *Agr*. *Forest Meteorol*. **123**, 13-39 (2004).
35 Sims, D. A., Rahman, A. F., Vermote, E. F. & Jiang, Z. Seasonal and inter-annual variation in view angle effects on MODIS vegetation indices at three forest sites. *Remote Sens*. *Environ*. **115**, 3112-3120 (2011).
36 Reichstein, M. *et al*. Reduction of ecosystem productivity and respiration during the European summer 2003 climate anomaly: a joint flux tower, remote sensing and modelling analysis. *Global Change Biol*. **13**, 634-651 (2007).
37 Sims, D. A. *et al*. A new model of gross primary productivity for North American ecosystems based solely on the enhanced vegetation index and land surface temperature from MODIS. *Remote Sens*. *Environ*. **112**, 1633-1646 (2008).
38 Vicca, S. *et al*. Urgent need for a common metric to make precipitation manipulation experiments comparable. *New Phytol*. **195**, 518-522 (2012).
39 Garbulsky, M. F., Peñuelas, J., Gamon, J., Inoue, Y. & Filella, I. The photochemical reflectance index (PRI) and the remote sensing of leaf, canopy and ecosystem radiation use efficiencies A review and meta-analysis. *Remote Sens*. *Environ*. **115**, 281-297 (2011).
40 Goerner, A. *et al*. Remote sensing of ecosystem light use efficiency with MODIS-based PRI. *Biogeosci*. **8**, 189-202 (2011).
41 Balzarolo, M. *et al*. On the relationship between ecosystem-scale hyperspectral reflectance and CO_2 exchange in European mountain grasslands. *Biogeosci*. **12**, 3089-3108 (2015).
42 Breda, N., Huc, R., Granier, A. & Dreyer, E. Temperate forest trees and stands under severe drought: a review of ecophysiological responses, adaptation processes and long-term consequences. *Ann*. *For*. *Sci*. **63**, 625-644 (2006).
43 Vicente-Serrano, S. M., Begueria, S. & Lopez-Moreno, J. I. A Multiscalar Drought Index Sensitive to Global Warming: The Standardized Precipitation Evapotranspiration Index. *J*. *Clim*. **23**, 1696- 1718 (2010).
44 Allen, R. G., Pereiro, L. S., Raes, D. & Smith, M. Crop Evapotranspiration - Guidelines for Computing Crop Water Requirements. (Food and Agriculture Organization of the United Nations, Rome, Italy, 1998).
45 Granier, A., Breda, N., Biron, P. & Villette, S. A lumped water balance model to evaluate duration and intensity of drought constraints in forest stands. *Ecol*. *Model*. **116**, 269-283 (1999).
46 Papale, D. *et al*. Towards a standardized processing of Net Ecosystem Exchange measured with eddy covariance technique: algorithms and uncertainty estimation. *Biogeosci*. **3**, 571-583 (2006). 47 Reichstein, M. *et al*. On the separation of net ecosystem exchange into assimilation and ecosystem respiration: review and improved algorithm. *Global Change Biol*. **11**, 1424-1439 (2005).
48 Myneni, R. B. *et al*. Global products of vegetation leaf area and fraction absorbed PAR from year one of MODIS data. *Remote Sens*. *Environ*. **83**, 214-231 (2002).
49 Peñuelas, J., Filella, I. & Gamon, J. A. Assessment of photosynthetic radiation-use efficiency withspectral reflectance. *New Phytol*. **131**, 291-296 (1995).
50 Garbulsky, M. F., Peñuelas, J., Papale, D. & Filella, I. Remote estimation of carbon dioxide uptakeby a Mediterranean forest. *Global Change Biol*. **14**, 2860-2867 (2008).
51 Guarini, R. *et al*. The utility of MODIS-sPRI for investigating the photosynthetic light-use efficiency in a Mediterranean deciduous forest. *Int*. *J*. *Remote Sens*. **35**, 6157-6172 (2014).
52 Rahman, A. F., Cordova, V. D., Gamon, J. A., Schmid, H. P. & Sims, D. A. Potential of MODIS ocean bands for estimating CO2 flux from terrestrial vegetation: A novel approach. *Geophys Res*. *Lett*. **31** (2004).
53 Goerner, A., Reichstein, M. & Rambal, S. Tracking seasonal drought effects on ecosystem light use efficiency with satellite-based PRI in a Mediterranean forest. *Remote Sens*. *Environ*. **113**, 1101-1111 (2009).
54 Bai, J. & Perron, P. Computation and analysis of multiple structural change models. *J*. *Appl*. *Econometrics* **18**, 1-22 (2003).
55 Zeileis, A., Kleiber, C., Kramer, W. & Hornik, K. Testing and dating of structural changes in practice. *Comp*. *Stat*. *Data Anal*. **44**, 109-123 (2003).
56 Zeileis, A., Leisch, F., Hornik, K. & Kleiber, C. strucchange: An R package for testing for structural change in linear regression models. *J*. *Stat*. *Softw*. **7**, 1-38 (2002).

Chapter 6. A MODIS photochemical reflectance index (PRI) as an estimator of isoprenoid emissions in a temperate deciduous forest

This chapter is just now finished and going to be submitted to *Remote Sensing of Environment*.

Abstract

The quantification of isoprene and monoterpene emissions at the ecosystem level is not entirely satisfactory with available models and field measurements. Remote-sensing techniques can extend the spatial and temporal assessment of isoprenoid fluxes. Detecting the exchange of biogenic volatile organic compounds (BVOCs) using these techniques is, however, a very challenging goal. Recent evidence suggests that a simple remotely sensed index, the photochemical reflectance index (PRI) indicative of radiation-use efficiency and excess reducing power, is a good indirect estimator of foliar isoprenoid emissions. We tested the ability of PRI to assess isoprenoid fluxes in a temperate deciduous forest in central USA throughout the entire growing season and under moderate and extreme drought conditions. We compared PRI time series calculated with MODIS bands to isoprene emissions measured with eddy covariance. PRI was significantly correlated with isoprene emissions for most of the season, until emissions peaked. PRI was also able to detect the annual peak of emissions, even when it was advanced in response to drought conditions. PRI is thus a promising index to estimate isoprene emissions, especially when it is complemented by information on potential emission. It may also be used to further improve models of isoprene emission under drought and other stress conditions.

1. Introduction

Isoprene comprises the largest fraction of globally emitted biogenic volatile organic compounds (BVOCs). Isoprene emissions are of great importance in plant biology and ecology and they can substantially influence atmospheric chemistry and composition and processes of the climatic system (Peñuelas and Llusià, 2003). For example, isoprene plays a role in the formation of photochemical smog, ozone and other secondary pollutants such as peroxyacyl nitrates and secondary organic aerosols (Andreae, 1997; Chameides et al., 1988; Fuentes et al., 2000) and has implications for regional air quality and global climate change (Peñuelas and Staudt, 2010).

The quantification of isoprenoid emissions at the ecosystem level is not entirely satisfactory with available models and field measurements. Isoprene emissions at canopy to regional levels can be directly measured by applying techniques of eddy covariance (Gu et al., 2017; Spirig et al., 2005; Westberg et al., 2001), but these measurements are limited to a few sites. Isoprenoid emissions can also be estimated using models based on capacities of foliar emission, such as the Model of Emissions of Gasses and Aerosols from Nature (MEGAN) model (Guenther et al., 2012), with algorithms based on foliar emissions that are driven by temperature and light (Guenther et al., 1993). Model simulations, however, remain unsatisfactory because foliar-emission capacities are highly variable and acclimate seasonally and over environmental gradients (Niinemets et al., 2010a, 2010b). For example, MEGAN was not able to detect the peak of emissions concurrent with episodic and extreme droughts (Potosnak et al., 2014; Seco et al., 2015). A reassessment of current models is therefore required to better predict changes in the seasonal dynamics of the capacities of both basal and total isoprenoid emissions, especially under the increasing occurrence of drought stress (IPCC, 2014). Current efforts are now being made to base the modeling on a fundamental understanding of the links between emissions and the biological processes that affect these emissions (Monson et al., 2012; Morfopoulos et al., 2013; Niinemets et al., 2010a), but uncertainty remains high (Monson et al., 2012; Morfopoulos et al., 2013).

Remote-sensing techniques can offer quick and intensive monitoring of spatial and temporal isoprene emissions at the ecosystem level with global coverage. Various approaches have been developed for remotely sensing isoprenoid emissions, such as indirect estimation by the remote detection of formaldehyde, a product of isoprenoid

oxidation, in the atmosphere (Barkley et al., 2008; Foster et al., 2014; Palmer et al., 2003). This approach, however, is based on highly uncertain assumptions associated with the oxidant chemistry of isoprenoids to formaldehyde (Barkley et al., 2008; Valin et al., 2016) and require a model of atmospheric chemistry to apply satellite observations to isoprene emissions. A new simple approach has recently been suggested for estimating isoprenoids using remotely sensed data (Peñuelas et al., 2013). Assuming that photosynthetic reducing power for isoprenoid production was higher under lower radiation-use efficiencies (RUEs) (Morfopoulos et al., 2014; Owen and Peñuelas, 2005; Peñuelas and Llusià, 2004), (Peñuelas et al., 2013) found that the photochemical reflectance index (PRI), a proxy of RUE, at the foliar level together with factors of basal emission could predict isoprenoid emission similarly to some standard emission models, and combined with these models improved their predictions of isoprene emission (Peñuelas et al., 2013). This remote-sensing capacity is based on the inverse relationship between isoprenoid emission and RUE and because PRI has already been widely tested as a good estimator of RUE at the foliar, canopy and ecosystem levels at different temporal scales (Peñuelas et al., 2011; Zhang et al., 2016). PRI is also related to isoprene emissions, because the pathways of both isoprene biosynthesis and xanthophyll-cycle dissipation co-vary, both increasing when more reducing power is available (Morfopoulos et al., 2014), and on the diurnal time scale PRI measures reflectance changes caused by the interconversion and dissipation of xanthophylls (Peñuelas et al., 1995). The next step is to test the ability of PRI to estimate isoprenoid emissions at larger scales, e.g. canopy or ecosystem levels, and throughout the season. Adding the temporal scale constitutes an additional challenge, because the relationships of both PRI and isoprene with RUE can also vary throughout the season.

Diurnal PRI variation is mainly driven by changes in the xanthophyll cycle (Gamon et al., 1992; Peñuelas et al., 1995), which are considered facultative changes in pigments. On seasonal time scales (over weeks and months) PRI variation can be a combined function of the xanthophyll cycle and changes in the pools of carotenoids and chlorophylls (Filella et al., 2009; Porcar-Castell et al., 2012; Sims and Gamon, 2002; Stylinski et al., 2002; Wong and Gamon, 2015), which are considered constitutive changes in pigments. Recent studies have indicated these constitutive changes in pigment pool size have a dominant influence on CCI (a PRI calculated using chlorophyll absorption band as reference) over long time spans (Wong & Gamon, 2015, Gamon et al. 2016). Similarly,

the relationship between PRI and isoprene emission is strongly influenced at longer timescales by constitutive changes in the size of carotenoid pigment pools (Harris et al., 2016) presenting the interesting hypothesis that carotenoid pigments are causally related to isoprene emissions over seasonal time spans. This relationship may be due to the link (either direct, e.g. via substrate availability, or indirect, e.g. via complementary functionality) between potential isoprenoid emission and carotenoid synthesis at timescales of days to weeks (Owen and Peñuelas, 2013). Also, the ability of PRI to predict seasonal variations in isoprene emission due to environmental factors other than light and temperature (Geron et al., 2000; Harley et al., 1994; Pressley et al., 2005) and under stress conditions (Potosnak et al., 2014; Seco et al., 2015) remains unknown. It is likely that, over long time scales, PRI provides a general "stress indicator" that integrates the influence of a number of environmental factors on plant biochemistry, photosynthetic physiology, and isoprene emission.

Isoprene emissions at the ecosystem level based on eddy covariance were measured throughout two consecutive growing seasons in a temperate deciduous forest in central Missouri, USA (Potosnak et al., 2014; Seco et al., 2015). The site experienced a mild drought in 2011 and an extreme drought in 2012. Both droughts were concurrent with high isoprene fluxes. This data set of measurements represents an exceptional resource for testing the ability of PRI to monitor the spatial and temporal emission of isoprene at the ecosystem level over long time spans. The occurrence of different drought intensities during the measurement period adds another important test for PRI. We tested (a) the utility of PRI as an estimator of isoprene emissions at the ecosystem level, (b) the utility of PRI as an estimator of seasonal isoprene emissions and (c) the sensitivity of PRI to the changes in isoprene emission caused by moderate and extreme drought.

2. Materials and Methods

2.1, Site description

The study was conducted in central Missouri (38°44.650N, 92°12.000W, 219 m a.s.l.) at the Missouri Ozark Forest Flux Site (MOFLUX, Gu *et al*., 2006), a broadleaf deciduous forest dominated by isoprene-emitting oaks, in the Baskett Wildlife Research and Education Area of the University of Missouri, which is included in the AmeriFlux Network. The main tree species include white, post and black oaks (*Quercus alba L*., *Q*.

stellata Wangenh. and *Q. velutina* Lam., respectively), shagbark hickory (*Carya ovata* (Mill.) K. Koch), sugar maple (*Acer saccharum* Marsh.) and eastern red cedar (*Juniperus virginiana* L.). The area has a warm, humid, continental climate (Critchfield, 1966), with mean January and July temperatures of -1.3 and 25.2 °C, respectively, and a mean annual precipitation of 1083 mm (National Climatic Data Center 1981–2010 climatic normals, Columbia Regional Airport, Missouri). We compared PRI time series derived from the Multi-Angle Implementation of Atmospheric Correction (MAIAC, MODIS Terra, col. 6) product to measurements of isoprene emission based on eddy covariance (measured continuously by proton transfer reaction mass spectrometry (PTR-MS) and a fast isoprene sensor (FIS)).

2.2, Flux data

The study site has an eddy-covariance system for measuring the flux of CO_2 between the ecosystem and the atmosphere (see Potosnak *et al*. (2014) and Seco *et al*. (2015)). An additional system was deployed to measure BVOCs. Isoprene was measured in 2011 by the eddy-covariance system based on the FIS (Guenther & Hills, 1998). Isoprene, monoterpenes and methanol were measured by PTR-MS (Ionicon, Innsbruck, Austria) (Karl et al., 2002) in 2012 using virtual disjunct eddy covariance. The eddy-covariance flux and meteorological parameters were measured on a 32-m walkup scaffold tower, approximately 10 m above the canopy. Complete details of the eddy-covariance technique and BVOCs measurements are provided by Potosnak *et al*. (2014) for the 2011 campaign and by Seco *et al*. (2015) for the 2012 campaign. Measurements were recorded from May to September 2011 and from May to October 2012.

CO_2-flux data were gap-filled and partitioned using marginal distribution sampling described by (Reichstein et al., 2005). The CO_2 fluxes (net ecosystem exchange, NEE) were partitioned into two components: gross primary production (GPP) and ecosystem respiration (Reco). This method is a nighttime-based approach where Reco is estimated by nightitme data using a respiration model, and GPP is then calculated as the difference between Reco and NEE. We considered only days with photosynthetically active radiation (PAR) >600 μmol m^{-2} s^{-1} and calculated the average values for GPP and isoprene emissions between 10:00 and 12:00 (CST) to coincide with the overpass of MODIS Terra to obtain daily flux data. Daily RUE was calculated as:

RUE= GPP/fAPAR

The fraction of absorbed PAR (fAPAR) was derived by (Monteith, 1993):

$fAPAR = 1 - PAR_{bc}/PAR_{in}*e^{1.35}$

where PAR_{bc} is PAR below the canopy and PAR_{in} is incident PAR. e^1.35 represents the mean effect of the absorptivities in the spectral bands of PAR and global solar radiation. Additional meteorological variables were measured continuously at the site. Incident PAR above the canopy, air temperature and volumetric soil-water content (SWC) at 10 cm were also measured. See (Potosnak et al., 2014; Seco et al., 2015) for details.

2.3, Satellite data

PRI was derived from MODIS on-board the Terra satellite, and the data were processed using the MAIAC algorithm. MAIAC provides a daily 1-km gridded terrestrial bidirectional reflectance factor (BRF, also known as surface reflectance) for MODIS bands 1-12, which are derived from a time series as long as 16-day moving windows of MODIS measurements. Except for atmospheric correction, the MAIAC algorithm also uses a new technique for masking clouds for obtaining cloud-free data.

A time series of surface reflectance was extracted for the 1-km grid that included the location of the flux tower. PRI was then calculated as the average of the nine closest pixels around the Missouri Ozark site, all within 2 km of the study site. All high-quality cloud-free observations and view zenith angles <45° were used. PRI from the MODIS satellite sensor (MODIS PRI, also known as the chlorophyll carotenoid index (CCI) (Gamon et al., 2016), and here on named PRI) was calculated as:

MODIS PRI (CCI) = (band 11 - band 1)/(band 11 + band 1)

where band 11 (526-536 nm) is the detection band and band 1 (620-670 nm) is the reference band.

PRI values were standardized as described by (Goerner et al., 2009; Rahman et al., 2004) to ensure positive values more comparable to commonly used remotely sensed indicators such as the normalized difference vegetation index:

sPRI = (1+PRI)/2

2.4. Statistical analyses

The patterns of isoprene emission were hierarchically partitioned using the R 'hier.part package' version 0.5–1 (Mac Nally and Walsh, 2004) to determine the importance of the explanatory variables, temperature, RUE and SWC, independently of the other covariates. We used the 'visreg' R package (Breheny and Burchett, 2013) to visualize this relationship between isoprene emissions and each explanatory variable while the other

variables were held constant. We calculated the standardized regression coefficients using the "lm.beta" function in the R package QuantPsyc from the linear-regression model. ANCOVAs were used to compare slopes and intercepts of the relationships between RUE and isoprene emissions with PRI and between PRI-estimated and MEGAN-estimated isoprene emissions. We used R to develop an empirical model based on the relationship of isoprene emission with MEGAN data complemented with PRI data. We cross-validated the model using 50% of the data as a sampling set and the remaining 50% as the testing set and repeated this procedure 1000 times, randomizing both subsets. All data treatments and analyses were conducted using R statistical software (version 3.2.5) (R Core Team, 2015).

3. Results

3.1. Seasonal variation in isoprene emissions, water availability, temperature and RUE

SWC at a depth of 10 cm continuously decreased in 2011 from mid-July (day of the year (DOY) 190-195) to early August (DOY 215) from 0.5 to 0.25 m^3 m^{-3} (Figure 1). This decrease coincided with decreases in water-vapor pressure deficit, predawn foliar water potential and net ecosystem production (Potosnak et al., 2014) indicative of water stress. Temperature during the study period was higher in 2012 than 2011, and SWC began to decrease from the beginning of the season (around DOY 140) to its minimum (<0.23 m^3 m^{-3} at 10 cm) at the end of August (DOY 243). Some indicators such as NEE, SWC, atmospheric vapor-pressure deficit, predawn foliar water potential and ecophysiological data indicated severe drought stress at the site during this period (Seco et al., 2015).

The pattern of isoprene emission differed between the two years due to differences in water availability. Isoprene fluxes increased in 2011 from the beginning of May to a peak at the end of July (around DOY 214) and then decreased. Isoprene emissions peaked a few weeks earlier in 2012, at the end of June (DOY 175) (Figure 1). High isoprene emissions were concurrent with the droughts in 2011 (moderate) and 2012 (more severe). The temporal patterns of isoprene emission, temperature and RUE described two scenarios in both years. Isoprene emissions initially increased to a maximum (increasing phase) as temperature increased and GPP and RUE decreased. Emissions then began to decrease (decreasing phase) when GPP and RUE remained low. Temperature decreased

concurrently with emissions in 2011, but temperature began to decrease later than emissions in 2012. Emissions in the decreasing phase were decoupled from RUE in both years and also from temperature in 2012 (Figure 1).

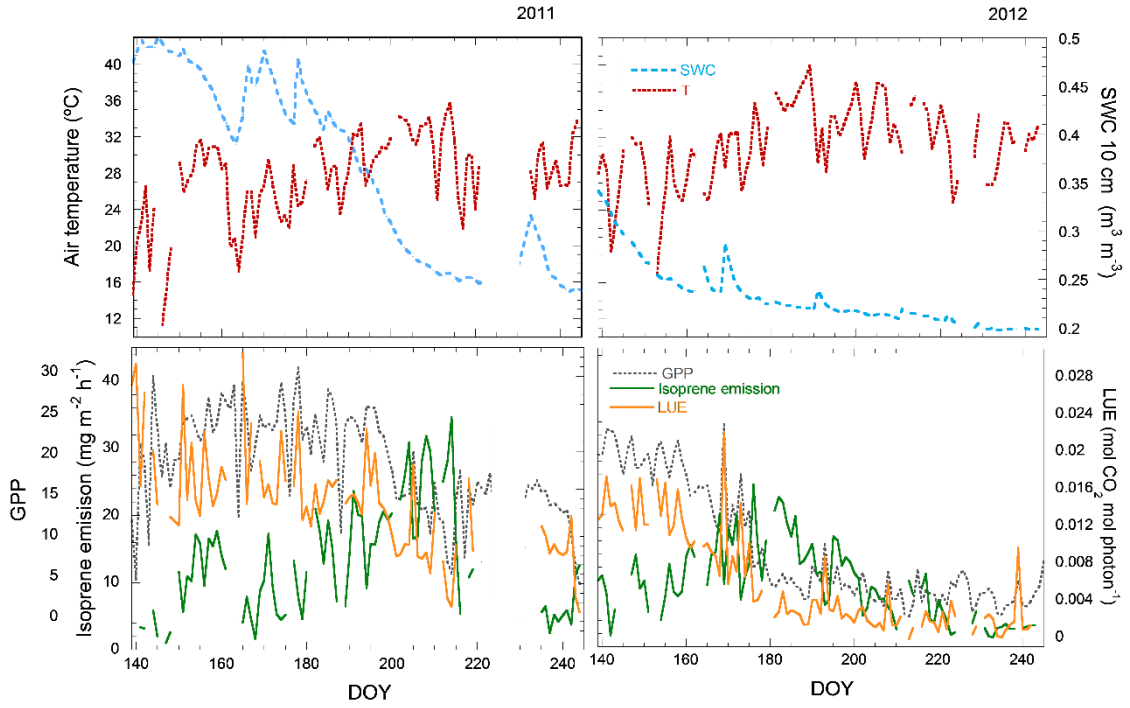

Figure 1. Seasonal variation of air temperature (T), SWC, GPP, isoprene emissions and RUE at the MOFLUX site in 2011 and 2012.

3.2. Influence of temperature, RUE and SWC on isoprene emissions

The patterns of isoprene emission were hierarchically partitioned to measure the importance of the explanatory variables, temperature, RUE and SWC. The independent effects of temperature, RUE and SWC predictors were statistically significant in both years (Figure 2). These variables together explained 88 and 89% of the variance in 2011 and 2012, respectively. Temperature had the highest independent contribution to the total explained variance (48.9% for 2011, 49.4% for 2012), but the contributions of RUE (20.8% for 2011, 31.7% for 2012) and SWC (30.3% for 2011 and 18.9% in 2012) were also important.

SWC was highly correlated with both RUE (R^2= 0.60) and PRI (R^2=0.56). PRI was thus able to detect the effect of low SWC on RUE and thus presumably on isoprene

emissions.

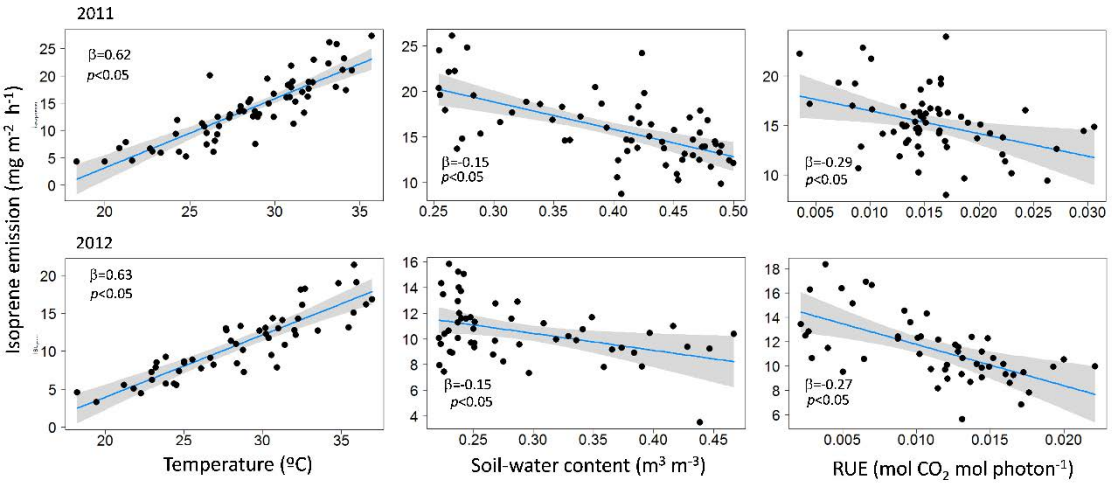

Figure 2. Partial residual plots of the relationships between isoprene emissions and temperature, soil-water content and RUE during the increasing phase of emissions. Shading represents the 95% confidence intervals. β is the standardized regression coefficient.

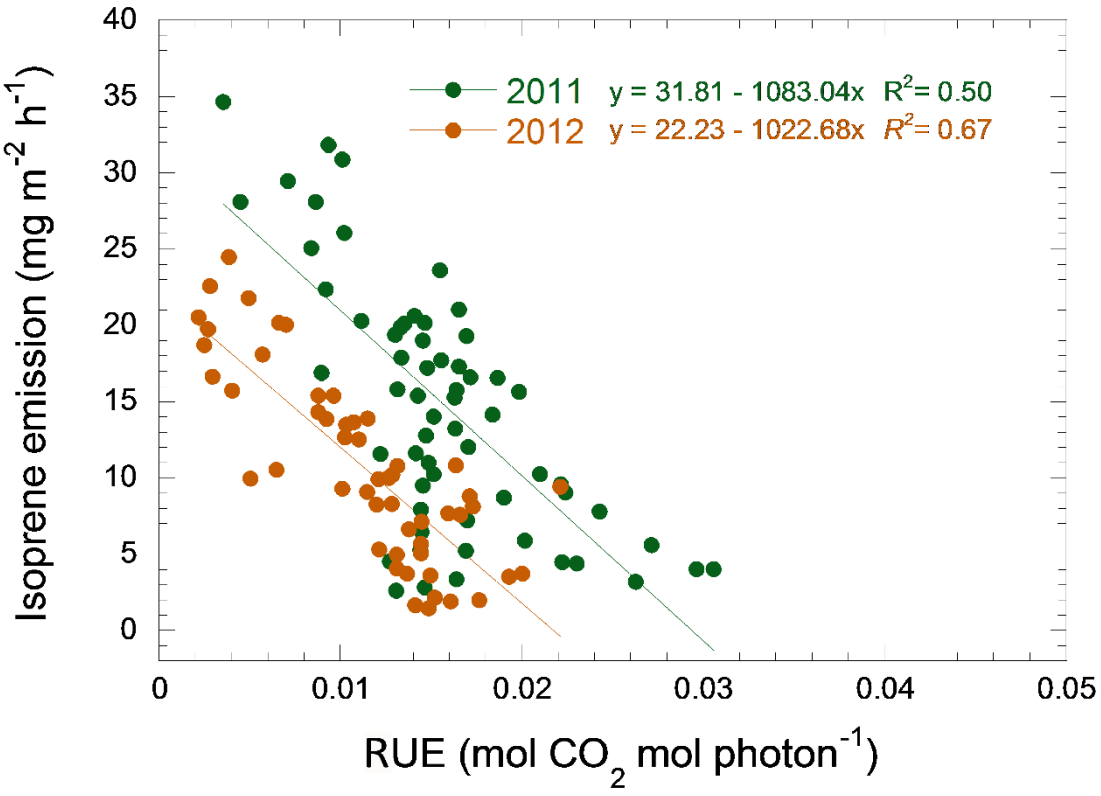

Figure 3. Relationship between isoprene emissions and RUE at the MOFLUX site during the increasing phase for 2011 and 2012.

3.3. Relationship between isoprene emission and RUE

Isoprene emission was negatively correlated with RUE during the increasing phase (Figure 3). The seasonal pattern of variation in RUE was opposite to that of isoprene emission, peaking on the days with lower emissions and being lower when emission was higher, but only until maximum emission, and then began to decrease (Figure 1). RUE accounted for 50 and 67% of the variance in isoprene emissions during the increasing phase in 2011 and 2012, respectively (Figure 3). The slope of the relationship was the same in both years (ANCOVA, $p>0.05$), but the intercept differed, with a lower emission for the same RUE in 2012.

3.4. Relationship between RUE and PRI

PRI varied seasonally in parallel to RUE throughout the entire measurement period (Figure 4). PRI accounted for 52 and 72% of the variance in RUE in 2011 and 2012, respectively. The relationship between RUE and PRI had similar slopes and intercepts in the two years (ANCOVA, $p>0.05$).

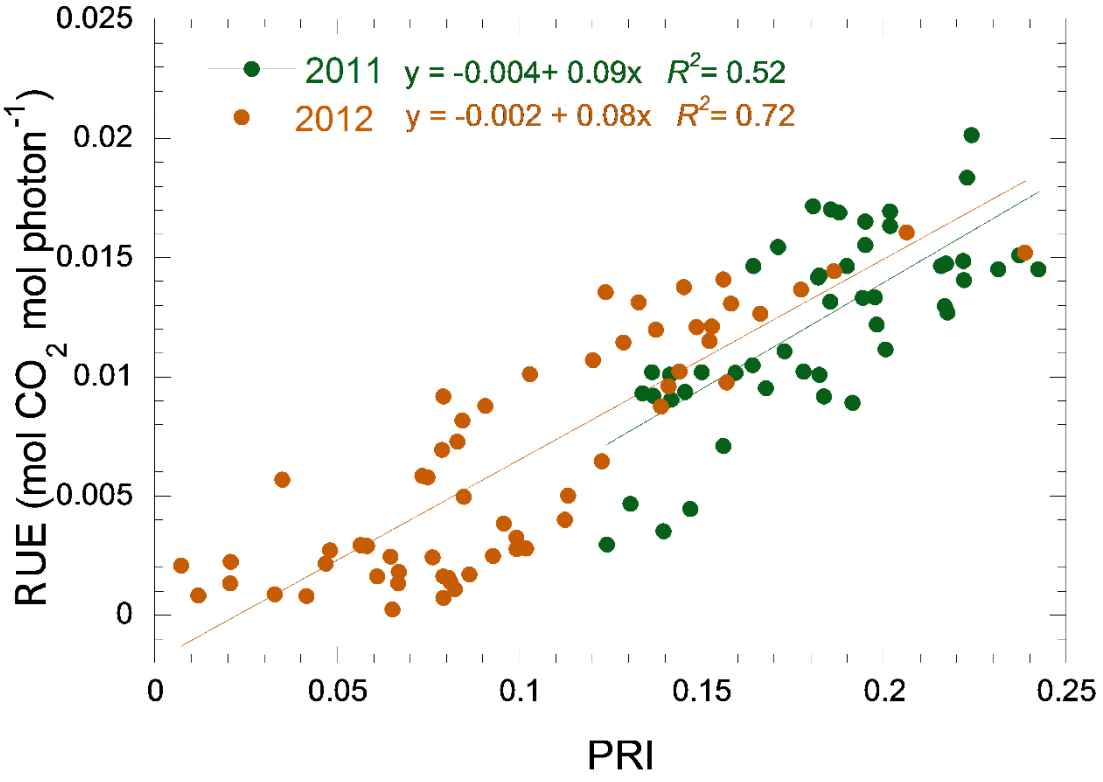

Figure 4. Relationship between radiation-use efficiency (RUE) and the photochemical reflectance index (PRI) at the MOFLUX site for 2011 and 2012.

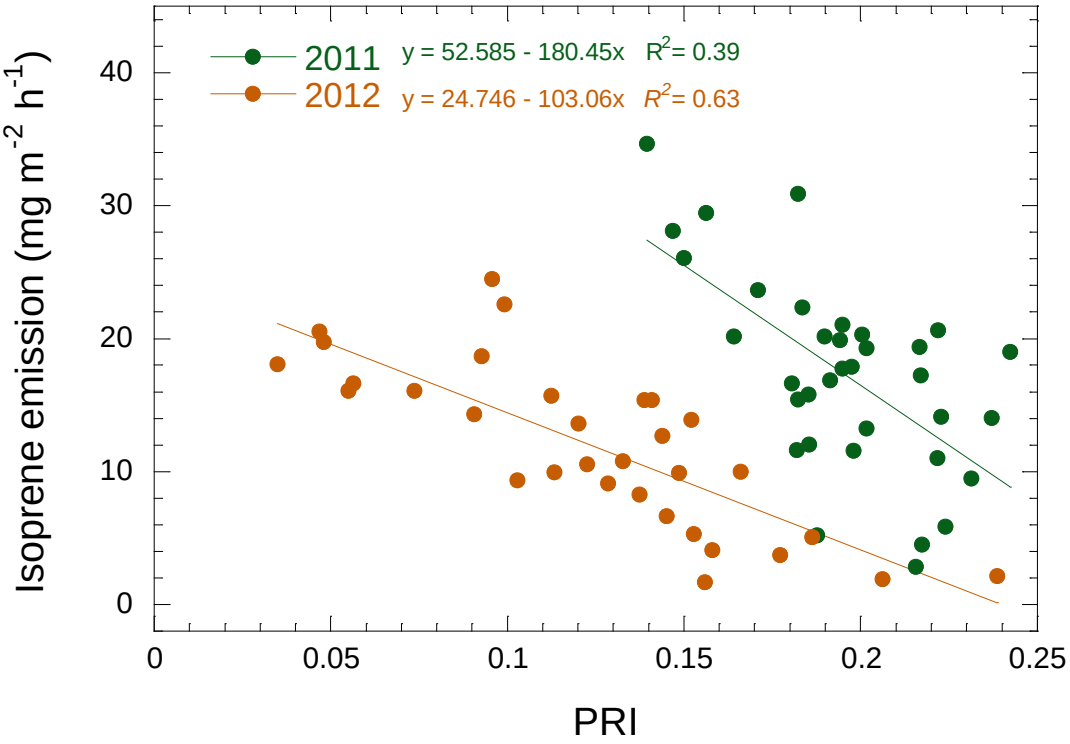

Figure 5. Relationship between isoprene emission and the photochemical reflectance index (PRI) at the MOFLUX site during the increasing phase in 2011 and 2012.PRI was significantly and negatively correlated with isoprene emissions during the increasing phase when we tested PRI as a proxy of RUE for estimating emissions (Figure 5). PRI explained 39 and 63% of the variance in isoprene emissions in 2011 and 2012, respectively. The slope of the relationship was similar (ANCOVA, p>0.1) for both years but the intercept differed, with lower emission for the same isoprene values in 2012.

3.5. Estimation of isoprene emissions using PRI (and MEGAN)

Midday isoprene flux estimated by the MEGAN model agreed well with the measured emissions for most of the annual cycle (Figure 6), but the model underestimated emissions during the onset of drought conditions in 2011 when the emissions were higher (Figures. 6 and 7, Potosnak *et al*., 2014), and estimate errors were larger for 2012 when drought conditions were stronger (Figures. 6 and 7, Seco *et al*., 2015). Isoprene emissions were mostly higher than predicted for both 2011 and 2012 after SWC decreased below 0.26 m^3 m^{-3}. Emission began to decrease in 2012 when SWC reached the wilting point for this ecosystem (0.23 m^3 m^{-3}, Seco *et al*., 2015), earlier than the MEGAN estimates.

The seasonal PRI inflection point in the decreasing phase coincided with the emission

peaks in both 2011 and 2012 and was thus sensitive to the advance of the emission peak in 2012. The MEGAN estimates and temperature coincided with the emission peak in 2011 but not 2012, when the measured peak was earlier (Figure 7).

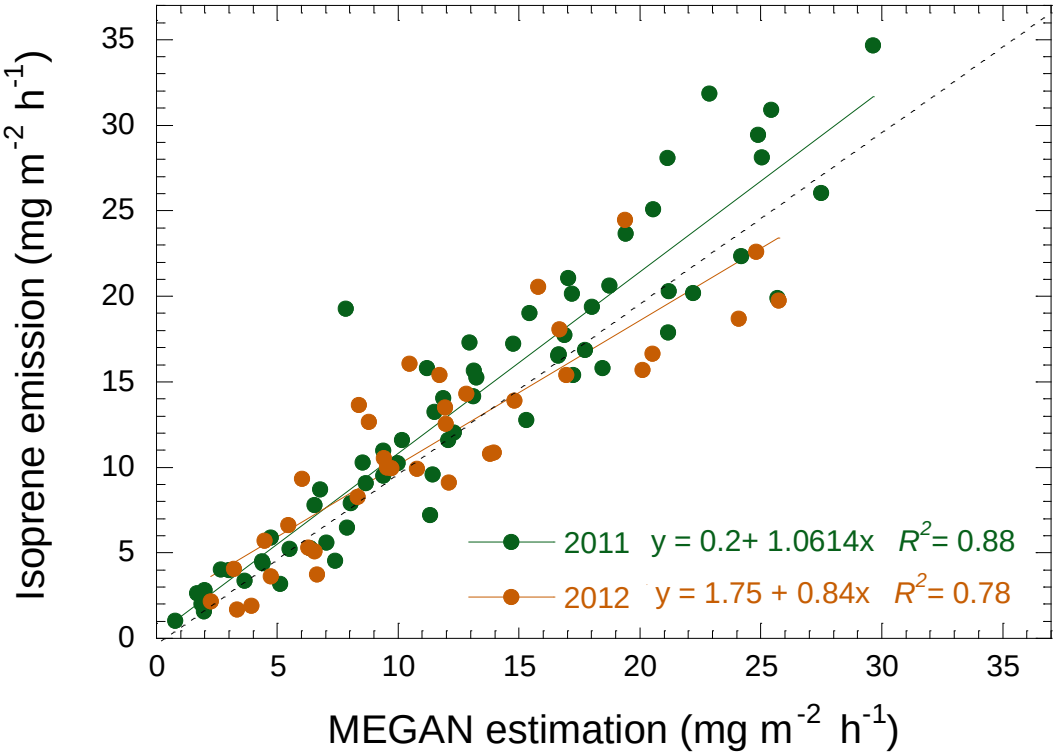

Figure 6. Relationship between isoprene emission and the results of the isoprene emissions estimation by MEGAN model for the MOFLUX site during the increasing phase for 2011 and 2012. The dotted line is the 1:1 line.

We randomly selected 50% of the data from the increasing phase for both 2011 and 2012 together as a training set for creating two models to estimate isoprenoid emission, one model using MEGAN and another using MEGAN and PRI. The remaining 50% of the data was used for validation. This procedure was repeated 1000 times. Complementing MEGAN algorithms with PRI produced more precise estimates (slopes were 0.89 using MRGAN and 0.98 using MEGAN+PRI) of isoprene emission (Figure 8). Both estimates had the same coefficient of correlation with measured isoprene fluxes, but the model combining MEGAN and PRI was more sensitive to higher emissions, indicated by the better adjustment of the model to the 1:1 line.

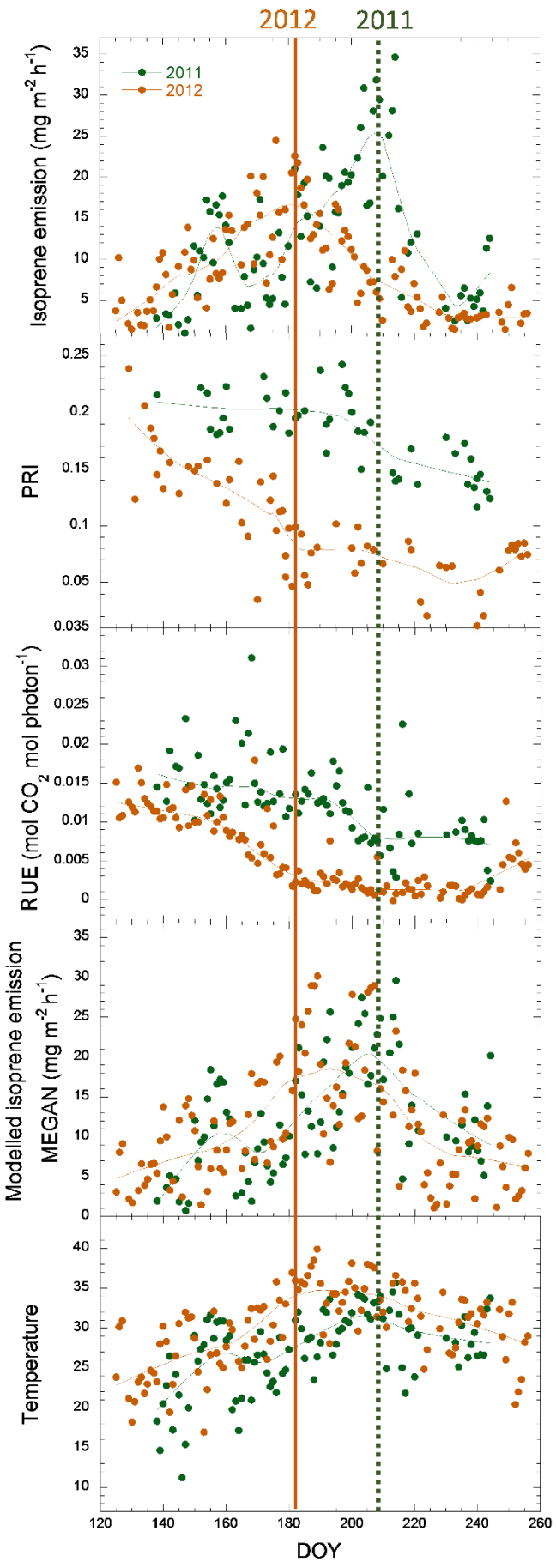
2012
2011
2011
2012
Isoprene emission (mg m-2 h-1)
PRI
RUE (mol CO2 mol photon-1)
Modelled isoprene emission
MEGAN (mg m-2 h-1)
Temperature
DOY

Figure 7. Comparison of the seasonal variation of isoprene emissions, PRI, RUE, emissions estimated by MEGAN and temperature for 2011 and 2012. The solid lines are spline fits. Vertical dotted lines show the period of maximum isoprene emissions in 2011 and 2012.

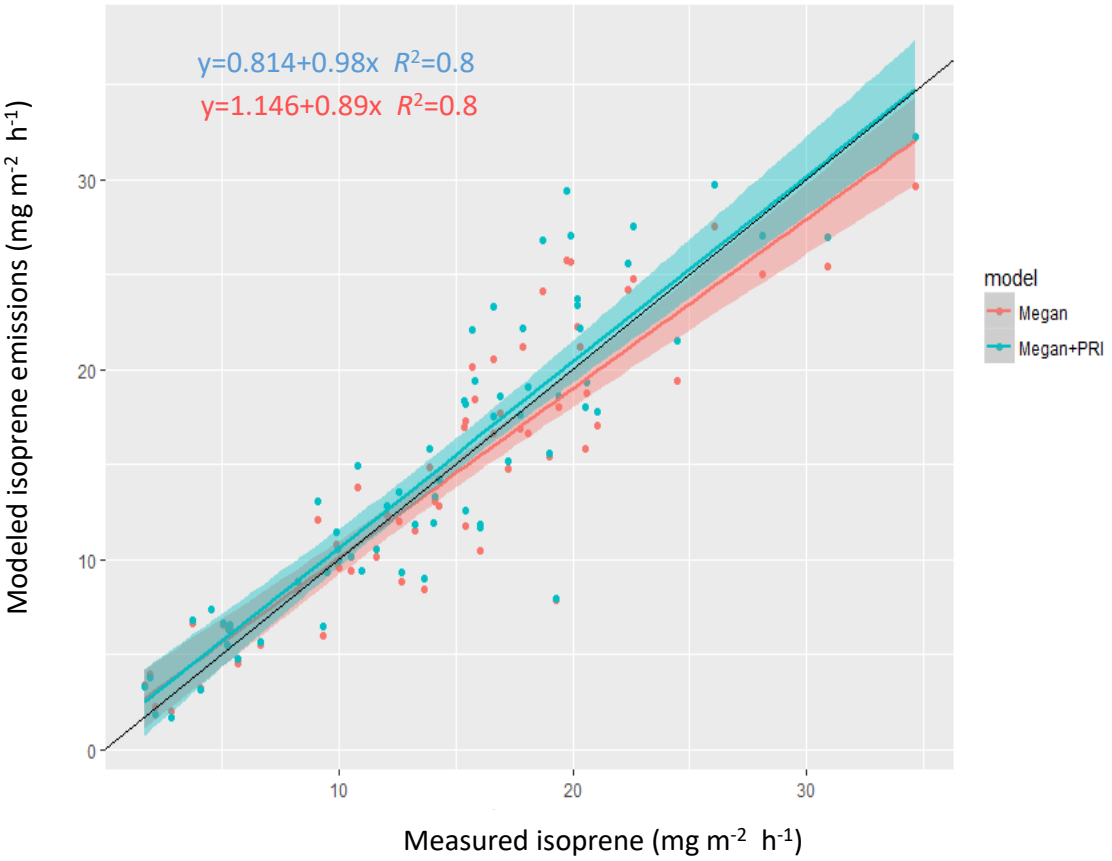

Figure 8. Measured versus estimated isoprenoid emissions using the MEGAN model and MEGAN model+PRI. The black line is the 1:1 line, and the shading represents the 95% confidence intervals.

4. Discussion

The relationship between isoprene emissions and PRI supported our hypothesis that estimates of isoprenoid emission could be improved by using remotely sensed PRI at the ecosystem level, under conditions of both moderate and extreme drought stress. This capacity of PRI, a good estimator of RUE at foliar, canopy and ecosystem levels (Gamon et al., 1992; Garbulsky et al., 2011; Peñuelas et al., 2011, 1995; Zhang et al., 2016), is based on the inverse relationship between isoprenoid emissions and RUE due to the

higher availability of photosynthetic reducing power for isoprenoid production under lower RUEs (Morfopoulos et al., 2014; Owen and Peñuelas, 2005; Peñuelas and Llusià, 2004) and to the direct relationship between PRI (via changes in the xanthophyll cycle) and isoprene biosynthesis (Morfopoulos et al., 2014). Additionally, MODIS PRI (or CCI, as calculated here) follows the seasonal change in carotenoid pigment pool sizes (relative to chlorophyll), and these carotenoid pigments are possibly related to isoprene biosynthesis (Harris et al., 2016; Owen and Peñuelas, 2013). The emission peak of isoprene coincided with the lowest RUEs of the vegetation after the seasonal increasing phase. PRI was sensitive to the isoprene-emission peak coinciding with the drought in 2011, a peak that MEGAN underestimated. PRI was also sensitive to the advance of the emission peak due to severe stress in 2012.

Isoprene emissions are not well explained by light and temperature under high stress (Genard-Zielinski et al., 2014; Tani et al., 2011). The stimulation of ecosystem isoprene emissions under various abiotic stresses reported in some studies (see references in Peñuelas & Llusià (2004), Niinemets *et al*. (2010a) and Genard-Zielinski *et al*. (2014)) were likely associated with the excess reducing power under stress conditions (Morfopoulos et al., 2014, 2013). Residual reducing power not used by carbon assimilation can support increased isoprene emission under drought (Dani et al., 2014). The balance between the availability of reducing power and its use in carbon assimilation may determine the rate of constitutive isoprenoid emission in plants (Dani et al., 2014). The highest isoprene emissions coinciding with the peak of the drought in 2011 in our study (a decrease in SWC, predawn foliar water potential and net ecosystem production; Potosnak *et al*., 2014), were higher than expected due solely to the conditions of light and temperature. This increase in isoprene emissions could be partly due to an increase in foliar temperature caused by drought-induced reductions in stomatal conductance (Niinemets, 2010; Potosnak et al., 2014), but it may also be due to the excess reducing power (Figure 1, DOY 203-215). RUE explained part of the variance in isoprene emissions (Figure 2), and water stress and RUE were strongly correlated.

PRI was not as good as an estimator of isoprene emissions later in the season, likely because the decrease in emissions was caused by substrate limitation and lower temperatures in 2011 and by substrate limitation in 2012, so PRI was decoupled from excess reducing power. Carbon availability may have critically limited emission under the severe drought at the site in 2012, because isoprene is produced in the chloroplast via

the methylerythritol phosphate (MEP) pathway (Sharkey et al., 2008), which requires both reducing power and carbon skeletons provided by photosynthesis (Loreto and Schnitzler, 2010).

Photosynthesis and isoprene emissions were decoupled seasonally, as previously described under drought conditions (e.g. (Bertin and Staudt, 1996; Brilli et al., 2007; Fortunati et al., 2008; Funk et al., 2005, 2004; Genard-Zielinski et al., 2014; Pegoraro et al., 2004; Potosnak et al., 2014; Tani et al., 2011; Wu et al., 2015). Isoprenoid emissions continued to increase concurrently with a decrease in photosynthetic CO_2 fixation (GPP) during the increasing phase. Mild stress may decrease carbon assimilation, but isoprene emissions would not be affected, because *the rate of* electron transport would be maintained and reserve carbon in the form of sugars and starch would support the production of isoprenoids (Niinemets, 2010). Isoprene might reduce cell oxidation and increase cell stabilization in plants (Sharkey et al., 2008; Velikova et al., 2012), so increasing the allocation of the recently assimilated carbon to isoprene would constitute an additional mechanism of drought resistance (Genard-Zielinski et al., 2014). Increased emission under drought is sustained if the intensity of drought remains within a species-specific tolerance threshold (Dani et al., 2015). Under extreme stress conditions isoprene emission starts declining for a length of time which depends on the species studied, until emissions are fully inhibited (Bruggemann and Schnitzler, 2002; Llusià et al., 2016; Rodríguez-Calcerrada et al., 2013). Isoprene emission in our study was mostly higher than predicted when SWC was <0.26 m^3 m^{-3}, and emission began to decrease when SWC reached the wilting point for this ecosystem (0.23 m^3 m^{-3}; (Seco et al., 2015). This seasonal decrease occurred earlier in 2012 than 2011 and earlier than modeled. Water limitation can override the physiological effects of high temperature on isoprene emission during severe stress (Fortunati et al., 2008), perhaps due to a very limited amount of recently produced dimethylallyl pyrophosphate (DMAPP), an isoprene substrate (Tani et al., 2011). (Bruggemann and Schnitzler, 2002) attributed the decrease in isoprene emission during drought to a limitation of the carbon supply rather than to a downregulation of isoprene synthase, an enzyme used during isoprene production.

The relationship of PRI with isoprene differed between the two years, as indicated by the different intercepts in the fit (Figure 5). However, the PRI-RUErelationship followed the same regression line for the two years (Figure 4), indicating the good performance of PRI in estimating RUE. The relationship between isoprene emissions and

RUE, however, was year-dependent even though the slopes were similar (Figure 3), suggesting that the proportion of available photosynthetic reducing power for isoprene formation differed between the two years. This difference might have been due to a higher competition between photorespiration and the MEP pathway under drought stress as the rate of photorespiration increases and reducing power and carbon supply for the MEP pathway decrease (Dani et al., 2014), because carbon availability can limit emission rates under severe drought and photorespiratory stresses (Dani et al., 2014) and isoprene emission may be regulated by substrate availability (Funk et al., 2004). The residual reducing power not invested in carbon assimilation is shared by non-photosynthetic sinks such as photorespiration or the MEP pathway (Dani et al., 2014), and isoprene emission may be most strongly influenced by pathways co-located with the MEP pathway in the chloroplast, such as photorespiration, because they compete directly for both reducing power and photosynthetic carbon (Dani et al., 2015).

In summary, we hypothesize that seasonal isoprene emissions would be primarily driven by temperature but modulated by reducing power and substrate availability, based on observations and previous conceptual models (Dani et al., 2015; Potosnak et al., 2014). Photosynthesis, photorespiration and the MEP pathway directly depend on reducing power and substrate availability. The availability of reducing power and substrate for the MEP pathway is thus dependent on photosynthesis and photorespiration. Isoprene emission would thus be stimulated by an increase in available reducing power when drought conditions decrease photosynthesis but would begin to decrease later in the season, despite the high availability of reducing power, because temperature would begin to decrease and substrate would become limiting. Photorespiration increases under severe drought conditions, causing a decrease in isoprene emissions, and photosynthesis (GPP) becomes minimal, so the carbon supply for the MEP pathway is exhausted earlier, advancing the seasonal decrease in isoprene emissions.

Based on the improved model results after including PRI, we propose a model of the performance of PRI in estimating isoprene emissions throughout the season (Figure 9). PRI is highly correlated with isoprene emissions at the beginning of the season and can thus be used to estimate them. Emissions and RUE become decoupled when RUE (GPP) is lowest and stabilizes; RUE remains low and isoprene emissions begin to decrease.

The effect of photorespiration on the relationship between RUE and isoprene emissions under severe drought conditions can disturb the ability of PRI to estimate

isoprene emission and can prevent the standardization of the PRI signal, even for the same species or the same ecosystem. The lack of correlation between emissions and RUE late in the season also hinders the use of PRI as a unique estimator for the entire season. Additionally, PRI measured from satellite data represents conditions at the top of canopies, but estimates of GGP using eddy covariance are integrated over the entire canopy (Goerner et al., 2009), which, together with the scatter of eddy covariance measurements, could account for some of the unexplained variability in the RUE-PRI relationship.

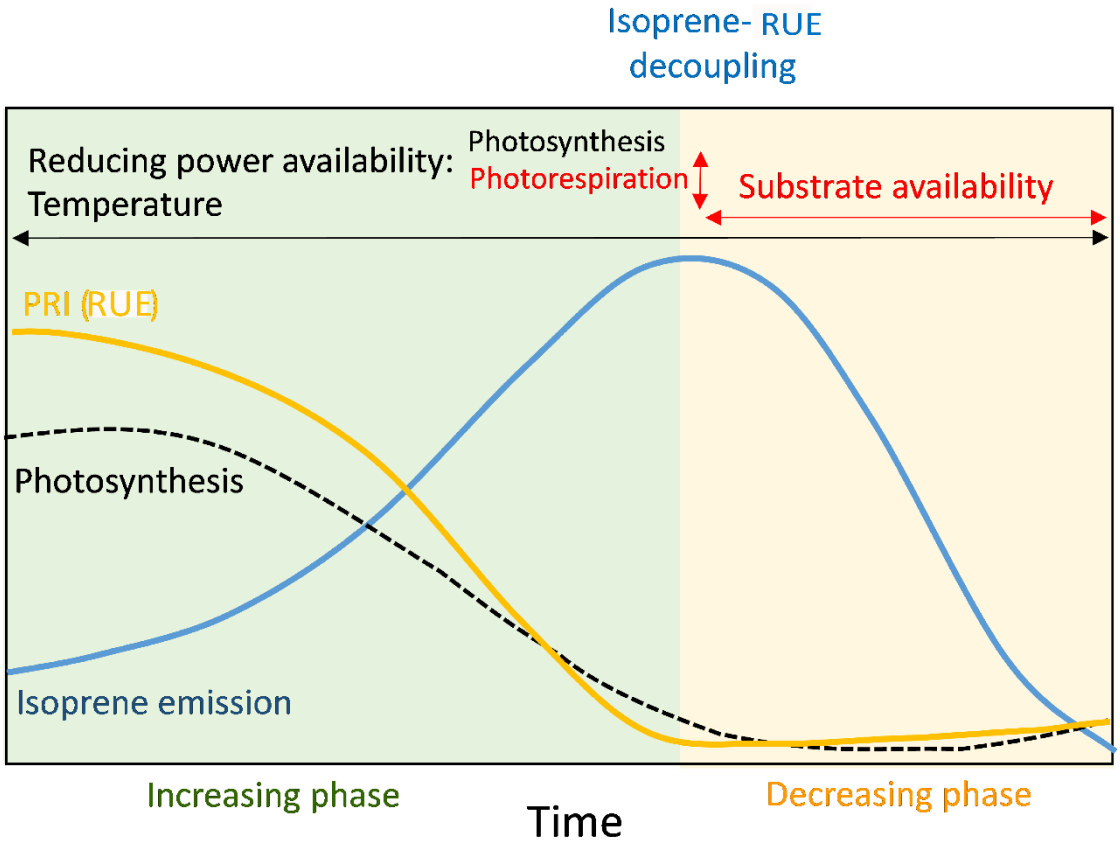

Figure 9. Conceptual model of the seasonal behavior of PRI and isoprene emissions, with the main drivers that affect their relationship. The variables in red affect isoprene emissions independently of RUE and thus alter the ability of PRI to estimate isoprene emissions.

PRI, however, was more sensitive than the MEGAN model to temporal changes in isoprene emissions, because it followed changes in RUE, so PRI could be used to improve MEGAN, consistent with previous foliar level studies where PRI combined with basal emission factors was as good a predictor of isoprenoid emissions as some standard

emission models and where a combination of MEGAN and PRI provided the best predictions (Peñuelas et al., 2013). PRI was thus accounting for additional residual variance not explained by the factors considered in MEGAN. Furthermore, the high temporal resolution and spatially extensive nature of remotely sensed data can help the detection of some of the spatial and temporal variability in emissions that other models may miss (Peñuelas et al., 2013).

In addition to the diurnal relationship between PRI and RUE mediated by the xanthophyll cycle and indicating excess reducing power, seasonal changes in PRI are primarily influenced by carotenoid pool sizes (relative to chlorophyll). The relationship between PRI and isoprene emissions is strongly influenced by these constitutive changes in pigments (Harris et al., 2016), so understanding how the isoprene-PRI relationship is affected by both long-term changes in pools of carotenoid pigments and short-term dynamic adjustments of RUE are important in studies with seasonal temporal scales. MODIS PRI (CCI) has been developed to assess shifts in the levels of chlorophyll and carotenoid pigments rather than the xanthophyll de-epoxidation cycle per se, particularly when sampled over seasonal cycles in coniferous forests (Gamon et al., 2016). Knowledge of the long-term pigment changes would add information for their effect on isoprene emission, facilitating the interpretation of PRI for monitoring isoprene emissions.

5. Conclusions

This study is the first demonstration that a MODIS PRI (also called CCI) sensitive to carotenoid pool sizes, could be used to remotely assess isoprene emissions at the ecosystem level. PRI was also able to monitor emission increases during the onset of drought conditions.

Complementing MEGAN with PRI improved MEGAN performance under drought conditions. PRI was able to estimate isoprene emissions under standard and drought conditions, but only until emissions reached their maxima. The subsequent decrease in isoprene emissions, attributed to the lack of carbon substrates instead of reducing power, was not well assessed by PRI.

Direct estimation of isoprene emission by PRI is, however, limited, because PRI estimates RUE, and the relationship between RUE and isoprene emissions can be modified by stress conditions. Further research is thus needed to resolve this limitation.

Additionally, further research is needed on the seasonal pigment responses involved to clarify the individual roles of xanthophyll cycle pigments versus other carotenoid pigments in the PRI signals linked to isoprene emissions

References

Andreae, M.O., Crutzen, P. J. 1997. Atmospheric aerosols: Biogeochemical Sources and Role in Atmospheric Chemistry. Science, 276, 1052–1058.doi:10.1126/science.276.5315.1052

Barkley, M.P., Palmer, P.I., Kuhn, U., Kesselmeier, J., Chance, K., Kurosu, T.P., Martin, R. V, Helmig, D., Guenther, A., 2008. Net ecosystem fluxes of isoprene over tropical South America inferred from Global Ozone Monitoring Experiment (GOME) observations of HCHO columns. J. Geophys. Res. 113. doi:10.1029/2008jd009863

Bertin, N., Staudt, M., 1996. Effect of water stress on monoterpene emissions from young potted holm oak (*Quercus ilex* L) trees. Oecologia 107, 456–462. doi:10.1007/bf00333935

Breheny, P., Burchett, W., 2013. Visualization of regression models using visreg. R Packag. 1–15.

Brilli, F., Barta, C., Fortunati, A., Lerdau, M., Loreto, F., Centritto, M., 2007. Response of isoprene emission and carbon metabolism to drought in white poplar (*Populus alba*) saplings. New Phytol. 175, 244–254. doi:10.1111/j.1469-8137.2007.02094.x

Bruggemann, N., Schnitzler, J.P., 2002. Comparison of isoprene emission, intercellular isoprene concentration and photosynthetic performance in water-limited oak (*Quercus pubescens* Willd. and *Quercus robur* L.) Saplings. Plant Biol. 4, 456–463. doi:10.1055/s-2002-34128

Chameides, W.L., Lindsay, R.W., Richardson, J., Kiang, C.S., 1988. The role of biogenic hydrocarbons in urban photochemical smog: Atlanta as a case study. Science. 241, 1473–1475. doi:10.1126/science.3420404

Critchfield, H.J., 1966. General Climatology. Prentice-Hall, Englewood Cliffs, N.J.

Dani, K.G.S., Jamie, I.M., Prentice, I.C., Atwell, B.J., 2015. Species-specific photorespiratory rate, drought tolerance and isoprene emission rate in plants. Plant Signal. Behav. 10, e990830. doi:10.4161/15592324.2014.990830

Dani, K.G.S., Jamie, I.M., Prentice, I.C., Atwell, B.J., 2014. Increased ratio of electron transport to net assimilation rate supports elevated isoprenoid emission rate in eucalypts under drought. Plant Physiol. 166, 1059–1072. doi:10.1104/pp.114.246207

Filella, I., Porcar-Castell, A., Munne-Bosch, S., Back, J., Garbulsky, M.F., Peñuelas, J., 2009. PRI assessment of long-term changes in carotenoids/chlorophyll ratio and short-term changes in de-epoxidation state of the xanthophyll cycle. Int. J. Remote Sens. 30, 4443–4455. doi:10.1080/01431160802575661

Fortunati, A., Barta, C., Brilli, F., Centritto, M., Zimmer, I., Schnitzler, J.-P., Loreto, F., 2008. Isoprene emission is not temperature-dependent during and after severe drought-stress: a physiological and biochemical analysis. Plant J. 55, 687–697. doi:10.1111/j.1365-313X.2008.03538.x

Foster, P.N., Prentice, I.C., Morfopoulos, C., Siddall, M., van Weele, M., 2014. Isoprene emissions track the seasonal cycle of canopy temperature, not primary production: evidence from remote sensing. Biogeosciences 11, 3437–3451. doi:10.5194/bg-11-3437-2014

Fuentes, J.D., Lerdau, M., Atkinson, R., Baldocchi, D., Bottenheim, J.W., Ciccioli, P., Lamb, B., Geron, C., Gu, L., Guenther, A., Sharkey, T.D., Stockwell, W., 2000. Biogenic hydrocarbons in the atmospheric boundary layer: a review. Bull. Am. Meteorol. Soc. 81, 1537–1575.doi:10.1175/1520-0477(2000)081<1537:BHITAB>2.3.CO;2

Funk, J.L., Jones, C.G., Gray, D.W., Throop, H.L., Hyatt, L.A., Lerdau, M.T., 2005. Variation in isoprene emission from *Quercus rubra*: sources, causes, and consequences for estimating fluxes. J. Geophys. Res. 110. doi:10.1029/2004jd005229

Funk, J.L., Mak, J.E., Lerdau, M.T., 2004. Stress-induced changes in carbon sources for isoprene production in *Populus deltoides*. Plant Cell Environ. 27, 747–755. doi:10.1111/j.1365-3040.2004.01177.x

Gamon, J.A., Huemmrich, K.F., Wong, C.Y.S., Ensminger, I., Garrity, S., Hollinger, D.Y., Noormets, A., Peñuelas, J., 2016. A remotely sensed pigment index reveals photosynthetic phenology in evergreen conifers. Proc. Natl. Acad. Sci. 113, 13087–13092. doi:10.1073/pnas.1606162113

Gamon, J.A., Peñuelas, J., Field, C.B., 1992. A narrow-waveband spectral index that tracks diurnal changes in photosynthetic efficiency. Remote Sens. Environ. 41, 35–44. doi:10.1016/0034-4257(92)90059-s

Garbulsky, M.F., Peñuelas, J., Gamon, J., Inoue, Y., Filella, I., 2011. The photochemical

reflectance index (PRI) and the remote sensing of leaf, canopy and ecosystem radiation use efficiencies. A review and meta-analysis. Remote Sens. Environ. 115, 281–297. doi:10.1016/j.rse.2010.08.023

Genard-Zielinski, A.-C., Ormeno, E., Boissard, C., Fernandez, C., 2014. Isoprene emissions from downy oak under water limitation during an entire growing season: what cost for growth? PLOS One 9. doi:10.1371/journal.pone.0112418

Geron, C., Guenther, A., Sharkey, T., Arnts, R.R., 2000. Temporal variability in basal isoprene emission factor. Tree Physiol. 20, 799–805.

Goerner, A., Reichstein, M., Rambal, S., 2009. Tracking seasonal drought effects on ecosystem light use efficiency with satellite-based PRI in a Mediterranean forest. Remote Sens. Environ. 113, 1101–1111. doi:10.1016/j.rse.2009.02.001

Gu, D., Guenther, A.B., Shilling, J.E., Yu, H., Huang, M., Zhao, C., Yang, Q., Martin, S.T., Artaxo, P., Kim, S., Seco, R., Stavrakou, T., Longo, K.M., Tóta, J., de Souza, R.A.F., Vega, O., Liu, Y., Shrivastava, M., Alves, E.G., Santos, F.C., Leng, G., Hu, Z., 2017. Airborne observations reveal elevational gradient in tropical forest isoprene emissions. Nat. Commun. 8, 15541. doi:10.1038/ncomms15541

Gu, L., Meyers, T., Pallardy, S.G., Hanson, P.J., Yang, B., Heuer, M., Hosman, K.P., Riggs, J.S., Sluss, D., Wullschleger, S.D., 2006. Direct and indirect effects of atmospheric conditions and soil moisture on surface energy partitioning revealed by a prolonged drought at a temperate forest site. J. Geophys. Res. 111. doi:10.1029/2006jd007161

Guenther, A.B., Hills, A.J., 1998. Eddy covariance measurement of isoprene fluxes. J. Geophys. Res. 103, 13145–13152. doi:10.1029/97jd03283

Guenther, A.B., Jiang, X., Heald, C.L., Sakulyanontvittaya, T., Duhl, T., Emmons, L.K., Wang, X., 2012. The Model of Emissions of Gases and Aerosols from Nature version 2.1 (MEGAN2.1): an extended and updated framework for modeling biogenic emissions. Geosci. Model Dev. 5, 1471–1492. doi:10.5194/gmd-5-1471-2012

Guenther, A.B., Zimmerman, P.R., Harley, P.C., Monson, R.K., Fall, R., 1993. Isoprene and monoterpene emission rate variability - model evaluations and sensitivity analyses. J. Geophys. Res. 98, 12609–12617. doi:10.1029/93jd00527

Harley, P.C., Litvak, M.E., Sharkey, T.D., Monson, R.K., 1994. Isoprene emission from velvet bean leaves. Plant Physiol. 105, 279–285.

Harris, A., Owen, S.M., Sleep, D., Pereira, M. da G. dos S., 2016. Constitutive changes in pigment concentrations: implications for estimating isoprene emissions using the photochemical reflectance index. Physiol. Plant. 156, 190–200. doi:10.1111/ppl.12361

IPCC, 2014. Climate Change 2014: impacts, adaptation, and vulnerability. Part A: global and sectoral aspects contribution of working group II to the fifth assessment report of the Intergovernmental Panel on Climate Change. Cambridge University Pres, Cambridge.

Karl, T.G., Spirig, C., Rinne, J., Stroud, C., Prevost, P., Greenberg, J., Fall, R., Guenther, A., 2002. Virtual disjunct eddy covariance measurements of organic compound fluxes from a subalpine forest using proton transfer reaction mass spectrometry. Atmos. Chem. Phys. 2, 279–291.

Llusià, J., Roahtyn, S., Yakir, D., Rotenberg, E., Seco, R., 2016. Photosynthesis, stomatal conductance and terpene emission response to water availability in dry and mesic Mediterranean forests 749–759. doi:10.1007/s00468-015-1317-x

Loreto, F., Schnitzler, J.-P., 2010. Abiotic stresses and induced BVOCs. Trends Plant Sci. 15,154–166.doi:10.1016/j.tplants.2009.12.006

Mac Nally, R., Walsh, C.J., 2004. Hierarchical partitioning public-domain software. Biodivers. Conserv. 13, 659–660. doi:10.1023/B:BIOC.0000009515.11717.0b

Monson, R.K., Grote, R., Niinemets, U., Schnitzler, J.-P., 2012. Modeling the isoprene emission rate from leaves. New Phytol. 195, 541–559. doi:10.1111/j.1469-8137.2012.04204.x

Monteith, J.L., 1993. Using tube solarimeters to measure radiation intercepted by crop canopies and to analyse stand growth. Delta-T Devices.1–11.

Morfopoulos, C., Prentice, I.C., Keenan, T.F., Friedlingstein, P., Medlyn, B.E., Peñuelas, J., Possell, M., 2013. A unifying conceptual model for the environmental responses of isoprene emissions from plants. Ann. Bot. 112, 1223–1238. doi:10.1093/aob/mct206

Morfopoulos, C., Sperlich, D., Peñuelas, J., Filella, I., Llusià, J., Medlyn, B.E., Niinemets, U., Possell, M., Sun, Z., Prentice, I.C., 2014. A model of plant isoprene emission based on available reducing power captures responses to atmospheric CO_2. New Phytol. 203, 125–

139. doi:10.1111/nph.12770
Niinemets, U., 2010. Mild versus severe stress and BVOCs: thresholds, priming and consequences. Trends Plant Sci. 15, 145–153. doi:10.1016/j.tplants.2009.11.008
Niinemets, U., Arneth, A., Kuhn, U., Monson, R.K., Peñuelas, J., Staudt, M., 2010a. The emission factor of volatile isoprenoids: stress, acclimation, and developmental responses. Biogeosciences 7, 2203–2223. doi:10.5194/bg-7-2203-2010
Niinemets, U., Monson, R.K., Arneth, A., Ciccioli, P., Kesselmeier, J., Kuhn, U., Noe, S.M., Peñuelas, J., Staudt, M., 2010b. The leaf-level emission factor of volatile isoprenoids: caveats, model algorithms, response shapes and scaling. Biogeosciences 7, 1809–1832. doi:10.5194/bg-7-1809-2010
Owen, S.M., Peñuelas, J., 2013. Volatile isoprenoid emission potentials are correlated with essential isoprenoid concentrations in five plant species. Acta Physiol. Plant. 35, 3109–3125. doi:10.1007/s11738-013-1344-4
Owen, S.M., Peñuelas, J., 2005. Opportunistic emissions of volatile isoprenoids. Trends Plant Sci. 10, 420–426. doi:10.1016/j.tplants.2005.07.010
Palmer, P.I., Jacob, D.J., Fiore, A.M., Martin, R. V, Chance, K., Kurosu, T.P., 2003. Mapping isoprene emissions over North America using formaldehyde column observations from space. J. Geophys. Res. 108. doi:10.1029/2002jd002153
Pegoraro, E., Rey, A., Greenberg, J., Harley, P., Grace, J., Malhi, Y., Guenther, A., 2004. Effect of drought on isoprene emission rates from leaves of *Quercus virginiana* Mill. Atmos. Environ. 38, 6149–6156. doi:10.1016/j.atmosenv.2004.07.028
Peñuelas, J., Filella, I., Gamon, J.A., 1995. Assessment of photosynthetic radiation-use efficiency with spectral reflectance. New Phytol. 131, 291–296. doi:10.1111/j.1469-8137.1995.tb03064.x
Peñuelas, J., Garbulsky, M.F., Filella, I., 2011. Photochemical reflectance index (PRI) and remote sensing of plant CO_2 uptake. New Phytol. 191, 596–599. doi:10.1111/j.1469-8137.2011.03791.x
Peñuelas, J., Llusià, J., 2004. Plant VOC emissions: making use of the unavoidable. Trends Ecol. Evol. 19, 402–404. doi:10.1016/j.tree.2004.06.002
Peñuelas, J., Llusià, J., 2003. BVOCs: plant defense against climate warming? Trends Plant Sci. 8, 105–109. doi:10.1016/s1360-1385(03)00008-6
Peñuelas, J., Marino, G., Llusià, J., Morfopoulos, C., Farre-Armengol, G., Filella, I., 2013. Photochemical reflectance index as an indirect estimator of foliar isoprenoid emissions at the ecosystem level. Nat. Commun. 4. doi:10.1038/ncomms3604
Peñuelas, J., Staudt, M., 2010. BVOCs and global change. Trends Plant Sci. 15, 133–144. doi:10.1016/j.tplants.2009.12.005
Porcar-Castell, A., Ignacio Garcia-Plazaola, J., Nichol, C.J., Kolari, P., Olascoaga, B., Kuusinen, N., Fernandez-Marin, B., Pulkkinen, M., Juurola, E., Nikinmaa, E., 2012. Physiology of the seasonal relationship between the photochemical reflectance index and photosynthetic light use efficiency. Oecologia 170, 313–323. doi:10.1007/s00442-012-2317-9
Potosnak, M.J., LeStourgeon, L., Pallardy, S.G., Hosman, K.P., Gu, L., Karl, T., Geron, C., Guenther, A.B., 2014. Observed and modeled ecosystem isoprene fluxes from an oak-dominated temperate forest and the influence of drought stress. Atmos. Environ. 84, 314–322. doi:10.1016/j.atmosenv.2013.11.055
Pressley, S., Lamb, B., Westberg, H., Flaherty, J., Chen, J., Vogel, C., 2005. Long-term isoprene flux measurements above a northern hardwood forest. J. Geophys. Res. 110. doi:10.1029/2004jd005523
R Core Team, 2015. R: A Language and Environment for Statistical Computing. R Found. Stat. Comput. 1, 1651.
Rahman, A.F., Cordova, V.D., Gamon, J.A., Schmid, H.P., Sims, D.A., 2004. Potential of MODIS ocean bands for estimating CO_2 flux from terrestrial vegetation: A novel approach. Geophys. Res. Lett. 31. doi:10.1029/2004gl019778
Reichstein, M., Falge, E., Baldocchi, D., Papale, D., Aubinet, M., Berbigier, P., Bernhofer, C., Buchmann, N., Gilmanov, T., Granier, A., Grünwald, T., Havránková, K., Ilvesniemi, H., Janous, D., Knohl, A., Laurila, T., Lohila, A., Loustau, D., Matteucci, G., Meyers, T., Miglietta, F., Ourcival, J.M., Pumpanen, J., Rambal, S., Rotenberg, E., Sanz, M., Tenhunen, J., Seufert, G., Vaccari, F., Vesala, T., Yakir, D., Valentini, R., 2005. On the separation of net ecosystem exchange into assimilation and ecosystem respiration: review and improved algorithm. Glob. Chang. Biol. 11, 1424–1439. doi:10.1111/j.1365-2486.2005.001002.x
Rodríguez-Calcerrada, J., Buatois, B., Chiche, E., Shahin, O., Staudt, M., 2013. Leaf isoprene emission declines in *Quercus pubescens*

seedlings experiencing drought - Any implication of soluble sugars and mitochondrial respiration? Environ. Exp. Bot. 85, 36–42. doi:10.1016/j.envexpbot.2012.08.001

Seco, R., Karl, T., Guenther, A., Hosman, K.P., Pallardy, S.G., Gu, L., Geron, C., Harley, P., Kim, S., 2015. Ecosystem-scale volatile organic compound fluxes during an extreme drought in a broadleaf temperate forest of the Missouri Ozarks (central USA). Glob. Chang. Biol. 21, 3657–3674. doi:10.1111/gcb.12980

Sharkey, T.D., Wiberley, A.E., Donohue, A.R., 2008. Isoprene emission from plants: Why and how. Ann. Bot. 101, 5–18. doi:10.1093/aob/mcm240

Sims, D.A., Gamon, J.A., 2002. Relationships between leaf pigment content and spectral reflectance across a wide range of species, leaf structures and developmental stages. Remote Sens. Environ. 81, 337–354. doi:10.1016/s0034-4257(02)00010-x

Spirig, C., Neftel, A., Ammann, C., Dommen, J., Grabmer, W., Thielmann, A., Schaub, A., Beauchamp, J., Wisthaler, A., Hansel, A., 2005. Eddy covariance flux measurements of biogenic VOCs during ECHO 2003 using proton transfer reaction mass spectrometry. Atmos. Chem. Phys. 5, 465–481.

Stylinski, C.D., Gamon, J.A., Oechel, W.C., 2002. Seasonal patterns of reflectance indices, carotenoid pigments and photosynthesis of evergreen chaparral species. Oecologia 131, 366–374. doi:10.1007/s00442-002-0905-9

Tani, A., Tozaki, D., Okumura, M., Nozoe, S., Hirano, T., 2011. Effect of drought stress on isoprene emission from two major *Quercus* species native to East Asia. Atmos. Environ. 45, 6261–6266. doi:10.1016/j.atmosenv.2011.08.003

Valin, L.C., Fiore, A.M., Chance, K., Abad, G.G., 2016. The role of OH production in interpreting the variability of CH_2O columns in the southeast U.S. Journal of Geophysical Research : Atmospheres 478–493. doi:10.1002/2015JD024012.Received

Velikova, V., Sharkey, T.D., Loreto, F., 2012. Stabilization of thylakoid membranes in isoprene-emitting plants reduces formation of reactive oxygen species. Plant Signal. Behav. 7, 139–141. doi:10.4161/psb.7.1.18521

Westberg, H., Lamb, B., Hafer, R., Hills, A., Shepson, P., Vogel, C., 2001. Measurement of isoprene fluxes at the PROPHET site. J. Geophys. Res. 106, 24347–24358. doi:10.1029/2000jd900735

Wong, C.Y.S., Gamon, J.A., 2015. Three causes of variation in the photochemical reflectance index (PRI) in evergreen conifers. New Phytol. 206, 187–195. doi:10.1111/nph.13159

Wu, C., Pullinen, I., Andres, S., Carriero, G., Fares, S., Goldbach, H., Hacker, L., Kasal, T., Kiendler-Scharr, A., Kleist, E., Paoletti, E., Wahner, A., Wildt, J., Mentel, T.F., 2015. Impacts of soil moisture on de novo monoterpene emissions from European beech, Holm oak, Scots pine, and Norway spruce. Biogeosciences 12, 177–191. doi:10.5194/bg-12-177-2015

Zhang, C., Filella, I., Garbulsky, M.F., Peñuelas, J., 2016. Affecting factors and recent improvements of the photochemical reflectance index (PRI) for remotely sensing foliar, canopy and ecosystemic radiation-use efficiencies. Remote Sensing, 8(9), 677. doi:10.3390/rs8090677

Conclusions

1. Our review integrated more than 20 years' analysis of studying PRI. The results indicate that PRI is a good proxy of RUE and GPP at different spatial and temporal scales. Diurnal changes of PRI were mainly associated with xanthophyll-cycle pigments across different vegetation functional types at leaf and canopy level. Seasonal changes of PRI, however, were significantly impacted by chlorophyll and carotenoid pool sizes. Other biochemical and physical factors such as additional photoprotective mechanisms, canopy structure, illumination, and view/solar geometry etc. complicate PRI interpretation and further constrain the generalization of the PRI-RUE relationships. Interestingly, improvements in PRI implementation received remarkable achievements. For example, correcting PRI by decreasing the influence of physical or physiological factors, or combining PRI with solar-induced fluorescence (SIF) and optical indices for biomass greenness could greatly improve remote sensing of RUE.

2. We demonstrated for the first time, as far as we know, the capability of optical signals to assess seasonal photosynthesis dynamics in an overwintering evergreen species. We found out that all wavelengths of the leaf-level fluorescence spectral, from 670 to 800 nm have substantial and similar potential to track seasonal photosynthetic dynamics. In addition, we showed that different optical signals, fluorescence, PRI, and WI can track photosynthesis via different mechanisms. It was NPQ that controlled changes in spectral fluorescence, carotenoid contents that regulated changes in PRI and the WI was correlated with WC. We suggest that a combination of different optical indices is preferable for maximising physiological information content retrieval, and can provide a non-destructive and robust approach to track photosynthetic dynamics during complex winter-spring transitions.
3. PRI and reflectance-ratio based ChlF R690/R630 both decreased with progressively enhanced drought stress, and significantly correlated with A, F_V/F_M, and Yield. The

differential values resulting from subtracting the PRI and R690/R630 values of drought treatments from the respective values of their corresponding recovery treatments $\Delta PRI_{recovery}$ and $\Delta R690/R630_{recovery}$ were correlated with $\Delta A_{recovery}$, $\Delta F_V/F_{Mrecovery}$ and $\Delta Yield_{recovery}$. Our result demonstrated that PRI and R690 were not only sensitive to progressively enhanced drought but also to the recovery of the photosynthesis after drought stress.

4. PRI but not NDVI captured the seasonal changes of photosynthesis in a Mediterranean shrub submitted to a long-term experimental warming and drought. The seasonality of water content was captured by WI. Warming enhanced winter photosynthetic activity, and both warming and drought enhanced the summer midday depression of photosynthesis. ΔPRI (midday PRI subtracted from morning PRI) was significantly correlated to photosynthetic midday depression both under warming and drought treatments. We concluded that using PRI and ΔPRI to monitor the variability in photosynthesis could provide a simple method to remotely sense photosynthetic seasonality and midday depression in response to ongoing and future environmental stresses.
5. The generally used remote sensing products including MODIS GPP and PRI were not reliable to detect the effect of drought on *in situ* observed GPP in forest. However, the MODIS PRI normalized by absorbed light (APAR) (sPRIn) detected such drought effects on GPP for Mediterranean forest but not for grassland ecosystem in where the conventional greenness indices such as NDVI performed better than PRI and sPRIn. We conclude that sPRIn provided a useful estimation of vegetation functioning that is difficult to be captured by the other greenness indices in Mediterranean forests, and is a promising indicator that allows to improve the detection of drought effects on GPP from space.
6. MODIS PRI was significantly correlated with isoprene emissions measured with eddy covariance for most of the season until there was a seasonal emission peak. The subsequent decrease in isoprene emissions due to the lack of carbon substrates elicited its decoupling with PRI. PRI also efficiently track the annual changes of

isoprene emissions, even during the onset of drought conditions. We conclude that PRI can be a promising index to estimate isoprene emissions, especially when it is complemented by information on potential emission. It may also be used to further improve models of isoprene emission under drought and other stress conditions.

Supplementary material

Chapter 2. Optical cues reveal the photosynthetic spring recovery in Scots pine needles

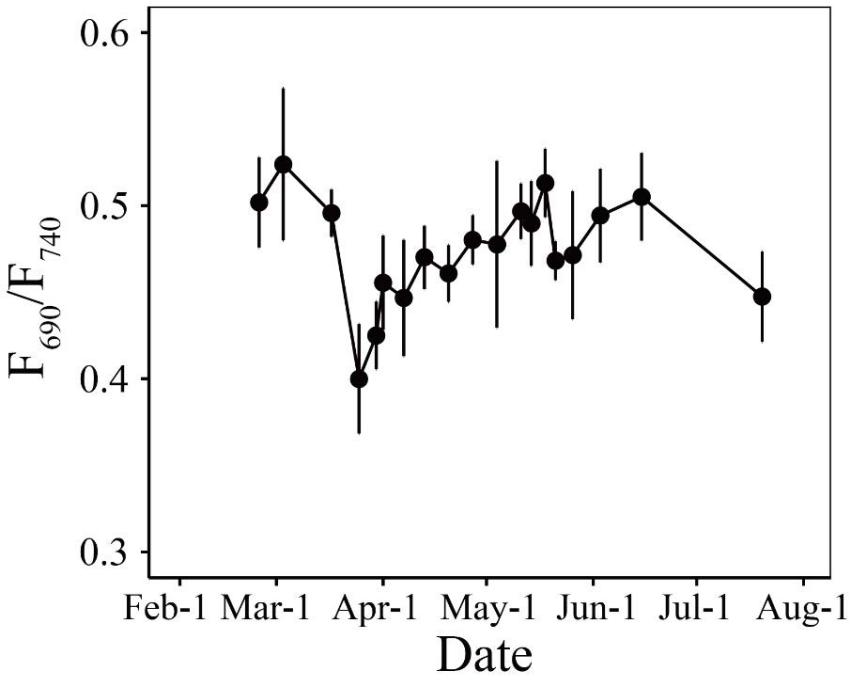

Figure S1. Seasonal variations in fluorescence ratio (F_{690}/F_{740}) for Scots pine needles. Points represent means of five biological replicates (n = 5). And standard error (SE; shown only when larger than symbols) was shown.

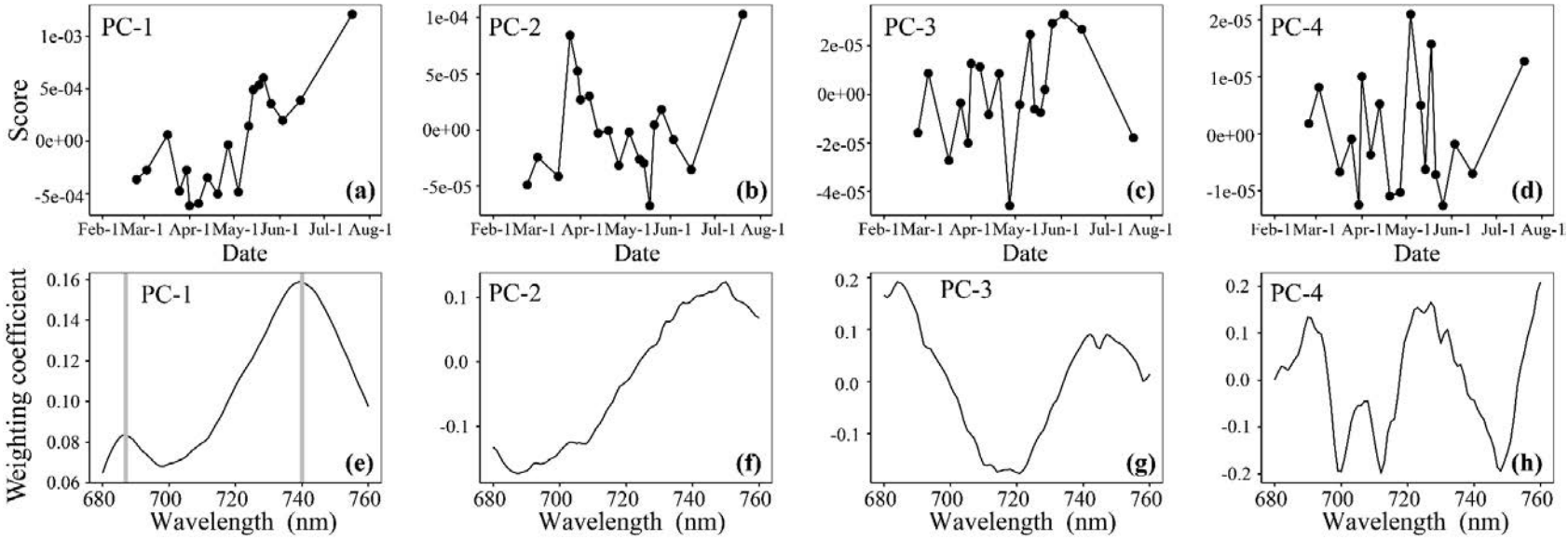

Figure S2. The first four Principle Component (PC) analysis for seasonally spectral fluorescence.

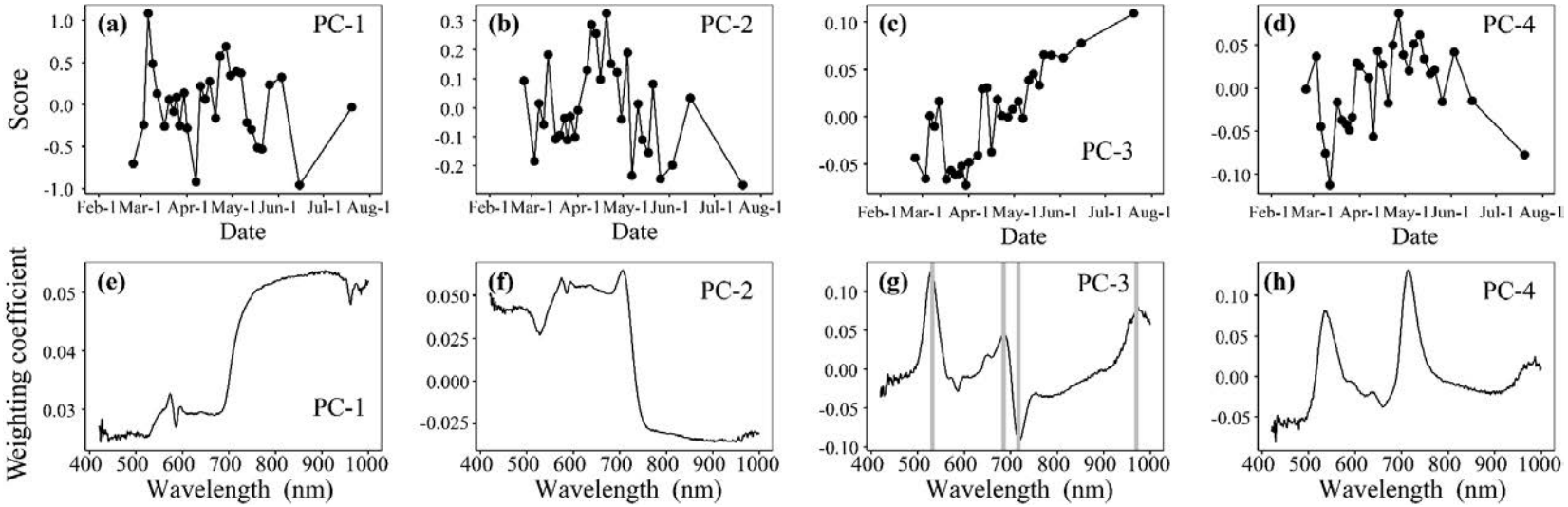

Figure S3. The first four Principle Component (PC) analysis for seasonally reflectance spectra.

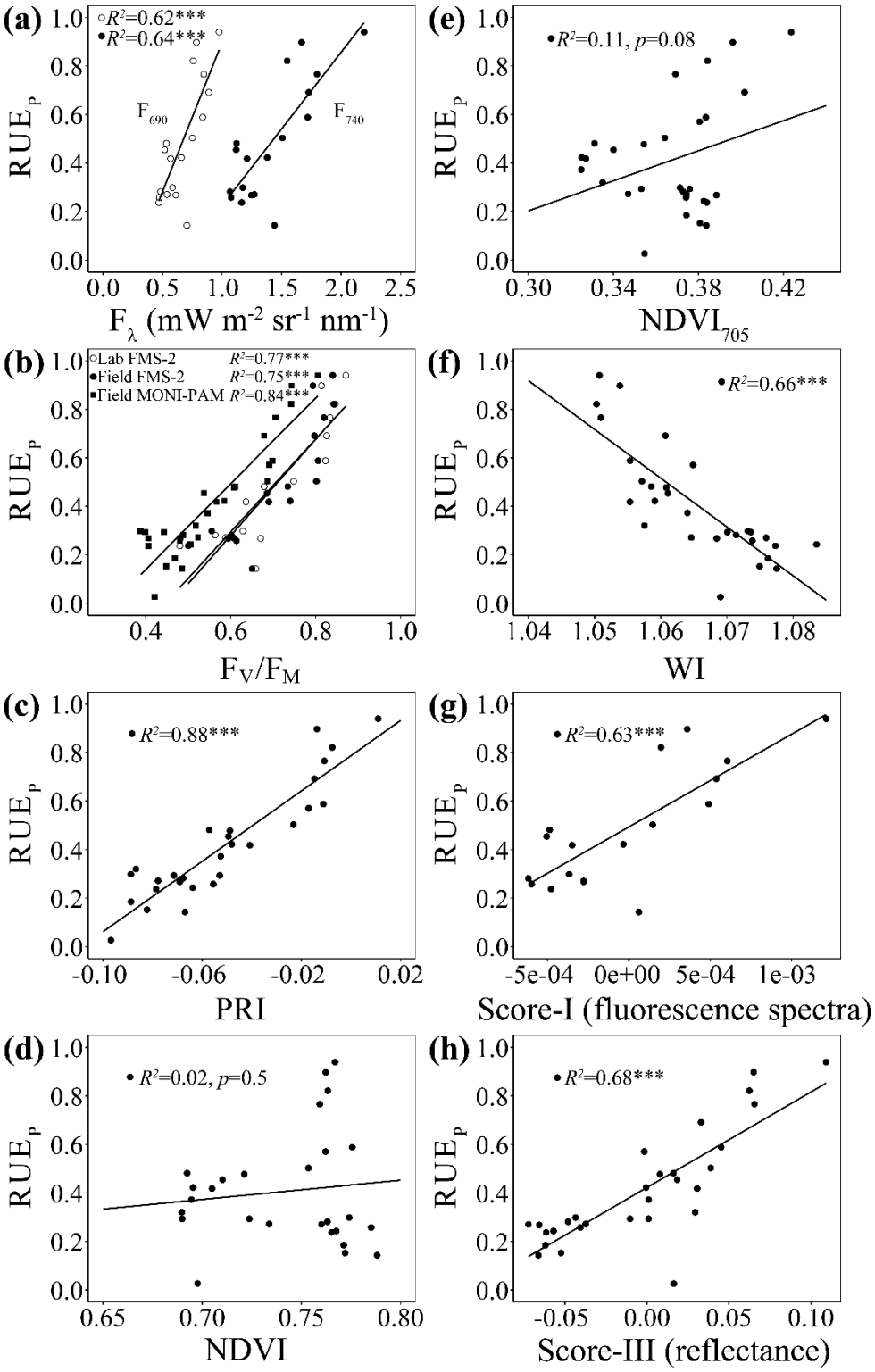

Figure S4. The linear correlations of optical indices in Figure 4 with rescaled normalized slope of linear function fitted to photosynthetic light response with low incident PAR before noon (RUE_p). Points represent means of five biological replicates (n = 5). ***p<0.001.

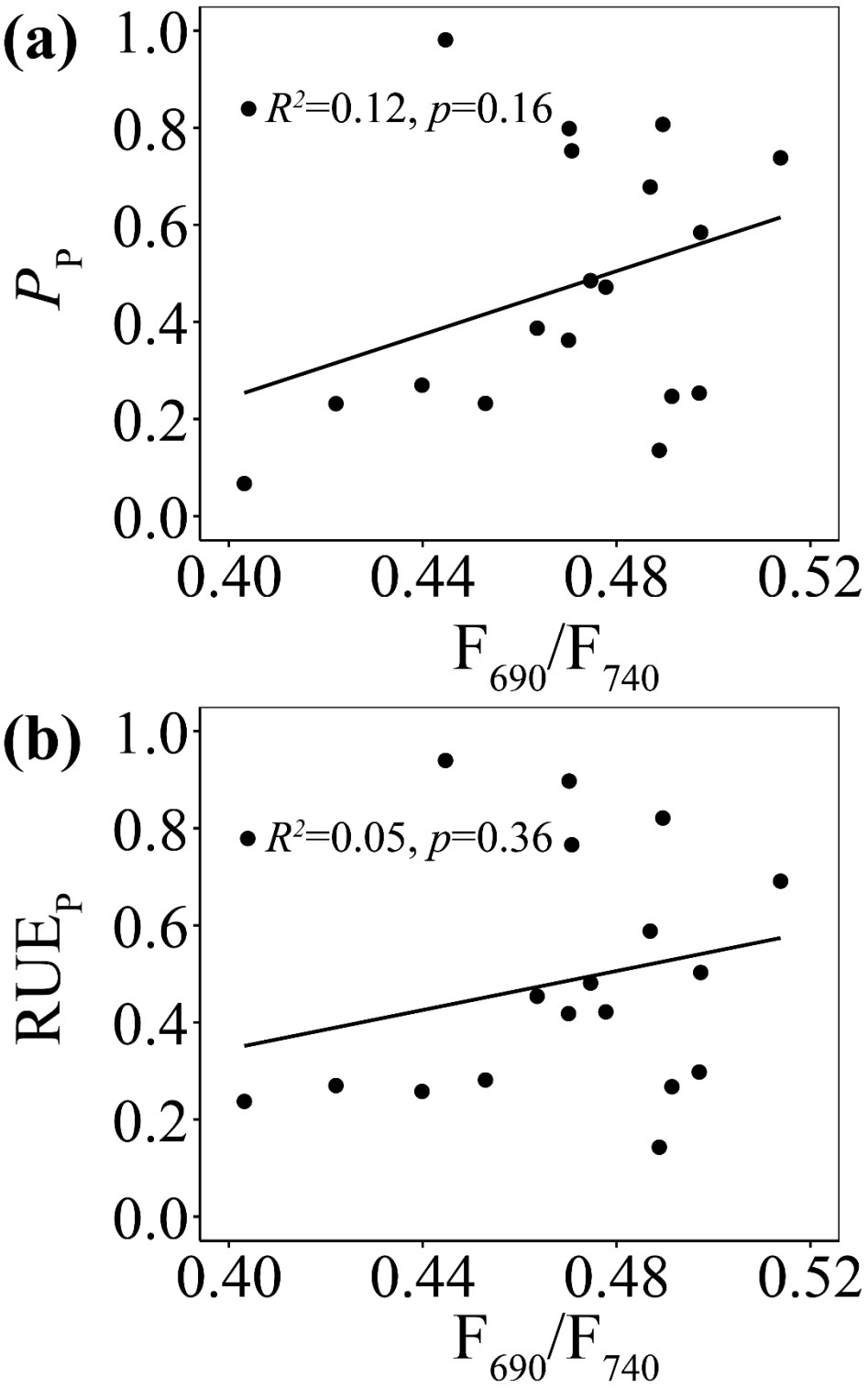

Figure S5. Relationships of F_{690}/F_{740} with rescaled normalized photosynthetic parameters (P_p and RUE_p). Points represent means of five biological replicates (n = 5).

Chapter 4. Photochemical reflectance index (PRI) for detecting responses of diurnal and seasonal photosynthetic activity to experimental drought and warming in a Mediterranean shrubland

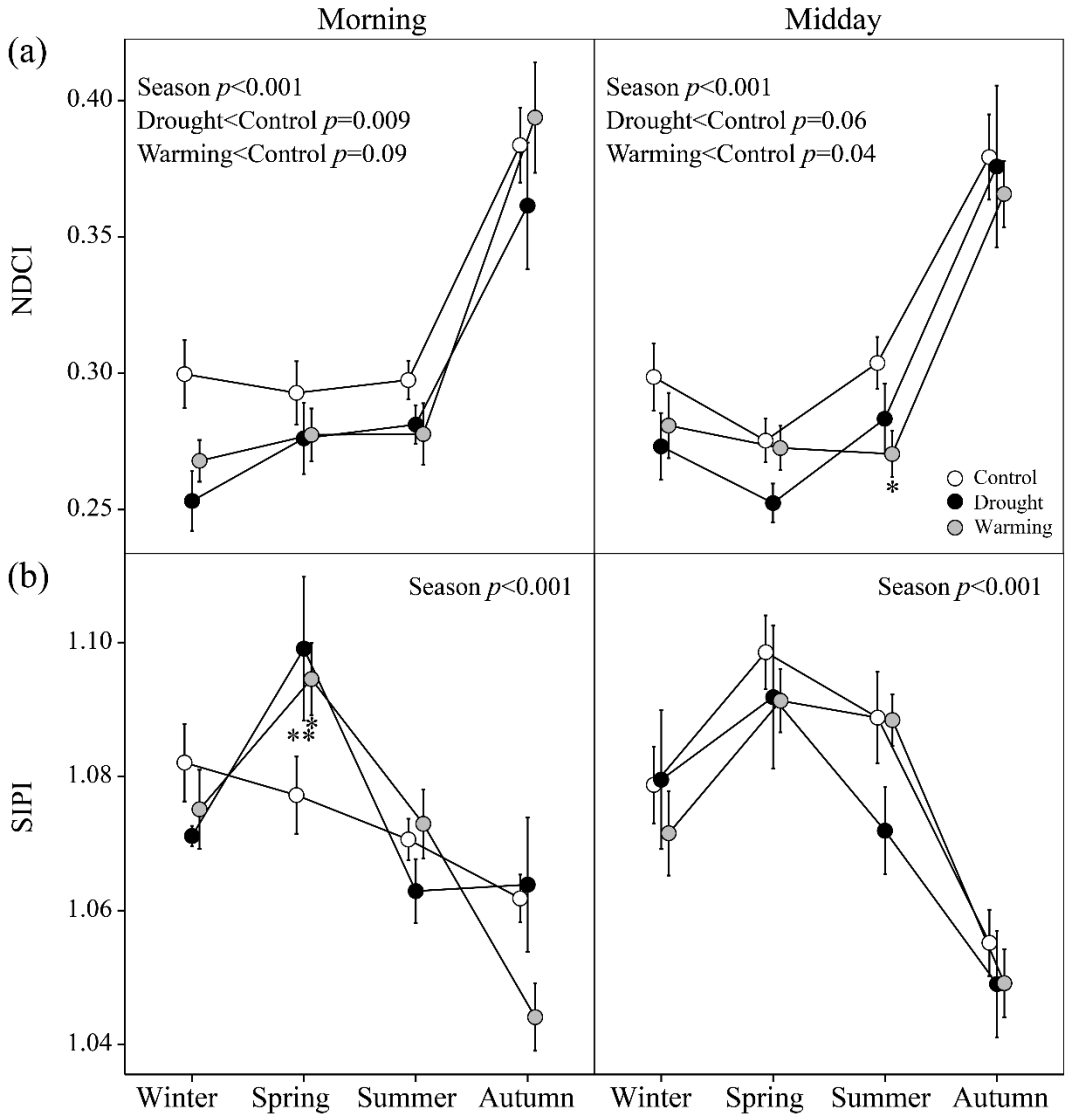

Figure S1. Seasonal variation of the normalized difference chlorophyll index (NDCI) (a) and the structure-independent pigment index (SIPI) (b) for *Erica multiflora* in 2014. Error bars are standard errors of the mean (n=9 for the drought and warming treatments, and n=18 for the control treatment). The significances of overall repeated-measures ANOVAs are depicted. *p<0.05 and **p<0.01 between treatments for each seasonal measurement.

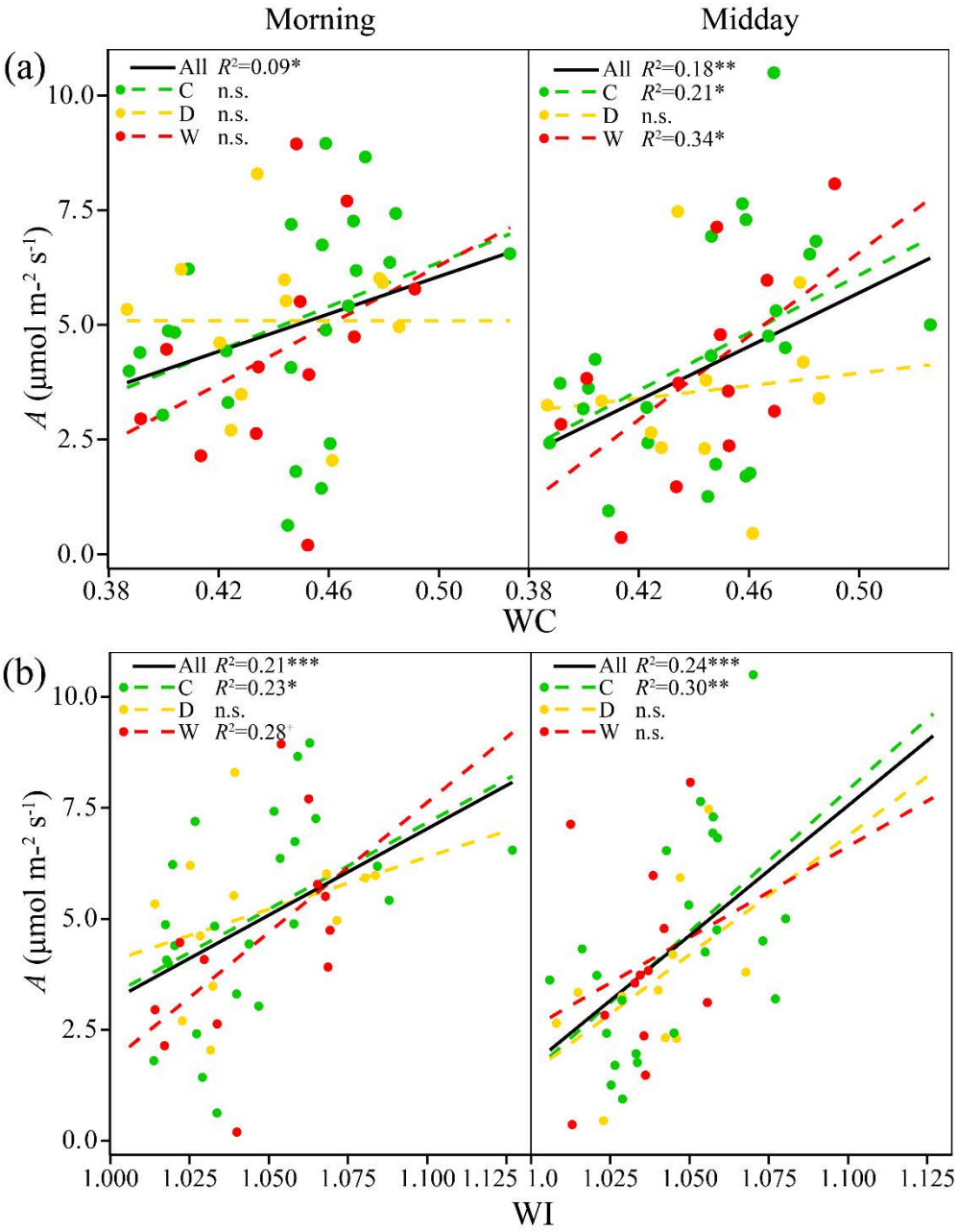

Figure S2. Relationships of CO_2 assimilation rate (*A*) with water content (WC) (a) and the water index (WI) (b) for *Erica multiflora* in 2014. The black lines represent the linear relationships over all three treatments. n.s. $p>0.1$, $^{+}p<0.1$, $*p<0.05$, $**p<0.01$ and $***p<0.001$ between variables. C, D and W indicate the control, drought and warming treatments, respectively.

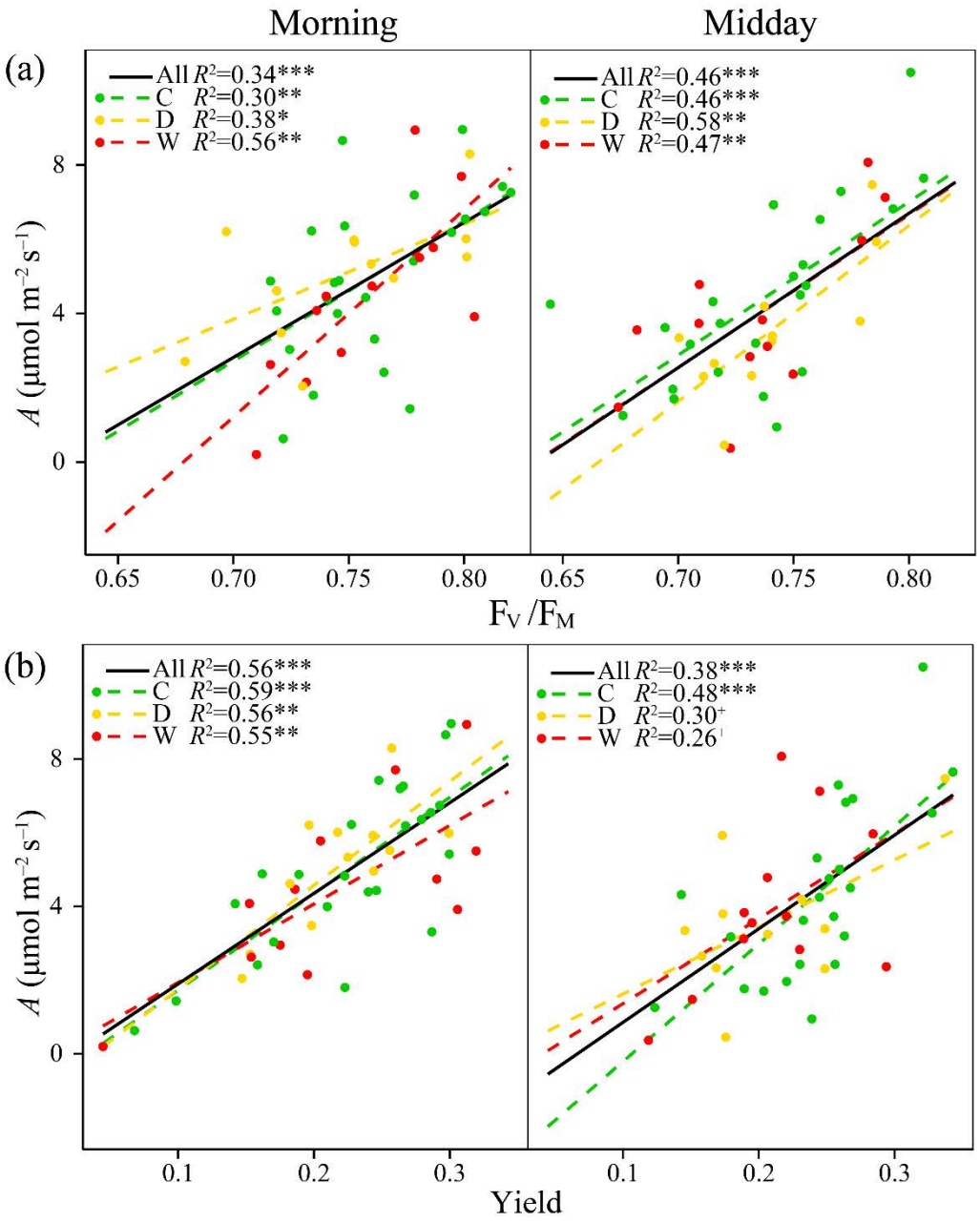

Figure S3. Relationships of CO_2 assimilation rate (*A*) with maximum (F_V/F_M) (a) and actual (Yield) (b) photochemical efficiency of PSII for *Erica multiflora* in 2014. The black lines represent the linear relationships over all three treatments. $^+p<0.1$, $*p<0.05$, $**p<0.01$ and $***p<0.001$ between variables. C, D and W indicate the control, drought and warming treatments, respectively.

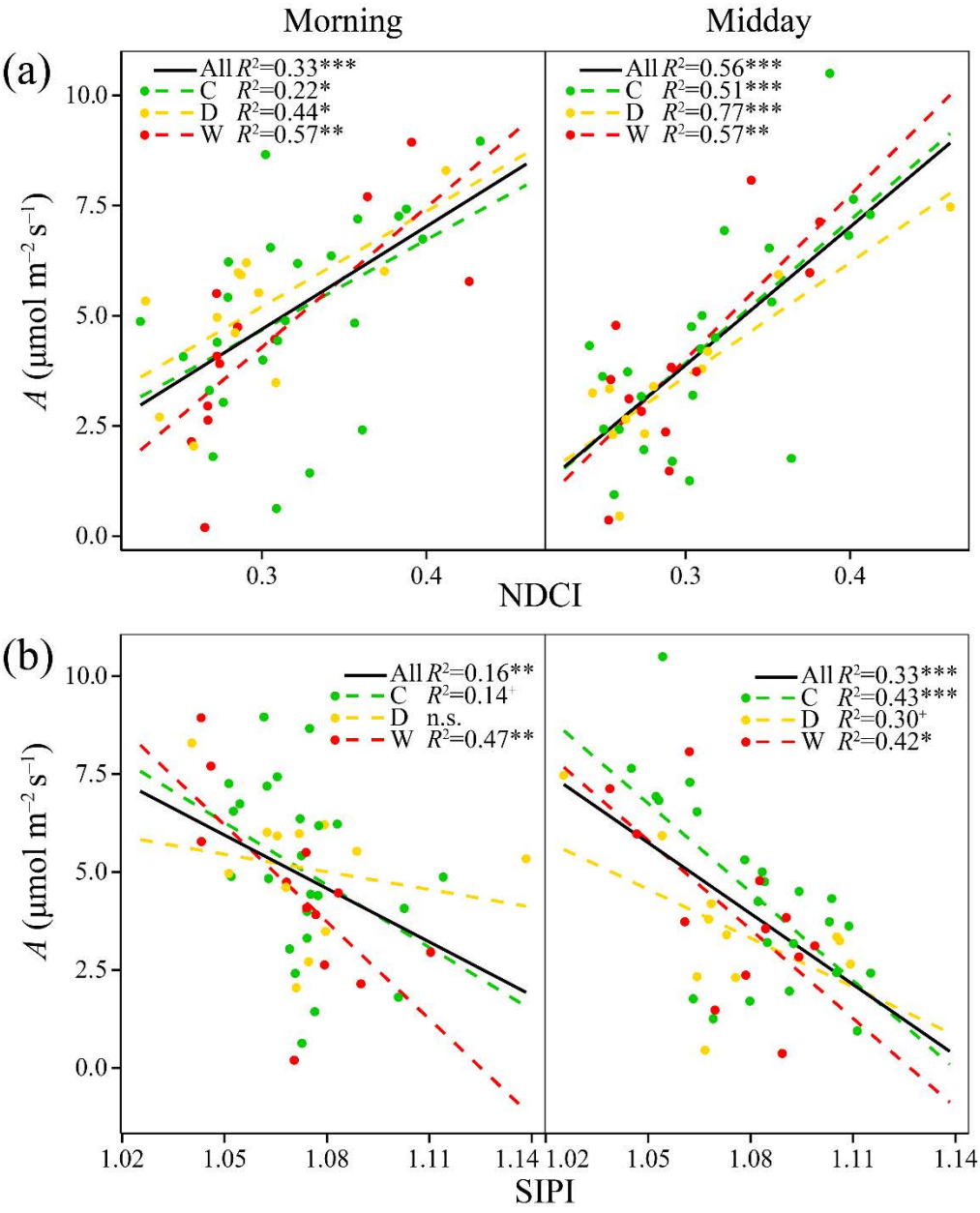

Figure S4. Relationships of CO_2 assimilation rate (A) with the normalized difference chlorophyll index (NDCI) (a) and the structure-independent pigment index (SIPI) (b) for *Erica multiflora* in 2014. The black lines represent the linear relationships over all three treatments. n.s. $p>0.1$, $^+p<0.1$, $*p<0.05$, $**p<0.01$ and $***p<0.001$ between variables. C, D and W indicate the control, drought and warming treatments, respectively.

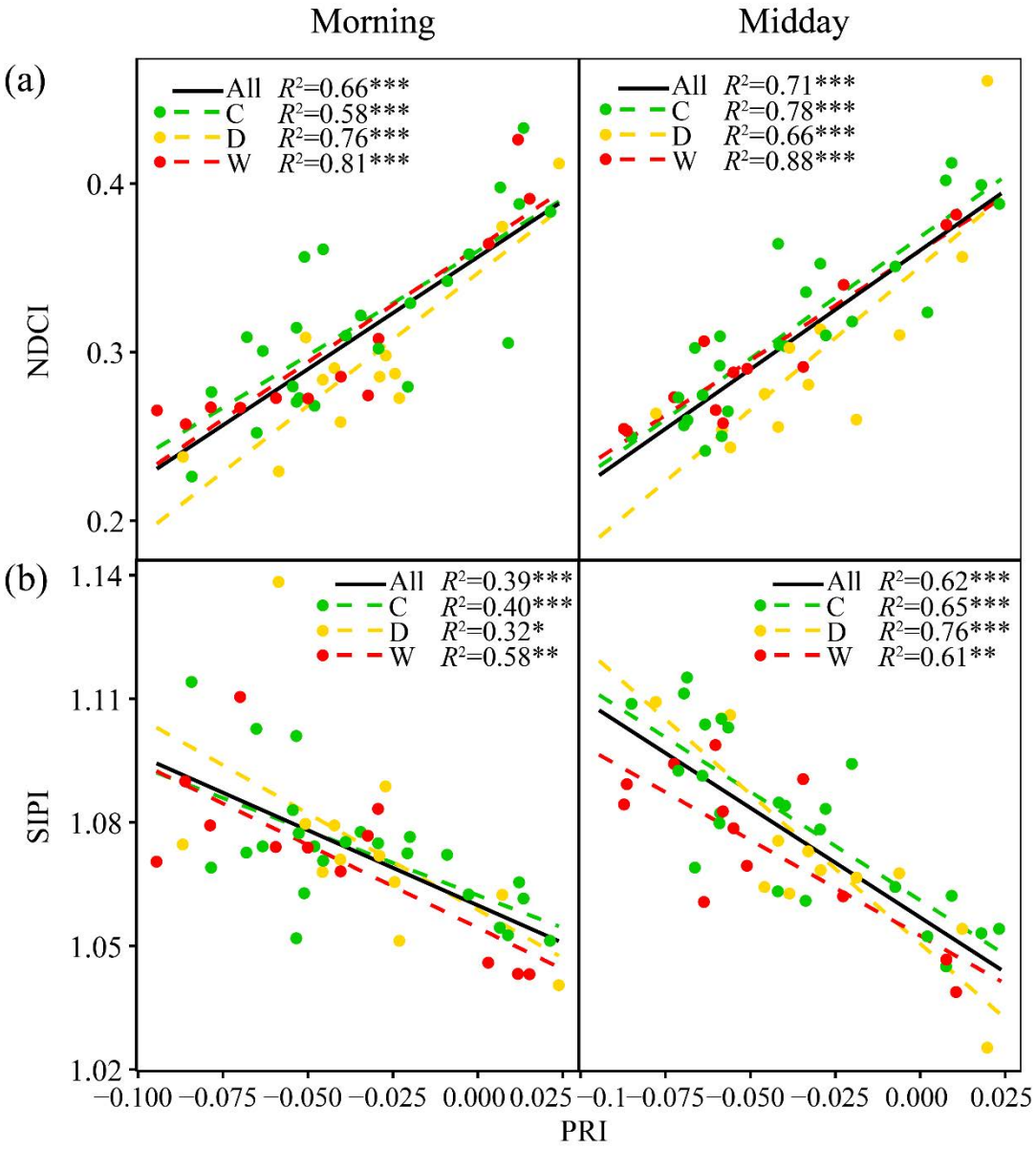

Figure S5. Relationships of the normalized difference chlorophyll index (NDCI) (a) and the structure-independent pigment index (SIPI) (b) with the photochemical reflectance index (PRI) for *Erica multiflora* in 2014. The black lines represent the linear relationships over all three treatments. *p<0.05, **p<0.01 and ***p<0.001 between variables. C, D and W indicate the control, drought and warming treatments, respectively.

Chapter 5. Remotely-sensed detection of effects of extreme droughts on gross primary production

Table S1. Main characteristics of the study sites: location, elevation (El), mean annual temperature (MAT), mean annual precipitation (MAP), vegetation type and dominant species and a key reference.

Site	Country	Location	El (m)	MAT (°C)	MAP (mm)	Vegetation (species)	Reference
Hesse	France	48.6742 N, 7.0656 E	300	9.2	885	Deciduous broadleaved forest (*Fagus sylvatica*)	[1]
Puéchabon	France	43.7414 N, 3.5958 E	61	13.4	883	Evergreen broadleaved forest (*Quercus ilex*)	[2]
Bugacpuszta	Hungary	46.6911 N, 19.6013 E	106	10.4	562	Semi-arid grassland (*Festuca pseudovina*, *Carex stenophylla*, *Salvia pratensis*)	[3]
Hainich	Germany	51.0793 N, 10.45 1E	445	7	800	Deciduous broadleaved forest (*Fagus sylvatica*)	[4]

Table S2. Description of the formulae used to derive the remote sensing indicators. The variable 'b' represents the reflectance values derived from MODIS: b1: 620 – 670 nm; b2: 841 – 876 nm; b3: 459 – 479 nm; b7: 2105 – 2155 nm, b11: 526 – 536 nm; b12: 546 – 556 nm.

Index	Formula	Use	Reference
Normalized Difference Vegetation Index (NDVI)	$\frac{b2-b1}{b2+b2}$	Greenness / biomass	5
Enhanced Vegetation Index (EVI)	$2.5 \cdot \frac{(b2-b1)}{b2+6 \cdot b1-7.5 \cdot b3+1}$	Greenness / biomass	5
Enhanced Vegetation Index 2 (EVI2)	$2.5 \cdot \frac{(b2-b1)}{b2+2.4 \cdot b1+1}$	Greenness / biomass	6
Simple Ratio (SR)	$\frac{b2}{b1}$	Greenness / biomass	5
Global Environmental Monitoring Index (GEMI)	$\eta(1-0.25\eta)-\frac{b1-0.125}{1-b1}$ $\eta=\frac{2(b2^2-b1^2)+1.5 \cdot b1+0.5b1}{b2+b1+0.5}$	Greenness / biomass	7
Normalized Difference Water Index (NDWI)	$\frac{b2-b7}{b2+b7}$	Leaf / canopy water content	8
Photochemical Reflectance Index (PRI)	$\frac{b11-b12}{b11+b12}$	Changes in carotenoid pigments (e.g. xanthophyll pigments)	9

Table S3. Field data for Hainich: plant area index (PAI, m^2 m^{-2}, is measured with the LAI-2000 sensor, which detects leaves and other plant organs such as fruits), leaf production (NPPl, g C m^{-2} y^{-1}), fruit production (NPPf, g C m^{-2} y^{-1}), wood production (NPPw, g C m^{-2} y^{-1}), and comments on important events in the forest (Mund M, Herbst M, Ammer C, Ghimire B, Kollascheck M, Knohl A, Schumacher J. (in preparation). It is not just a trade-off – Evidence for a complex control of vegetative and regenerative growth in an old-growth, mixed beech stand).

Year	PAI	NPPl	NPPf	NPPw	Comment
2003	6.2	175	24	199	
2004	5.5	158	100	157	masting + low spring temperatures
2005	5.8	176	8	218	
2006	6.0	163	115	190	masting
2007	5.7	179	42	254	
2008	6.5	184	10	222	
2009	6.1	175	172	194	masting
2010	6.7	181	13	175	
2011	NA	124	189	129	masting + dry spring + early bud break + late frost

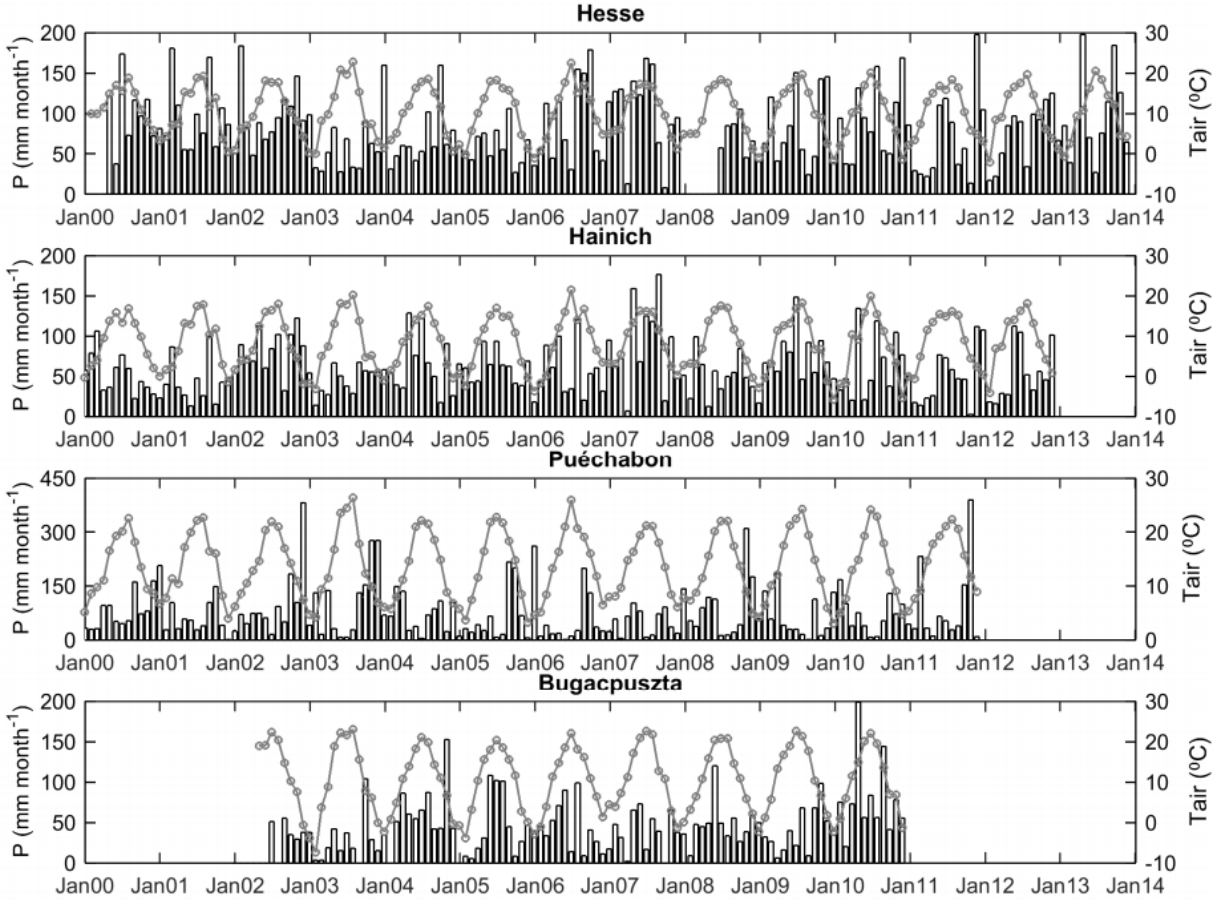

Figure S1 Time series of monthly precipitation (P; black bars) and mean monthly air temperature (Tair; grey symbols). Data were collected at the sites.

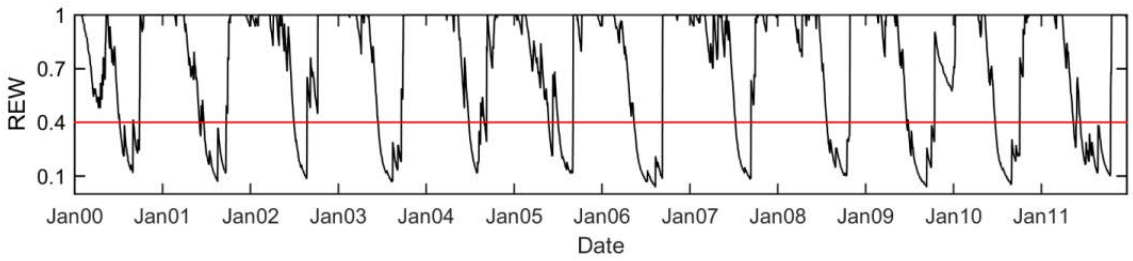

Figure S2. Relative extractable water (REW) for Puéchabon (black line). The red line indicates the common threshold of 0.4, indicative of drought stress. See manuscript text for further details.

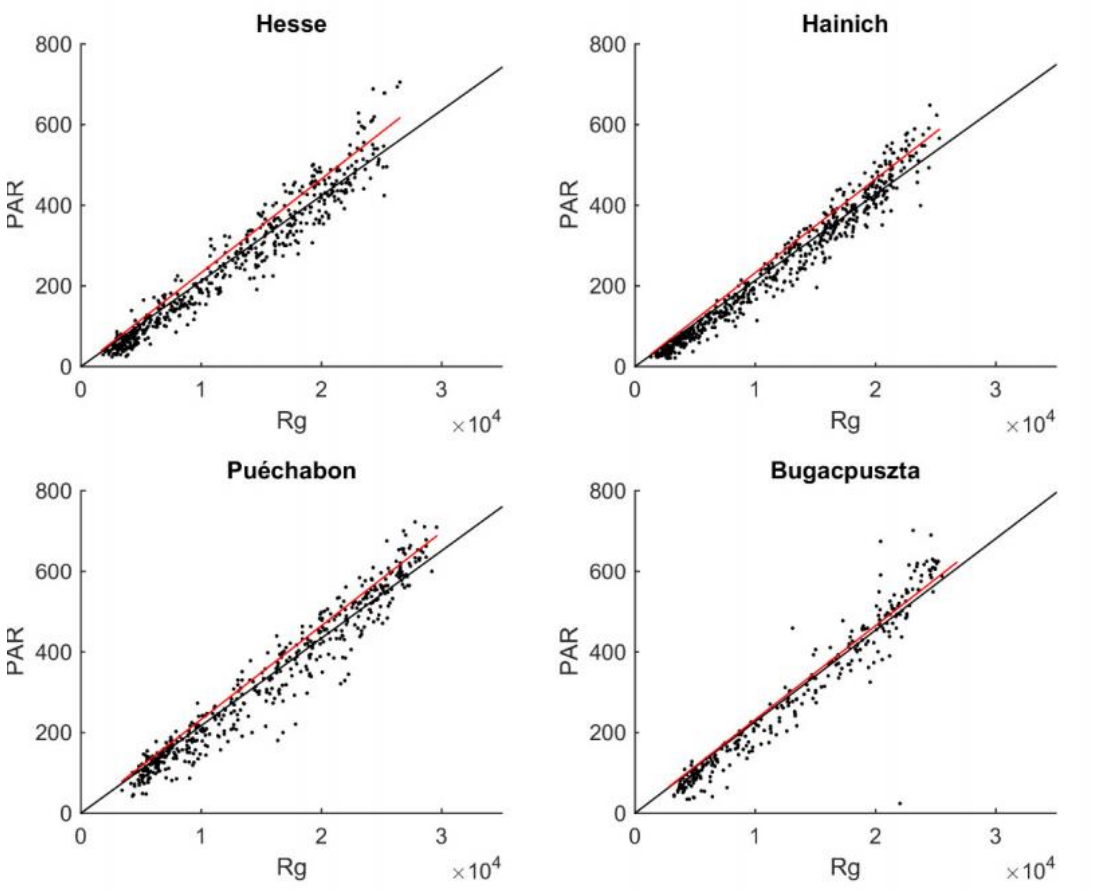

Figure S3. Relationship between photosynthetically active radiation (PAR; µmol m^{-2} s^{-1}; obtained from flux tower) and global radiation (Rg; $kJ.m^{-2}.d^{-1}$; obtained from JRC-MARS), for each of the studied sites. Linear fits through the origin are shown as black lines. We used the relationship PAR=Rg/43 (red lines) to calculate PAR from the JRC-MARS data set. This method has the advantage of removing data gaps in the field data and is especially interesting for the current study where the aim is to test how drought effects observed in the field can be detected using global databases (MODIS and JRC-MARS).

Hesse

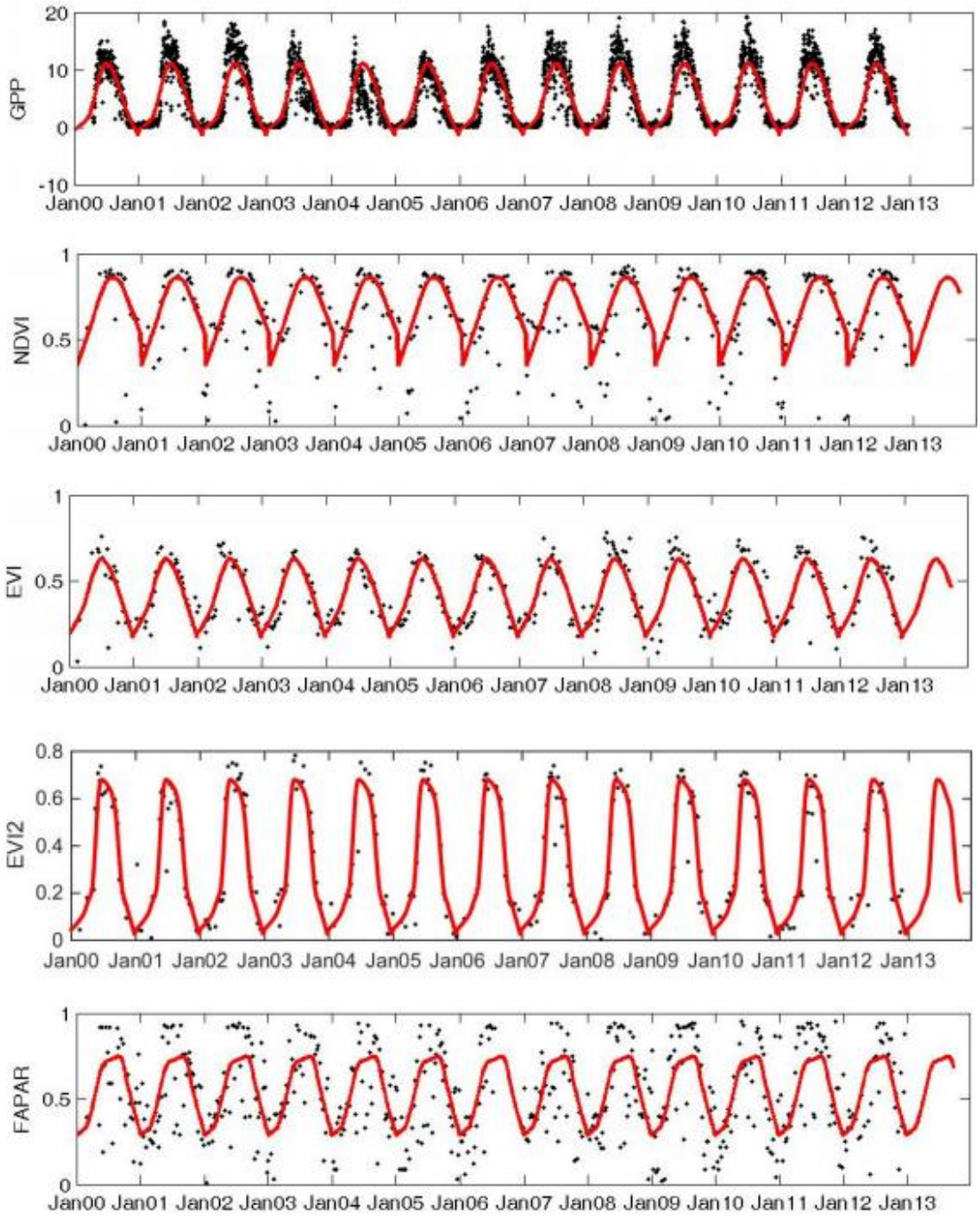
GPP
20
10
0
-10
NDVI
1
0.5
0
EVI
1
0.5
0
EVI2
0.8
0.6
0.4
0.2
0
FAPAR
1
0.5
0
Jan00 Jan01 Jan02 Jan03 Jan04 Jan05 Jan06 Jan07 Jan08 Jan09 Jan10 Jan11 Jan12 Jan13

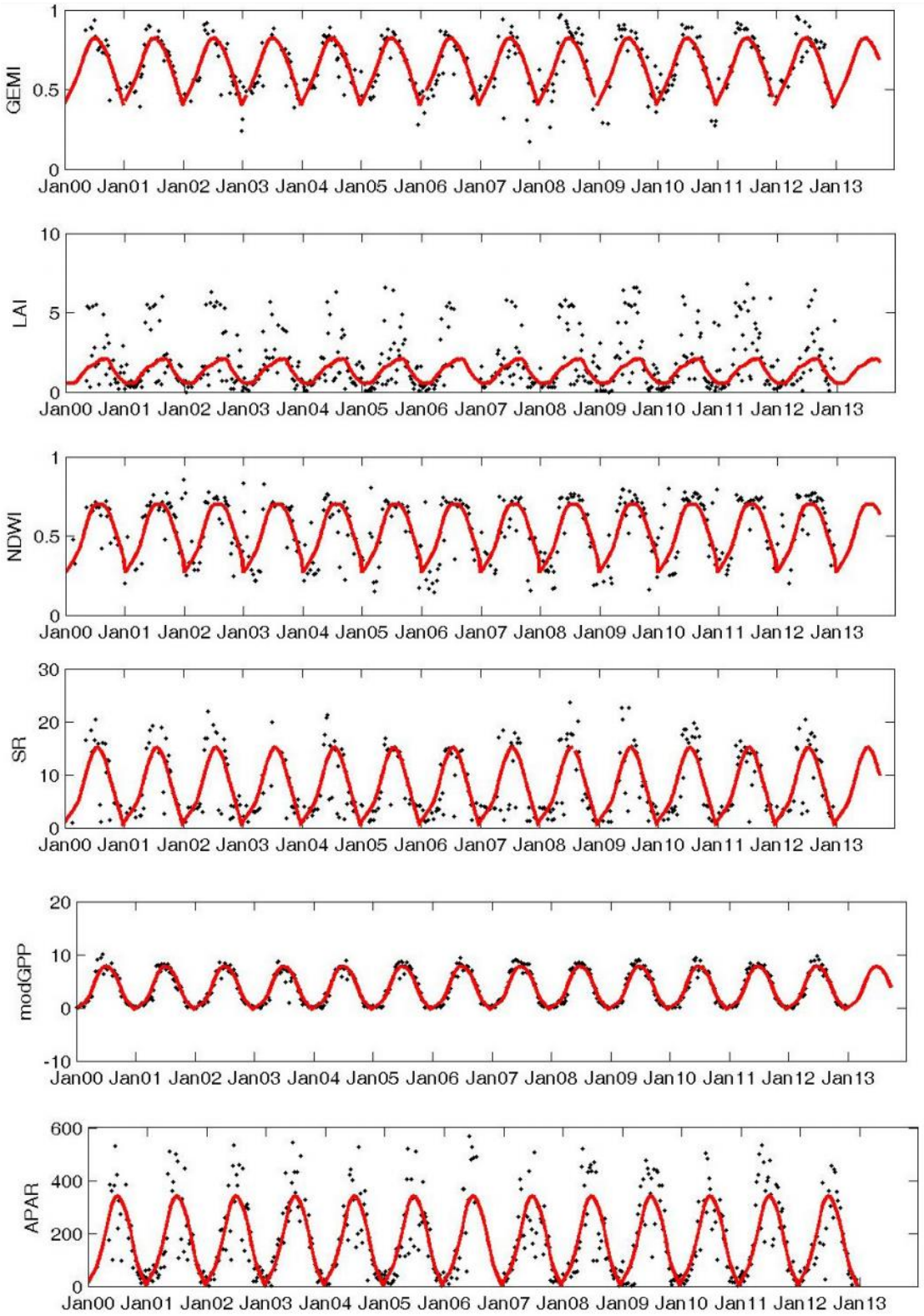
GEMI
1
0.5
0
LAI
10
5
0
NDWI
1
0.5
0
SR
30
20
10
0
modGPP
20
10
0
-10
APAR
600
400
200
0
Jan00 Jan01 Jan02 Jan03 Jan04 Jan05 Jan06 Jan07 Jan08 Jan09 Jan10 Jan11 Jan12 Jan13

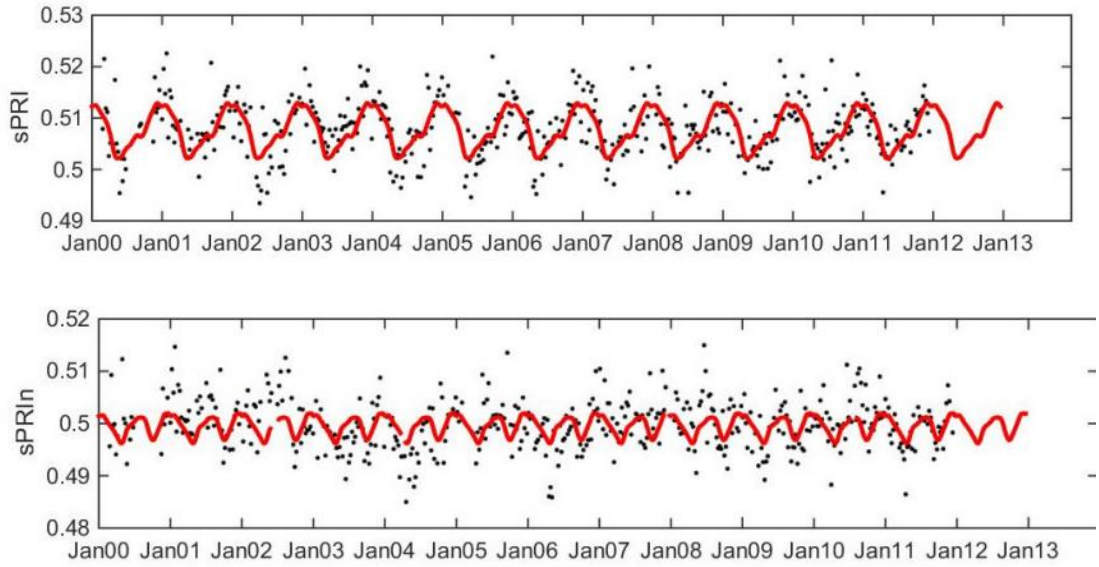
sPRI
0.53
0.52
0.51
0.5
0.49
Jan00 Jan01 Jan02 Jan03 Jan04 Jan05 Jan06 Jan07 Jan08 Jan09 Jan10 Jan11 Jan12 Jan13
sPRIn
0.52
0.51
0.5
0.49
0.48
Jan00 Jan01 Jan02 Jan03 Jan04 Jan05 Jan06 Jan07 Jan08 Jan09 Jan10 Jan11 Jan12 Jan13

Hainich

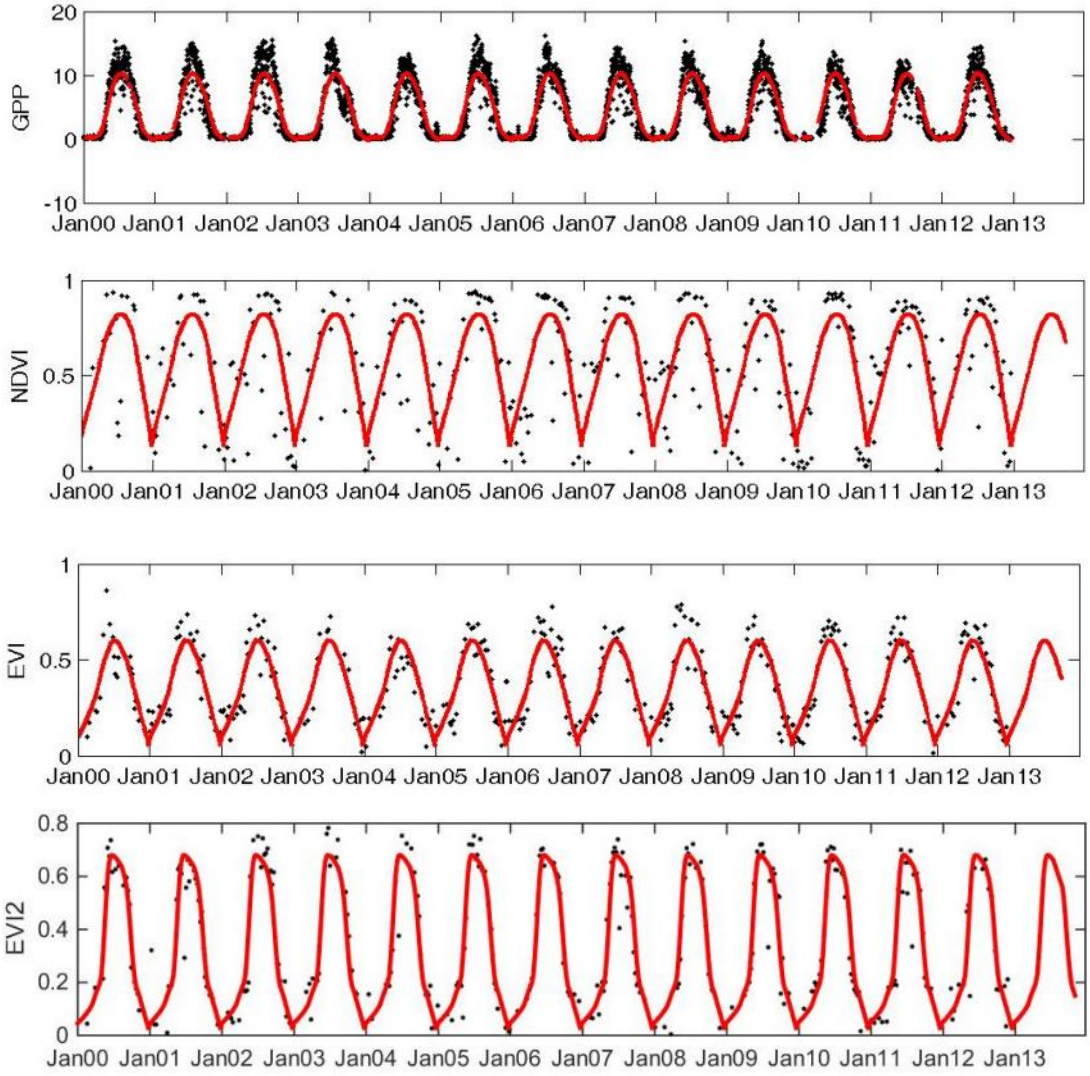
GPP
20
10
0
-10
Jan00 Jan01 Jan02 Jan03 Jan04 Jan05 Jan06 Jan07 Jan08 Jan09 Jan10 Jan11 Jan12 Jan13
NDVI
1
0.5
0
Jan00 Jan01 Jan02 Jan03 Jan04 Jan05 Jan06 Jan07 Jan08 Jan09 Jan10 Jan11 Jan12 Jan13
EVI
1
0.5
0
Jan00 Jan01 Jan02 Jan03 Jan04 Jan05 Jan06 Jan07 Jan08 Jan09 Jan10 Jan11 Jan12 Jan13
EVI2
0.8
0.6
0.4
0.2
0
Jan00 Jan01 Jan02 Jan03 Jan04 Jan05 Jan06 Jan07 Jan08 Jan09 Jan10 Jan11 Jan12 Jan13

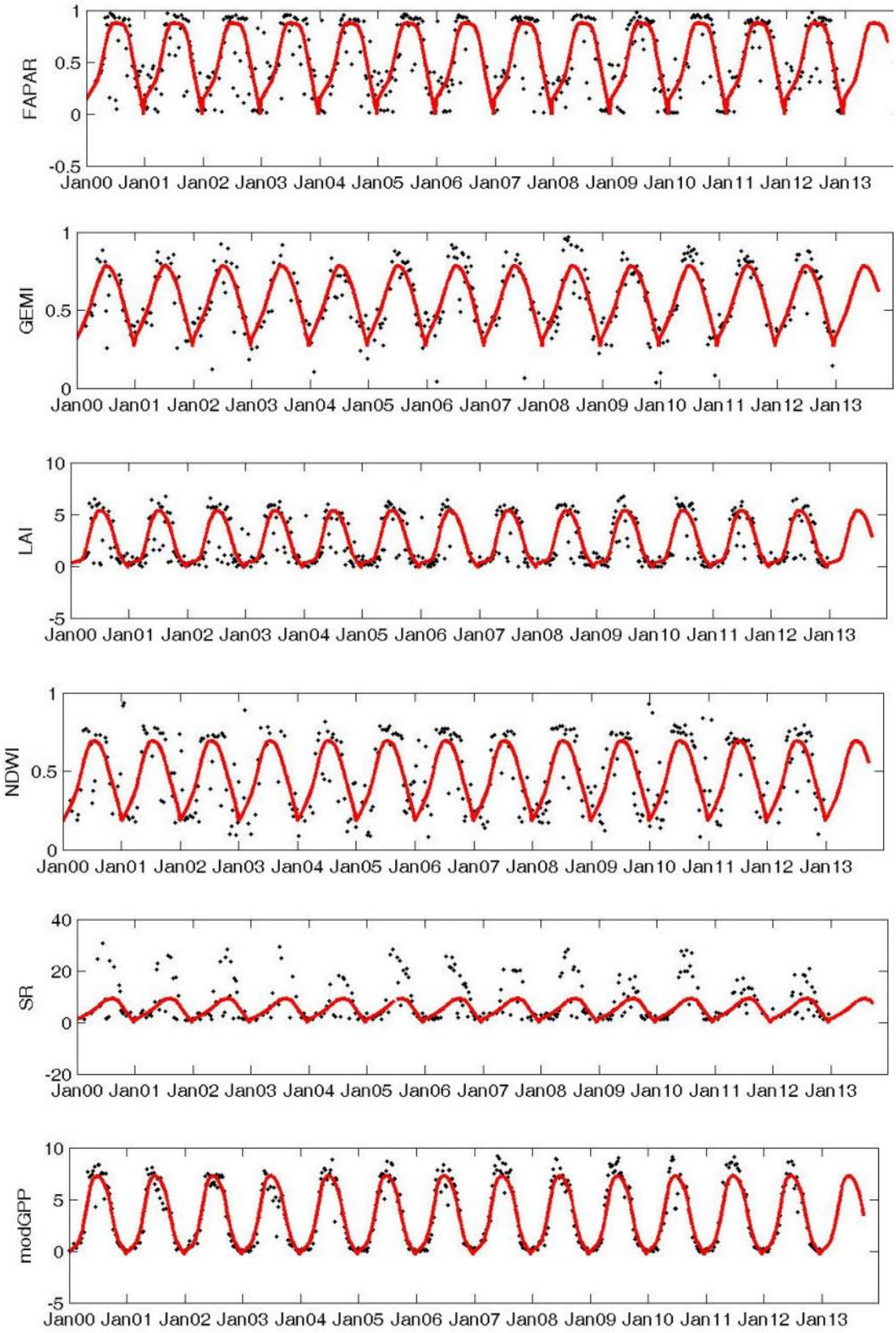
FAPAR
1
0.5
0
-0.5
Jan00 Jan01 Jan02 Jan03 Jan04 Jan05 Jan06 Jan07 Jan08 Jan09 Jan10 Jan11 Jan12 Jan13
GEMI
1
0.5
0
Jan00 Jan01 Jan02 Jan03 Jan04 Jan05 Jan06 Jan07 Jan08 Jan09 Jan10 Jan11 Jan12 Jan13
LAI
10
5
0
-5
Jan00 Jan01 Jan02 Jan03 Jan04 Jan05 Jan06 Jan07 Jan08 Jan09 Jan10 Jan11 Jan12 Jan13
NDWI
1
0.5
0
Jan00 Jan01 Jan02 Jan03 Jan04 Jan05 Jan06 Jan07 Jan08 Jan09 Jan10 Jan11 Jan12 Jan13
SR
40
20
0
-20
Jan00 Jan01 Jan02 Jan03 Jan04 Jan05 Jan06 Jan07 Jan08 Jan09 Jan10 Jan11 Jan12 Jan13
modGPP
10
5
0
-5
Jan00 Jan01 Jan02 Jan03 Jan04 Jan05 Jan06 Jan07 Jan08 Jan09 Jan10 Jan11 Jan12 Jan13

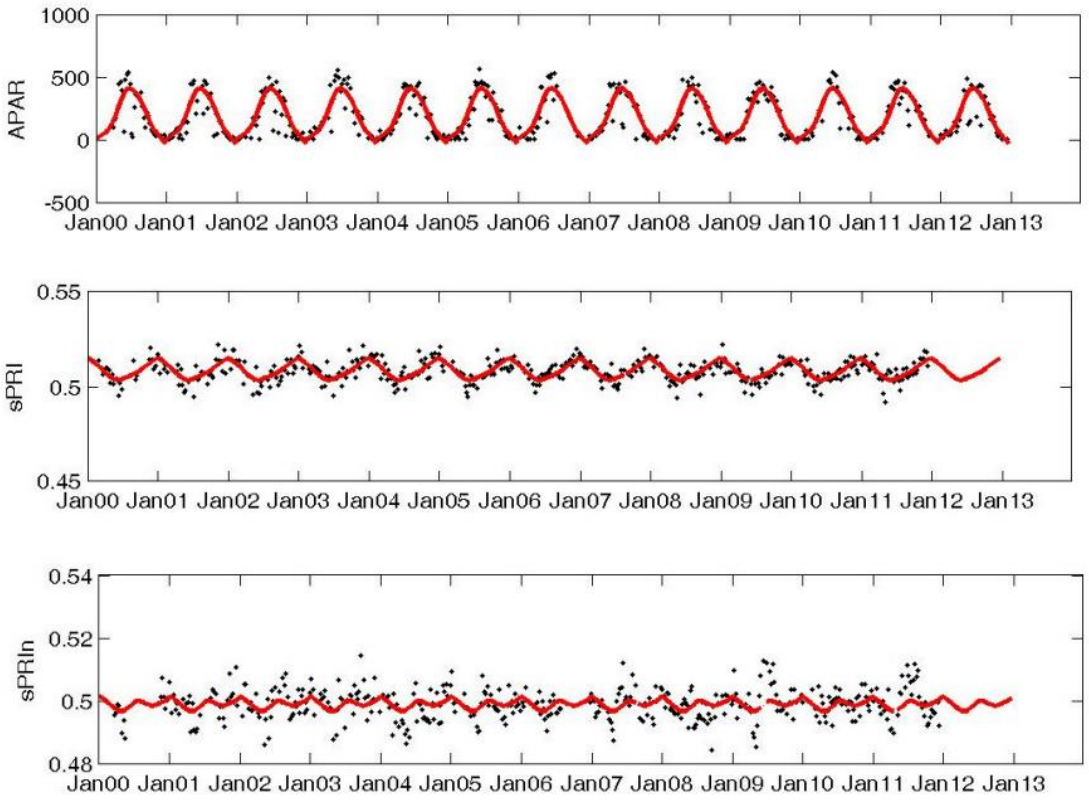
APAR
1000
500
0
-500
sPRI
0.55
0.5
0.45
sPRIn
0.54
0.52
0.5
0.48
Jan00 Jan01 Jan02 Jan03 Jan04 Jan05 Jan06 Jan07 Jan08 Jan09 Jan10 Jan11 Jan12 Jan13

Puéchabon

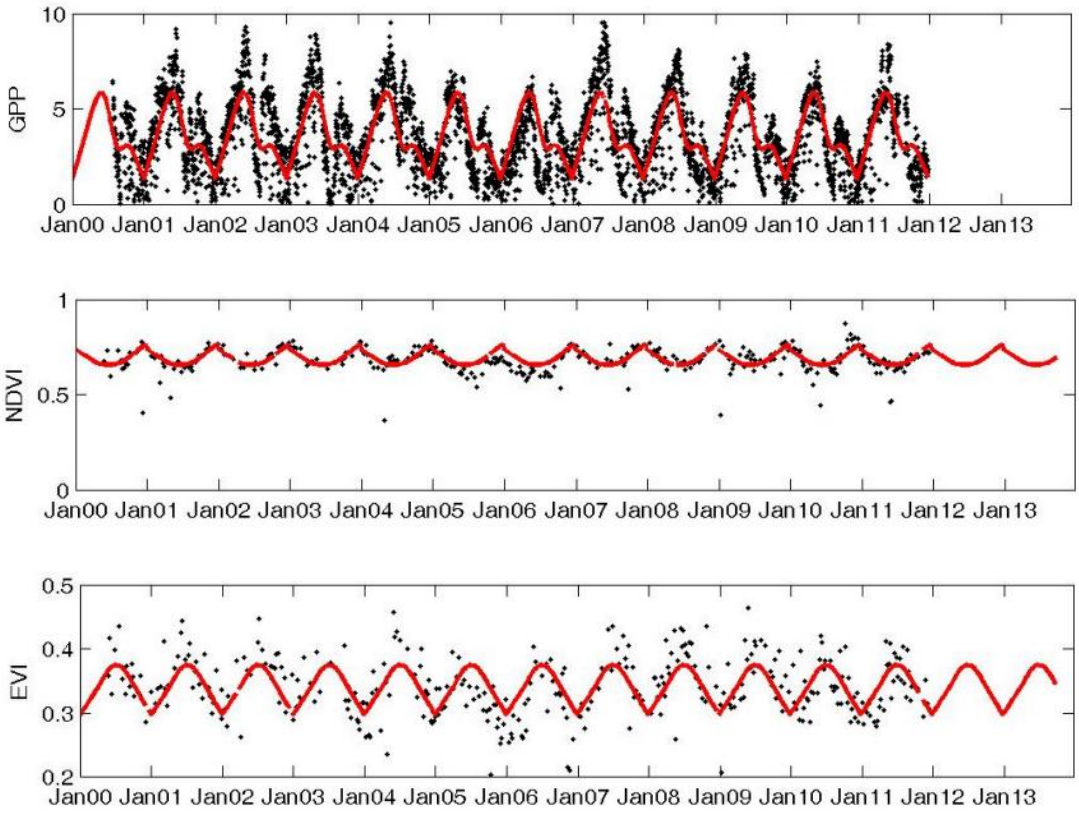
GPP
10
5
0
NDVI
1
0.5
0
EVI
0.5
0.4
0.3
0.2
Jan00 Jan01 Jan02 Jan03 Jan04 Jan05 Jan06 Jan07 Jan08 Jan09 Jan10 Jan11 Jan12 Jan13

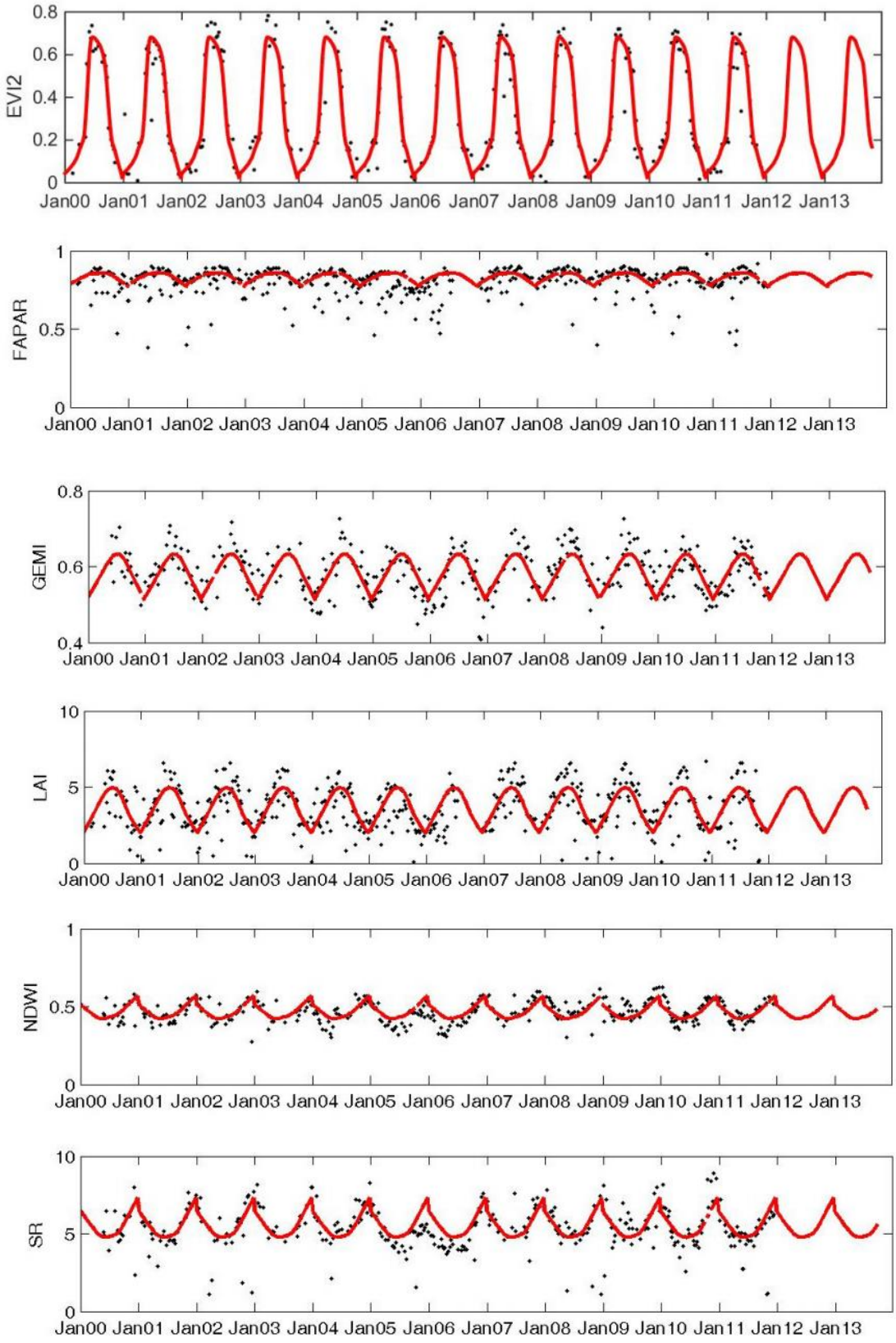
EVI2
0.8
0.6
0.4
0.2
0
Jan00 Jan01 Jan02 Jan03 Jan04 Jan05 Jan06 Jan07 Jan08 Jan09 Jan10 Jan11 Jan12 Jan13
FAPAR
1
0.5
0
Jan00 Jan01 Jan02 Jan03 Jan04 Jan05 Jan06 Jan07 Jan08 Jan09 Jan10 Jan11 Jan12 Jan13
GEMI
0.8
0.6
0.4
Jan00 Jan01 Jan02 Jan03 Jan04 Jan05 Jan06 Jan07 Jan08 Jan09 Jan10 Jan11 Jan12 Jan13
LAI
10
5
0
Jan00 Jan01 Jan02 Jan03 Jan04 Jan05 Jan06 Jan07 Jan08 Jan09 Jan10 Jan11 Jan12 Jan13
NDWI
1
0.5
0
Jan00 Jan01 Jan02 Jan03 Jan04 Jan05 Jan06 Jan07 Jan08 Jan09 Jan10 Jan11 Jan12 Jan13
SR
10
5
0
Jan00 Jan01 Jan02 Jan03 Jan04 Jan05 Jan06 Jan07 Jan08 Jan09 Jan10 Jan11 Jan12 Jan13

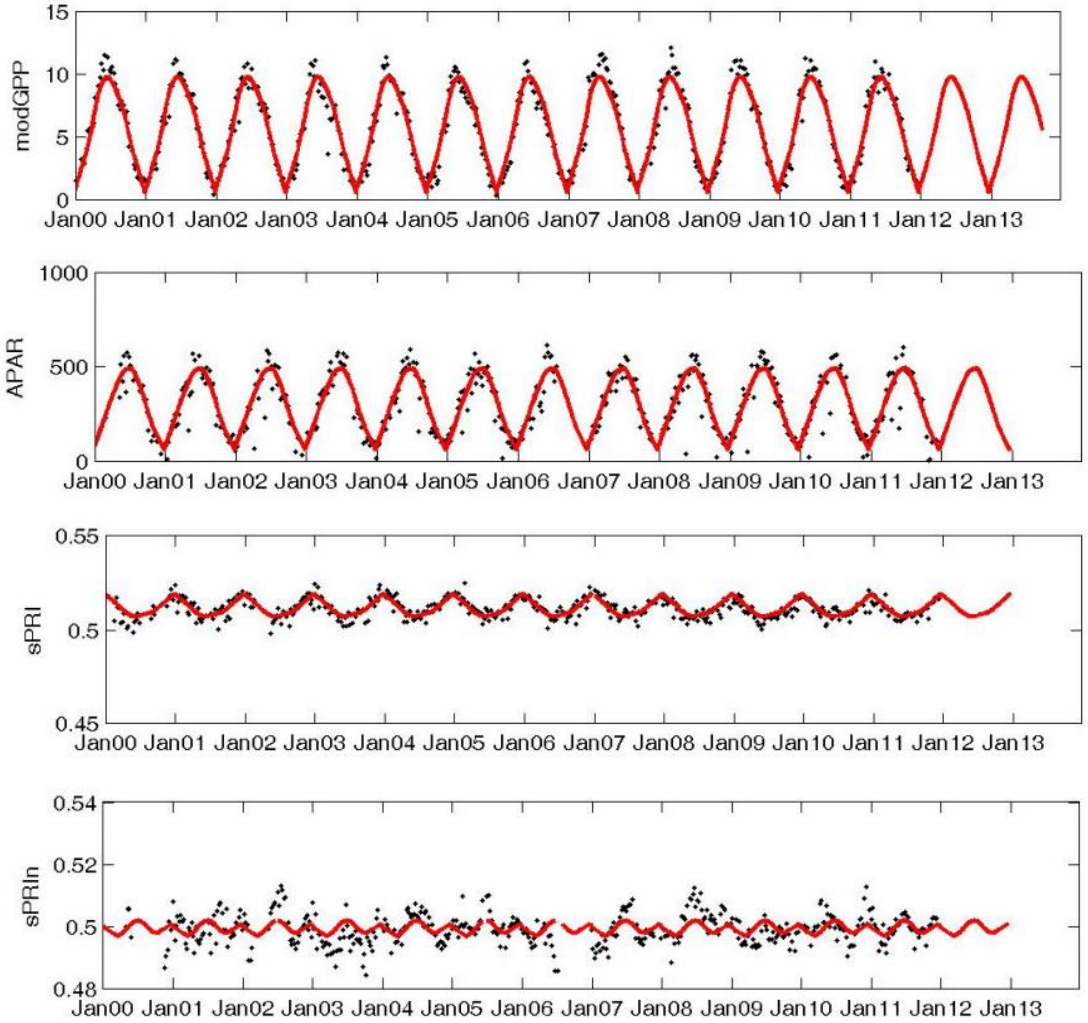

Bugacpuszta

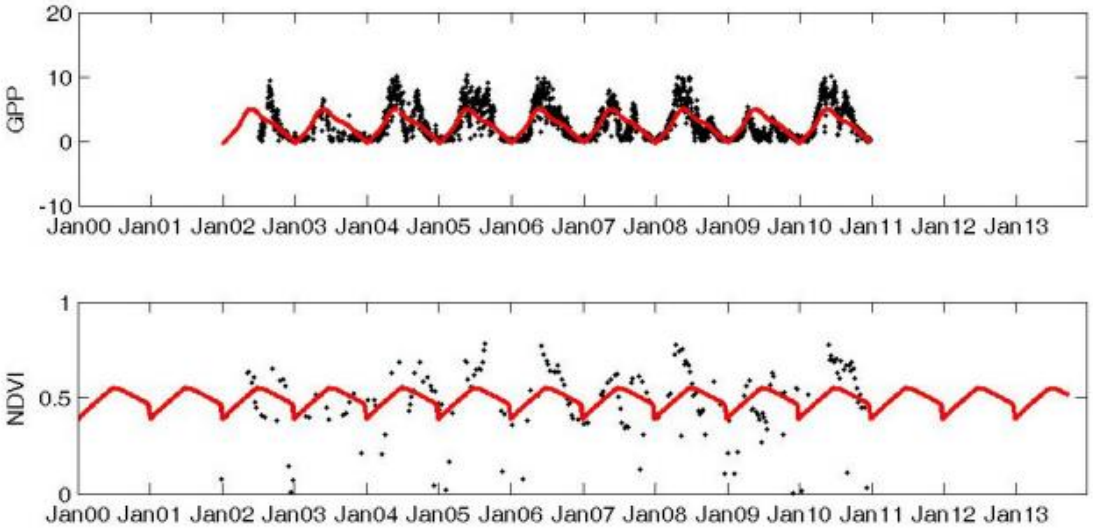

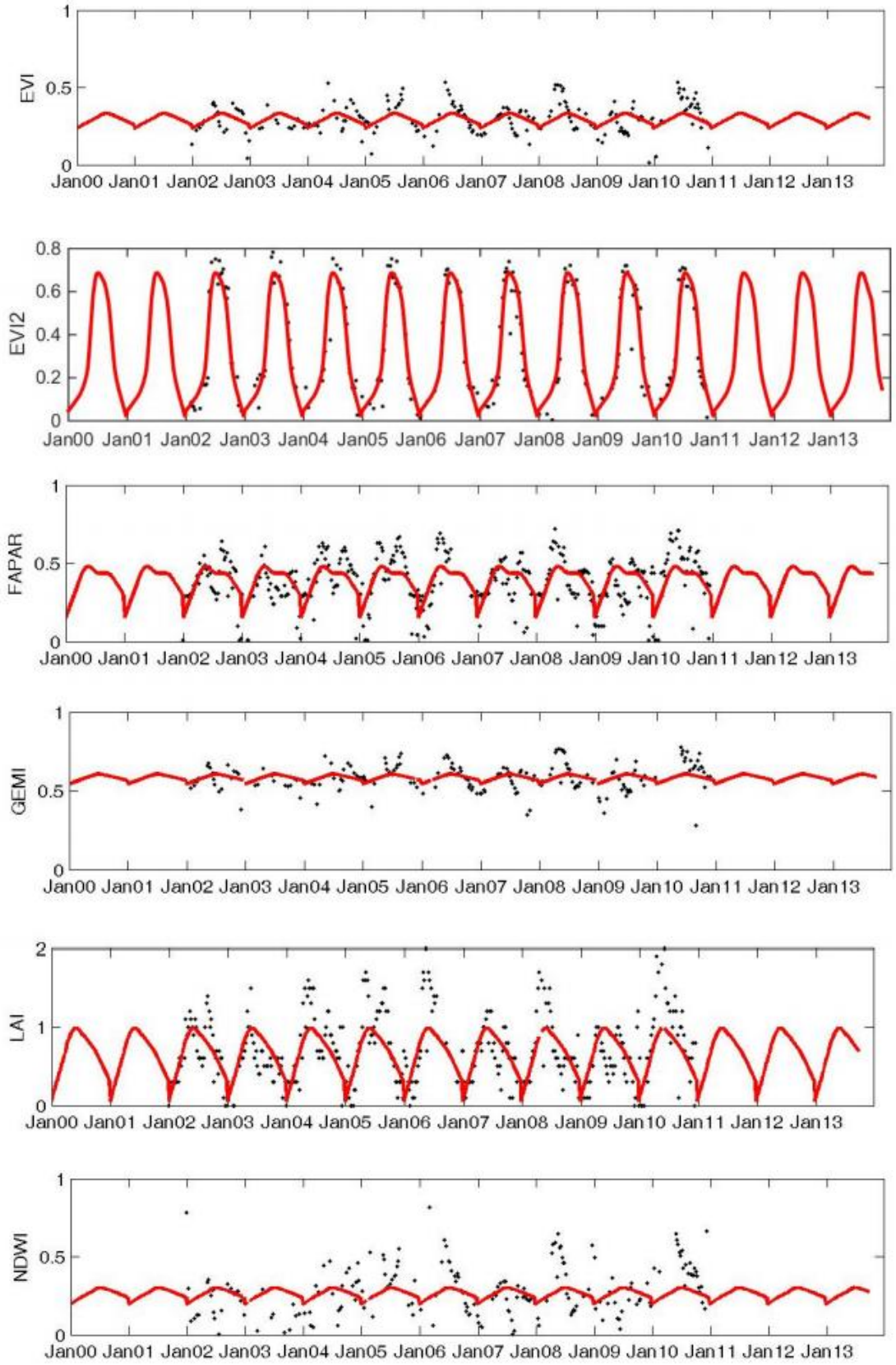
EVI
1
0.5
0
Jan00 Jan01 Jan02 Jan03 Jan04 Jan05 Jan06 Jan07 Jan08 Jan09 Jan10 Jan11 Jan12 Jan13
EVI2
0.8
0.6
0.4
0.2
0
Jan00 Jan01 Jan02 Jan03 Jan04 Jan05 Jan06 Jan07 Jan08 Jan09 Jan10 Jan11 Jan12 Jan13
FAPAR
1
0.5
0
Jan00 Jan01 Jan02 Jan03 Jan04 Jan05 Jan06 Jan07 Jan08 Jan09 Jan10 Jan11 Jan12 Jan13
GEMI
1
0.5
0
Jan00 Jan01 Jan02 Jan03 Jan04 Jan05 Jan06 Jan07 Jan08 Jan09 Jan10 Jan11 Jan12 Jan13
LAI
2
1
0
Jan00 Jan01 Jan02 Jan03 Jan04 Jan05 Jan06 Jan07 Jan08 Jan09 Jan10 Jan11 Jan12 Jan13
NDWI
1
0.5
0
Jan00 Jan01 Jan02 Jan03 Jan04 Jan05 Jan06 Jan07 Jan08 Jan09 Jan10 Jan11 Jan12 Jan13

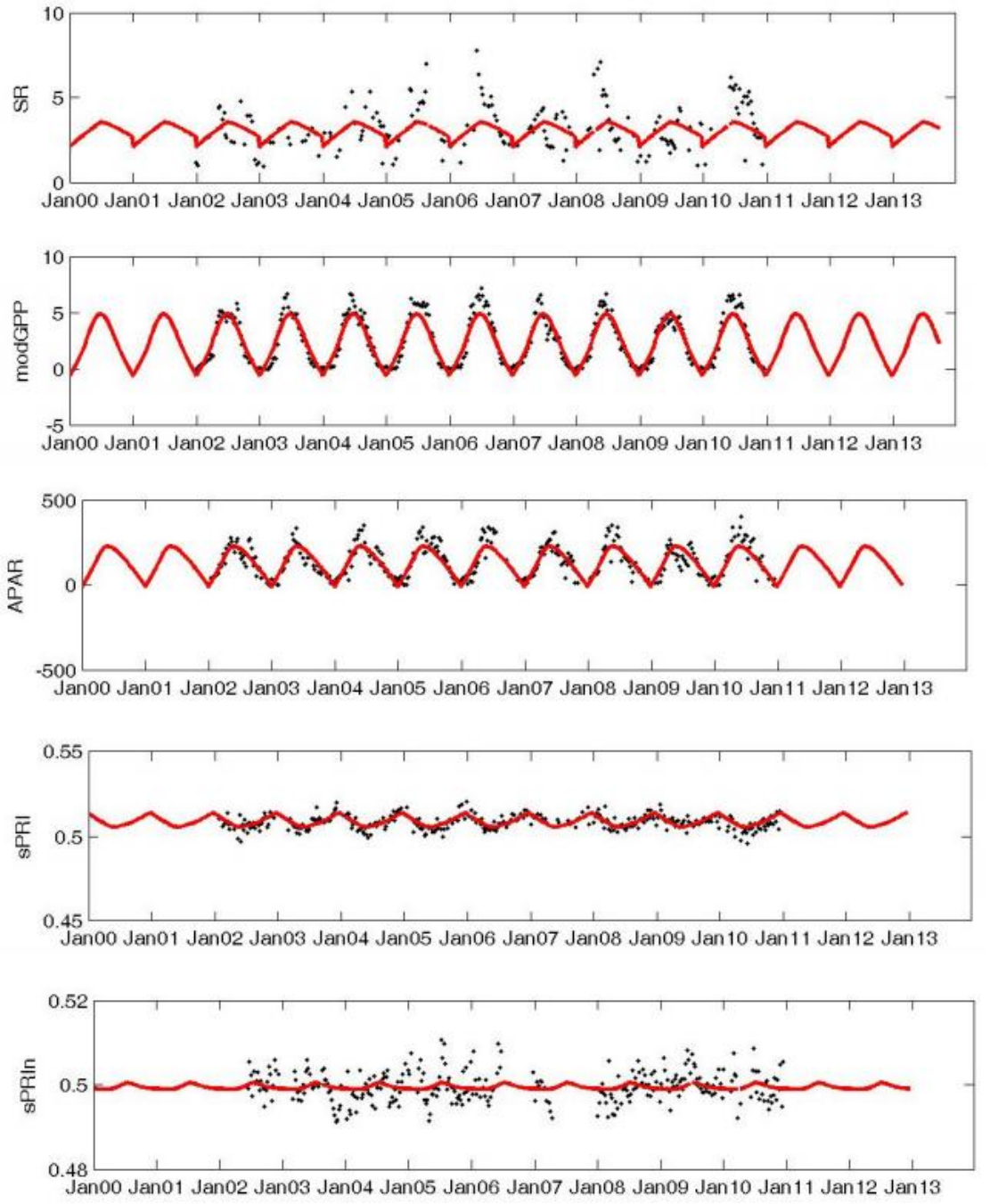

Figure S4. Seasonal patterns. The figures show the time series of flux or remotely sensed data (black points) and the average seasonal pattern (using a ~1-month moving window) used for calculating the anomalies (red lines) for the four sites.

Hainich

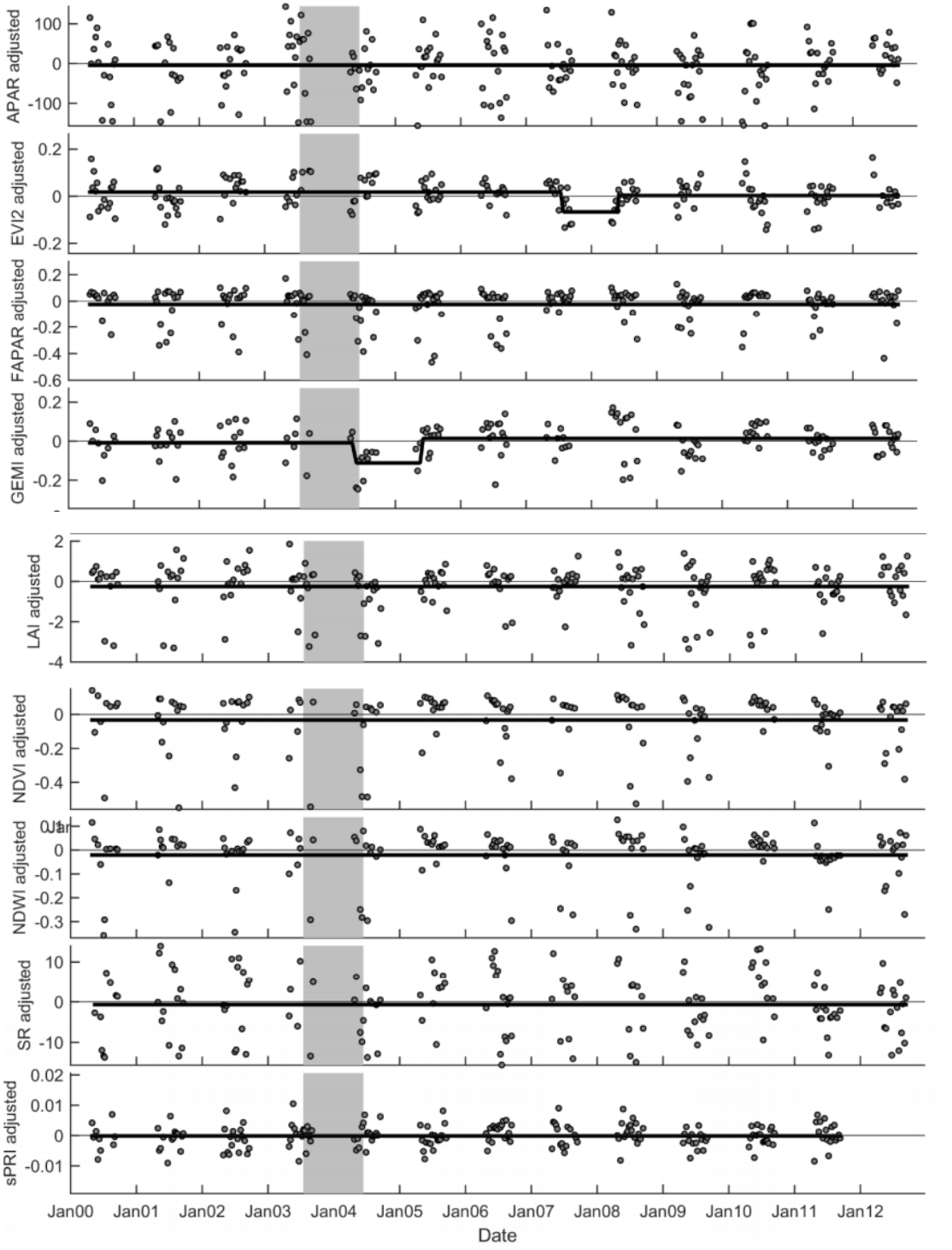
APAR adjusted
EVI2 adjusted
FAPAR adjusted
GEMI adjusted
LAI adjusted
NDVI adjusted
NDWI adjusted
SR adjusted
sPRI adjusted
Jan00
Jan01
Jan02
Jan03
Jan04
Jan05
Jan06
Jan07
Jan08
Jan09
Jan10
Jan11
Jan12
Date

Puéchabon

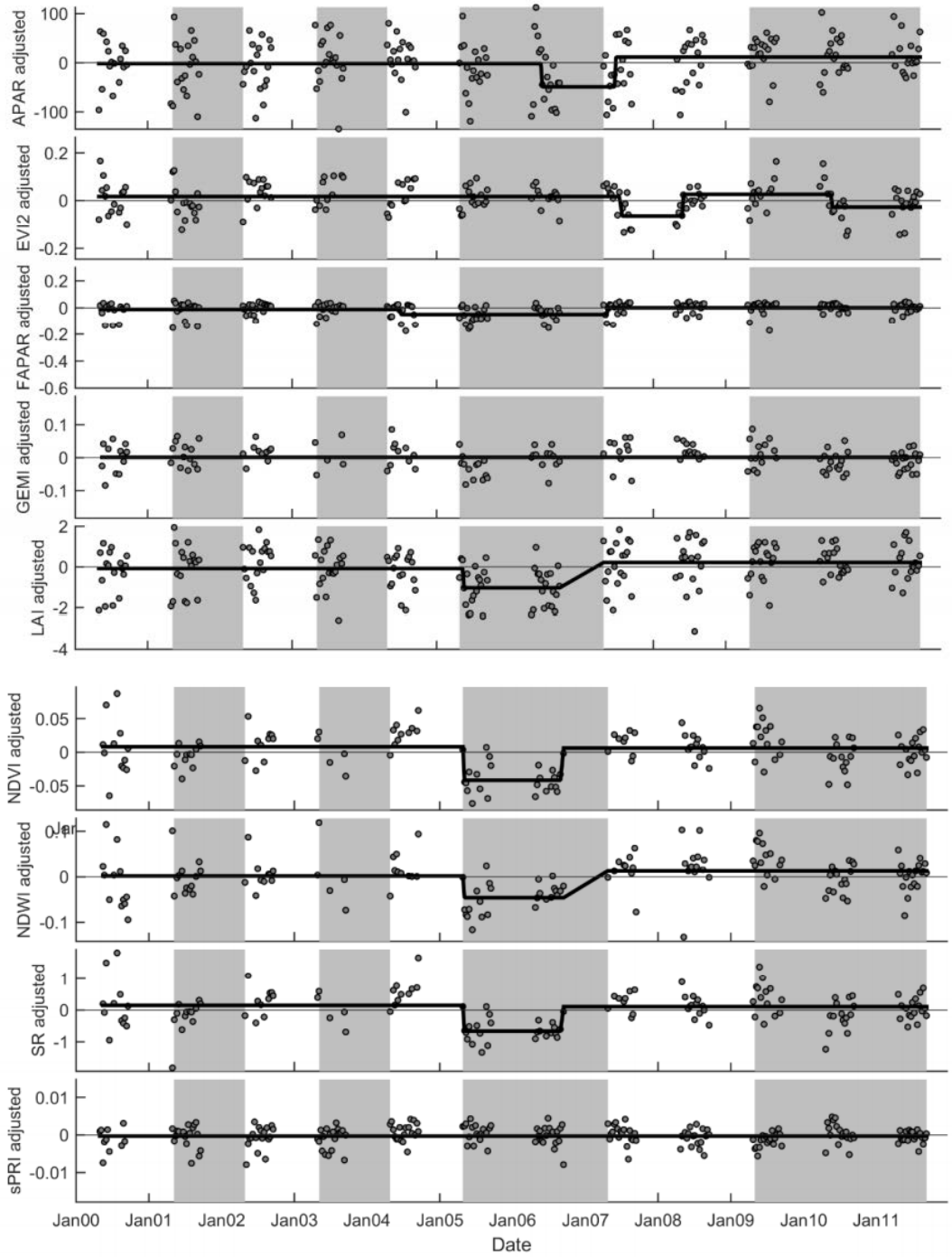
APAR adjusted
EVI2 adjusted
FAPAR adjusted
GEMI adjusted
LAI adjusted
NDVI adjusted
NDWI adjusted
SR adjusted
sPRI adjusted
Jan00
Jan01
Jan02
Jan03
Jan04
Jan05
Jan06
Jan07
Jan08
Jan09
Jan10
Jan11
Date

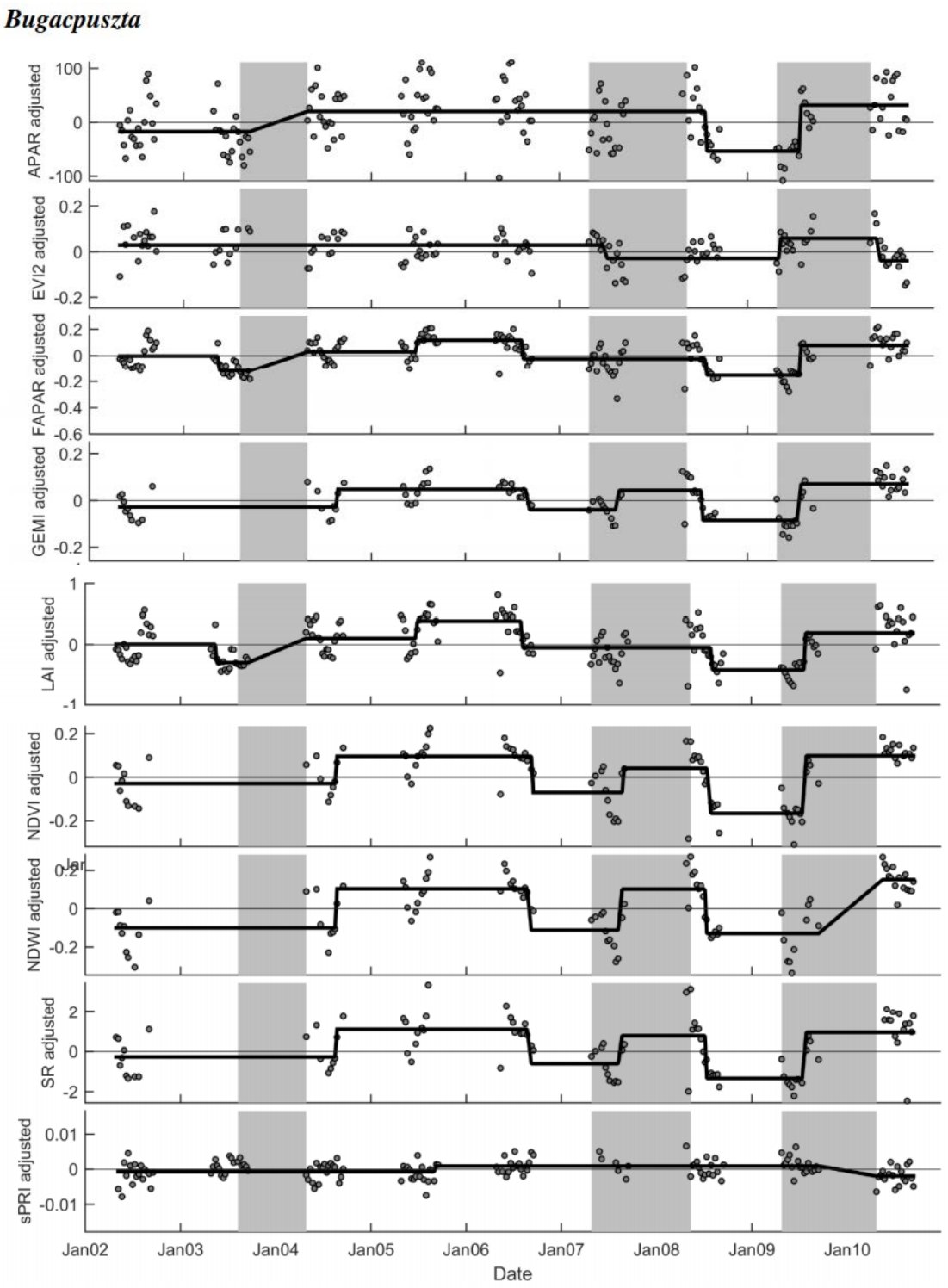

Figure S5. The results of the breakpoint analysis for the four sites.

Notes S1 Water availability metrics.

Plants experience a given reduction in precipitation (or SPEI) quite differently between sites e.g., because of differences in soil texture or groundwater access; see [10], and periods of drought are therefore best identified using site-specific data. The stress experienced by plants is ideally indicated by predawn leaf water potential[10], but this measurement is not usually available. In our dataset, predawn leaf water potential was available only for Puéchabon, where they were combined with measurements of soil-water content to compute the water stress integral WSI; see [11,12]. In this forest, WSI values ranging from -100 to -150 MPa day are representative of a wellwatered years, while the lowest WSI observed so far was – 358 MPa day[12]. We consider WSI ≤ - 250 MPa day to be indicative of moderate to severe drought, which corresponds to a probability of 0.3 given that average WSI was -213.6 MPa day, with a standard deviation of 73.35 MPa day. Another reliable indicator of water availability is the relative extractable water (REW) in soil, which can be calculated either from soil measurements[10] or with a water balance model[13]. The latter was used for Hesse and Hainich. The necessary data to run the model were not available for Bugacpuszta, but soil-moisture measurements provided an indication of the depletion of soil moisture for part of the time series under consideration. Soil-moisture measurements are not necessarily indicative of drought as experienced by the biota (e.g., when roots explore deeper soil layers; see also[10]), but these measurements were useful for verifying the plausibility of the SPEI results.

References

1 Granier, A., Breda, N., Longdoz, B., Gross, P. & Ngao, J. Ten years of fluxes and stand growth in a young beech forest at Hesse, North-eastern France. Ann. For. Sci. 65, 704 (2008).

2 Rambal, S. et al. Drought controls over conductance and assimilation of a Mediterranean evergreen ecosystem: scaling from leaf to canopy. Global Change Biol. 9, 1813-1824 (2003).

3 Nagy, Z. et al. The carbon budget of semi-arid grassland in a wet and a dry year in Hungary. Agriculture Ecosystems & Environment 121, 21-29 (2007).

4 Knohl, A., Schulze, E. D., Kolle, O. & Buchmann, N. Large carbon uptake by an unmanaged 250-year-old deciduous forest in Central Germany. Agr. Forest Meteorol. 118, 151-167 (2003). 22

5 Rouse, J. W., Haas, R. H., Schell, J. A. & Deering, D. W. in Proceedings of the Third Earth Resources Technology Satellite-1 Symposium 3010-3017 (Greenbelt, USA; NASA SP- 351, 1974).

6 Jiang, Z., Huete, A. R., Didan, K. & Miura, T. Development of a two-band enhanced vegetation index without a blue band. Remote Sens. Environ. 112, 3833-3845 (2008).

7 Pinty, B. & Verstraete, M. M. GEMI - A nonlinear index to monitor global vegetation from satellites. Vegetatio 101, 15-20 (1992).

8 Gao, B. C. NDWI - A normalized difference water index for remote sensing of vegetation liquid water from space. Remote Sens. Environ.58, 257-266 (1996).

9 Gamon, J. A., Penuelas, J. & Field, C. B. A narrow-waveband spectral index that tracks diurnal changes in photosynthetic activity. Remote Sens. Environ.41, 35-44 (1992).

10 Vicca, S. et al. Urgent need for a common metric to make precipitation manipulation experiments comparable. New Phytol.195, 518-522 (2012).

11 Myers, B. J. Water-stress integral – a link between short-term stress and long-term growth. Tree Physiol. 4, 315-323 (1988).

12 Rambal, S. et al. How drought severity constrains gross primary production (GPP) and its partitioning among carbon pools in a *Quercus ilex* coppice? Biogeosci.11, 6855-6869 (2014).

13 Granier, A., Breda, N., Biron, P. & Villette, S. A lumped water balance model to evaluate duration and intensity of drought constraints in forest stands. Ecol. Model. 116, 269-283 (1999).